



EURASIA GEOSCIENCE

CONGRESS AND EXHIBITION

10-13 NOVEMBER 2023, ANTALYA

Eurasia Geoscience Congress and Exhibition (EGCE2023)

ABSTRACT BOOK

15.11.2023

ISBN 978-605-136-740-8

ORGANIZED BY



www.eurasiacongress.org



"One day my mortal body will turn to dust, but the Turkish Republic will stand forever."

M. Kemal ATATÜRK

"The supreme guide in life is science."

M. Kemal ATATÜRK

We proudly celebrate the **100th** anniversary of the Republic of Türkiye, respectfully honoring the visionary founder of our Republic, Atatürk. As we look hopefully towards the future, we reaffirm our heartfelt dedication to the values of our Republic.

EGCE Organizing Committee



Eurasia Geoscience Congress and Exhibition 2023

November, 10-13, 2023, Antalya, TÜRKİYE



Organized by

Eurasia Geoscience Congress and Exhibition (EGCE2023)

ABSTRACT BOOK

Authors

M. Emin Candansayar, Prof. Dr., Ankara University

Pantelemion Soupios, Prof. Dr, King Fahd University of Petroleum and Minerals

Cansu Arican, MSc, Ankara University

15.11.2023

ISBN 978-605-136-740-8

Table of Contents

Welcome.....	i
Abstract Statistics	i
Organizing Committee.....	ii
Conveners/ Scientific Committee.....	ii
Topics.....	iv
Congress Overview	v
Technical Program (POSTER)	v
Technical Program (ORAL SESSIONS)	vi
ABSTRACTS and EXTENDED ABSTRACTS (FULL PAPER)	1
1.1 Northwestern Anatolia Lithospheric Resistivity Structure Revealed by 3D Inversion of Long Period Magnetotelluric Data: Comparison With Velocity Lithospheric Structure	2
1.2 IDENTIFYING AND LOCALIZING OF SEISMOGENIC EM ANOMALIES FROM DATA OBSERVED BY PERMANENT MT STATIONS.....	7
1.3 AN INSIGHT INTO THE EAST ANATOLIAN FAULT ZONE AND SURROUNDINGS THROUGH EARTHQUAKE TOMOGRAPHY: THE RELOCATION OF FEBRUARY 6, 2023 MAIN AND AFTERSHOCKS USING PAST SEISMIC ACTIVITY	12
1.4 WHAT ACTUALLY ROTATIONAL SEISMOLOGY MEANS TO A SEISMOLOGIST?	17
1.5 EVALUATING THE PERFORMANCE OF ROTATIONAL SENSORS ACROSS DIFFERENT SOURCE TYPES: EARTHQUAKES, EXPLOSIONS, AND VIBROSEIS SWEEPS.....	18
1.6 ANALYSIS OF SURFACE RUPTURE PATTERNS AND FAULT OFFSET VARIABILITY ASSOCIATED WITH THE 06 FEBRUARY 2023 PAZARCIK (KAHRAMANMARAS) EARTHQUAKE (MW 7.7) IN ISLAHIYE AREA, TURKIYE.....	19
1.7 EVALUATION OF RELATIVE TECTONIC ACTIVITY IN THE EASTERN PART OF KHAZAR FAULT ZONE, NORTH IRAN	25
1.8 PROBABILISTIC EARTHQUAKE RISK ANALYSES IN THE REGION OF SINDIRGI – SİNANPAŞA FAULT ZONE, TURKIYE	31
1.9 MORPHOTECTONIC CHARACTERISTICS AND PALEOSEISMOLOGICAL ANALYSIS OF ARAS FAULT ZONE (NW IRAN); PRELIMINARY RESULTS FROM REMOTE SENSING AND FIELD STUDIES	37
2.1 GEOPHYSICAL INSIGHTS INTO THE TECTONIC REGIME OF THE CHANIA BASIN IN THE AEGEAN REGION.....	45
2.2 SEISMIC SHIELDING OF URBAN AREAS BY USING INTEGRATED GEOPHYSICAL METHODS	46
2.3 RESISTIVITY IMAGE OF LEAKAGE FROM ÇANAKKALE OLD OPEN WASTE DISPOSAL SITE ..	47

2.4	INVESTIGATION OF THE MINERALOGICAL-PETROGRAPHICAL AND GEOCHEMICAL PROPERTIES OF DARENDE (MALATYA) REGION LIMESTONE	51
3.1	NON- DESTRUCTIVE GEOPHYSICAL INVESTIGATION OF SUPPORT STRUCTURE ELEMENT BY USING 3D INVERSION OF DIRECT CURRENT RESISTIVITY DATA	58
4.1	(NOT PRESENTED) Stratigraphy From the Pungalla Section, Ashdagh Mountain, North Eastern Iraq	62
4.2	EXHIBITION SIMILARITIES AND DISPARITIES UPPER CRETACEOUS SOURCE ROCKS FROM SOUTHEASTERN ANATOLIA FROM LITHOLOGICAL CONTENT PERSPECTIVE.....	63
4.3	CHARACTERIZATION OF AN UNCONVENTIONAL ORGANIC-RICH CARBONATE MUDSTONE, LATE JURASSIC OF SAUDI ARABIA	64
4.4	UNDERSTANDING THE ORIGIN OF QUARTZ CEMENTATION IN SANDSTONES FOR BETTER PRE-DRILL RESERVOIR QUALITY PREDICTION.....	65
5.1	LEVERAGING GENERATIVE ADVERSARIAL NETWORKS (GANS) TO ENHANCE WELL LOGGING DATA INTERPRETATION FOR SUSTAINABLE NEAR-FIELD EXPLORATION	66
5.2	POTENTIAL USE OF SONIC DATA FOR ROCK TYPING AND GEOSTEERING IN BIOTURBATED CARBONATE STRATA	70
5.3	CHALLENGES IN MICROSEISMIC TECHNOLOGY FOR RESERVOIR CHARACTERIZATION AND MONITORING: A BRIEF REVIEW	71
5.4	ELASTIC REVERSE TIME MIGRATION FOR IMAGING THROUGH GAS CLOUDS	72
5.5	AVA ANALYSIS OF MULTI-COMPONENT SEISMIC WAVE MODES (P-SV, SV-P).....	73
5.6	GAS-WATER DETECTION TECHNOLOGY AND APPLICATION OF LOTEM COMBINED WITH WELL LOGGING AND SEISMIC DATA	74
5.7	SIP DETECTION AND QUANTIFICATION OF IRON SULFIDE (FES) MATERIALS: A PATHWAY TO EARLY MONITORING	78
5.8	RECONSTRUCTION OF THE 3D SUBSURFACE OF THE AL-HASSA OASIS, EASTERN SAUDI ARABIA.....	79
5.9	DETERMINATION OF DEEP-SEATED FAULTS USING GRAVITY AND MAGNETIC METHODS: PRELIMINARY RESULTS FROM NORTH ADIYAMAN, SOUTHEASTERN TURKIYE	80
5.10	DETERMINING THE STRUCTURAL FEATURES OF THE GULF OF ANTALYA AND ITS OFFSHORE BY USING GRAVITY-MAGNETIC METHODS.....	84
6.1	AI-BASED INTEGRATION OF GEOSCINCE AND OTHER DATA FOR CARBON SEQUESTRATION AND ENHANCED OIL RECOVERY	85
6.2	USING ELECTROMAGNETIC FLUID IMAGING DURING THE ENERGY TRANSITION.....	88
6.3	HOW IMPORTANT IS MULTIPHYSICS FOR ELECTROMAGNETIC IMAGING	89
6.4	VOLCANIC MASSIVE SULFIDE (VMS) ORE DEPOSIT IN WESTERN SAUDI ARABIA: A GEOPHYSICAL STUDY.....	90

6.5	(NOT PRESENTED) GeoCluster-ExpertNet: A Proposed Model Integrating Unsupervised Learning with Expert for Optimal Geothermal Drilling	91
6.6	(NOT PRESENTED) Investigation of the Relationship Between the Topography and the Fluid Circulation Depth on the Geothermal Systems of Central Anatolia Region	92
6.7	3D VELOCITY STRUCTURE AND FLUID FLOWS INFERRED FROM THE MICROSEISMIC EVENTS IN THE GEOTHERMAL FIELD, TURKEY.....	93
6.8	MAGNETOTELLURIC SYSTEM NORD	104
6.9	DIG: A RESEARCH PROJECT TO ASSESS IRELAND'S GEOTHERMAL ENERGY POTENTIAL ..	105
6.10	GEOELECTRICAL CHARACTERIZATION OF GEOTHERMAL RESERVOIRS – CASE STUDIES FROM GEDİZ GEOTHERMAL AREA (TÜRKİYE).....	106
7.1	PHOENIX NEW GENERATION MT/CSAMT TECHNOLOGIES WITH REAL TIME DATA TRANSFER CAPABILITIES.....	107
7.2	JOINT APPLICATION OF ELECTROMAGNETIC PROSPECTING METHODS FOR MINERAL EXPLORATION: CASE STUDIES	108
7.3	REAL TIME MONITORING OF THE NATURAL BROADBAND EM SIGNALS: APPLICATIONS FOR MONITORING OF ACTIVE VOLCANOES.....	109
7.4	MAGNETOTELLURICS IN DEEP MINING OPERATIONS: CASE STUDIES FROM NORTH AMERICA.....	110
7.5	KMS ARRAY SYSTEM FOR CSEM/MT.....	111
7.6	LITHIUM-THE IMPORTANT RESOURCE OF GREEN TECHNOLOGY: PROPERTIES, GEOLOGY AND TURKEY'S POTENTIAL	112
7.7	THE GEOCHEMISTRY OF CLAYS ÇAVUŞÇUGÖL (ILGIN, KONYA)	116
7.8	A LARGE SCALE ERT SURVEY FOR LOCATING CLAY MINERALS	117
7.9	USING MARINE CSEM FOR RESERVOIR MONITORING BASED ON PETROPHYSICAL MODELING.....	118
8.1	COMPARING THE EFFICIENCY OF SYNTHETIC VS NATURAL-BASED LIQUID ACTIVATED CARBON IN REMOVING ORGANIC POLLUTANTS FROM CONTAMINATED WATER.....	123
8.2	RESISTIVITY IMAGING OF AQUIFER STRUCTURE WITH 2D/3D INVERSION OF DIRECT CURRENT RESISTIVITY AND AUDIO-MAGNETOTELLURIC DATA.....	127
9.1	GEOPHYSICAL AND REMOTE SENSING SURVEYS AT THE ARCHAEOLOGICAL SITE OF PHILIPPI, N. GREECE.....	131
9.2	IMAGING ARCHAEOLOGICAL RUINS BY GPR AND ERT SURVEYS: THE CASE OF ANCIENT SELEUKEIA SIDERA IN PISIDIA.....	132
9.3	WATER-BORNE ARCHAEOGEOPHYSICAL INVESTIGATIONS AT LAKE İZNIK	136
10.1	ESTIMATING THE ELECTRICAL ANISOTROPY COEFFICIENT, STRIKE DIRECTION, AND DIP ANGLE USING SQUARE ELECTRODE ARRAY DATA WITH GENERALIZED REGRESSION NEURAL NETWORKS	140



Eurasia Geoscience Congress and Exhibition 2023

November, 10-13, 2023, Antalya, TÜRKİYE



Organized by

10.2 CONSTRAINED INVERSION OF GEOPHYSICAL DATA WITHOUT REGULARIZATION PARAMETER USING PARETO-OPTIMAL SWARM INTELLIGENCE: APPLICATION TO MAGNETOTELLURIC PROBLEM	144
10.3 A NEW SOFTWARE FOR 3-DIMENSIONAL INVERSION OF MAGNETOTELLURIC AND GRAVITY DATA: PART 1: SOFTWARE INTERFACE AND GRAVITY INVERSION	145
10.4 A NEW MAGNETOTELLURIC 3D MODELING ALGORITHM: COMPARISON BASED ON DIFFERENT DIRECT AND ITERATIVE SOLVER PERFORMANCES.....	146
10.5 SEISMIC VELOCITY INVERSION BY IMPROVED INVERSIONNET DEEP MODEL: NOISY AND NOISELESS TRAINING DATA SETS	151
P.1 ELECTRIC FIELD MEASUREMENT IN POOR GROUNDING CONDITIONS.....	152
P.2 AIRBORNE MAGNETIC INVESTIGATION FOR DETECTION OF EXPLODED AND UNEXPLODED ORDNANCE USING UAV SYSTEMS IN A FORMER MILITARY AREA	153
P.3 THE MAGNETOTELLURIC METHOD IN GEOTHERMAL EXPLORATION: CASE STUDIES	160
Sponsors & Exhibitors & Supporters	161

Welcome

On behalf of the Organizing Committee, it is a pleasure and a great honor for us to welcome you to **Eurasia Geoscience Congress and Exhibition 2023 (EGCE2023)**.

Ankara University organizes this event with support of King Fahd University of Petroleum and Minerals (KFUPM). The congress is also supported by national universities (ÇOMU, Kocaeli, KTÜ, Afyon Kocatepe, Süleyman Demirel...). Leading supporters are the Chamber of Geophysical Engineers of Turkey and the Turkish Oil Company (TPAO). Without their support, we cannot make this congress. I would like to thank all of them.

In this event, we have 57 oral and 2 poster presentations on various topics. The topics about the geological and geophysical investigation of the deep earth, Oil and Gas Exploration to CO2 monitoring, Mining Geophysics to Mining Geology, Geothermal Exploration to Site Investigation will undoubtedly attract geoscientists, engineers, representatives of oil, energy and mining companies, researchers and students from many different countries. We have participants not only from Türkiye, but also from Saudi Arabia, the USA, Iraq, China, Canada, and Iran.

We have a diamond sponsor (Phoenix/Tezcür), Gold Sponsors (FNC and TPIC), and 5 exhibitor companies. We also thank sponsors and exhibitors. We expect that you will all have an exciting and rewarding time attending talks, visiting the exhibition, and enjoying the Venue Hotel. For three days and during the congress, we will be together, and we can discuss new potential collaboration and joint Projects in different applications.

We would like to express our appreciation and congratulations to all those involved in organizing the EGCE2023.

Prof. Dr. M. Emin CANDANSAYAR & Prof. Dr. Pantelis SOUPIO
Congress Chairman Technical Program Chairman

Abstract Statistics

	Number of Abstracts	Number of International Abstracts	Number of Abstracts from Turkey
Oral	54	28	26
Poster	3	2	1
Total	57	30	27

Participating Countries (in Alphabetic order): Canada, China, Germany, Greece, Ireland, Norway, Russia, Saudi Arabia, Türkiye, USA

Country	Canada	China	Germany	Greece	Ireland	Norway	Russia	Saudi Arabia	Türkiye	USA
Number of Abstracts	3	2	2	2	1	1	4	11	27	4

Note that three abstracts, two from Türkiye (ID: 6.5 and 6.6) and one from Iraq (ID 4.1) is not presented in the congress. Therefore they are removed from the “Abstract Book”.

Organizing Committee

Prof. Dr. M. Emin Candansayar	Ankara University, Turkey	Congress Chairman
Prof. Dr. Pantelis Soupios	King Fahd University of Petroleum and Minerals, Saudi Arabia	Technical Program Chairman
Cansu Arıcan	Ankara University	General Secretary
Demet Över	Ankara University	Responsible for Exhibition

Conveners/ Scientific Committee

(according to the topic number in alphabetic order)

Topic No	Name SURNAME	Title	University, Department	Country
1	Bülent KAYPAK	Prof. Dr.	Ankara Univ., Geophysical Eng.Dept.	Türkiye
1	Veysel Işık	Prof. Dr.	Ankara Univ., Geological Eng.Dept.	Türkiye
1	Bülent TANK	Prof.Dr.	Boğaziçi Univ.	Türkiye
1	Erhan ERDOĞAN	Dr.	Phoenix Geophysics Limited	Canada
1	Naser MEQBEL	Dr.	3D Consulting Geo.	Germany
1	Özlem HACIOĞLU	Dr.	Karadeniz Technical Univ., Geophysical Eng. Dept	Türkiye
2	Emin U. ULUGERGERLİ	Prof.Dr.	Çanakkale Onsekiz Mart Univ., Geophysical Eng. Dept.	Türkiye
2	Ertan PEKŞEN	Assoc.Prof.	Kocaeli Univ., Geophysical Eng. Dept.	Türkiye
3	Selma KADIOĞLU	Prof.Dr.	Ankara Univ., Geophysical Eng.Dept.	Türkiye
3	N. Yıldırım GÜNDOĞDU	Dr.	Ankara Univ., Geophysical Eng.Dept.	Türkiye
4	Khalid RAMADAN	Prof. Dr.	King Fahd University of Petroleum and Minerals, Dept. of Geoscience	Saudi Arabia
4	John D. HUMPHREY	Assoc. Prof.	King Fahd University of Petroleum and Minerals, Dept. of Geoscience	Saudi Arabia
5	Ammar ELHUSSEINY	Assoc. Prof.	King Fahd University of Petroleum and Minerals, Dept. of Geoscience	Saudi Arabia

5	SanLinn KAKA	Assoc. Prof.	King Fahd University of Petroleum and Minerals, Dept. of Geoscience	Saudi Arabia
6	Kurt STRACK	Dr.and CEO	KMS Tech.Inc.	USA
6	Pantelis SOUPIO	Prof. Dr.	King Fahd University of Petroleum and Minerals, Dept. of Geoscience	Saudi Arabia
7	M. Emin CANDANSAYAR	Prof. Dr.	Ankara Univ., Geophysical Eng.Dept.	Türkiye
7	Shunguo WANG	Dr.	Norwegian University of Science and Technology	Norway
7	Ahmet YILDIZ	Prof. Dr.	Afyon Kocatepe Univ.	Türkiye
7	Özcan ÖZYILDIRIM	Dr.	Afyon Kocatepe Univ.	Türkiye
8	Husam Musa Mahmoud BAALOUSHA	Assoc. Prof.	King Fahd University of Petroleum and Minerals, Dept. of Geoscience	Saudi Arabia
8	Bassam TAWABINI	Assoc. Prof.	King Fahd University of Petroleum and Minerals, Dept. of Geoscience	Saudi Arabia
9	İrfan AKCA	Assoc.Prof.	Ankara Univ., Geophysical Eng.Dept	Türkiye
9	Alexandros STAMPOLIDIS	Dr.	Aristotle University of Thessaloniki, Dept. of Geology	Greece
10	Çağlayan Balkaya	Prof. Dr.	Süleyman Demirel Univ., Geophysical Eng. Dept.	Türkiye
10	İsmail Demirci	Dr.	Ankara Univ., Geophysical Eng.Dept.	Türkiye
11	Theis SOLLING	Prof. Dr.	King Fahd University of Petroleum and Minerals, Dept. of Geoscience	Saudi Arabia

Thanks to...

We would like to thank our Scientific Committee for their valuable assistance in preparing the technical program of EGCE2023.

Topics

1- Geophysics and Geology Studies for deep Earth investigations

- 1.1. Seismology, Seismic Imaging, Crustal Fluids & Seismic Activity,
- 1.2. Tectonics, Geochemistry
- 1.3. Magnetotelluric, Gravity, and Magnetic, Heat Flow studies

2- Site Investigation with Geophysics and Geology Studies

- 2.1 Engineering Seismology /Seismic Methods (Refraction, MASW, REMI, Microtremor)
- 2.2 Electric and EM Methods (DC Resistivity, IP, GPR, Controlled Source EM)
- 2.3 Geotechnical, SPT, CPT Test

3- Geophysical Methods and other Non-Destructive Studies of Buildings before and After Earthquake

- 3.4. Earthquake Engineering
- 3.5. How to design an earthquake-resistant structure?
- 3.6. Micro-seismic, Structural GPR, and Micro DC Resistivity
- 3.7. Civil engineering in non-destructive structure investigation

4- Petroleum Geology

- 4.1. Sedimentology and impact of diagenesis on reservoir quality
- 4.2. Applications of carbonate diagenesis to petroleum reservoir characterization
- 4.3. Sedimentology and stratigraphy of carbonate sediments and rocks

5- Geological and geophysical investigations for Oil and Gas Exploration and development

- 5.1. Onshore and offshore geophysics (active/ passive seismic and non-seismic)
- 5.2. Seismic Reflection, Full Waveform Inversion
- 5.3. Integration of geophysics and geological data in E & P
- 5.4. Geological, geophysical, and petrophysical evaluation and monitoring of conventional and unconventional reservoir rocks
- 5.5. Application of AIs in oil and gas E & P

6- Geophysics contribution to the Energy transition (Geothermal, CO₂, wind, solar, minerals)

- 6.1. Geothermal
- 6.2. CO₂ monitoring
- 6.3. Special mineral exploration

7- Mining Geology and Mining Geophysical Studies, Geothermal Exploration

- 7.1. Airborne Geophysics
- 7.2. IP/DC
- 7.3. Drone/Airborne Geophysics
- 7.4. Geothermal Exploration

8- Hydrogeology and Hydrogeophysics Studies

- 8.1. Groundwater modeling and monitoring
- 8.2. Aquifer storage and recovery (ASR)
- 8.3. Groundwater pollution assessment and control
- 8.4. Sustainable use of natural resources (water, minerals, energy, etc.)

9- Archaeometry, Archaeogeophysics and Archaeogeology

10- Modeling, Inversion and Optimization in Geoscience

- 10.1. Inversion and Joint inversion of different geophysical data sets
- 10.2. Global optimization and Deep Learning Algorithm in Geoscience

11- Exhibitor Session

Congress Overview

Overview		
Date	Time	Event Name
10 November 2023 Friday	17:00-18:00	Icebreaker and Congress Photo LOCATION: Amphitheater in front of the swimming pool NOTE: Please take your drinks from the bar with you.
11 November 2023 Saturday	9:00-9:20	Opening Ceremony
	9:20-9:40	Exhibitor Session: Exhibition Companies Short (3 minutes) Presentations Opening Exhibition
	10:30-12:30	Technical Program and Exhibition
	12:30-13:30	Lunch Time
	13:30-17:30	Technical Program and Exhibition
12 November 2023 Sunday	08:40-12:30	Technical Program and Exhibition
	12:30-13:30	Lunch Time
	13:30-17:30	Technical Program and Exhibition
	13:30- 17:00	Course
13 November 2023 Monday	9:00-12:00	Check out and safe back to home
Note: Registration desk will be open everyday between 9:00-18:00		

Technical Program (POSTER)

Sunday - 12 November 2023 - Morning Sessions		
Time	ID	POSTER PROGRAM
10:30	P1	Electric field measurement in poor grounding conditions NIKITA ZORIN (STC NORD-WEST), DMITRII EPISHKIN (STC NORD-WEST), ANDREY YAKOVLEV (MOSCOW STATE UNIVERSITY), DENIS YAKOVLEV (NORD-WEST)
10:40	P2	Airborne Magnetic Investigation For Detection of Exploded and Unexploded Ordnance Using UAV Systems in a Former Military Area COSKUN ERTUGRUL (SAGTECH GEOPHYSICS)
11:00	P3	The magnetotelluric method in geothermal exploration: case studies N. PALSHIN (SHIRSHOV INST.OF OCEANOLOGY RAS), D. EPISHKIN (STC NORD-WEST), A.YAKOVLEV (MOSCOW STATE UNIV.), D. YAKOVLEV (NORD-WEST), NIKITA ZORIN (STC NORD-WEST)

Technical Program (ORAL SESSIONS)

Saturday - 11 November 2023 (MORNING SESSIONS)		
Time	ID	ORAL SESSION HALL A
09:00		OPENING CEREMONY
09:20		Exhibition Session: Exhibition Companies Short (3 minutes) Presentation
10:00		Exhibition Opening - (Exhibition Area)
10:00-10:30		Tea/Coffee Break
SESSION 6: Geophysics contribution to the Energy transition (Geothermal, CO ₂ , wind , solar, minerals)		
		Conveners: Kurt M. STRUCK, Pantelis SOUPIO
10:30	6.1	AI-Based Integration of Geoscience and other Data for Carbon Sequestration and Enhanced Oil Recovery Fred AMINZADEH (Energy Transition International)
10:50	6.2	Using Electromagnetic Fluid Imaging During the Energy Transition Kurt M STRACK (KMS TECHNOLOGIES), C. BARAJAS-OLALDE (EERC UNIV. NORTH DAKOTA), P. SOUPIO (KFUPM)
11:10	6.3	How important is multiphysics for electromagnetic imaging Kurt M. STRUCK (KMS TECHNOLOGIES)
11:30	6.4	Volcanic Massive Sulfide (VMS) Ore Deposit in Western Saudi Arabia: A Geophysical Study A. KHOGALI (KFUPM), K. CHAVANIDIS (KFUPM), A. STAMPOLIDIS (ARISTOTLE UNIV. OF THESSALONIKI), R. COLES (GOLDS AND MINERALS COMPANY LTD.), S. HANAFY ((KFUPM), Pantelis SOUPIO (KFUPM)
11:50	6.5	GeoCluster-ExpertNet: A Proposed Model Integrating Unsupervised Learning with Expert for Optimal Geothermal Drilling Orkun TEKE (Manisa Celal Bayar Univ.) NOT PRESENTED /Removed from Abstract book
12:30-13:30		LUNCH
Saturday - 11 November 2023 (AFTERNOON SESSIONS)		
Time	ID	ORAL SESSION HALL A
SESSION 5: Geological and geophysical investigations for Oil and Gas Exploration and development		
		Conveners: Sanlın I. KAKA, Can ÖREN
13:30	5.1	ONLINE: Leveraging Generative Adversarial Networks (GANs) to Enhance Well Logging Data Interpretation for Sustainable Near-Field Exploration Abdulrahman AL-FAKIH (KFUPM), S.I. KAKA (KFUPM), A. KOESHİDAYATULLAH (KFUPM)
13:50	5.2	ONLINE: Potential use of Sonic data for rock typing and geosteering in bioturbated carbonate strata Ammar EL-HUSSEİNY (KFUPM), H. ELTOM (KFUPM)
14:10	5.3	Challenges In Microseismic Technology for Reservoir Characterization and Monitoring: A Brief Review. Sanlın I. KAKA (KFUPM)
14:30	5.4	Elastic reverse time migration for imaging through gas clouds Can ÖREN (TPAO), Saygın İLERİ (TPAO)
14:50	5.5	AVA analysis of multi-component seismic wave modes (P-Sv, Sv-P) Saygın İLERİ (TPAO)
15:10-15:30		Tea/Coffee Break
SESSION 5: Geological and geophysical investigations for Oil and Gas Exploration and development		
		Conveners: Sanlın I. KAKA, Saygın İLERİ
15:30	5.6	Gas-Water detection technology and application of LOTEM combined with well logging and seismic data Liangjun YAN (YANGTZE UNIVERSITY)
15:50	5.7	SIP Detection and Quantification of Iron Sulfide (FeS) Materials: A Pathway to Early Monitoring Panagiotis KİRMİZAKİS (KFUPM), A. EL-HUSSEİNY (KFUPM), M. MAHMOUD (KFUPM), P. SOUPIO (KFUPM)
16:10	5.8	Reconstruction of the 3D subsurface of the Al-Hassa Oasis, Eastern Saudi Arabia Abid KHOGALI (KFUPM), P. KİRMİZAKİS (KFUPM), K. CHAVANIDIS (KFUPM), A.L. ASHADI (KFUPM), A. STAMPOLIDIS (ARISTOTLE UNIV. OF THESSALONIKI), M. Emin CANDANSAYAR (ANKARA UNIVERSITY), PANTELIS SOUPIO (KFUPM)
16:30	5.9	Determination of Deep-seated Faults Using Gravity and Magnetic Methods: Preliminary Results From North Adıyaman, Southeastern Türkiye Bahar DİNÇER (TPAO), V. İŞİK (Ankara U.), R. SABER (Ankara U.), A. ÇAĞLAYAN (Ministry Of Environment, Urbanisation and Climate Change), R.N. BEKTAŞ (Ankara U.)
16:50	5.10	Determining the Structural Features of the Gulf of Antalya and Its offshore by using Gravity-Magnetic Methods Ahmet KİRMİZİTAS (TPAO), M.A.SÜNNETÇİOĞLU (TPAO)
NOTE: The speakers names are written in red colored font.		

Saturday - 11 November 2023 (MORNING SESSIONS)		
Time	ID	ORAL SESSION HALL B
09:00		
09:20		
10:00		
10:00-10:30		Tea/Coffee Break
SESSION 4: Petroleum Geology		
		Conveners: Imad GHAFOR, Mehmet HAZAR
10:30		
10:50	4.1	Stratigraphy From the Pungalla Section, Ashdagh Mountain, North Eastern Iraq Imad GHAFOR (UNIV. OF SULAIMANI) NOT PRESENTED /Removed from Abstract book
11:10	4.2	Exhibition Similarities and Disparities Upper Cretaceous Source Rocks from Southeastern Anatolia from Lithologic Content Perspective Mehmet HAZAR (TPAO), T. ISCIMEN (TPAO), Y. D. ERDAL (TPAO), S.G. KOSE (TPAO)
11:30	4.3	ONLINE: Characterization of an Unconventional Organic-Rich Carbonate Mudstone, Late Jurassic Of Saudi Arabia John HUMPHREY (KFUPM), Septriandi CHAN (KFUPM)
11:50	4.4	ONLINE: Understanding the origin of Quartz Cementation in Sandstones for Better Pre-Drill Reservoir Quality Prediction Khalid AL-RAMADAN (KFUPM)
12:30-13:30		LUNCH
Saturday - 11 November 2023 (AFTERNOON SESSIONS)		
Time	ID	ORAL SESSION HALL B
SESSION 2: Site Investigation with Geophysics and Geology Studies		
		Conveners: Emin U. ULUGERGERLİ, Ertan PEKŞEN and Bassam TAWABINI
13:30	3.1	Non-Destructive Geophysical Investigation of Support Structure Element By Using 3D Inversion of Direct Current Resistivity Data Cansu ARICAN (Ankara Univ.), M. E. CANDANSAYAR (Ankara Univ.), N. Y. GÜNDOĞDU (Ankara Univ.)
13:50	2.1	Geophysical Insights into the Tectonic Regime of the Chania Basin in the Aegean Region Panagiotis KIRMIZAKIS (KFUPM), U. DİKMEN (Ankara Univ.), Pantelis SOUPIO (KFUPM)
14:10	2.2	Seismic shielding of urban areas by using integrated geophysical methods Panagiotis KIRMIZAKIS (KFUPM), G. KRITIKAKIS (Technical Univ. of Crete), E. KOKKINO (Hellenic Mediterranean Univ.), N. THEODULIDIS (Inst. of Eng. Seismology and Earthquake Engineering), B. MARGARIS, N. PAPADOPOULOS (Inst. For Mediterranean Studies, Foundation for Research & Technology Hellas), M. STEIAKAKIS (Tech. Univ. Of Crete), U. DİKMEN (Ankara Univ.), M.-D. Mangriotis (Univ. of Southampton), A. SAVVAIDIS (Univ. of Texas), C. LOUPASAKIS (Nat. Univ. Of Athens), A. VAFIDIS (Tech. Univ. Of Crete), Pantelis SOUPIO (KFUPM)
14:30	2.3	Resistivity image of leakage from Çanakkale Old Open Waste Disposal Site Ebru Ş. ULUOCAK (Çanakkale Onsekiz Mart Univ.), Emin U. ULUGERGERLİ (Çanakkale Onsekiz Mart Univ.)
14:50	2.4	Investigation of the mineralogical-petrographical and geochemical properties of Darende (Malatya) region limestone Metin BAĞCI (Aydın Kocatepe Univ.)
15:10-15:30		Tea/Coffee Break
SESSION 10: Modeling, Inversion and Optimization in Geoscience		
		Conveners: Çağlayan BALKAYA, İsmail DEMİRCİ
15:30	10.1	Estimating the Electrical Anisotropy Coefficient, Strike Direction, and Dip Angle using Square Electrode Array Data with Generalized Regression Neural Networks Ertan PEKŞEN (Kocaeli Univ.), D. DURDAĞ (Kocaeli Univ.), E. GASIMOV (Kocaeli Univ.)
15:50	10.2	Constrained inversion of geophysical data without regularization parameter using Pareto-optimal swarm intelligence: Application to magnetotelluric problem Ersin BÜYÜK (TÜBİTAK-MAM)
16:10	10.3	A new Software for 3-Dimensional Inversion of Magnetotelluric and Gravity data: Part 1: Software Interface and Gravity Inversion Özcan ÖZYILDIRIM (Aydın Kocatepe Univ.)
16:30	10.4	A New Magnetotelluric 3D Modeling Algorithm: Comparison Based on Different Direct and Iterative Solver Performances İsmail DEMİRCİ (Ankara Univ.)
16:50	10.5	Seismic Velocity Inversion by Improved InversionNet Deep Model: Noisy and Noiseless Training Data sets Mojtaba NAJAFIKHATOUNABAD (Ankara U.), H. Y. KELEŞ (Hacettepe U.), S. KADIOĞLU (Ank.U.)
NOTE: The speakers names are written in red colored font.		

Sunday - 12 November 2023 -Morning Sessions		
Time	ID	ORAL SESSION - HALL A
SESSION 1: Geophysics and Geology Studies for deep Earth investigations		
		Chairpersons: Bülent KAYPAK, Veysel IŞIK
08:40	1.1	Northwestern Anatolia Lithospheric Resistivity Structure Revealed by 3D Inversion of Long Period Magnetotelluric Data: Comparison With Velocity Lithospheric Structure M. Emin CANDANSAYAR (Ankara Üniv.), İ. DEMİRCİ (Ankara Üniv.), N.Y. GÜNDOĞDU (Ankara Üniv.), H. YILMAZ (Sivas Cumhuriyet Univ.)
09:00	1.2	Identifying and Localizing of Seismogenic EM Anomalies from Data Observed by Permanent MT Stations Wenbao HU (Yangtze Univ.)
09:20	1.3	An Insight Into The East Anatolian Fault Zone And Surroundings Through Earthquake Tomography: The Relocation of February 6, 2023 Main and Aftershocks Using Past Seismic Activity Bülent KAYPAK (Ankara Üniv.), Begüm KOCA (Ankara Üniv.)
09:40	1.4	ONLINE (Invited Speaker): What actually Rotational Seismology Means to a Seismologist? Gizem İZGİ (University of Potsdam)
10:00	1.5	ONLINE (Invited Speaker): Evaluating the Performance of Rotational Sensors Across Different Source Types: Earthquakes, Explosions, and Vibroseis Sweeps Gizem İZGİ (University of Potsdam), Eva P.S. EIBL (University of Potsdam), Frank Krüger (University of Potsdam), Felix Bernauer (Ludwig-Maximilians Universität München)
10:20-10:50		Tea/Coffee Break
SESSION 6: Geophysics contribution to the Energy transition (Geothermal, CO ₂ , wind , solar, minerals)		
		Conveners: Duygu KIYAN and Burcu TURHAN
10:50	6.6	Investigation of the Relationship Between the Topography and the Fluid Circulation Depth on the Geothermal Systems of Central Anatolia Region Sultan BURHANUDDIN (Marmara Üniv.), Kamil ERKAN (Marmara Üniv.) NOT PRESENTED /Removed from Abstract book
11:10	6.7	3D Velocity structure and fluid flows inferred from the microseismic events in the geothermal field, Turkey Burcu TURHAN (TPAO) , T. BİLGİC (MİKROİSİMİK MÜH.DAN. LTD.ŞTİ.), Ü.S. SELEK (MİKROİSİMİK MÜH.DAN. LTD.ŞTİ.), K. BALCI (MASPO ENERGY SAN. ve TİC.A.Ş), A. YILDIRIM (MASPO ENERGY SAN. ve TİC.A.Ş), B. KAYPAK (ANKARA UNIV.)
11:30	6.8	Magnetotelluric system NORD D. EPİSHKIN (STC NORD-WEST), A. Yakovlev (Lomonosov Moscow State Univ.) and N. Zorin (STC Nord-West)
11:50	6.9	DIG: A Research Project to Assess Ireland's Geothermal Energy Potential Duygu KIYAN (DUBLIN INSTITUTE FOR ADVANCED STUDIES)
12:10	6.10	Goelectrical Characterization of Geothermal Reservoirs – Case Studies from Gediz Geothermal Area (Türkiye) Özlem HACIOĞLU (Kardemir Teknik Üniv.), A.T. BAŞOKUR (LEMNİS Geoscience)
12:30-13:30		LUNCH
Sunday - 12 November 2023 - Afternoon Sessions		
Time	ID	ORAL SESSION - HALL A
SESSION 7: Mining Geology and Mining Geophysical Studies, Geothermal Exploration		
		Chairpersons: M. Emin CANDANSAYAR, Erhan ERDOĞAN
13:30	7.1	Phoenix New Generation MT/CSAMT Technologies with Real Time Data Transfer Capabilities Erhan ERDOĞAN (PHOENIX GEOPHYSICS Limited)
13:50	7.2	Joint application of electromagnetic prospecting methods for mineral exploration: case studies Anastasiya SOLOVYEVA (NORD-WEST), D.EPİSHKIN (STC NORD-WEST), V.KULIKOV (MOSCOW STATE UNIVERSITY), D. YAKOVLEV (NORD-WEST), N. ZORIN (STC NORD-WEST)
14:10	7.3	Real time Monitoring of the Natural Broadband EM Signals: Applications for monitoring the active volcanoes Erhan ERDOĞAN (PHOENIX GEOPHYSICS Limited)
14:30	7.4	Magnetotellurics in Deep Mining Operations: Case studies from North America Erhan ERDOĞAN (PHOENIX GEOPHYSICS Limited)
14:50		
15:10-15:30		Tea/Coffee Break
SESSION 7: Mining Geology and Mining Geophysical Studies, Geothermal Exploration		
		Chairpersons: Ahmet YILDIZ, Özcan ÖZYILDIRIM
15:30	7.5	KMS array system for CSEM/MT Kurt STRACK (KMS Technologies)
15:50	7.6	Lithium-The Important Resource of Green Technology: Properties, Geology and Turkey's Potential Ahmet YILDIZ (AFYON KOCATEPE UNIV.)
16:10	7.7	The Geochemistry of Clays Çavuşçuöl (Ilgın, Konya) Hakan FİDAN (Kütahya Dumlupınar Univ.), G.YANIK(Kütahya Dumlupınar Univ.), A.YILDIZ(Afyon Kocatepe Univ.),C.ÖZKUL(Kütahya Dumlupınar Univ.)
16:30	7.8	A large scale ERT survey for locating clay minerals Alexandros STAMPOLİDİS (Aristotle Univ. of Thessaloniki), P. LOUVARIS , E. AMANATİDOU, K. POLYDOROPOULOS, N. KORDATOS
16:50	7.9	ONLINE: Using Marine CSEM For Reservoir Monitoring Based on Petrophysical Modeling Mohammed ETTAYEBİ (Norwegian University of Science and Technology), Shunguo WANG (Norwegian University of Science and Technology), Martin LANDRØ (Norwegian University of Science and Technology)
NOTE: The speakers names are written in red colored font.		

Sunday - 12 November 2023 - Morning Sessions		
Time	ID	ORAL SESSION - HALL B
SESSION 9: Archaeometry, Archaeogeophysics and Archaeogeology SESSION 8: Hydrogeology and Hydrogeophysics Studies		
		Chairpersons: İrfan AKCA, Alexandros STAMPOLİDİS, N. Yıldırım GÜNDOĞDU
08:40	8.1	Comparing The Efficiency of Synthetic Vs Natural-Based Liquid Activated Carbon in Removing Organic Pollutants from Contaminated Water Bassam TAWABİNİ (KFUPM), T. SALEH (KFUPM), M. AL-RAYYAN (SAUDİ ARAMCO), R. NASSER (SAUDİ ARAMCO), P. SOUPIO (KFUPM), P. KİRMİZAKİS (KFUPM)
09:00	8.2	Resistivity Imaging of Aquifer Structure With 2D/3D Inversion of Direct Current Resistivity and Audio-Magnetotelluric Data N. Yıldırım GÜNDOĞDU (ANKARA UNIV.), M. Emin CANDANSAYAR (ANKARA UNIV.)
09:20	9.2	Geophysical and remote sensing surveys at the archaeological site of Philippi, N. Greece Alexandros STAMPOLİDİS (ARİSTOTLE UNIVERSITY OF THESSALONİKİ), A. KARAMİTROU (UNIVERSITY OF SOUTHAMPTON), G. TSOKAS (ARİSTOTLE UNIVERSITY OF THESSALONİKİ)
09:40	9.3	Imaging Archaeological Ruins By GPR and ERT Surveys: The Case of Ancient Seleukeia Sidera In Pisidia Çağlayan BALKAYA (Süleyman Demirel Univ.), O. ÇAKMAK (Süleyman Demirel Univ.), H.E. TÛTÛNSATAR (Isparta Univ.)
10:00	9.4	Water-Borne Archaeogeophysical Investigations at Lake İznik İrfan AKCA (Ankara Univ.), Mustafa ŞAHİN (Uludağ Univ.)
10:20-10:50	ID	Tea/Coffee Break
SESSION 1: Geophysics and Geology Studies for deep Earth investigations		
		Conveners: Veyisel İŞİK, Rıza SABER
10:50	1.6	Analysis of Surface Rupture Patterns and Fault Offset Variability Associated with the 06 February 2023 Pazarcık (Kahramanmaraş) Earthquake (Mw 7.7) In Islahiye Area, Türkiye Ayşe ÇAĞLAYAN (Ministry Of Environment, Urbanisation and Climate Change), V. İŞİK (Ankara Univ.),R. SABER (Ankara Univ.), H. ÜNAL (GEOMEK Mühendislik) F. CHİTEA (Bucharest University)
11:10	1.7	Evaluation of Relative Tectonic Activity in The Eastern Part Of Khazar Fault Zone, North Iran Marjan TOURANİ (Ankara Univ.), R. SABER (Ankara Univ.), V. İŞİK (Ankara Univ.), A. ÇAĞLAYAN (Ministry Of Environment, Urbanisation And Climate Change), Fiorina CHİTEA (Bucharest University)
11:30	1.8	Probabilistic Earthquake Risk Analyses In The Region Of Sındırgı – Sinanpaşa Fault Zone, Türkiye Ayca GÜNAY (Ankara Univ.), A. ÇAĞLAYAN (Ministry Of Environment, Urbanization And Climate Change), R. SABER (Ankara Univ.), V. İŞİK (Ankara Univ.),
11:50	1.9	Morphotectonic Characteristics And Paleoseismological Analysis of Aras Fault Zone (Nw Iran); Preliminary Results From Remote Sensing and Field Studies Rıza SABER (Ankara Univ.), V. İŞİK (Ankara Univ.), A. ÇAĞLAYAN (Ministry Of Environment, Urbanisation And Climate Change), F. CHİTEA (Bucharest University)
12:10		
12:30-13:30		LUNCH
Sunday - 12 November 2023 - Afternoon Sessions		
Time	ID	ORAL SESSION - HALL B
		Course Title: Artificial Intelligence AI and Data Analytics DA For Energy Exploration and Production Lectuter: Fred Aminzadeh
13:30		
13:50		
14:10		
14:30		
14:50		
15:10-15:30		Tea/Coffee Break
		Course Title: Artificial Intelligence AI and Data Analytics DA For Energy Exploration and Production Lectuter: Fred Aminzadeh
15:30		
15:50		
16:10		
16:30		
16:50		
NOTE: The speakers names are written in red colored font.		

ABSTRACTS and EXTENDED ABSTRACTS (FULL PAPER)

Please note that the organizing committee is not responsible for any misprinting of the abstract published in this book. All responsibility ar belongs to the corresponding authors.

1.1 NORTHWESTERN ANATOLIA LITHOSPHERIC RESISTIVITY STRUCTURE REVEALED BY 3D INVERSION OF LONG PERIOD MAGNETOTELLURIC DATA: COMPARISON WITH VELOCITY LITHOSPHERIC STRUCTURE

M. Emin Candansayar^{1*}, İsmail Demirci¹, N.Yıldırım Gündoğdu¹, Hüseyin Yılmaz²

¹Ankara University, Engineering Faculty, Geophysical Eng. Dept., Geophysical Modeling Group, 06830, Golbasi, Ankara, TURKIYE

²Sivas Cumhuriyet University, Engineering Faculty, Geophysical Eng. Dept., Sivas, TURKIYE

*Corresponding e-mail: candansayar@ankara.edu.tr

ABSTRACT

In this study, we revealed lithospheric resistivity structure of northwestern Anatolia by using 3D inversion of Magnetotelluric (MT) data. The survey area is approximately 300kmx200km in size, located between N38°30' - N41°05' latitudes and D29°30' - D32°00' longitudes in Northwestern Anatolia. We collected broadband MT data on 358 stations and long period magnetotelluric (LMT) data on the 64 stations along 4 parallel lines in the survey area. The broadband data collected between 2007-2011 under the TUBITAK project, numbered 105G145. The LMT data collected under our another TUBITAK project, numbered 119Y197 between the years, 2020-2022. The MT lines are crossing main tectonic traverses such as North Anatolia Fault Zones, Intra-Pontid Suture zones. After the time series analysis and main data processing procedure such as phase tensor decomposition and static shift correction, we combined broadband and LMT data for each line and interpreted by using two dimensional inversion algorithm. The 2D inversion results showed us the main tectonic units. We also inverted combined set of MT ve LMT data by using three dimensional inversion algorithm. The three dimensional resistivity model also showed us to main tectonic units as two dimensional resistivity models. Additionally, crust and lithosphere relations also revealed. We obtained upper and lower crust boundary by using magnetic data and crust depth by using gravity data. Those results are also validated our resistivity models obtained from MT data inversion. We also revealed lithosphere asthenosphere boundary from the 3D resistivity model. We compared resistivity lithospheric structure obtained in this study and velocity lithospheric structure that already obtained by the other researcher studies. The both lithospheric structures are supports each other.

KEYWORDS: Northwestern Anatolia, Lithosphere, Magnetotelluric, 3D, Inversion

INTRODUCTION

The magnetotelluric (MT) method is widely used to investigate the structure of the lithosphere. There are many studies conducted in the last 15 years on the investigation of the upper crust-lower crust boundary and tectonic structures, suture zones and fault zones within the crust with MT (e.g. Becken et al. 2008, Bertrand et al. 2012; Zeng et al., 2015). Many international projects

have been carried out in the last 20 years to investigate the relationship between the lithosphere and the crust within it using the magnetotelluric method (e.g. Wei vd. 2001; Unsworth 2010; Xie 2016).

There are many studies investigating the main tectonic zones, fault zones and crustal structure in Western Anatolia (e.g. Gürer and Bayrak 2007; Ulugergerli et al. 2007; Kaya 2010). Studies on investigating the upper crust-lower crust relationship, suture zones and fault zones in Northwest Anatolia were carried out within the scope of our previous TÜBİTAK project (Candansayar et al. 2009, 2010, 2012; Kaya 2010). So far, a resistivity lithosphere model has not been obtained with the MT method in Western Anatolia. The aim of this study is to investigate upper-lower crust relation, Moho depth and resistivity lithospheric structure of the survey area. Within the scope of the study, broadband and long-term MT (MT and LMT) data were measured in approximately 200 by 300 km area between approximately 38°-41° latitudes and 29°-31° longitudes in Northwest Anatolia.

METHOD and APPLICATION

MT is natural (or passive) source geophysical electromagnetic method. It is mainly used for investigating deep resistivity structure. In this method, in each station vertical electric fields (E_x and E_y) and vertical and horizontal magnetic fields (H_x , H_y and H_z) is measured as a function of time. This data transferred to frequency domain by using fast Fourier transform and in frequency domain impedance and tipper tensor data is obtained.

In this study, we used MT and LMT data collected on 358 and 64 stations, respectively. (Figure 1). LMT data are collected new generation Phoenix MTU-5C receiver. This receiver has network card that enable us to transfer time series data via GSM operator during measurement. Therefore, we can make quality control of MT data during measurement. There are approximately 12 years slots between MT and LMT data measurements. However, when we compare MT and LMT data that collected approximately on the same station locations, we can see that the data obtained for the same periods are mostly fit the each other (Figure 2).

We first did phase tensor analysis (Caldwell et al. 2004) before 2D and 3D inversion. There is no constant shift effect in the phase tensor data, and in recent years, $\beta(^{\circ})$, obtained from the phase tensor and known as the "phase tensor skew angle", is used instead of "skew" in dimensionality analysis (Patro et al. 2014; Xue et al. 2021; Kirkby et al. 2020; Zhao et al. 2022). As $\beta(^{\circ})$ moves away from zero degrees, the medium becomes three-dimensional. As a result of phase tensor analysis, $\beta(^{\circ})$ values obtained at all stations and periods in a direction were drawn as a cross section. As an example, we present $\beta(^{\circ})$ section for Profile 1. When looking at beta sections, the beta angle is around zero degrees in low periods (shallow sections), while this angle value is significantly away from zero degrees in high periods (deep). It is seen that the beta angle is scattered in some regional areas. Therefore, it seems that a meaningful model cannot be found with 2D inversion of very deep structures. After MT data analysis, we did 2D and 3D inversion of MT and LMT data.

DISCUSSION and RESULTS

We combined MT and LMT data sets for each line. We did 2D inversion of all lines data. As an representative, we showed 2D inversion result of Line 1 (Figure 4). We also did 3D inversion of MT and LMT data collected from all stations along four lines. Xz-section obtained from 3D inversion result showed in Figure 5. We interpreted the upper and lower crust boundary and crust and upper mantle boundary (Moho discontinuity) from 2D and 3D resistivity model. We also obtained solid lithosphere and asthenosphere boundary from 3D MT inversion result. We compared our result with Gravity, Magnetic and passive seismic tomography result.

CONCLUSION

Within the scope of the study, a 3D resistivity model of the region up to a depth of 200 km was obtained by 3D inversion of MT and LMT data. As a result of the interpretation of the 3D resistivity model, it was found that the upper crust and lower crust boundary varies between 8-23km in the region. Moho depth was found to vary between 28-51 km. The boundary between lithosphere and asthenosphere was found between depths of 80-120 km. All these borders deepen from south to north. The results obtained are supported by previously conducted Seismology, Gravity and Magnetic studies.

REFERENCES

- Becken, M., Ritter, O., Park, S. K., Bedrosian, P. A., Weckmann, U., & Weber, M. 2008. "A deep crustal fluid channel into the San Andreas Fault system near Parkfield, California". *Geophysical Journal International*, 173(2), 718-732.
- Bertrand, E., Unsworth, M., Chiang, C. W., Chen, C. S., Chen, C. C., Wu, F., ... & Hill, G. 2009. "Magnetotelluric evidence for thick-skinned tectonics in central Taiwan". *Geology*, 37(8), 711-714.
- Candansayar M.E., Kaya C., Güler A., v.d., 2008. "NW_Anatolia_CSGM Project: an investigation of N-W Anatolian Crust Structure by using Geophysical Methods". IAGA WG 1.2 on Electromagnetic Induction in the Earth, Beijing, China, October 23- October 29, 2008
- Candansayar, M.E. vd. 2012. "Deep Crustal Structure of Thrace Region Revealed by 2D Inversion of Magnetotelluric Data". Extended Abstract, 21st EM Induction Workshop, Darwin, Australia, July 25-31, 2012
- Candansayar M. E., C.Kaya, Ü.Dikmen v.d. 2010 "Crustal structure of Northwestern Turkey, revealed by magnetotelluric surveys with the help of Seismology, Gravity and Magnetic Data". IAGA WG 1.2 on Electromagnetic Induction in the Earth 20th Workshop Abstract, Giza, Egypt , September 18-24, 2010
- Candansayar M. E., C.Kaya, Ü.Dikmen v.d. 2010 "Crustal structure of Northwestern Turkey, revealed by magnetotelluric surveys with the help of Seismology, Gravity and Magnetic Data". IAGA WG 1.2 on Electromagnetic Induction in the Earth 20th Workshop Abstract, Giza, Egypt , September 18-24, 2010
- Caldwell, T. Grant, Hugh M. Bibby, and Colin Brown. "The magnetotelluric phase tensor." *Geophysical Journal International* 158.2 (2004): 457-469
- Güler, A., & Bayrak, M. (2007). Relation between electrical resistivity and earthquake generation in the crust of West Anatolia, Turkey. *Tectonophysics*, 445(1-2), 49-65.
- Kaya, C. (2010). Deep crustal structure of northwestern part of Turkey. *Tectonophysics*, 489(1), 227-239.
- Wei, W., Unsworth, M., Jones, A., Booker, J., Tan, H., Nelson, D., ... & Jin, S. (2001). Detection of widespread fluids in the Tibetan crust by magnetotelluric studies. *Science*, 292(5517), 716-719.
- Unsworth, M. (2010). Magnetotelluric studies of active continent–continent collisions. *Surveys in Geophysics*, 31(2), 137-161.

Xie, C., Jin, S., Wei, W., Ye, G., Jing, J., Zhang, L., ... & Xia, R. (2016). Crustal electrical structures and deep processes of the eastern Lhasa terrane in the south Tibetan plateau as revealed by magnetotelluric data. *Tectonophysics*, 675, 168-180.

Zeng, S., Hu, X., Li, J., Xu, S., Fang, H., & Cai, J. (2015). Detection of the deep crustal structure of the Qiangtang terrane using magnetotelluric imaging. *Tectonophysics*, 661, 180-189.

ACKNOWLEDGEMENT

This study supported by TUBITAK (The Scientific and Technological Research Council of Turkey) Project with Grant Number 119Y197. We thanks TUBITAK for their support.

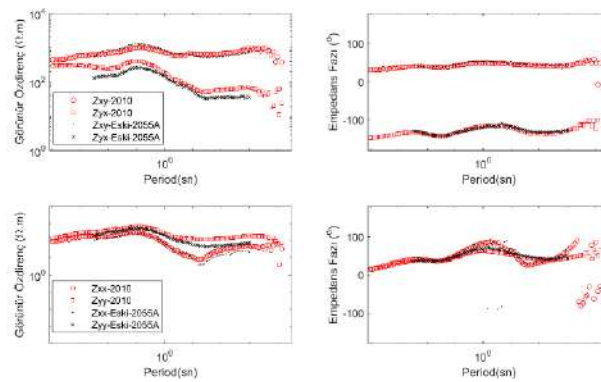


Figure 2. Comparison of the measured LMT data at station number 2010 with the MT data measured around this station 12 years ago. Apparent resistivity and Phase curves for Zxy, Zyx, Zxx and Zyy impedance components.

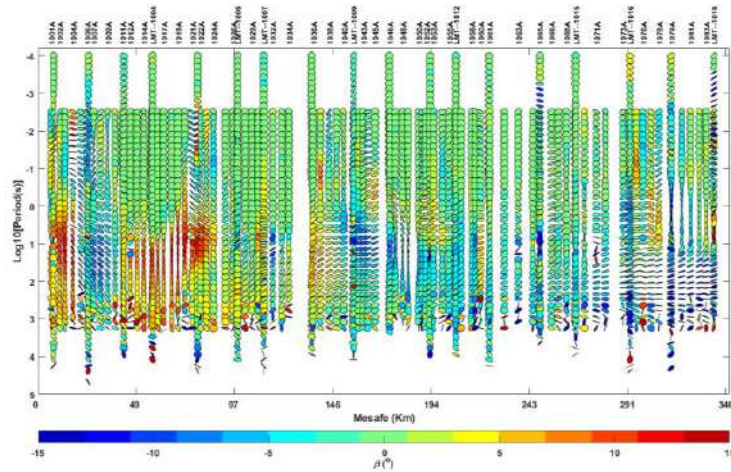


Figure 3. Line 1 $\beta(^{\circ})$ section. Here at LMT stations, the lowest period is 0.0001 and the highest period is usually over 10,000s. At MT stations, the lowest period is 0.03 sec. and the highest period is generally around 2000 s. Therefore, not all MT stations were added to the section to avoid overlapping of stations.

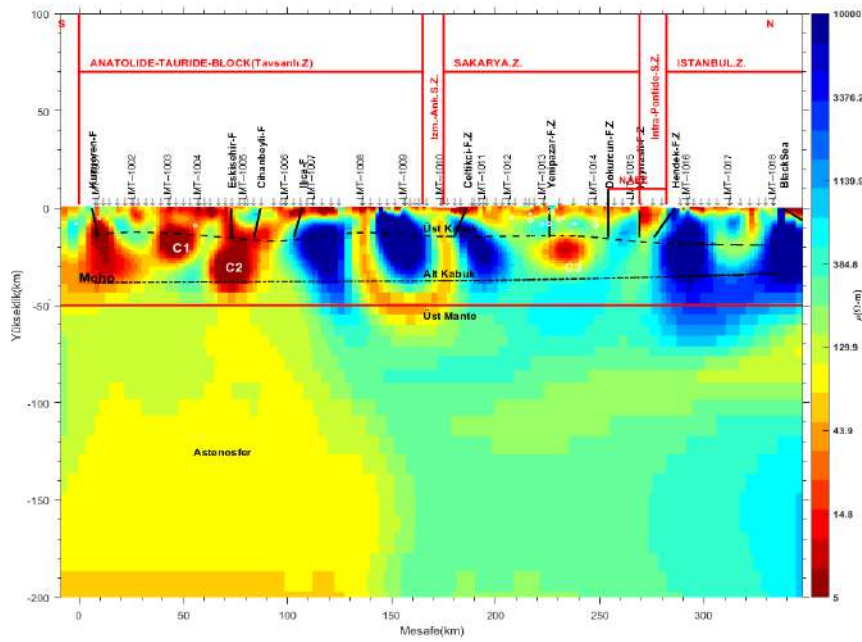


Figure 4. (a) Line-1 2D inversion result. The Curie point depth calculated from magnetic data is shown on the model with thick black lines, and the Moho depth obtained from gravity data is shown with black dotted lines. The red line shows the lower bound of the model obtained from the 2D inversion of MT data. The main tectonic zones are shown on the top of the resistivity model.

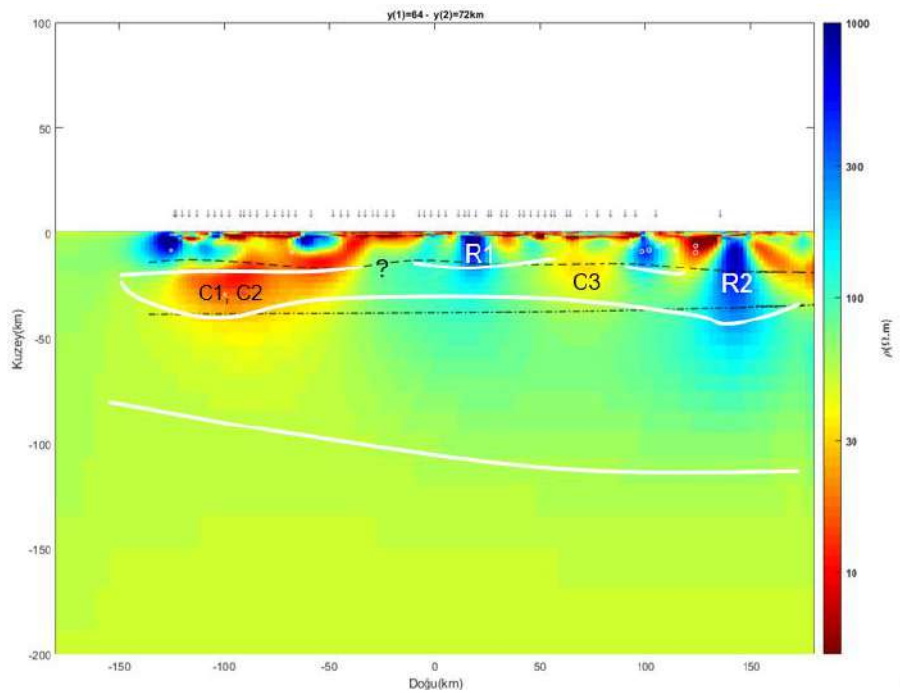


Figure 5. xz-section close to the Line-1 profile direction as a result of the 3D inversion. Solid white lines indicate the upper and lower crustal boundary, Moho depth, and lithosphere-asthenosphere boundary, respectively, from shallowest to deepest.

1.2 IDENTIFYING AND LOCALIZING OF SEISMOGENIC EM ANOMALIES FROM DATA OBSERVED BY PERMANENT MT STATIONS

W. Hu^{1*}, B. Han², X. Chen^{2,3}, Y. Fan^{2,4} and K. Hu⁵

1Professor, Key Laboratory of Exploration Technologies for Oil and Gas Resources of MOE, Yangtze University, Wuhan, China

2Researcher, State Key Laboratory of Earthquake Dynamics, Institute of Geology, Beijing, China

3Senior Researcher, National Institute of Natural Hazards, Ministry of Emergency Management, Beijing, China

4Researcher, China Earthquake Network Center, Beijing, China

5Research Assistant Professor, Department of Earth and Space Sciences, Southern University of Science and Technology, Shenzhen, China

**Corresponding author e-mail: hwb@yangtzeu.edu.cn*

ABSTRACT

The observed data from permanent magnetotelluric (MT) stations in the Southern segment of South-north Earthquake Belt of China have indicated potential seismogenic-induced electromagnetic disturbances. To simulate the seismogenic electromagnetic (SEM) anomaly, we combined the MT responses with responses from an arbitrarily oriented electric dipole underground. Synthetic results have shown that seismogenic EM radiation can produce recognizable apparent resistivity and phase anomaly in MT data for station, even far from the seismogenic zone. Long-term MT data obtained from Dali and Lijiang stations in Yunnan Province, China, were processed base on daily variation. We extracted the background (quietperiod) responses of these stations and identified two sections of data with SEM anomalies serving as precursors of two earthquake events (Yunlong & Yangbi). Selecting certain anomalous responses according to experimental criteria, we used them for inversion to determine the parameters of dipole location, including depth and orientation, and the spectrum of moment. The distribution of predicted dipoles are mostly located in or near the seismogenic area, and their azimuth generally exhibits good directivity toward the seismogenic fault, indicating the feasibility of this method in predicting the seismogenic zone. By analyzing the spatial distribution and time-varying characteristics of the inversion results of SEM anomalies in MT data, in conjunction with the geological and electrical structural characteristics of the predicted area and a comprehensive evaluation of seismic activity, it is expected to achieve imminent earthquake prediction.

KEYWORDS: Seismogenic EM anomaly, MT responses, dipole responses, identifying SEM, positioning SEM by inversion

INTRODUCTION

Both conventional seismic monitoring networks and permanent MT stations monitor variations of EM fields and underground electrical structures through continuous observation at fixed points. If a certain intensity of low-frequency electromagnetic radiation is generated during the

process of earthquake preparation, the electromagnetic fields recorded by MT station are the superposition of the induced fields generated by natural field source variations and the electromagnetic radiation fields of earthquake preparation underground.

The MT sounding method has the characteristics of the wide frequency band and multicomponent observation. Using MT data from permanent stations to identify and extract SEM anomaly have following advantages. (1) The ratio of the mutually orthogonal electric and magnetic field is used to obtain the electric impedance of the earth and then the apparent resistivity and impedance phase. Thus the influence of earth electromagnetic field variations can be automatically eliminated. (2) Reliable regional background resistivity information at different depths can be obtained from long-term observation by the network, which is convenient for identifying and extracting SEM anomalies. (3) The impedance anomaly of a MT station not only includes the change in the resistivity of the underlying earth media caused by stress change and fracture development in the adjacent areas but also includes the electromagnetic radiation generated by pressure changes on rock body.

IDENTIFYING SEM ANOMALIES

On May 18, 2016, an M5.0 magnitude earthquake occurred in Yunlong, Yunnan, with its epicenter located at 26.10°N and 99.53°E, and focal depth ranging from 3~17 km. On March 27, 2017, an M5.1 earthquake occurred in Yangbi, with its epicenter located at 25.89°N, 99.80°E, and at depth of approximately 12 km. Figure 1 shows the epicenter and aftershock zone (light red area) of these two earthquakes, as well as the relative positions of the Dali and Lijiang MT stations near the earthquake area. The Dali Station is approximately 82.93km from the Yunlong epicenter and 47.18 km from the Yangbi epicenter. Lijiang Station is about 127.88km away from the Yunlong epicenter and 143.12km from the Yangbi epicenter.

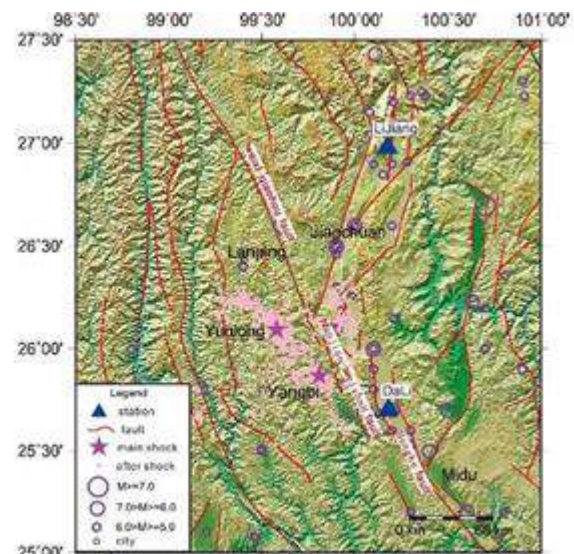


Fig. 1 The epicenters of the Yunlong and Yangbi earthquakes, and location of Dali and Lijiang station

During the quiet period, the signals observed by MT stations mainly come from the natural electromagnetic fields and induced fields in the earth near the station. The natural field source has the characteristics of a plane wave, while the earth's resistivity during the quiet period has characteristics of invariant in time. In this way, through long-term statistical averaging of station observed data, background field information with high SN ratio and high reliability can be obtained. Under the premise of excluding interference effects, responses deviated from the background field by a certain amplitude can be identified as responses containing SEM anomalies. Firstly, routine MT processing was performed on the daily observation data to obtain the apparent resistivity (ρ_{xy} , ρ_{yx}) and phase (ϕ_{xy} , ϕ_{yx}) responses of two polarization modes. Due to significant

differences in apparent resistivity and phase values between different stations, or for different frequencies and polarization modes for same station, the observed apparent resistivity and phase are normalized using the background values of the corresponding frequencies of each station to unify the criteria for identifying anomalies. In this way, when the ratio is greater than 1, it indicates an enhanced response, and when it is less than 1, it indicates a weakened response. At the same time, confidence intervals (or empirical thresholds) for different components are determined based on the characteristics of electromagnetic environmental interference sources at each station. The SEM anomaly identification is then carried out according to the time-varying curve of normalized response for each frequency. Due to the varying degrees of influence of natural source fluctuations and human interferences on MT responses at different frequencies, to choose frequency with relatively stable background is recommended for identifying anomaly.

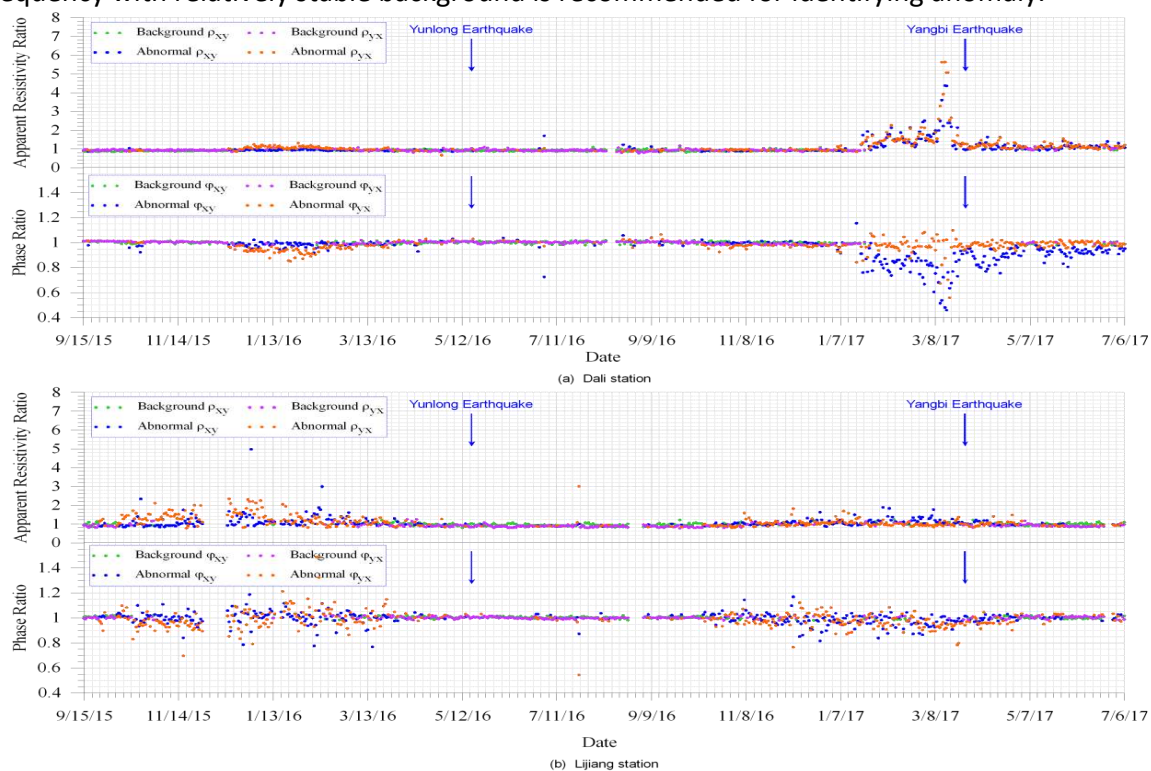


Fig. 2 Normalized apparent resistivity and phase of Dali and Lijiang Stn. for time period 9/15/2015~7/6/2017

Identifiable apparent resistivity and phase anomalies were observed at both Dali and Lijiang station before the Yunlong and Yangbi earthquake. Figure 2 shows the normalized timevarying curves of the apparent resistivity and phase at $f=74\text{Hz}$ for both stations. The green and blue data points in the plots represent the background and abnormal response of normalized ρ_{xy} and ρ_{yx} , respectively, while the purple and orange data points represent normalized background and abnormal ϕ_{yx} and ϕ_{xy} respectively. It can be seen from Fig. 2 that the identifying process has effectively achieved the classification of observed responses. The normalized background response obtained is close to 1 and has continuity, while the abnormal response is prominent. At the same time, the abnormal responses for these four parameters have good consistency. From the distribution of anomalous data points on the time-varying curve, it can be seen that the SEM anomalies begin to appear long before the earthquake, but not completely continuous.

Therefore, manual analysis and judgment need to be conducted based on the time-varying characteristics of long-term observation responses for each station.

SEM POSITIONING BY INVERSION

Combination of the MT background field and the anomalous radiation field in the ground can be used to simulate the observed MT response containing SEM disturbances, the objective function for inversion can then be established. The responses of arbitrarily oriented dipoles in n-layered earth are calculated by algorithm of Hu et al. (2023). The existed inversion algorithms can be applied to obtain the physical parameters of the earth and the parameters of the radiation source in the ground. The parameters of the dipole radiation source obtained through inversion include source moment, location (x-y coordinates and burial depth), and state (azimuth and inclination) parameters. The differential ant-stigmergy inversion algorithm (Liu et al., 2015) is adopted to invert parameters of multiple dipole sources using multi-station data since this algorithm is robust to initial model.

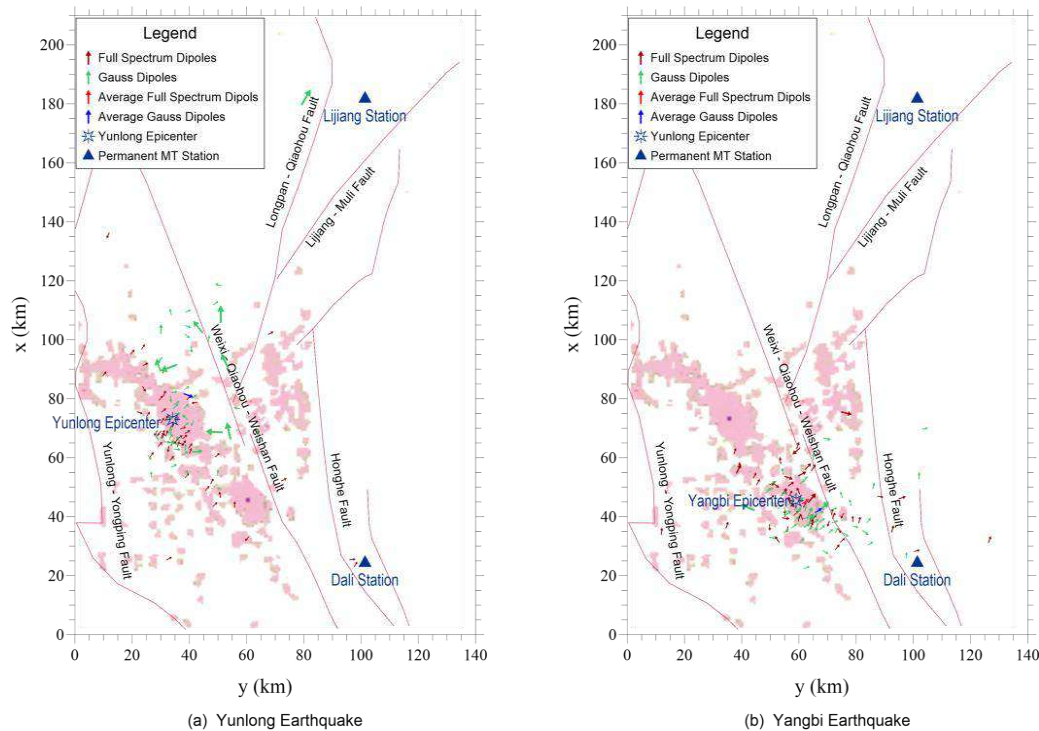


Fig.3 Location map of the underground dipoles predicted by inversion of the observed SEM anomalies of Dali and Lijiang station before the Yunlong and Yangbi earthquake

Figure 3 shows the distribution map of the underground dipole source obtained from inversion. The dark red arrow represents dipole of equal amplitude spectrum, and the green arrow represents the Gaussian dipole with high central frequency obtained from the inversion of daily anomalies. The direction of the arrow indicates the azimuth of the dipole, and its length is proportional to the dipole moment. Figure 3(a) shows the inversion results from the identified 51 abnormal daily data before the Yunlong earthquake. It can be seen that although the inversion

results are scattered, the overall predicted dipoles are located in or near the seismogenic zone. The predicted equal spectrum dipoles are mainly distributed in the seismogenic area near the epicenter at average depth of 15km, with little spatial scattering. The orientation of most dipoles is approximately perpendicular to the Weixi Qiaohou - Weishan fault near the epicenter. Predicted high-frequency dipoles are at shallower depth (~7km) and more scattered in spatial distribution, with a portion distributed on both sides of the Weixi Qiaohou - Weishan fault besides the area near the epicenter; several dipoles are located near the Dali station, which may be a reflection of the observed data being interfered by the nearby noise.

Figure 3(b) shows the distribution map of inverted dipoles from the selected 55 SEM anomalies observed before Yangbi earthquakes. The spatial dispersion of the predicted dipoles is not significant, and the amplitude difference of the source moments is also small. The predicted dipoles are mainly distributed in the seismogenic area near the epicenter near the Dali station, possibly due to the fact that the Yangbi epicenter is relatively close to the Dali station and the observed anomalies have relatively large amplitude at the Dali station. In addition, there are several predicted dipoles fall near the Dali station, which may be the result of observed data being interfered by noise near the station.

CONCLUSION

The SEM anomaly causes disturbance in the apparent resistivity and phase observed at MT stations. By averaging the responses observed during the quiet period as the background and simulating responses of electric dipoles as the anomalous field, we can obtain the total observed MT field containing SEM disturbances by stacking these responses in the form of complex components of EM field. The synthesized responses can be used to invert parameters of multiple SEM radiation sources underground, and to achieve positioning of the radiation source (or seismogenic center).

It's important to note that this study is still in its preliminary stages, with limited examples. However, the research results indicate that the feasibility of applying an underground dipole source to equivalently simulate SEM radiation, followed by the inversion and positioning of underground radiation sources. Based on the comprehensive evaluation of regional geology, geoelectric structural characteristics and seismic activity, it is expected to achieve the goal of using SEM anomalies for imminent earthquake prediction.

ACKNOWLEDGEMENT

The authors would like to express gratitude to the National Natural Science Foundation of China for supporting of project No. 41574064.

REFERENCES

- Hu, K.Y., Hu, W.B. and Huang, Q.H. (2023). Electromagnetic fields excited by arbitrarily oriented dipoles in horizontally layered earth. *Chinese Journal of Geophysics*, 66(8):3290-3301.
- Liu, J.T., Hu, W.B. and Hu, X.Y. (2015). Two-dimensional magnetotelluric inversion using differential anti-stigmery algorithm. *Oil Geophysical Prospecting*, 50(3):548-555.

1.3 AN INSIGHT INTO THE EAST ANATOLIAN FAULT ZONE AND SURROUNDINGS THROUGH EARTHQUAKE TOMOGRAPHY: THE RELOCATION OF FEBRUARY 6, 2023 MAIN AND AFTERSHOCKS USING PAST SEISMIC ACTIVITY

B. Kaypak^{1,2*} and B. Koca^{1,2}

¹Department of Geophysical Engineering, Ankara University, Ankara, Türkiye

²Earthquake Research and Application Center, Ankara University, Ankara, Türkiye

*Corresponding author e-mail: kaypak@eng.ankara.edu.tr

ABSTRACT

The North Anatolian Fault and the East Anatolian Fault Systems are two of the most significant fault zones in Turkey. Over thousands of years, they have witnessed substantial and destructive earthquakes. The most recent of these devastating earthquakes occurred on February 6, 2023, along the East Anatolian Fault System (EAFS) in a manner rarely observed. On February 6, 2023, two major earthquakes, with magnitudes of 7.8 and 7.6 Mw, respectively, occurred. Despite nine months having passed since these earthquakes, aftershocks are still ongoing, causing considerable destruction and loss of life. Since the first day, more than 40,000 earthquakes have occurred in the region in total. In order to shed light on the occurrence of these earthquakes, the region's 3D subsurface seismic velocity structure was determined using the local earthquake tomography method. A two-stage tomography study was conducted. In the first stage, earthquakes that occurred in the region from 1900 to February 6, 2023, were used, while in the second stage, earthquakes, including main shocks and aftershocks, from that date to the present were considered. This study focuses on the first stage's research and its results. Out of the approximately 37,000 earthquakes that occurred in the region before the Kahramanmaraş earthquakes, 1951 earthquakes were selected based on criteria such as the GAP and RMS values. Travel time data for 16,865 P-waves and 9,438 S-waves recorded at 29 stations were utilized. Initially, a 1-D velocity model with seven layers down to 50 km depth was established for the region, and subsequently, a 3-D tomographic velocity structure of the region was obtained by modeling in the lateral direction with 20x20 km grid points and in the vertical direction with 5 km node spacing. The distribution of low and high seismic velocity anomalies, Moho topography, magmatic intrusions, and similar structures were identified from the tomographic images, and attempts were made to determine their relationship with earthquakes. Additionally, using the 3-D velocity model obtained from tomographic inversion, the coordinates and depths of the Kahramanmaraş earthquakes with magnitudes of 7.8 and 7.6 that occurred on February 6, 2023, were calculated more precisely.

KEYWORDS : Tomography, earthquake, Kahramanmaraş, seismicity, relocation.

DATA and METHOD

To determine the 3-D deep seismic velocity structure of a region using the local earthquake tomography method, travel times of the P and S phases of earthquakes that have occurred in the same region are required. For this purpose, earthquakes that occurred within the period from 1900 to the first mainshock of the Kahramanmaraş earthquake on February 6, 2023, in the vicinity of the Eastern Anatolian Fault Zone (EAFZ) as shown in Figure 1 were utilized. Out of approximately 44,000 earthquakes, those with a GAP value less than 180° , an RMS value below 2 seconds, and at least 10 P-wave observations at various stations were used for calculations. All earthquake-related data were obtained from the ISC data portal. The data were collected solely from operational earthquake observation stations within the region. Despite the presence of various types of 82 stations belonging to AFAD and Kandilli Observatory Earthquake Research Institute from 1900 to the present in the region, data could only be acquired from 55 stations. The distribution of these stations is also depicted in Figure 1. Initially, the 1-D velocity structure of the region was determined using the VELEST (Kissling, 1988; Kissling vd., 1994; Kissling vd., 1995) algorithm. For this purpose, 1576 selected earthquakes were used based on specific criteria. In this stage, first the 1-D P-wave velocity structure was determined, and then, additional data with at least 5 S-wave readings to P-phase observations were incorporated to calculate the 1-D P&S wave velocity structure of the region. Finally, the obtained velocity model was also utilized as a reference velocity model for 3-D tomographic solutions. The SIMUL2000 (Thurber 1983, 1993; Eberhart-Phillips 1993; Thurber and Eberhart-Phillips, 1999) algorithm was employed for obtaining the 3-D tomographic velocity model of the region. Similar to the 1-D velocity model, the V_p velocity structure was initially determined, and then the V_p/V_s structure was computed. For these studies, only the P-wave observation count was reduced to eight, while the other criteria remained the same. Consequently, 1825 earthquakes were used in the inverse modeling processes. Given the extensive coverage of the region, horizontal grid points were set at 20x20 km spacing, and vertical spacing was set at 5 km intervals.

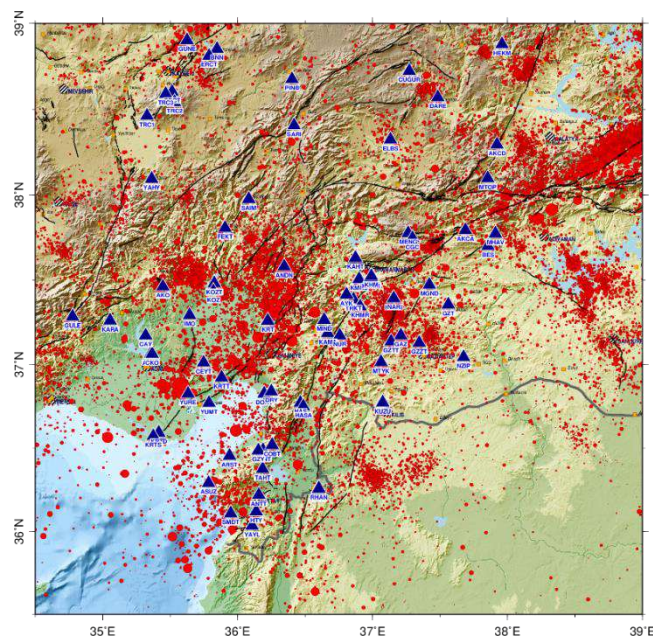


Figure1 The distribution of earthquakes (red dots) and stations (blue triangles) in the region.

RESULTS

This study has yielded the following results:

- 1-D P- and S-wave velocity structure of the region.
- 3-D Vp and Vp/Vs structure of the region.
- Relocation of earthquakes.
- Recalculation of the locations of Kahramanmaraş earthquakes and aftershocks.

The 1-D velocity structure of the region could be modeled down to a depth of approximately 50 km. It has been observed that up to this depth, the region consists of approximately seven layers (Figure 2). It was determined that there is a low-velocity layer ($V_p \sim 2.8$ km/s; $V_s \sim 0.7$ km/s) up to a depth of 5 km from the surface, and after this depth, there is a sudden increase in velocity. The Moho depth was estimated to be approximately 35-36 km from the 1-D crustal velocity model (Figure 2).

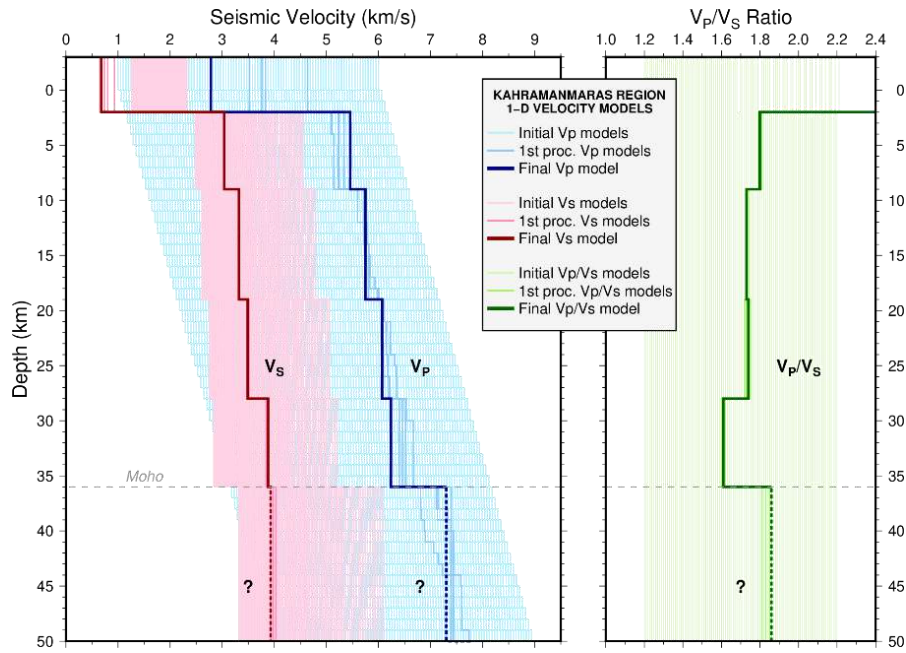


Figure2 1-D crustal velocity model for P- and S- wave in the region.

When examining the tomographic velocity models (V_p and V_p/V_s) obtained through 3-D inversion, it was observed that V_p values fall within the range of 2.7-8.8 km/s, and V_p/V_s ratios are between 1.4 and 2.0 down to a depth of approximately 50 km. In the 3-D velocity structure, where tomographic anomalies are observed down to about 50 km depth, it was determined that the Moho discontinuity is located at depths of 30-35 km (Figure 3). Additionally, in basin-like areas, low V_p values were observed, while anomalies with high V_p values occasionally extend from deeper regions towards the surface.

As a result of the relocation conducted based on the obtained 3-D velocity model, all earthquakes that occurred in the region have been relocated as accurately as possible in terms of their real coordinates and depths. Furthermore, the obtained new 3-D velocity model of the region has allowed for a more accurate calculation of the locations and depths of the main shocks of the

Kahramanmaraş earthquakes (Figure 4). The depth of the first shock was approximately 20 km, while the depth of the second main shock was determined to be 13 km."

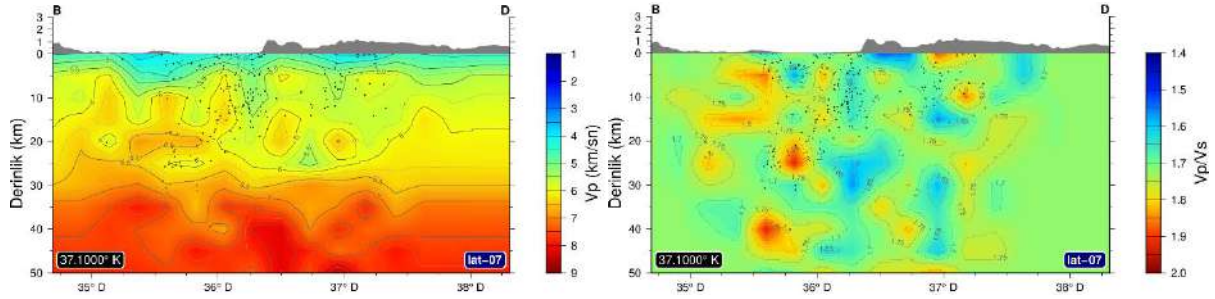


Figure3 The vertical cross-section derived from the 3D tomographic inverse solution velocity model. The left side represents the Vp, while the right side depicts the Vp/Vs model.

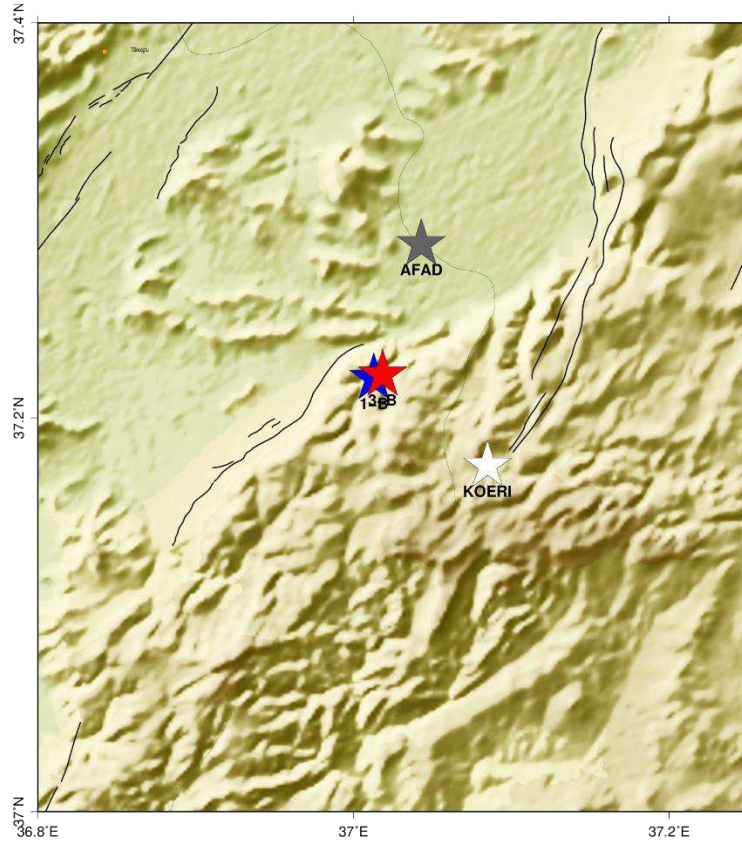


Figure4 The new location of the first main shock of Kahramanmaraş earthquake (red and blue stars) calculated using the 3-D velocity model.

CONCLUSION

The deep traces of the complex tectonic structure of the region have been determined with the tomographic velocity structures obtained along the EAFZ. The effects of the region being a tectonic plate boundary can also be observed in the deep velocity structures. Structures with anomalous features, such as the continuation of surface faults in the depths, structures

resembling mantle uplifts within the crust, and fundamental depths of basin areas, have been revealed. Furthermore, the positioning errors arising from lateral velocity deficiencies in the earthquake locations determined using 1-D velocity models have been rectified with 3-D velocity models. As a result, the locations of the main shocks of the Kahramanmaraş earthquakes have been more accurately determined. The second part of this study, which constitutes the initial section of tomographic imaging, will address tomographic studies conducted with the aftershocks of the Kahramanmaraş earthquakes after February 6, 2023.

REFERENCES

- Eberhart-Phillips, D., 1990. Three-dimensional P and S velocity structure in the Coalinga region, California. *J. Geophys. Res.* 95, 15,343–15,363.
- Kissling, E., 1988. Geotomography with local earthquake data, *Rev. Geophys.*, 26, 659–698.
- Kissling, E., Ellsworth, W.L., Eberhart-Phillips, D. & Kradolfer, U., 1994. Initial reference models in local earthquake tomography, *J. Geophys. Res.*, 99, 19 635–19 646.
- Kissling, E., Kradolfer, U. & Maurer, H., 1995. VELEST User's Guide—Short Introduction, Institute of Geophysics and Swiss Seismological Service, ETH.
- Thurber, C.H., 1983. Earthquake locations and three-dimensional crustal structure in the Coyote Lake area, central California. *J. Geophys. Res.* 88, 8226–8236.
- Thurber, C.H., 1993. Local earthquake tomography: velocities and Vp/Vs-theory. In: Iyer, H.M., Hirahara, K. (Eds.), *Seismic Tomography: Theory and Practice*. Chapman and Hall, London, pp. 563–583.
- Thurber, C.H., Eberhart-Phillips, D., 1999. Local earthquake tomography with flexible gridding. *Comput. G*

1.4 WHAT ACTUALLY ROTATIONAL SEISMOLOGY MEANS TO A SEISMOLOGIST?

G. İzgi^{1*}

¹*Institute of Geosciences, University of Potsdam, Karl-Liebknecht-Str. 24/25, 14476 Potsdam, Germany*

**Corresponding author e-mail: gizem.izgi@uni-potsdam.de*

ABSTRACT

Rotational seismology is a branch of seismology that focuses on the measurement and analysis of rotational ground motion caused by seismic events. Traditional seismology primarily deals with the study of translational (vertical and horizontal) ground motion, but rotational seismology extends this focus to include the rotation of the ground about a vertical axis. This rotational motion can provide valuable insights into the dynamics of seismic events and the Earth's subsurface properties. Rotational seismology involves the use of specialized sensors, known as rotational seismometers, to record the angular motion of the ground in response to seismic waves. These sensors are designed to measure the rate of rotation (angular velocity) and sometimes the angle of rotation (orientation) of the ground based on Sagnac's effect. Although being relatively new and evolving field, and its integration with traditional translational seismology has the potential to provide a more comprehensive understanding of seismic phenomena. Researchers and seismologists use rotational data alongside translational data to gain insights into earthquake sources, ground motion, and seismic hazard assessments.

KEYWORDS: Rotational seismology, gradient, full wavefield

1.5 EVALUATING THE PERFORMANCE OF ROTATIONAL SENSORS ACROSS DIFFERENT SOURCE TYPES: EARTHQUAKES, EXPLOSIONS, AND VIBROSEIS SWEEPS

G. İzgi^{1*}, E.P.S. Eibl¹, F. Krüger¹, F. Bernauer²

¹*Institute of Geosciences, University of Potsdam, Karl-Liebknecht-Str. 24/25, 14476 Potsdam, Germany*

²*Department für Geo- und Umweltwissenschaften, Ludwig-Maximilians Universität München,
80333 München, Germany*

*Corresponding author e-mail: gizem.izgi@uni-potsdam.de

ABSTRACT

Complete seismic wavefield description requires incorporating rotational motions in addition to translation and strain. The blueSeis-3A (exail), a recently introduced portable fiber-optic gyroscope designed specifically for seismological applications, offers high sensitivity for direct rotation measurement. To assess the performance of these rotational sensors, we utilized two distinct datasets collected from the same region.

In the first dataset, we deployed six rotational and three translational instruments in a tightly grouped configuration between August 26th and September 2nd, 2019, at the Fürstenfeldbruck observatory. We analyzed the self-noise characteristics of these instruments, examining their correlation, coherency, and probabilistic power spectral densities. Additionally, we investigated coherent noise spectrograms within four distinct groups and discussed observations related to the ML 3.4 Dettingen Earthquake that occurred on August 29, 2019.

In the second dataset, we aimed to further assess and compare the rotational sensors. In November 2019, we conducted an active experiment in the same region, involving the detonation of five explosions with varying yields and characteristics, as well as the operation of a vibroseis truck generating 480 sweep signals across a broad frequency range spanning from 7 to 120 Hz at 160 different locations. We estimated back azimuths for both the explosions and the sweeps.

When estimating the back azimuths of explosions, using only rotational sensors yielded favorable results. However, utilizing vertical rotation rates and transverse acceleration also proved feasible, particularly when we observed the presence of SH-type energy caused by scattering. The accuracy of these estimates depended on factors such as the signal-to-noise ratio, distance from the source, and the yield of explosives. Unlike conventional methods that rely on P waves, our approach for tracking vibroseis movements relied on S waves, as rotational sensors are primarily capable of recording S-type waves. Notably, for distances exceeding 700 meters, the method relying solely on rotational sensors exhibited substantial deviations, underscoring the need to select the appropriate method for calculating the back azimuth based on the source type.

In summary, our findings indicate that using a single rotational sensor to estimate the direction of various source types (e.g., earthquakes, explosions, and vibroseis sweeps) can be successful, taking into account the associated method limitations.

KEYWORDS: Portable rotational sensor, active experiment, huddle test

1.6 ANALYSIS OF SURFACE RUPTURE PATTERNS AND FAULT OFFSET VARIABILITY ASSOCIATED WITH THE 06 FEBRUARY 2023 PAZARCIK (KAHRAMANMARAS) EARTHQUAKE (MW 7.7) IN ISLAHIYE AREA, TURKIYE

A. Caglayan^{1*}, V. Isik², R. Saber³, H. Unal⁴, F. Chitea^{5,6}

¹Dr., Department of Geological Survey, Ministry of Environment, Urbanisation and Climate Change, General Directorate of Spatial Planning, Ankara, Türkiye

²Prof. Dr., Department of Geological Engineering, Ankara University, Ankara, Türkiye

³Dr., Department of Geological Engineering, Ankara University, Ankara, Türkiye

⁴Mr., Geomtek Mühendislik, Geoteknik, Proje, Ankara, Türkiye

⁵Lect. Dr., Department of Engineering Geology and Geophysics, Bucharest University, Bucharest, Romania

⁶Lect. Dr., Institute of Geodynamics of the Romanian Academy, Bucharest, Romania

*Corresponding author e-mail: ayse.caglayan@csb.gov.tr

ABSTRACT

Numerous destructive earthquakes have occurred in Türkiye, part of the Alpine-Himalayan Orogenic Belt, both in historical and instrumental periods, resulting in many appalling casualties. Pazarcık earthquake (Mw 7.7), the first major earthquake of the 06 February 2023 Kahramanmaraş earthquake sequences, occurred along the so-called East Anatolian Fault Zone. A total surface rupture was approximately 250 km long from Golbasi to Antakya. A maximum left-lateral offset of 4-4.5 m has been documented, with various dip-slip displacements from tens of cm to a few meters. The overall direction of surface rupture changes noticeably from NE to SE, forming NW-facing arc-shaped geometry. The evidence of surface faulting is traceable along hillslopes, valleys and plain terrain, as well as on modern manufactured structures such as roads, garden walls, houses and barns.

Various well-developed surface faulting geometries were observed in field studies, high-resolution satellite images, and UAV-based aerial photos. Different morphological features, including simple and complex fault traces, pop-up structures, sag ponds, fault splays and lateral spreading related to surface deformation, were observed in the Islahiye area. The lateral width of the surface ruptures varies from a few to a hundred meters. Formation of typical Riedel fractures is evident in the entire study area, indicating development stages of surface faulting. Left lateral fault offsets were measured, ranging from tens of cm to approximately 3 m, while the vertical displacement was documented to be confined to about 50 cm. Our geological and geomorphological field observations along the active main fault surface indicate that there have been numerous fault activities causing historical and/or prehistorical earthquakes. So far, The results emphasize the importance of adopting risk-based approaches in establishing settlement areas around active fault zones.

KEYWORDS: Twin earthquakes, Surface rupture, Active tectonics, East Anatolian Fault Zone, Southeastern Türkiye

INTRODUCTION

The Anatolian Plate, a western domain of the so-called Turkish-Iranian Plateau, includes significant intra-plate deformation zones formed due to the collision of the Arabian and Eurasian Plates (e.g., Şengör and Kidd 1979). In the literature, different times have been suggested by researchers for the initiation of the collision between the Arabian and Eurasian Plates, such as Late Cretaceous (e.g., Berberian and King 1981), late Eocene to middle Miocene (e.g., Dewey et al. 1986), early Oligocene (e.g., McQuarrie and van Hinsbergen 2013), late Oligocene to late Miocene (e.g., Fakhari et al. 2008) and Pliocene (e.g., Falcon 1974). The most preferred initiation time of the collision is 36–20 Ma (e.g., Zhang et al. 2016), where most of the tectonic responses to the collision occurred after 20 Ma (Su and Zhou 2020). The collision has resulted in the formation of different deformation zones within Anatolia, including the East Anatolian Fault Zone (Arpat and Şaroğlu 1972), North Anatolian Fault Zone (Caglayan et al. 2019), Central Anatolia Deformation Zones (Isik et al. 2014), Western Anatolia Extensional Zones (Isik et al. 2003).

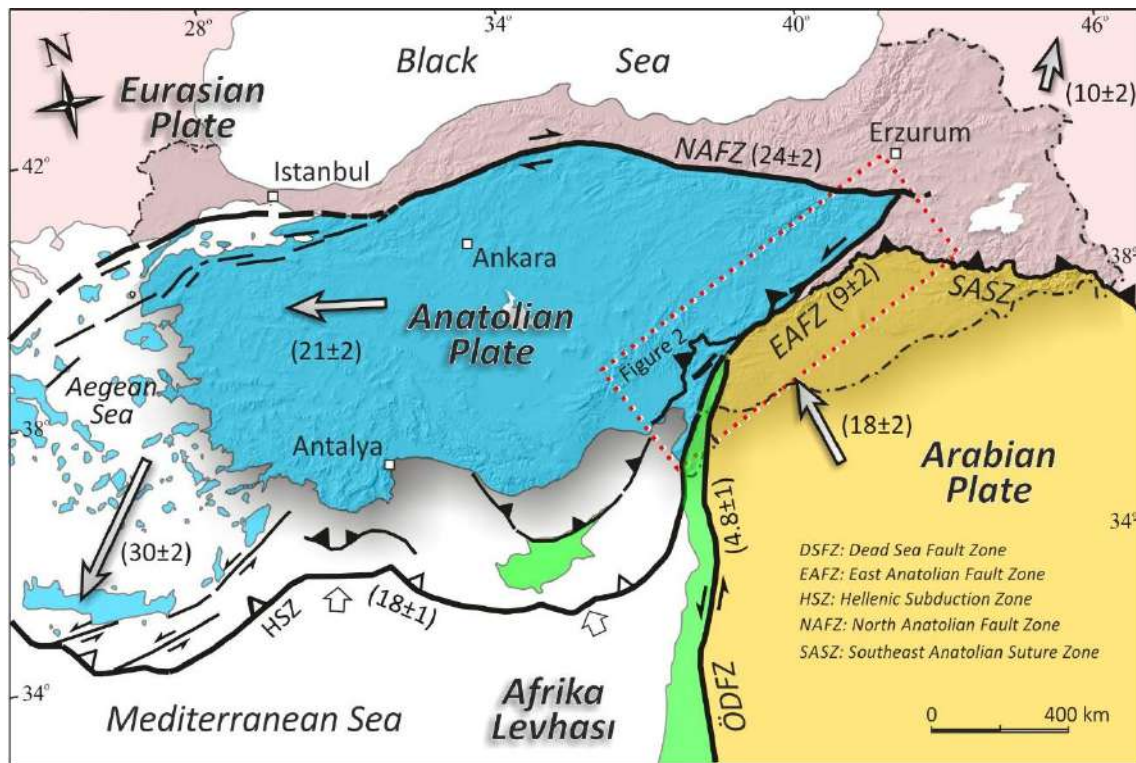


Figure1 A map showing the interaction between different tectonic plates in Türkiye and the surrounding area

The East Anatolian Fault Zone (EAFZ) is a major active fault zone in Türkiye that extends for more than 600 kilometers from the Karlıova (Bingöl) to the Mediterranean Sea (e.g. Arpat and Şaroğlu 1972). The EAFZ is a complex system of faults that includes multiple branches or segments with localized pull-apart basins and push-up zones, with controversial age estimations, likely between Late Miocene-Early Pliocene (e.g., Şengör et al. 1985) or Late Pliocene (e.g., Emre and Duman, 2007) and slip rate of 6 mm/yr to 10 mm/yr. (Taymaz et al. 1991). Historical and instrumental records reveal significant seismic activity along the EAFZ. The largest known historical earthquakes along the EAFZ occurred on November 29, 1114 ($M > 7.8$), March 28, 1513 ($M > 7.4$) and March 2, 1893 ($M > 7.1$) (Ambraseys and Jackson 1998). In contrast, these large devastating

historical earthquakes contrast with few significant earthquakes during the last century on December 4, 1905 Mw 6.8 earthquake (Nalbant et al., 2002), January 24, 2020 Mw 6.8 earthquake (Pousse-Beltran et al. 2020), and lately destructive February 06, 2023 Mw: 7.8 Earthquake. The latter earthquake has produced a surface rupture of more than 300 km in length from north of Gölbaşı (Adıyaman) to the Antakya (Hatay) in the SW. The remote sensing observations revealed the curved shape and complex nature of the surface rupture.

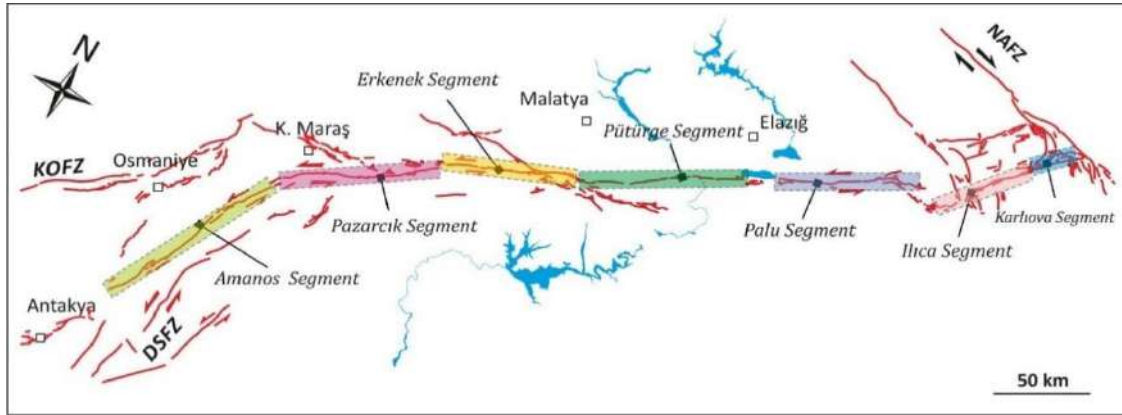


Figure2 A map showing different fault segments of the East Anatolian Fault Zone.

In this study, an optical post-event satellite image investigation was conducted to obtain the whole distribution of co-seismic surface rupture by using high-resolution Maxar images. After determining the location of possible ruptures derived from satellite images, the field survey was carried out with a high-precision mapping drone, and the surface rupture data were gathered. Subsequently, all collected data were processed to measure fracture patterns and fault offset amounts.

METHOD and APPLICATION

The study included two stages: office-based remote sensing studies and field surveys. Firstly, resolution precious Maxar optical images were acquired on February 08, 2023 and are available online for research purposes. Using Maxar images, the surface ruptures were generally mapped, and the potential locations for field observation, drone flight areas and detailed mapping were selected. A DJI Phantom 4 RTK (real-time kinematic) drone with vertical positioning accuracy of 1.5 cm + 1 ppm and a ground resolution of 2.74 cm at a 100 m flight altitude was used for photogrammetry studies. All captured digital images were imported into Agisoft Metashape 1.8.5 software. The software automatically recognizes the relative position and direction of each photo, calculates the aerial triangulation and performs 2D and 3D reconstructions using the generated point cloud data. As a result, DEMs, DSMs, orthophotos, and 3D models could be extracted from processed data. Finally, detailed surface rupture maps along the study area were generated.

RESULTS

The surface deformation map shows that the main area impacted by the Pazarcık earthquake in the İslahiye area is approximately 6 × 12 km. The rupture zone presents two main fault branches

propagating in the SW direction (Figure 3). This is consistent with the preexisting tectonic landforms, morphological features and outcrop evidence of fresh and relatively older fault slickensides, suggesting the repetition of several destructive historical earthquakes in the study area. Left lateral fault offsets were measured, ranging from tens of cm to approximately 3 m. while the vertical displacement was documented to be confined to about 50 cm. (Figure 3). Continuous rupture traces with lengths ranging from several meters to tens of meters were observed in the field investigations. Based on the branching of the fault strike, the surface rupture of the earthquake in this area can be roughly divided into two sections. The western section, which has a strike of N30°E to N70°E, consists of intermittent fractures with different lengths. The eastern fault branch strikes N25°-30°E and has a length of ~10 km with highly discontinuous and intermittent geometry (Figure 3).

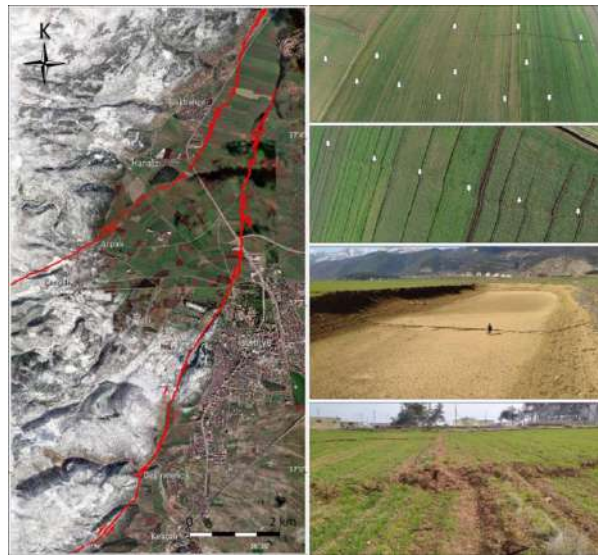


Figure3 Maxar satellite image (left), and field and drone images (right) of surface faulting along the İslahiye area.

In the İslahiye area, surface faulting is mainly characterized by simple shear on the surface, representing various Riedel fractures arranged in en-echelon geometries (Figures 4 and 5). Various types of Riedel fractures and morphological features, such as push-up and small-scale pull-apart structures, were found in field observations and laboratory studies. On the obtained orthophotos, all the fracture strikes were measured and projected onto the rose diagram (Figures 4 and 5). Comparison of The results indicate two main distribution types of rupture patterns. The first type is R, P and T, with a minority of R' Riedel fractures. The angular difference between main populations of fractures with principal displacement zone does not exceed 15°-20°, demonstrating nearly linear propagation of surface faulting.

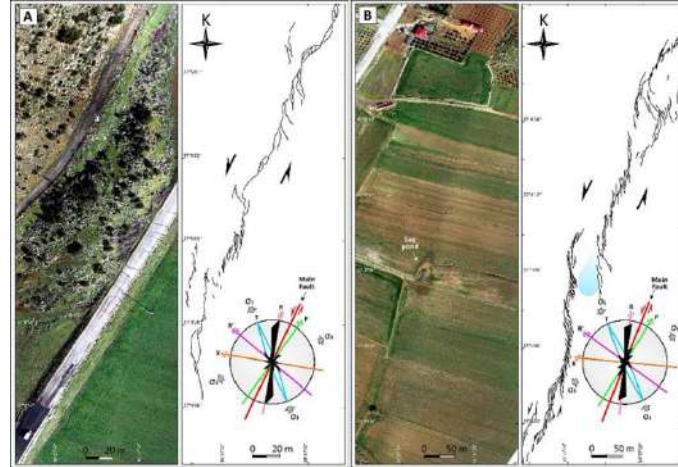


Figure4 Orthophotos and sketch drawings of surface ruptures on the western fault branch during the Pazarcık earthquake.

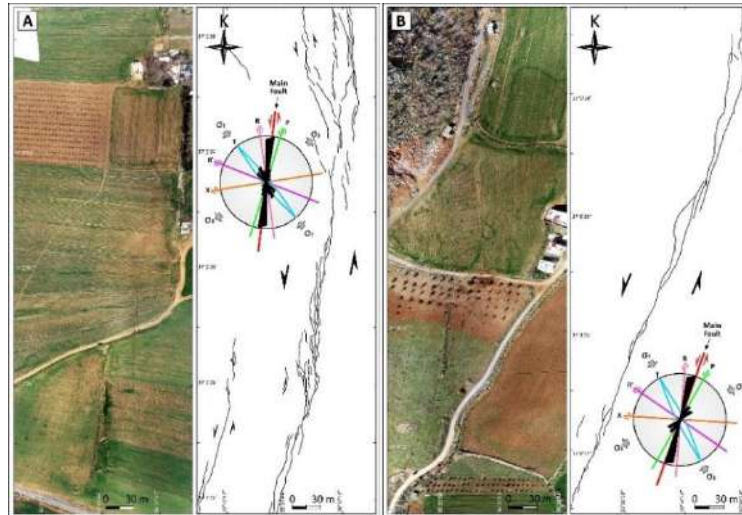


Figure5 Orthophotos and sketch drawings of surface ruptures on the eastern fault branch during the Pazarcık earthquake.

The second type indicates that the several meters to several tens of meters long en-echelon shears represent major structures along the study area (Figures 4 and 5). The angular difference between the orientations of the en-echelon shears and the principal displacement zone is 20°–30°. The fault stepping along the surface ruptures have formed several typical push-up and sag pond structures (Figures 4 and 5). Finally, drone observations reveal that geomorphological features such as ruts, gullies, and streams and modern structures such as roads, walls, and buildings were displaced horizontally and vertically by a fault along the rupture zone (Figures 4 and 5). These indicate that the Pazarcık earthquake resulted in a primarily left-lateral strike-slip motion.

CONCLUSIONS

The main conclusions reached in this study are:

1. Different morphological features, including simple and complex fault traces, pop-up structures, sag ponds, fault splays and lateral spreading related to surface deformation, were observed in the

Islahiye area. The lateral width of the surface ruptures varies from a few to a hundred meters. The lateral width of the surface ruptures varies from a few to a hundred meters.

2. Formation of typical Riedel fractures is evident in the entire study area, indicating development stages of surface faulting. The R, P and T, with a minority of R' Riedel fractures, are dominant fractures along the study area. The several meters to several tens of meters long en-echelon shears represent major structures also.

3. Left lateral fault offsets were measured, ranging from tens of cm to approximately 3 m, while the vertical displacement was documented to be confined to about 50 cm.

4. The consistency between surface faulting with the preexisting tectonic landforms, morphological features and outcrop evidence of fresh and relatively older fault slickensides, suggesting the repetition of several destructive historical earthquakes in the study area.

REFERENCES

- Ambraseys, N.N., Jackson, J. A. 1998. Faulting associated with historical and recent earthquakes in the Eastern Mediterranean region. *Geophys. J. Int.*, 133, pp. 390–406.
- Arpat, A. E., Şaroğlu, F. 1972. Doğu Anadolu Fayı ile ilgili bazı gözlem ve düşünceler. *Bulletin of the Mineral Research and Exploration*, 73, 1–9.
- Berberian, M., King, G. 1981. Toward a paleogeography and tectonic evolution of Iran. *Canadian Journal of Earth Science* 18, 502–557.
- Caglayan, A., Isik, V., Saber, R. 2019. Paleoseismologic evidence for Holocene activity on 1944 earthquake segment, north Anatolian fault zone. *Geoscience Journal*, 23, 805–22. <https://doi.org/10.1007/s12303-018-0075-3>.
- Dewey, J.F., Hempton, M.R., Kidd, W.S.F., Şaroğlu, F., Şengör, A.M.C. 1986. Shortening of continental lithosphere: the neotectonics of Eastern Anatolia a young collision zone. In "Collision tectonics" eds. M. P. Coward and A. C. Ries, *Geol. Soc. Spec. Publ.*, 19, pp. 3–36.
- Emre, O., Duman, T.Y., 2007. The East Anatolian Fault: Structural Pattern and Relationship with the Dead Sea Transform. *American Geophysical Union, Fall Meeting 2007, Abstract #T42B-01*
- Fakhari, M., Axen, G., Horton, B., Hassanzadeh, J., Amini, A. 2008. Revised age of proximal deposits in the Zagros foreland basin and implications for Cenozoic evolution of the high Zagros. *Tectonophysics* 451, 170–85.
- Isik, V., Seyitoglu, G., Cemen, I., 2003. Ductile–brittle transition along the Alas, ehir detachment fault and its structural relationship with the Simav detachment fault, Menderes Massif, western Turkey. *Tectonophysics* 374, 1–18.
- Isik, V., Uysal, I. T., Caglayan, A., Seyitoglu, G. 2014. The evolution of intraplate fault systems in central Turkey: structural evidence and Ar–Ar and Rb–Sr age constraints for the Savcili Fault Zone. *Tectonics* 33, 1875–99. <https://doi.org/10.1002/2014TC003565>.
- McQuarrie, N., van Hinsbergen, D. 2013. Retrodeforming the Arabia–Eurasia collision zone: age of collision versus magnitude of continental subduction. *Geology* 41, 315–8.
- Nalbant, S., McCloskey, J., Steacy, S., Barka, A. 2002. Stress accumulation and increased seismic risk in eastern Turkey. *Earth Planetary Science Letters* 195, 291–298.
- Pousse-Beltran, L., Nissen, E., Bergman, E. A., Cambaz, M. D., Gaudreau, E., Karasözen, E., Tan, F. (2020). The 2020 Mw 6.8 Elazığ (Turkey) Earthquake Reveals Rupture Behavior of the East Anatolian Fault. *Geophysical Research Letters*, 47 (13), e2020GL088136. doi: 10.1029/2020GL088136
- Su, H., Zhou, J. 2020. Timing of Arabia–Eurasia collision: constraints from restoration of crustal-scale cross-sections. *Journal of Structural Geology* 135, 104041.
- Şengör, A. M. C. & Kidd, W. S. F. 1979. Post-collisional tectonics of the Turkish–Iranian Plateau and a comparison with Tibet. *Tectonophysics* 55, 361–76.
- Şengör, A. M. C., Görür, N., Şaroğlu, F. 1985. Strike-slip faulting and related basin formation in zones of tectonic escape: Turkey as a case study, Strike-Slip Deformation, Basin Formation and Sedimentation. Biddle, K.T., Christie Bick, N. (Eds.), *Soc. Eco., Palaeo. Mineral. Spec. Publ.*, 37, pp. 227–264.
- Taymaz, T., Jackson, J., McKenzie, D. P. 1991. Active tectonics of the north and central Aegean Sea. *Geophysical Journal International*, 106, 433–490.
- Zhang, Z., Xiao, W., Majidifard, M., Zhu, R., Wan, B., Ao, S., Chen, L., Rezaeian, M., Esmaeili, R. 2016. Detrital zircon provenance analysis in the Zagros Orogen, SW Iran: implications for the amalgamation history of the Neo-Tethys. *International Journal of Earth Sciences* 106, 1223–38.

1.7 EVALUATION OF RELATIVE TECTONIC ACTIVITY IN THE EASTERN PART OF KHAZAR FAULT ZONE, NORTH IRAN

M. Tourani^{1*}, R. Saber², V. Isik³, A. Caglayan⁴ and F. Chitea⁵

¹Mrs., Department of Geological Engineering, Ankara University, Ankara, Türkiye

²Dr., Department of Geological Engineering, Ankara University, Ankara, Türkiye

³Prof. Dr., Department of Geological Engineering, Ankara University, Ankara, Türkiye

⁴Dr., Department of Geological Survey, Ministry of Environment, Urbanisation and Climate Change, General Directorate of Spatial Planning, Ankara, Türkiye

⁵Lect. Dr., Department of Engineering Geology and Geophysics, Bucharest University, Bucharest, Romania

*Corresponding author e-mail: tourani@ankara.edu.tr

ABSTRACT

The Alborz Mountain range, a typical orogenic region located in North Iran, was formed due to the collision of the Iran and Eurasian Plates. This mountain range is characterized by active range-parallel fold and thrust structures that reflect the ongoing tectonic processes in the region. The Khazar Fault Zone is the main active north-bounding fault of the range, characterized by a south-dipping reverse/thrust fault with a left-lateral component. The Khazar Fault Zone represents a significant source of seismic hazard for the entire Alborz Mountain range, especially for densely populated cities on the region's northern side. We employ quantitative geomorphometric analysis techniques to assess the relative tectonic activity within the eastern segment of the Khazar Fault Zone and to explore the variations in deformation along its length. We computed seven geomorphic indices, including Stream length-gradient index (SI), Drainage basin asymmetry (Af), Valley floor width-valley height ratio (Vf), Index of drainage basin shape (Bs), Mountain-front sinuosity ratio (Smf), Normalized steepness index (Ksn), and Hypsometric curve/Hypsometric integral (Hi), for 39 drainage basins along the study area. Along the eastern part of the zone, the low Smf values (ranging from 1.04 to 1.66) and Vf values predominantly less than 1 across the entire study area indicate relatively straight mountain fronts and young V-shaped valleys respectively. Moreover, measured uplift rates due to these indices show that the uplift rate is higher than 0.5 mm/yr in the entire area. The values of Af and Bs suggest that most basins indicate notable tilting and elongation. The SI and Ksn values show a rising trend from west to east in the study area. The Hi results also show that most valleys are young in terms of geological age and deeply excavated. Our results emphasize that relative tectonic activity increases toward the east of the Khazar Fault Zone within the study area. The overall result of the geomorphometric analysis shows that the deformation forces associated with the intense tectonic process along the eastern part of the Khazar Fault Zone are the dominant factors in shaping the surface topography. The geomorphometric results also correlate well with seismological observations, the landscape evolution in the east of the Khazar Fault Zone reflecting the increasing tectonic activity towards this part of the fault.

KEYWORDS: Geomorphic indices, Alborz Mountains, Khazar Fault Zone, Active tectonics, North Iran, Turkish-Iranian Plateau

INTRODUCTION

Geomorphological, geodetic, and geological data are commonly employed to analyze and define deformation occurring within tectonically active regions (e.g., Molin et al., 2004; Saber et al., 2022). Since the early 2000s, the utilization of geomorphic indices has been crucial in establishing the correlation between erosion mechanisms and the tectonic activity of the region (e.g., Silva et al. 2003; Bull 2007; El Hamdouni et al., 2008; Saber et al. 2020; Caglayan et al. 2021). Also, Geomorphic indices serve as valuable tools in evaluating tectonic activity and deformation along active faults, enabling the segmentation of fault sections into intervals of relative tectonic activity (e.g., Rockwell 1984; Saber et al. 2018). Our study focuses on quantitative geomorphometric analysis techniques to assess the relative tectonic activity within the eastern segment of the Khazar Fault Zone located at Alborz Mountain Range in northern Iran. The Alborz Mountains stand out as one of the remarkable morphological features within the Turkish-Iranian Plateau (Fig 1a). This mountain range is characterized by its curved shape with ~ 600 km in length and ~ 100 km in width, located in northern Iran (Fig 1b). The Alborz Mountain range is one of the regions where earthquakes most frequently occur, and active fault zones have historically and instrumentally caused numerous destructive earthquakes (Fig 1b). Both structural and seismological information indicates that parallel and sub-parallel reverse/thrust and strike-slip faults are widespread tectonic structures developed along the range (e.g., Jackson et al., 2002; Allen et al., 2003; Rashidi, 2021; Nazari et al., 2021).

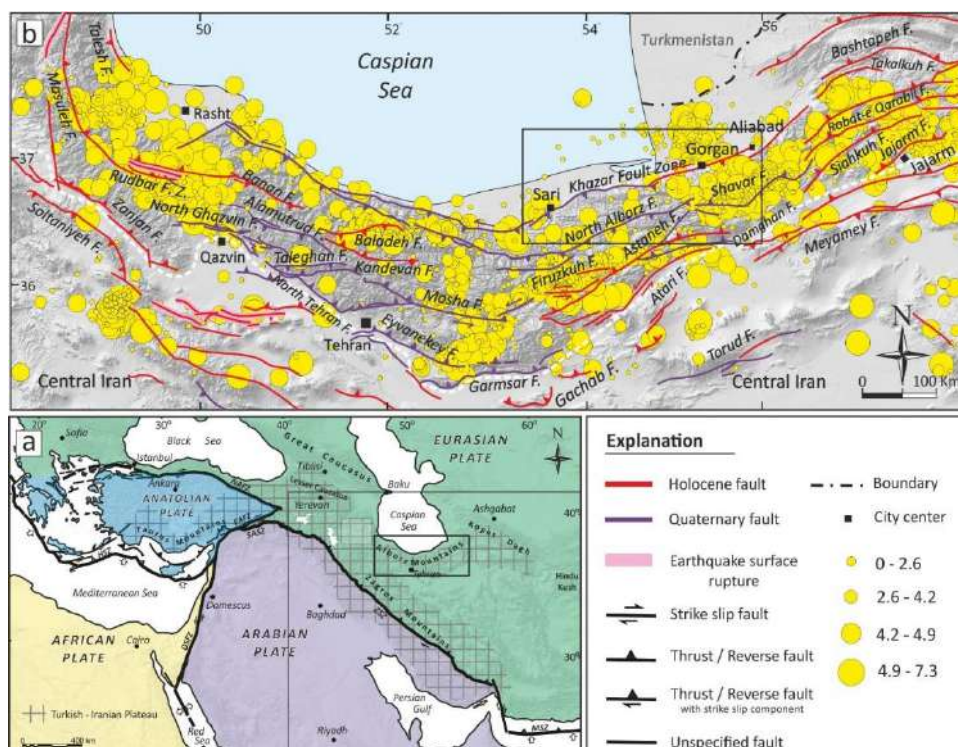


Figure1 (a) A simplified tectonic map showing the relationship of the Eurasian, Arabian, African and Anatolian Plates (re-drawn from Isik et al., 2021), (b) A map showing active fault zones and the distribution of earthquake epicenters (ISC earthquake catalog) since 1964 along the Alborz Range. Active faults and earthquake focal mechanisms are adopted from the International Institute of Earthquake Engineering and Seismology (2013) and Oveisi et al. (2019).

The Khazar Fault Zone is defined as an active south-dipping, reverse/thrust fault 600 km long located in northern foothills of the Alborz mountains (Rashidi, 2021; Nazari et al., 2021) (Fig. 1b). The Khazar Fault Zone has formed a distinctive morphological landscape between the Caspian Sea and the Alborz Mountains (Allen et al., 2003; Rashidi, 2021). Ghassemi (2005) states that in the eastern Alborz, the Khazar Fault Zone is usually hidden, segmented and indicated as fault-propagation folds. On the hanging wall of this part of the Khazar Fault Zone, there are low-grade metamorphosed rocks (Fig 2). The eastern part of the Khazar Fault Zone has juxtaposed Percamberin, Paleozoic, Mesozoic and Neogene units over Quaternary deposits (Fig 2). Several destructive historical (Ambraseys and Melville, 1982) and instrumental earthquakes (e.g., the 1985 October 29 Gorgan earthquake - Mw 6.2: Priestly et al., 1994 and the 2004 May 28 Baladeh earthquake - Mw 6.2: Tatar et al., 2007) attributed to the Khazar Fault Zone. Therefore, the Khazar Fault Zone is the most active structure, representing a notable seismic hazard for the entire Alborz Mountain range, especially for densely populated cities on the region's northern side (Nazari et al. 2021).

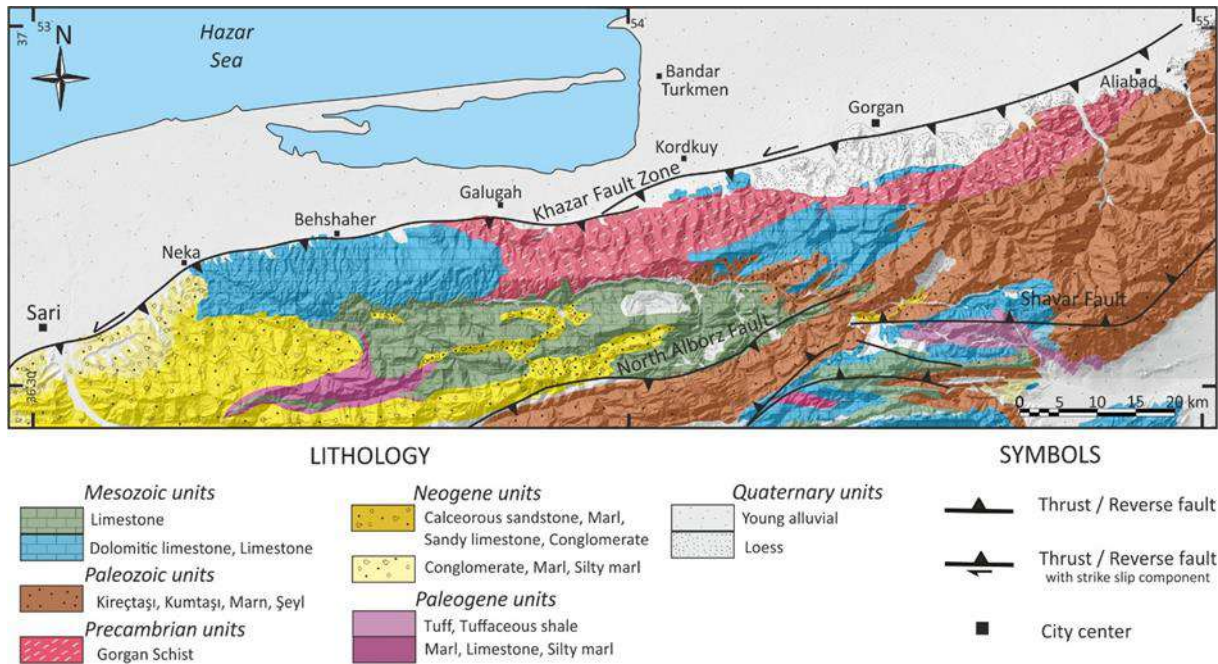


Figure2 Simplified geological map of the study area (modified from 1:250,000 geological maps of the Geological Survey of Iran).

METHOD and APPLICATION

We employ quantitative geomorphometric analysis using geomorphic indices to assess the relative tectonic activity within the eastern segment of the Khazar Fault Zone and to explore the variations in deformation along its length. The geomorphic indices are extracted with the help of 1 arc second Shuttle Radar Topography Digital Elevation Model (SRTM DEM) data of 30m resolution. Geomorphic indices were calculated and analyzed using the Matlab-based TecDEM toolbox (Shahzad and Gloaguen, 2011), Topo-Toolbox (Schwanghart and Scherler, 2014) and ArcGIS (10.3) modules and some other graphical programs. We computed seven geomorphic indices in Table 1 for 39 drainage basins along the study area (Fig 3a).

Table1 Morphometric indices were used in the study.

S. No.	Geomorphic Indices	Formula	Reference
1	Mountain front sinuosity (Smf)	$Smf = Lmf/Ls$	Bull (1977); Keller and Pinter (2002),
2	Drainage basin asymmetry (AF)	$AF = 100 \cdot Ar/At$	Keller and Pinter (2002); Saber et al., (2018)
3	Valley floor width to valley height ratio (Vf)	$Vf = 2Vw/[(Eld-Esc) + (Erd-Esc)]$	Keller and Pinter (2002); Silva et al., (2003).
4	Hypsometric Integral and Curve (Hi)	$HI = Hmean - Hmin / Hmax - Hmin$	Keller and Pinter (2002); Saber et al (2022)
5	Stream length gradient index (SL)	$SI = (\Delta H / \Delta L) L$	Hack (1973); Keller and Pinter (2002)
6	Index of drainage basin shape (Bs)	$Bs = Bl/Bw$	El Hamdouni et al., (2008)
7	Normalized steepness index (Ksn)	$S = Ksn \cdot A^{-u}$, and therefore $Ksn = S/A^{-u}$,	Hack (1973); Flint (1974)

RESULTS and CONCLUSIONS

The calculated Vf values along the study area mainly vary between 0.12-0.97 (Fig 4b). The low Vf values, predominantly less than 1 across the study area, indicate relatively young V-shaped valleys. The Smf values range from 1.04 to 1.66 (Fig 4c), and these low values of smf also indicate straight mountain fronts due to relatively high tectonic activity. Moreover, measured uplift rates due to these indices show that the uplift rate is higher than 0.5 mm/yr in the area (Fig 3). According to Af values, 15 basins (38.46%) belong to class 1, 11 basins (28.21%) belong to class 2 and 13 basins (33.33%) belong to class 3 (Fig 4d). So, the majority of drainage basins show high tilting amounts around the fault zone. The Bs values show that 53.85% of drainage basins represent elongated shapes in the study area, and the majority of these elongated basins are located in the eastern section of the study area, suggesting higher tectonic activity (Fig 4e).

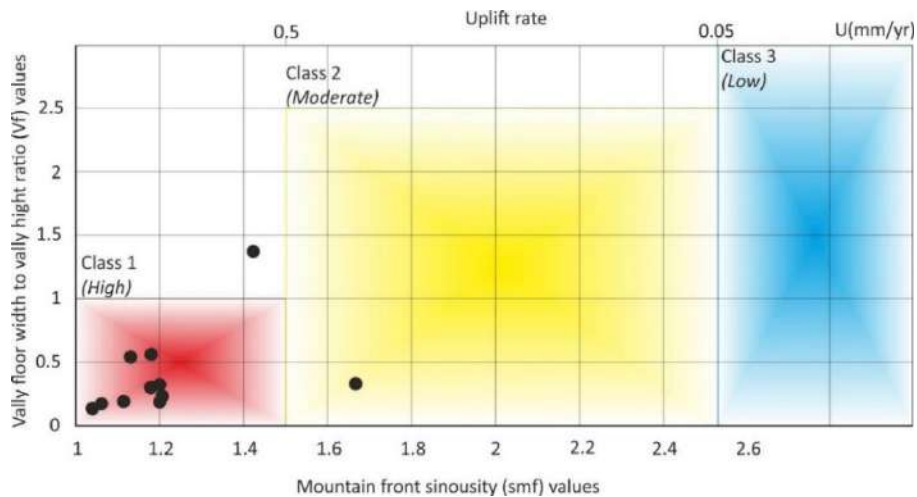


Fig. 3. Chart showing Smf (mountain-front sinuosity ratio) values versus Vf (valley floor width–valley height ratio) values for the mountain fronts of each segment, along with inferred activity classes. The numbers at the top represent inferred uplift rates U (mm/yr) based on Rockwell et al. (1984).

The SI values range from <200 to >800, indicating a rising trend from west to east in the study area. This suggests that in the eastern part, the SI anomalies dominantly result from tectonic activities, specifically faulting (Fig 3f). The Ksn values range from 0.005 to 43.38. the Ksn values,

also the same as SI values, show a rising trend from west to east in the study area (Fig 4g). The high values of Ksn in the study area highlight mainly the effect of tectonic processes indicating rapid uplift. The calculated Hi values along the study area vary between 0.15-0.55 and show a rising trend from west to east in the study area (Fig. 4h). The majority of the basins (76.92%) exhibit low Hi values in the study area and these low values show that most valleys are young in terms of geological age and deeply excavated. Our results emphasize that relative tectonic activity increases toward the east of the Khazar Fault Zone within the study area. The overall result of the geomorphometric analysis shows that the deformation forces associated with the intense tectonic process along the eastern part of the Khazar Fault Zone are the dominant factors in shaping the surface topography. The geomorphometric results also correlate well with seismological observations, the landscape evolution in the east of the Khazar Fault Zone reflecting the increasing tectonic activity towards this part of the fault zone.

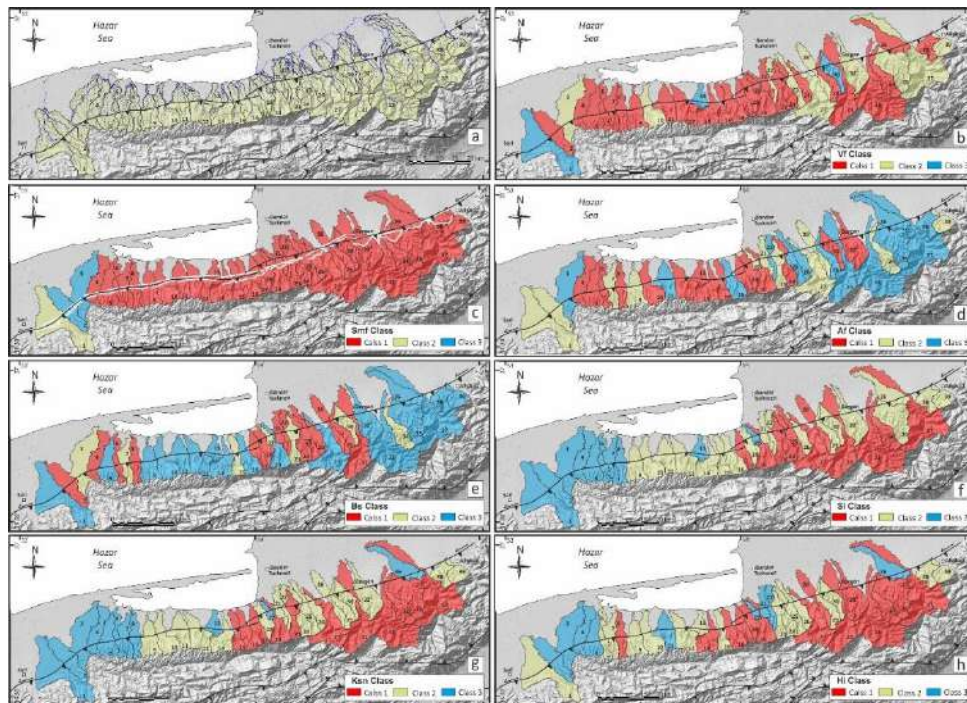


Figure 4 Maps displaying morphometric analysis results along the eastern segment of the Khazar Fault Zone. (a) Extracted drainage basins, (b) Ratio of valley floor width to valley height (Vf), (c) Mountain-front sinuosity ratio (Smf), (d) Drainage basin asymmetry (Af), (e) Drainage basin asymmetry (Bs), (f) Stream length gradient (SL), (g) Normalized steepness index (Ksn) and (h) Hypsometric integral (Hi).

REFERENCES

- Allen, M.B., Vincent, S.J., Alsop, G.I., Ismailzadeh, A., Flecker, R. 2003. Late Cenozoic deformation in the South Caspian region: effects of a rigid basement block within a collision zone. *Tectonophysics*, 366, 223-239.
- Ambraseys, N.N., Melville, C.P. 1982. A history of Persian earthquakes. Cambridge Univ, Cambridge.
- Bull, W.B., 2007. Tectonic Geomorphology of Mountains: A New Approach to Paleoseismology. Wiley-Blackwell, Oxford, pp. 328.
- Bull, W.B. 1977. Tectonic geomorphology of the Mojave Desert, California. In the US Geological Survey contract report. 14-0-001-G-394 (p. 188). Menlo Park, CA: Office of Earthquakes, Volcanoes, and Engineering.
- Caglayan, A., Saber, R., Isik, V., 2021. Geomorphic evidence of active faulting in the Simav Half-graben, Western Turkey. 11th Congress of the Balkan Geophysical Society 10-14 October 2021, Bucharest.

- El Hamdouni, R., Irigaray, C., Fernández, T., Chacón, J., Keller, E.A. 2008. Assessment of relative active tectonics, southwest border of the Sierra Nevada (southern Spain). *Geomorphology* 96, 150-173.
- Flint, J.J. 1974. Stream gradient as a function of order, magnitude, and discharge. *Water Resour. Res.* 10, 969-973. <http://dx.doi.org/10.1029/WR010i005p00969>.
- Ghassemi, M.R. 2005. Drainage evolution in response to fold growth in the hanging wall of the Khazar fault, north-eastern Alborz, Iran. *Basin Res.* 17, 425-436.
- Hack, J.T. 1973. Stream-profile analysis and stream-gradient index. *Journal of Research of the U.S. Geological Survey*, 1(4), 421-429.
- Isik, V., Saber, R., Caglayan, A. 2021. November 08, 2019 Turkmanchay earthquake (Mw 5.9) in NW Iran: an assessment of the earthquake using DInSAR time-series and field evidence. *Natural Hazards*. <https://doi.org/10.1007/s11069-020-04439-1>
- Jackson, J.A., Priestley, K., Allen, M., Berberian, M. 2002. Active tectonics of the South Caspian Basin. *Geophys. J. Int.* 148, 214-245.
- Keller, E.A., Pinter, N. 2002. *Active tectonics: Earthquakes, uplift, and landscape* (2nd ed., p. 362). Upper Saddle River, NJ: Prentice Hall.
- Molin, P., Pazzaglia, F.J., Dramis, F. 2004. Geomorphic expression of active tectonics in a rapidly deforming forearc, Sila massif, Calabria, southern Italy. *Am. J. Sci.* 304, 559-589.
- Nazar, i H., Ritz, J.F., Burg, J.P., Shokri, M., Haghipour, N., Vizheh, M.M., Avagyan, A., Nashli, H.F., Ensani, M. 2021. Active tectonics along the Khazar fault (Alborz, Iran). *J Asian Earth Sci.* <https://doi.org/10.1016/j.jseae.2021.104893>
- Oveisi, B., Sabour, M., Sadeghi, M., Heibati, Z. 2019. Seismotectonic map of Iran, Version I- mint/6294-5890. Ministry of Industry, Mine and Trade. Geol Surv Iran Seismotectonic Department, Tehran, Iran.
- Priestley, K. Baker, C. Jackson, J. 1994. Implications of earthquake focal mechanism data for the active tectonics of the South Caspian Basin and surrounding regions. *Geophys J Int.* <https://doi.org/10.1111/j.1365-246X.1994.tb04679.x>
- Rashidi, A. 2021. Geometric and kinematic characteristics of the Khazar and North Alborz Faults: Links to the structural evolution of the North Alborz-South Caspian boundary, Northern Iran. *J Asian Earth Sci.* <https://doi.org/10.1016/j.jseae.2021.104755>.
- Rockwell, T.K., Keller, E.A., Johnson, D.L., 1984. Tectonic geomorphology of alluvial fans and mountain fronts near Ventura, California. In: Morisawa, M. (Ed.), *Tectonic Geomorphology. Proceedings of the 15th Annual Geomorphology Symposium*. Allen and Unwin Publishers, Boston, MA, pp. 183-207.
- Saber, R., Caglayan, A. Isik, V. 2018. Relative tectonic activity assessment and kinematic analysis of the North Bozghush fault Zone, NW Iran. *Journal of Asian Earth Sciences* 164, 219-36. <https://doi.org/10.1016/J.JSEAES.2018.06.023>.
- Saber, R., Isik, V. Caglayan, A. 2020. Tectonic geomorphology of the Aras drainage basin (NW Iran): implications for the recent activity of the Aras Fault Zone. *Geological Journal.* 55, 5022-48. <https://doi.org/10.1002/gj.3724>.
- Saber, R., Caglayan, A. Isik, V. 2022. Landscape response to deformation in Sabalan area, NW Iran: Inferred from quantitative morphological and structural analysis. *Earth Environ. Sci. Trans. R. Soc. Edinb.* 113, 227-252. <https://doi.org/10.1017/S1755691022000135>
- Schwanghart, W., Scherler, D. 2014. Short communication: TopoToolbox 2-MATLAB-based software for topographic analysis and modeling in earth surface sciences. *Earth Surf. Dynam.* 2 (1), 1-7.
- Shahzad, F., Gloaguen, R. 2011. TecDEM: a MATLAB-based toolbox for tectonic geomorphology, Part 1: drainage network preprocessing and stream profile analysis. *Comput. Geosci.* 37, 250-260.
- Silva, P.G., Goy, J.L., Zazo, C., Bardají, T. 2003. Fault generated mountain fronts in southeast Spain: geomorphologic assessment of tectonic and seismic activity. *Geomorphology.* 50, 203-225.
- Tatar, M., Jackson, J., Hatzfeld, D., Bergman, E. 2007. The 2004 May 28 Baladeh earthquake (Mw 6.2) in the Alborz, Iran: over thrusting the South Caspian Basin margin, partitioning of oblique convergence and the seismic hazard of Tehran. *Geophys J Int.* <https://doi.org/10.1111/j.1365-246X.2007.03386.x>

1.8 PROBABILISTIC EARTHQUAKE RISK ANALYSES IN THE REGION OF SINDIRGI – SİNANPAŞA FAULT ZONE, TÜRKİYE

A. Günay^{1*}, A. Çağlayan², R. Saber³ and V. Isik⁴

¹Miss., Department of Geological Engineering, Ankara University, Ankara, Türkiye

²Dr., Department of Geological Survey, Ministry of Environment, Urbanisation and Climate Change, General Directorate of Spatial Planning, Ankara, Türkiye

³Dr., Department of Geological Engineering, Ankara University, Ankara, Türkiye

⁴Prof. Dr., Department of Geological Engineering, Ankara University, Ankara, Türkiye

*Corresponding author e-mail:: aycan_gunay@hotmail.com

ABSTRACT

The Sındırgı-Sinanpaşa Fault Zone is one of the most significant active fault zones in western Anatolia, Türkiye. Numerous historical (1728 – M ?, 1875 - M:6.1) and instrumental period earthquakes (1944 – Ms 6.0, 1970 – Ms 5.9, 27 June 2011 – M 5.0) have occurred along the fault zone. Therefore, Understanding the seismic behavior of the zone is critical for determining suitable settlement areas in the region. The earthquake recurrence interval was determined as the best-case and the worst-case scenario data for the region. According to the best-case scenario, the average recurrence period of earthquakes with magnitude of 5.5, 6 and 6.5 is 4 - 19 years, 19 - 68 years, and 34 - 258 years, respectively. In addition, the probability of an earthquake with a magnitude of 7.0 occurring within 50 years is 5.0% - 44.5%. In the worst-case scenario, the average recurrence period of earthquakes with magnitudes of 5.5, 6 and 6.5 is 4 – 9, 13 – 34, and 49 – 131 years, respectively. Additionally, the probability of an earthquake with a magnitude of 7.0 occurring within 50 years is 9.4% - 24.3%. Lastly, the average ground acceleration is 0.23 - 0.56 g, with a probability of exceeding 99% - 45% in 50 years for earthquakes with a radius of 100 km in the region. Our findings suggest that the region is seismically active, where risk-based approaches should be employed in establishing settlement areas.

KEYWORDS: Earthquake, Probabilistic analysis, Risk analyses, Active fault zone, Western Türkiye

INTRODUCTION

95% of earthquakes occur at active plate boundaries (Işık and Çağlayan 2018). Türkiye is located in a region where the relative movements of the Eurasian, African, and Arabian plates (Şengör and Yılmaz 1981, Çağlayan et al. 2019). The west and southwest movements of the Anatolian plate are provided by the North Anatolian Fault Zone (NAFZ) and the East Anatolian Fault Zone (EAFZ). These fault zones are the most important fault zones in Türkiye (Figure 1A).

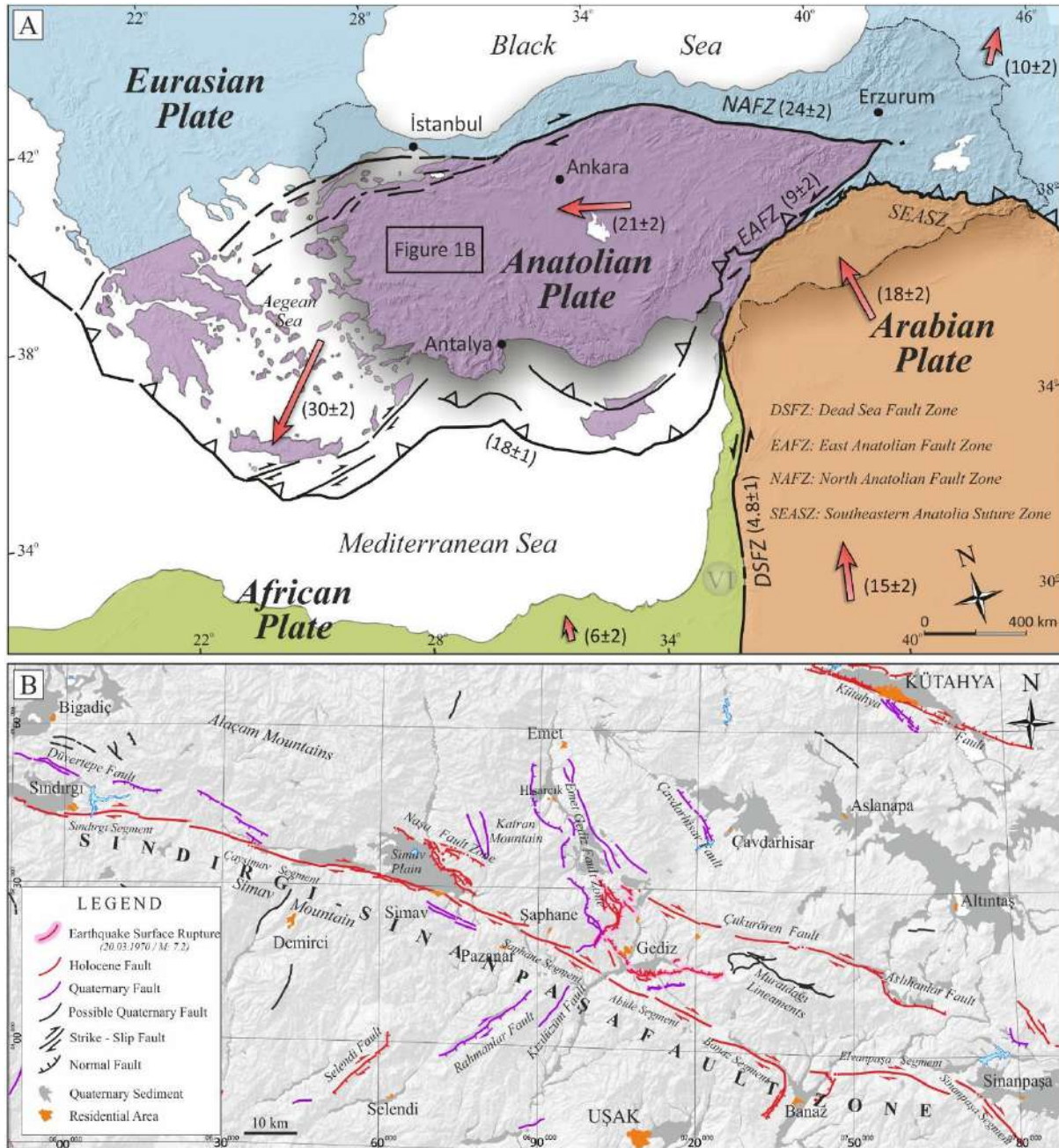


Figure1 (A) The map shows the plate geometries of Türkiye and its surroundings (taken from Caglayan et al. 2019). (B) The map shows the Sındırgı-Sinapaşa Fault Zone and active- possible active faults in the region (Faults and quaternary areas were simplified and redrawn from Emre et al. 2013)

Another important fault zone is the Sındırgı – Sinapaşa Fault Zone (Figure 1B). Although there are different opinions about the characteristics of the fault zone, it is drawn as a strike-slip fault on the Active Faults Map of Türkiye. In the literature, the features of this zone have also been presented as a normal fault, or that the faulting began as a strike-slip fault and later progressed to a normal fault. Moreover, it is an active fault zone in western Türkiye that has been classified into seven segments (Emre et al. 2013). These segments are named Sındırgı, Çayşimav, Şaphane, Abide, Banaz, Elvanpaşa, and Sinapaşa. In addition, it is a N60°W fault zone with a length of approximately 200 km between the residential areas of Sındırgı (Balıkesir) in the northwest and

Sinapaşa (Afyon) in the southeast. The activity of the Sındırgı-Sinapaşa Fault Zone and its surroundings is recorded in historical (e.g., 1728-M:?, 1875-M: 6.1, 1896-M:?) and instrumental period earthquake data (e.g., 1928-Ms: 6.1, 1944-Ms: 6.0, 28 Mart 1970-Mw: 7.2, 1970-Ms: 5.9, 17 Şubat 2009-Mw: 5.3, 19 Mayıs 2011-Mw: 5.9, 27 Haziran 2011-M: 5.0, 3 Mayıs 2012-Mw: 5.8) (Figure 2).

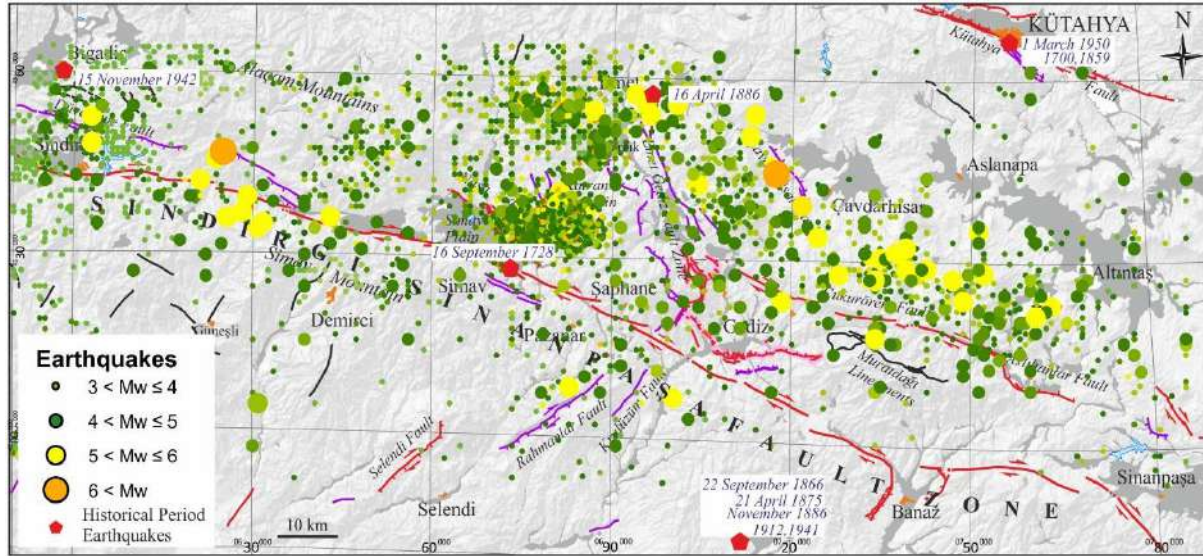


Figure2 The map shows historical and instrumental period earthquake data

The fault zone affects many settlements with medium or high population such as Alacaatlı, Sındırgı, Pürsünler, Osmanlar, İzzettin, Söğütcük, Yeniköy, Hisarbey, Ahmetli, Demirci, Simav, Yeşilköy, Kuşdemir, Hatipler, Kaplangı, Paşacık, Çayhisar. As a result, it is critical to study the tectonic activity of the Sındırgı- Sinapaşa Fault Zone, determine the earthquakes that have occurred in the past and understand the potential risks in the future.

METHOD and APPLICATION

Earthquakes of magnitude 4.5 or more that occurred along the Sındırgı-Sinapaşa Fault Zone throughout the instrumental period were determined, and a probabilistic earthquake risk analysis was performed along the zone. Earthquake data were obtained from the Boğaziçi University Kandilli Observatory and the Earthquake Research Institute Regional Earthquake-Tsunami Monitoring and Evaluation Center website. In addition, the data were taken both within a radius of 100 km from the center of the zone and regionally throughout the fault zone, and these data were compared. Moreover, four different types of earthquake magnitude data were obtained. These are body-wave magnitude (Mb), local magnitude (MI), duration-dependent magnitude (Md), and the largest magnitude value among the magnitude values given in the earthquake catalog (xM). Furthermore, Ms magnitude data were converted from MI, Md, and Mb magnitudes with formulas, and xM size was directly evaluated and interpreted. Additionally, the results obtained were interpreted both regionally and along the fault zone. Finally, the Zemin Jeofizik Analiz software prepared by Özçep (2005) was used for the study. The earthquake recurrence

interval and Poisson probability distribution were determined as the best-case and the worst-case scenario data for the region.

RESULTS

Firstly, instrumental period earthquakes with a magnitude of 4.5 and above occurring in the fault zone within a circular area with a radius of 100 km were used for the probability analysis. In the table, the Poisson probability distribution and recurrence periods were calculated according to xM and the data obtained by converting three different earthquake magnitudes into Ms magnitude (Table 1).

Table1 Poisson probability distribution and recurrence periods of the fault zone within a circular area with a radius of 100 km

	Probability for D (Year)(%)				Probability for D (Year)(%)				Probability for D (Year)(%)				Recurrence interval			
	50				75				100				(Year)			
Magnitude (M)	xM	MI	Md	Mb	xM	MI	Md	Mb	xM	MI	Md	Mb	xM	MI	Md	Mb
4.5	100	100	100	100	100	100	100	100	100	100	100	100	0	1	0	1
5	100	100	100	100	100	100	100	100	100	100	100	100	1	2	1	2
5.5	100	99.8	100	100	100	100	100	100	100	100	100	100	4	8	5	5
6	97.7	83.9	95.0	97.5	99.6	93.5	98.9	99.6	99.9	97.4	99.8	99.9	13	27	17	14
6.5	64.1	41.5	58.7	77.1	78.5	55.2	73.4	89.0	87.1	65.8	82.9	94.7	49	93	57	34
7	24.3	14.5	22.9	44.5	34.2	21	32.4	58.7	42.7	27.0	40.6	69.2	179	318	192	85

Table2 Poisson probability distribution and recurrence periods of the region with coordinates of 39.252992°N-28.048134°E / 38.661007°N – 30.248331°E

	Probability for D (Year)(%)				Probability for D (Year)(%)				Probability for D (Year)(%)				Recurrence interval			
	50				75				100				(Year)			
Magnitude (M)	xM	MI	Md	Mb	xM	MI	Md	Mb	xM	MI	Md	Mb	xM	MI	Md	Mb
4.5	100	100	100	100	100	100	100	100	100	100	100	100	1	1	1	2
5	100	100	100	100	100	100	100	100	100	100	100	100	2	5	4	6
5.5	99.6	93.7	97.7	93.2	100	98.4	99.6	98.2	100	99.6	99.9	99.5	9	18	13	19
6	76.9	51.9	67.5	56.9	88.9	66.7	81.5	71.7	94.7	76.9	89.4	81.4	34	68	44	59
6.5	31.6	17.6	28.6	23.2	43.5	25.3	39.6	32.6	53.3	32.2	49.0	40.9	131	258	149	190
7	9.4	5.0	9.6	7.9	13.8	7.4	14.0	11.6	17.9	9.8	18.2	15.2	507	973	497	606

Secondly, instrumental period earthquakes with a magnitude of 4.5 and above occurring in the region with coordinates of 39.252992°N-28.048134°E / 38.661007°N – 30.248331°E were used for probability analysis. In the table, the Poisson probability distribution and recurrence periods were calculated according to xM and the data was obtained by converting three different earthquake magnitudes into Ms magnitude (Table 2).

Thirdly, instrumental period earthquakes that occurred both within a circular area with a radius of 100 km and at the coordinates of 39.252992°N-28.048134°E / 38.661007°N – 30.248331°E, according to the magnitude specified as xM in the catalog, were used. In the table, the Poisson probability distribution and recurrence periods were calculated according to xM (Table 3).

Table3 According to xM, Poisson probability distribution and recurrence periods of the fault zone within a circular area with a radius of 100 km, and at the coordinates of 39.252992°N-28.048134°E / 38.661007°N – 30.248331°E

	Probability for D (Year)(%)		Probability for D (Year)(%)		Probability for D (Year)(%)		Recurrence interval	
	50		75		100		(Year)	
Magnitude (M)	xM- 100km radius	xM- coordinates	xM- 100km radius	xM- coordinates	xM- 100km radius	xM- coordinates	xM- 100km radius	xM- coordinates
4,5	100	100	100	100	100	100	0	1
5	100	100	100	100	100	100	1	2
5,5	100	99.6	100	100	100	100	4	9
6	97.7	76.9	99.6	88.9	99.9	94.7	13	34
6,5	64.1	31.6	78.5	43.5	87.1	53.3	49	131
7	24.3	9.4	34.2	13.8	42.7	17.9	179	507

Lastly, in the study area, the danger level for 5.9 - 7.0 magnitude earthquakes has been calculated for a 50-year building life. The average ground acceleration was determined to vary between 0.23 and 0.56 g, and the probability of exceeding 99% - 45% was calculated. It was determined that such earthquakes pose a high danger for earthquakes with a radius of 100 km in the region.

CONCLUSIONS

The earthquake recurrence interval was determined as the best-case and the worst-case scenario data for the region. The best-case scenario was determined from the region limited by the coordinates and within a circular area with a radius of 100 km in the region. The worst-case scenario was determined from the region with both limited coordinates and the regional with xM values. Thus, the following results were obtained:

i) According to the best-case scenario, the average recurrence period of earthquakes with a magnitude of 5.5 is 4 - 19 years, while the average recurrence period of earthquakes with a magnitude of 6.0 is 13 - 68 years. Moreover, the average recurrence period of earthquakes with a magnitude of 6.5 is 34 - 258 years. In addition, the probability of an earthquake with a magnitude

of 7.0 occurring within 50 years is 5.0% - 44.5%, and the probability of an earthquake with a magnitude of 7.0 occurring within 100 years is 9.8% - 69.2%.

ii) In the worst-case scenario, the average recurrence period of earthquakes with magnitudes of 5.5, 6 and 6.5 is 4 – 9, 13 – 34, and 49 – 131 years, respectively. Additionally, the probability of an earthquake with a magnitude of 7.0 occurring within 50 years is 9.4% - 24.3%, and the probability of an earthquake with a magnitude of 7.0 occurring within 100 years is 17.9% - 42.7%.

The average ground acceleration is 0.23 - 0.56 g, with a probability of exceeding 99% - 45% in 50 years for earthquakes within a circular area with a radius of 100 km in the region. Our findings suggest that the region is seismically active and that risk-based approaches should be employed in establishing settlement areas.

REFERENCES

- Çağlayan, A., Isik, V. and Saber, R. 2019. Paleoseismologic evidence for Holocene activity on 1944 earthquake segment, north Anatolian fault zone. *Geosciences Journal*, 23(5), 805–822. <https://doi.org/10.1007/s12303-018-0075-3>.
- Emre, Ö., Duman, T.Y., Özalp, S., Olgun, Ş., Elmacı, H. and Şaroğlu, F. 2013. Açıklamalı Türkiye Diri Fay Haritası. MTA, Özel Yayın Serisi-30, Ankara.
- Isık V. and Çağlayan A., 2018. Afet Risk Azaltma Politikaları Ders Kitabı, Bölüm 6: Doğa Kaynaklı Afet Risk Azaltma Stratejileri-I: Deprem. Eskişehir: Anadolu Üniversitesi, 156-181, ISBN: 978-975-06-2327-1, Yayın Nu:2545
- Özçep, F. 2005. "Zemin Jeofizik Analiz", Microsoft® Excel Programı, G.Ü. Müh. Fak. Jeofizik Müh. Böl., İstanbul.
- Şengör, A. M. C. and Yılmaz, Y. 1981. Tethyan evolution of Turkey: A plate tectonic approach. *Tectonophysics*, 75, pp. 181-241.

1.9 MORPHOTECTONIC CHARACTERISTICS AND PALEOSEISMOLOGICAL ANALYSIS OF ARAS FAULT ZONE (NW IRAN); PRELIMINARY RESULTS FROM REMOTE SENSING AND FIELD STUDIES

R. Saber^{1*}, V. Isik², A. Caglayan³, F. Chitea^{4,5}

¹Dr., Department of Geological Engineering, Ankara University, Ankara, Türkiye

²Prof. Dr., Department of Geological Engineering, Ankara University, Ankara, Türkiye

³Dr., Department of Geological Survey, Ministry of Environment, Urbanisation and Climate Change, General Directorate of Spatial Planning, Ankara, Türkiye

⁴Lect. Dr., Department of Engineering Geology and Geophysics, Bucharest University, Bucharest, Romania

⁵Lect. Dr., Institute of Geodynamics of the Romanian Academy, Bucharest, Romania

*Corresponding author e-mail: reza-saber@hotmail.com

ABSTRACT

Remarkable geological features within the Alpine-Himalayan Orogenic belt can be mapped on the territory of Iran. Crustal-scale fault zones with different characteristics, surrounded by mountain ranges and a history of numerous destructive earthquakes, make the NW of Iran an open-space geodynamic laboratory. In NW Iran, the NE-SW striking left-lateral strike-slip Aras Fault Zone (AFZ) exhibits an approximately 240 km length and 0.6~35 km width on the Iran and Azerbaijan border. Morphotectonic features such as stream channel offsets, shutter and pressure ridges, fault-bonded young folds, and restraining and releasing bends were observed and documented along the Aras Main fault and other fault branches of the AFZ (Horadiz, Khodafarin, Aslanduz and Asadkandi).

The left lateral displacement amounts along the AFZ range from a few to hundreds of meters. Higher offset was observed on the SW parts of the Aras Main and Horadiz fault branches, whereas on the Aslanduz and Asadkandi branches in the NE sections, the offset gradually decreased. Four Paleoseismological trenches were excavated on different branches of AFZ to investigate faulting characteristics and to search for traces of historical seismic events embedded within the geological layers. Among the investigation techniques used in the research, the radiocarbon dating of samples was used for documenting the two historical seismic events. Occurred between 3600-2400 BC and 2050-750 BC. The results emphasize that no surface rupture is related to large earthquakes after 750 BC along the investigated segments. Additionally, they can be used for evaluating the earthquake recurrence, which, based on the 14C dating, is estimated within an interval between 1500 and 3000 years.

KEYWORDS: Tectonic geomorphology, Paleoseismology, 14C dating, Earthquake recurrence period, Iran

INTRODUCTION

The Alpine-Himalayan Belt represents a young orogeny, which has developed due to the collision of the Gondwana and Eurasian Plates. The orogeny extends for approximately 10.000 km from Spain in the west to Southeast Asia (e.g., Stocklin, 1968, McKenzie, 1978) (Figure 1A). NW Iran is one of the significant examples of intra-plate deformation areas due to hosting numerous regional-scale strike-slip fault zones (e.g., Masson et al., 2006, Berberian, 2014, Saber et al., 2020, 2021) (Figure1B).

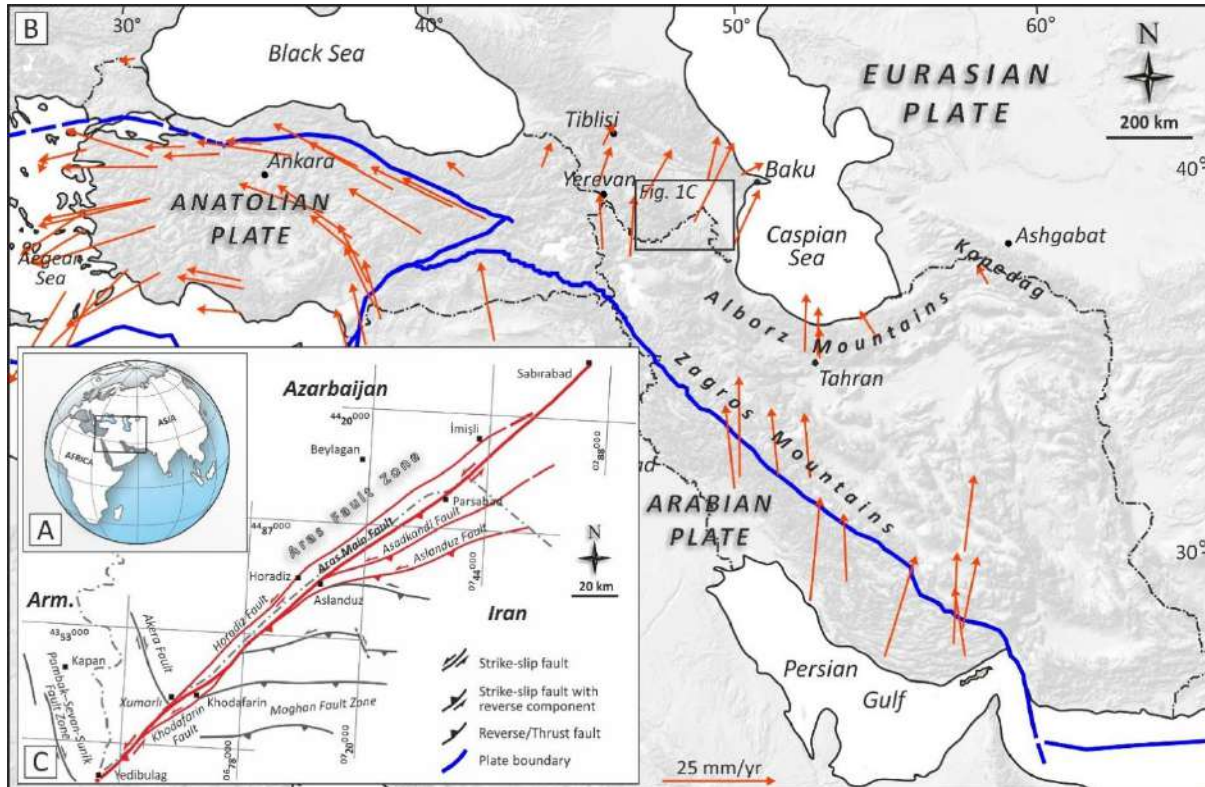


Figure1 (A and B) maps illustrating the global and regional location of the Aras Fault Zone, (C) a simplified map showing the geometry of the Aras Fault Zone.

In terms of neotectonic, Iran represents a prominent active intracontinental collision zone within the Alpine-Himalayan Orogenic Belt. The initial formation and evolution of the orogeny is linked to the collision of the African and European plates in the west (Cisternas and Philip 1997) and the collision of the Indian and Asian plates in the east. The Turkish-Iranian Plateau collision resulted in the development of structures such as right-lateral and left-lateral strike-slip faults, N-S-oriented normal faults, and thrust/reverse faults in the E-W direction (Şengör et al., 1985). Copley and Jackson (2006) explained the main structures as right-lateral and left-lateral strike-slip faults, N-S-oriented normal faults, and rotating blocks. NW Iran is one of the significant examples of intra-plate deformation areas due to hosting numerous regional-scale strike-slip fault zones (e.g., Berberian, 2014, Saber et al., 2018, 2020). The Aras Fault Zone (AFZ), as one of the best examples of the transpressional tectonic regime in the region, represents prominent morphological features in NW Iran (Saber et al., 2020, 2021) (Figure 2). The AFZ is an active fault zone situated on Iran and Azerbaijan border (Saber et al., 2021) (Figure 1C). The NE-SW striking fault zone extends from Yedigöller (Iran) to Sabirabad (Azerbaijan), which represents left-lateral strike-slip fault characteristics with a traceable length of about 240 km and a width of 0.6 km to ~35 km (Figure

2). However, the zone does not exhibit the same faulting geometry, patterns, and characteristics along its entire length. The southwestern part of the zone represents a relatively narrow zone, while the central part is characterized by anastomosing faulting geometry. In contrast, the zone displays horsetail fault geometry in the northeastern domain (Saber et al., 2021). The AFZ interacts with other major fault zones, NW-SE oriented Akera and Pambak-Sevan-Sunik, and E-W striking Moghan Fault Zones in its western and eastern blocks, respectively (Figure 1C).

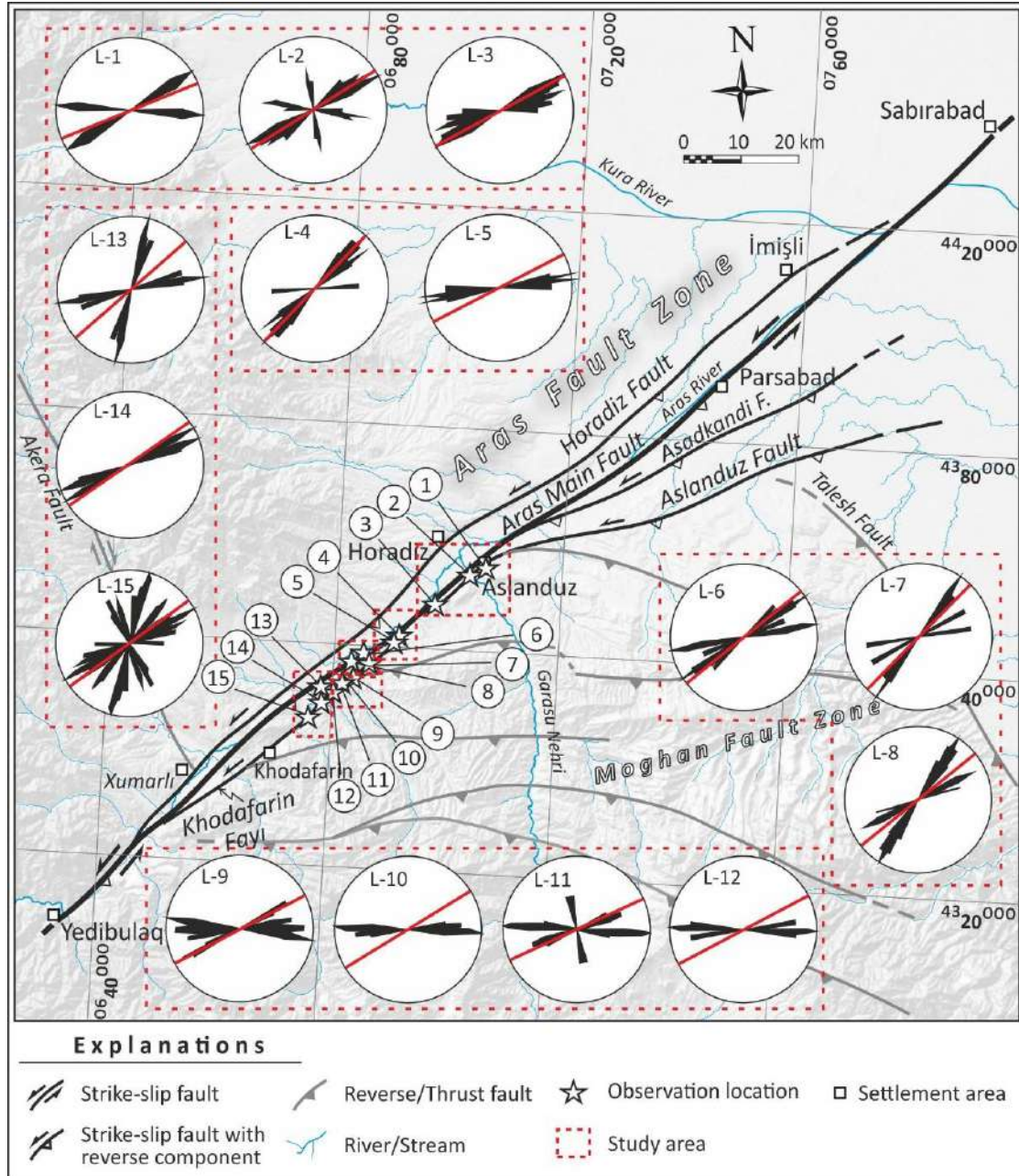


Figure2 A map showing the geometrical features of the Aras Fault Zone. Rose diagrams display the plane direction of the observed faults in field studies. Thick red lines represent the general direction of the AFZ in study locations. Digits within circles indicate study locations.

METHOD and APPLICATION

Various morphotectonic indicators were analyzed, distinguished, and mapped on different fault branches of the AFZ to estimate the current tectonic activity condition of the fault zone. For paleoseismology studies, several trenches were excavated in appropriate places on the AFZ and geological units and structural elements on the trench walls were documented. Furthermore, several samples were collected from the trench walls for ¹⁴C (Radiocarbon) dating studies. The dating results were then evaluated with the OxCal v4.4 program to estimate earthquake events and recurrence intervals.

RESULTS

Morphotectonic

The AFZ comprises five fault branches based on geometrical relationships and structural properties (Saber et al., 2020) called the Aras Main, Horadiz, Khodafarin, Asadkandi, and Aslanduz fault branches.

The NE–SW striking Aras Main fault extends between Yedibulaq (Iran) and Sabirabad (Azerbaijan) and terminates gradually in young deposits (Figure 2). The fault branch displays slightly curved geometry with a general direction between N43°–61°E and dip amounts of 50–85° to the SE, according to field observations. Field observations and remote sensing studies reveal a few hundred meters of left-lateral displacement along the Main fault (Figure 3A).

The Horadiz fault represents 110 km of traceable length, linking to the Aras Main fault in the SW and NE of Xumarlı and Imishli settlement areas, respectively (Figure 2). The slightly curved fault cuts Plio-Quaternary and Quaternary young deposits with the general direction of N36°–62°E (Figure 2). Distinct left-lateral displacements on stream channels are among characteristic morphotectonic features along the Horadiz Fault (Figure 3B, C). Additionally, shutter ridges, beheaded streams, and alluvial fan offsets have also developed due to the neotectonic activity of the Horadiz Fault (Figure 3B, C).

The Khodafarin fault represents a curved-shape fault branch that deviates from the Aras Main fault in the southwest of Khodafarin and constitutes a NE-SW oriented fault block by relinking to the Main Fault (Figure 2). The Khodafarin fault represents the shortest fault branch of the AFZ with approximately 50 km of N48°–57°E striking traceable length. Measured stream channel offsets reveal hundreds of meters of left-lateral displacement along the Khodafarin fault (Figure 4A).

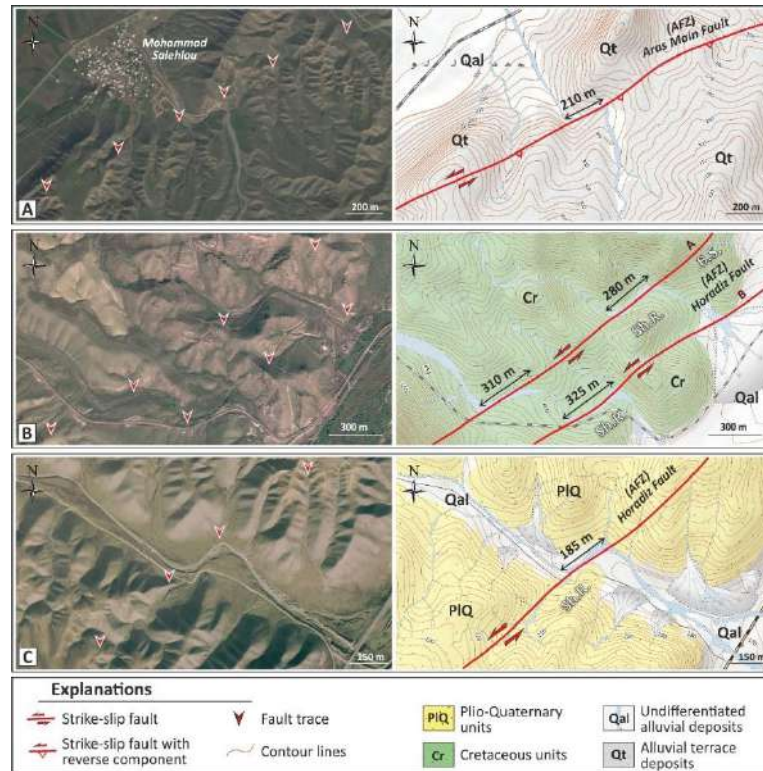


Figure3 Google Earth satellite images (left) and topographic maps (right) show morphotectonic indicators and offset stream channels along different fault branches of the AFZ. (A) The Aras Main Fault, (B, C) the Horadiz Fault.

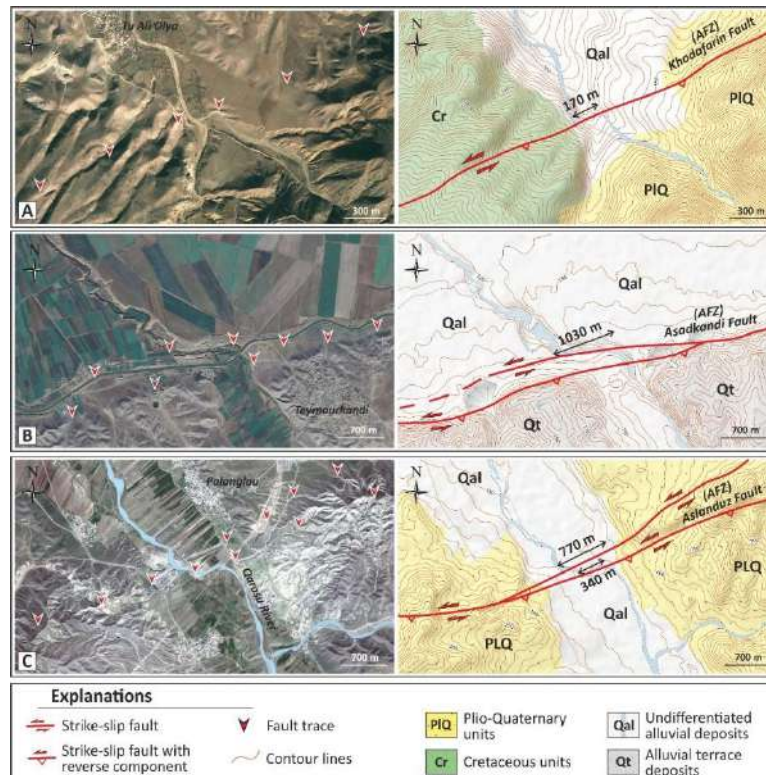


Figure4 Google Earth satellite images (left) and topographic maps (right) show morphotectonic indicators and offset stream channels along the AFZ. (A) The Khodafarin Fault, (B) the Asanduz Fault, (C) the Asadkandi Fault.

The Asadkandi and Aslanduz Faults represent the northeastern part of the AFZ. These fault branches deviate from the Aras Main Fault and form horsetail fault geometry (Figure 2). The Asadkandi Fault separates from the Aras Main Fault in NE of Aslanduz city with a general direction that varies between N59°–70°E and approximately 60 km of traceable length. The fault affects Quaternary units and terminates in young Holocene deposits to the northeast (Figure 2). Various amounts of vertical displacements, stream channel offsets, and the development of asymmetric and displaced alluvial fans were documented along the Asadkandi Fault (Figure 4B).

The curve-shaped Aslanduz fault deviates from the Aras Main Fault in the south of Marjan village and passes through the south of Aslanduz city, then terminates in Quaternary sediments and Holocene deposits of the Kura Basin to the north, with a traceable length of about 90 km (Figure 2). The direction of the fault varies slightly; while it exhibits a similar trend to the Aras Main Fault in the SW part, it presents a significant curvature geometry in the northeastern extension with N49°-79°E directions dipping to the SE. Linear mountain front, stream channel offsets, prominent displacements of alluvial fans, and asymmetrically developed fans are among distinct neotectonic morphological features along the Aslanduz Fault. About 770 m of left-lateral stream channel offset on the Qarasu River (Figure 4C) demonstrates the recent tectonic activity of the zone, as well.

Paleoseismology

The trench was excavated in the NE part of Aslanduz, near the new city hospital. The main purpose was to understand the geometry and potential seismic activity of the NE-SW trending Asadkandi Fault. The trench study was conducted on the N70°E striking fault trace cutting the Quaternary units. The length, width, and depth of the N20°W oriented trench were 25 m, 1.5-2 m, and 2.5 - 3 m, respectively (Figure 5).

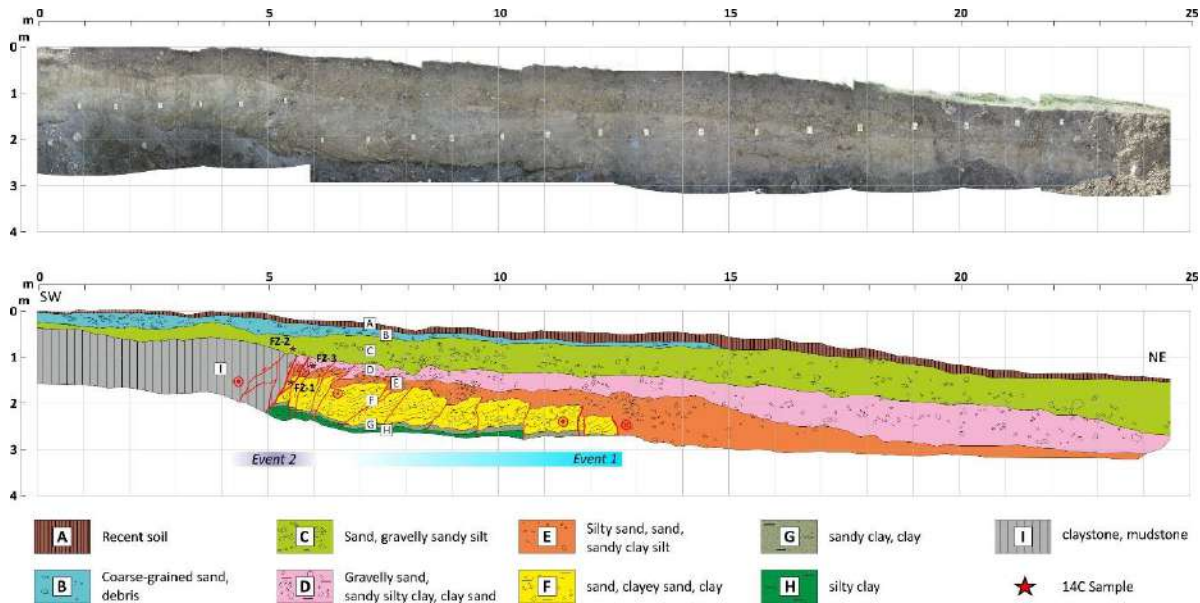


Figure 5 Photomosaic and log view of the western wall of the trench opened on the Asadkandi Fault.

14C dating results revealed the occurrence of at least two destructive earthquakes with surface faulting during the Holocene in this part of the AFZ. One of the events was estimated to have occurred between 3600 and 2400 BC, and the other between 2050 BC and 750 BC. Moreover, no evidence of surface faulting has been found in this part of this AFZ for the last 2750 years. Considering the results, the earthquake recurrence interval is quite wide and is calculated between 1500 and 3000 years (Figure 6). This recurrence interval explains the lack of destructive seismic records for the recent past along the Asadkandi Fault.

OxCal v4.4.4 Bronk Ramsey (2021); r:5 Atmospher?c data from Re?mer et al (2020)

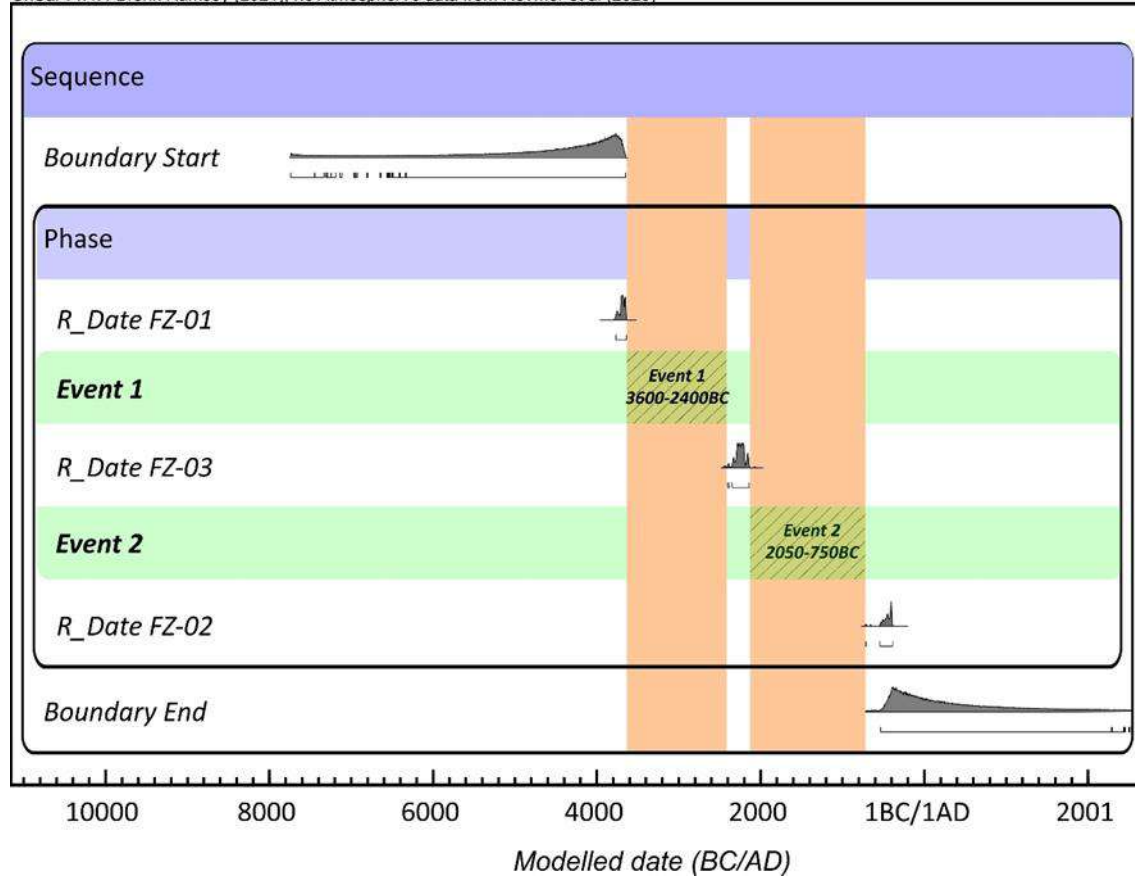


Figure6 Calibration of dating results obtained from a trench on the AFZ using the OxCal v4.4 (Reimer et al. 2020, Bronk Ramsey 2021).

CONCLUSIONS

The main conclusions reached in this study are:

1. The Aras Fault Zone is divided into 5 main fault branches of different lengths and widths, including numerous parallel or nearly parallel fault strands. The effect of recent faulting activity on stream channels and alluvial fans is considerable along the study area.
2. At least two destructive earthquakes with surface faulting during the Holocene in this part of the AFZ. One of the events was estimated to have occurred between 3600 and 2400 BC, and the other between 2050 BC and 750 BC. Moreover, no evidence of surface faulting has been found in this part of this AFZ for the last 2750 years. Considering the results, the earthquake recurrence

interval is quite wide and is calculated between 1500 and 3000 years. This result indicates the lack of destructive seismic records for the recent past along the fault zone.

REFERENCES

- Berberian, M., 2014. Earthquakes and Co-seismic active faulting on the Iranian plateau, a historical, social and physical approach. *Develop. Earth Surf. Processes*. 17, 776.
- Bronk Ramsey, C., Heaton, T.J., Schlolaut, G., Staff, R.A., Bryant, C.L., Brauer, A., Lamb, H.F., Marshall, M.H., and Nakagawa, T. 2020. Reanalysis of the atmospheric radiocarbon calibration record from Lake Suigetsu, Japan. *Radiocarbon*, 62, 989–999.
- Cisternas, A., and Philip, H. 1997. Seismotectonics of the Mediterranean region and the Caucasus. In: Giardini, D., Balassanian, S. (Eds.), *Historical and Prehistorical Earthquakes in the Caucasus*. Kluwer Academic Publishing, Dordrecht, the Netherlands, 39–77.
- Copley, A., Jackson, J. 2006. Active tectonics of the Turkish–Iranian plateau. *Tectonics*, 25, TC6006. <https://doi.org/10.1029/2005TC001906>.
- Masson, F., Djamour, Y., Van Gorp, S., Chery, J., Tatar, M., Tavakoli, F., Nankali, H., and Vernant, P. 2006. Extension in NW Iran driven by the motion of the south Caspian basin. *Earth Planetary Science Letters*, 252, 180–188.
- McKenzie, D., 1978. Active tectonics of the Alpine-Himalayan Belt: the Aegean Sea and surrounding regions. *Geophys. J. R. Astron. Soc.* 55, 217–254.
- Reimer, P.J., Austin, W.E.N., Bard, E., Bayliss, A., Blackwell, P.G., Bronk Ramsey, C., Butzin, M., Cheng, H., Edwards, R.L., Friedrich, M., Grootes, P.M., Guilderson, T.P., Hajdas, I., Heaton, T.J., Hogg, A.G., Hughen, K.A., Kromer, B., Manning, S.W., Muscheler, R., Palmer, J.G., Pearson, C., van der Plicht, J., Reimer, R.W., Richards, D.A., Scott, E.M., Southon, J.R., Turney, C.S.M., Wacker, L., Adolphi, F., Büntgen, U., Capano, M., Fahrni, S.M., Fogtmann-Schulz, A., Friedrich, R., Köhler, P., Kudsk, S., Miyake, F., Olsen, J., Reinig, F., Sakamoto, M., Sookdeo, A., and Talamo, S. 2020. The IntCal20 Northern Hemisphere radiocarbon age calibration curve (0–55 cal kBP). *Radiocarbon*, 62: 725–75.
- Saber, R., Caglayan, A., Isik, V. 2018. Relative tectonic activity assessment and kinematic analysis of the north Bozgush fault zone, NW Iran. *Journal of Asian Earth Sciences*, 164, 219–236. <https://doi.org/10.1016/J.JSEAES.2018.06.02>.
- Saber, R., Isik, V., Caglayan, A., 2020. Tectonic geomorphology of the Aras drainage basin (NW Iran): implications for the recent activity of the Aras Fault Zone. *Geol. J.* 55 (7), 5022–5048. <https://doi.org/10.1002/gj.3724>.
- Saber, R., Isik, V. and Caglayan, A. 2021. Structural styles of the Aras fault zone with implications for a transpressive fault system in NW Iran. *Journal of Asian Earth Sciences* 207, 104655. <https://doi.org/10.1016/j.jseaes.2020.104655>.
- Stocklin, J. 1968. Structural History and Tectonics of Iran: A Review. *American Association of Petroleum Geologists Bulletin*. 52, 1229–1258.
- Şengör, A.M.C., Görür, N. and Şaroğlu, F. 1985. Strike-slip faulting and related basin formation in zones of tectonic escape: Turkey as a case study, in *Strike-slip Faulting and Basin Formation*, edited by Biddke, K.T. and Christie-Blick, N., Society of Econ. Paleont. Min. Sp. Publ., 227-264.

2.1 GEOPHYSICAL INSIGHTS INTO THE TECTONIC REGIME OF THE CHANIA BASIN IN THE AEGEAN REGION

P. Kirmizakis¹, U. Dikmen² and P. Soupios^{1*}

¹*Department of Geosciences, College of Petroleum Engineering & Geosciences, King Fahd University of Petroleum & Minerals, Dhahran, Saudi Arabia*

²*Department of Geophysical Engineering, Ankara University, Ankara, Turkey*

**Corresponding author e-mail: panteleimon.soupios@kfupm.edu.sa*

ABSTRACT

This study focuses on one of the most seismically active regions within the Aegean area, where microzonation studies play a crucial role in earthquake engineering design. The study's purpose is to enhance understanding of the seismic behavior of the Chania basin, contributing valuable insights into its tectonic regime. Given the region's high seismic activity, the accurate determination of seismic parameters is essential for designing resilient structures. The research centers on the critical parameter of average S-wave velocity (V_{s30}) within the top 30 meters of subsoil, as mandated by EUROCODE 8, the European seismic-resistant design standard. A comprehensive geophysical field campaign was undertaken in the Chania basin to achieve these objectives. This campaign included various geophysical methods, encompassing seismic, electric, and electromagnetic surveys. The data collection involved diverse techniques, such as TEM soundings, circular seismic arrays, passive and active linear surface waves, seismic profiles, geoelectrical resistivity imaging, and HVSr measurements. These combined methods aimed to provide a holistic view of the basin's subsurface properties. The study's primary contribution lies in its application of modern geophysical techniques to unravel the tectonic dynamics of the Chania/Souda basin. Through the integration of various geophysical datasets, the study presents a preliminary understanding of the region's tectonic framework. The importance of employing surface geophysics as a powerful tool for large-scale tectonic investigations is highlighted, particularly for complex systems. The results obtained from TEM measurements were meticulously assessed and validated using borehole data, enhancing the reliability of the findings. Through the construction of 2D pseudo sections, the study successfully identified geological formations and new fault structures. This comprehensive knowledge of the basin's geological and tectonic characteristics is a foundational resource for future regional seismotectonic studies and earthquake vulnerability assessments. In conclusion, this research sheds light on the Chania basin's seismic behavior and tectonic regime through the innovative application of a wide array of geophysical methods. By providing valuable insights into the subsurface properties and fault structures, the study advances the understanding of this seismically active region and offers a basis for informed decision-making in earthquake hazard mitigation and infrastructure design.

KEYWORDS: seismic dynamis, transient electromagnetics, Chania basin, geophysical insights, tectonic regime

2.2 SEISMIC SHIELDING OF URBAN AREAS BY USING INTEGRATED GEOPHYSICAL METHODS

P. Kirmizakis^{1*}, G. Kritikakis², E. Kokkinou³, N. Theodoulidis⁴, B. Margaritis⁴, N. Papadopoulos⁵, M. Steiakakis², U. Dikmen⁶, M. Mangriotis⁷, A. Savaidis⁸, C. Loupasakis⁹, A. Vafidis² and P. Soupios¹

¹Department of Geosciences, College of Petroleum Engineering & Geosciences, King Fahd University of Petroleum & Minerals, Dhahran, Saudi Arabia

²School of Mineral Resources Engineering, Technical University of Crete, Chania, Greece

³Department of Agriculture, Hellenic Mediterranean University, Heraklion, Greece

⁴Institute of Engineering Seismology and Earthquake Engineering (EPPO), Thessaloniki, Greece

⁵Institute for Mediterranean Studies, Foundation for Research & Technology Hellas, Heraklion, Greece

⁶National Oceanography Centre Southampton (NOCS), University of Southampton, UK

⁷Department of Geophysical Engineering, Ankara University, Ankara, Turkey

⁸University of Texas, Texas, USA

⁹School of Mining and Metallurgical Engineering, National Technical University of Athens, Athens, Greece

*Corresponding author e-mail: p.kirmizakiss@kfupm.edu.sa

ABSTRACT

Estimating the strong motion parameters for the shallow geological formations is essential for engineering seismology, earthquake hazard assessment, design of structures, soil mechanics, and development of ground motion prediction equations. These parameters provide valuable information that helps engineers and seismologists design earthquake-resistant structures and infrastructure. For this reason, the sites of the accelerometer network must cover different geological settings and provide accurate measurements of ground motion during an earthquake. In this research, the Crete Island in Greece was selected as a well-known region prone to earthquakes, to characterize the subsurface of the accelerometer sites by using a combination of geophysical and geological data to analyze the strong motion parameters of shallow geological formations. The study area comprises a variety of geological and tectonic settings, making it an ideal location for investigating the effects of different geological conditions on ground motion parameters.

KEYWORDS : geocharacterization, multiphysics, earthquake hazard assessment

2.3 RESISTIVITY IMAGE OF LEAKAGE FROM ÇANAKKALE OLD OPEN WASTE DISPOSAL SITE

E. Ş. Uluocak¹, E. Ulugergerli^{1*}

¹Department of Geophysical Engineering, Çanakkale 18 March University, Çanakkale, Türkiye

*Corresponding author e-mail: emin@comu.edu.tr

ABSTRACT

In this study, we focus on an environmental geophysical study of the former open waste disposal site of Çanakkale, Turkey, which was actively used between 1989 and 2009. We investigate the spatiotemporal variations of pollution from the unregulated landfill using direct current (DC) electrical resistivity method and in situ pH and electrical conductivity measurements in leachate-contaminated water. The results indicate the variation of pollution from the open waste disposal site, which is characterized by low resistivity values (≤ 10 Ohm-m) in the 2D resistivity sections, during the years of geophysical measurements (2004–2008–2009). We propose that geochemical analyses and geophysical measurements that provide a robust approach to subsurface contaminant diffusion can be highly effective in municipal solid waste management studies within the context of sustainable environmental policies.

KEYWORDS: Environmental geophysics, DC resistivity, Leachate, Environmental sustainability

INTRODUCTION

In the relatively shallow geophysical surveys for environmental purposes, the general steps can be defined as follows; i) identification of the phenomenon that may cause a potential environmental problem (e.g., a source of pollutants); ii) definition of the main physical processes that can be affected by source(s) (e.g., decomposition, gas released, heavy metal accumulation in the soil and water, etc.); iii) determination of the suitability and limits of the geophysical method(s) together with multidisciplinary approaches; iv) survey design; v) applications; and finally vi) interpretations.

Specifically, in an open waste site, the geological structures (e.g., type and thickness of strata, bedrock), water table and its relationship with possible fractures, and spatiotemporal variation of contamination in relation to leachate are investigated by using geophysical methods. Here, we show a case study to analyze the potential pollution hazard caused by Çanakkale old open waste disposal site that was used actively during 1989 to 2009. Our results give important insight into diffusion of the pollutant, sourced by the waste area, by means of resistivity variation.

METHOD and APPLICATION

Electrical conductivity, generally, depends on properties of the ground, such as temperature, pressure, porosity, permeability, saturation, and the distribution of fluid. Further, the salinization

and resulting high ion concentration in the soil are important parameters that are affecting the electrical features of the medium. Gradual contamination of groundwater and soil over time, mainly owing to the leachate from chemical reactions with dissolved pollutants in the waste sites, increases the ion concentration and conductivity compared to their surroundings. Thus, it is possible to identify contaminated areas with geophysical methods that are sensitive to the conductivity (or resistivity) contrast beneath the surface. Given its non-destructive nature, fast and highly accurate results, and relatively low cost, the DC resistivity method we used in this study (Figure 1a) is one of the most widely used geophysical methods to characterize contamination in the subsurface. Accordingly, the geophysical survey was designed based on the conceptual model (Figure 1a) showing the profiles in Figure 1b oriented in the groundwater flow direction depending on the slope.

In this study, for the first time we also present pH and conductivity changes from in-situ measurements in the water, including the samples in the creek which may have been mixed with leachate, to define the landfill-induced environmental pollution in the study region.

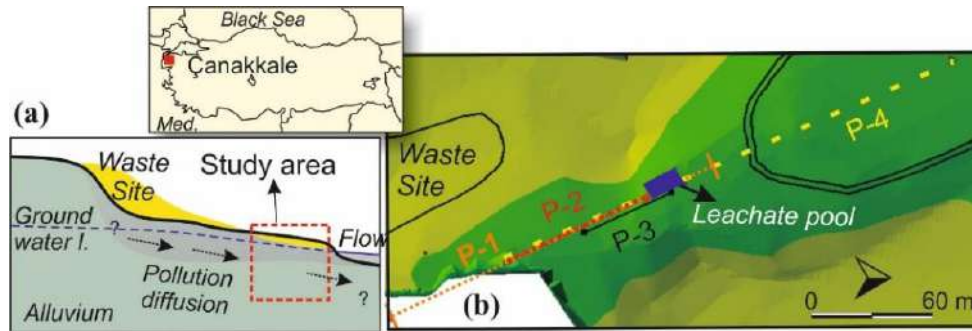


Figure1 (a) Conceptual model of the study area (inset show location of Çanakkale). (b) Profiles for geophysical survey (Şengül Uluocak & Uluggerli, 2023 and references therein).

DISCUSSION and RESULTS

2D resistivity sections in Figures 2a and 2b show low resistivity zones (≤ 10 Ohm-m) that can be interpreted as contaminated areas caused by diffused leachate beneath the region. In the SE, a zone closest to the waste site, the penetration of pollutants is characterized by very low resistivity values of ≤ 2 Ohm-m. Similarly, high conductivity zone obtained towards the NW in P-1 (Figure 2a) indicates the pollution that leaks from the artificial leachate pool and cannot be observed from the surface during the survey.

Our water analyses support the studies suggesting a linear relationship between the age of a landfill and leachate's pH values (Özkıdık, 1995). The locations of in-situ measurements made in the years of 2004 and 2009 are shown in Figure 3. Accordingly, both pH and electrical conductivity (Ec) variations (Table 1) resulted from the pollutant concentration in the samples are considerably higher than those recommended for meteoric waters and/or the inland water quality standards (e.g., Öz & Ertaş, 2016). Conductivity values, as expected, decrease in 2004 (Table 1) following the decreasing pollutant concentration especially in the samples of 1 and 2 mixed with surface water in the creek. However, same samples (1 and 2) appear to have become more contaminated over years (i.e., from 2004 to 2009, Table 1) due to the ongoing leachate transport from the waste site.

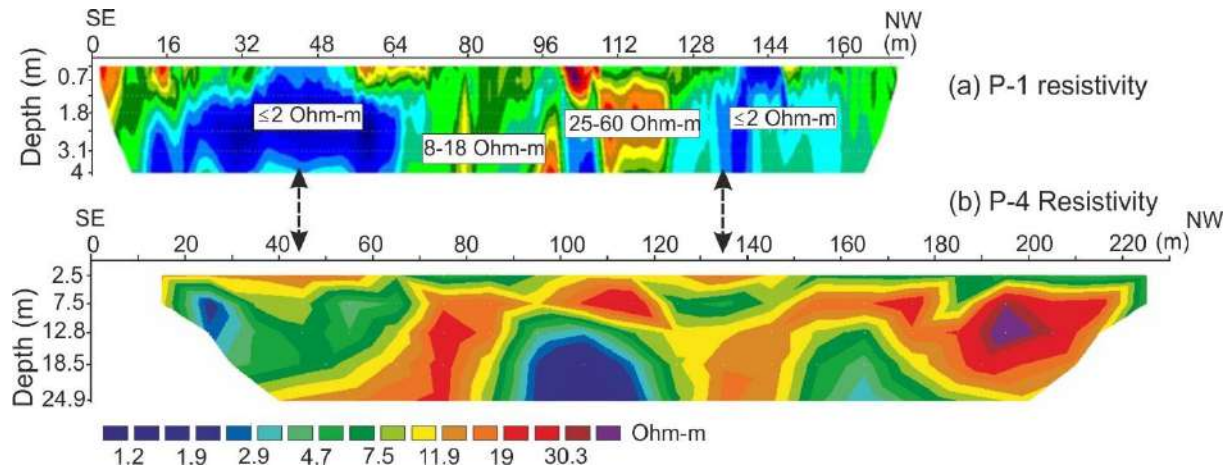


Figure2 2D resistivity section obtained from electrical measurements in (a) P-1 (in 2004, Şengül, 2004; Kaya et al., 2007) and (b) Profile P-4 (2009, Beşkardeş, 2009).

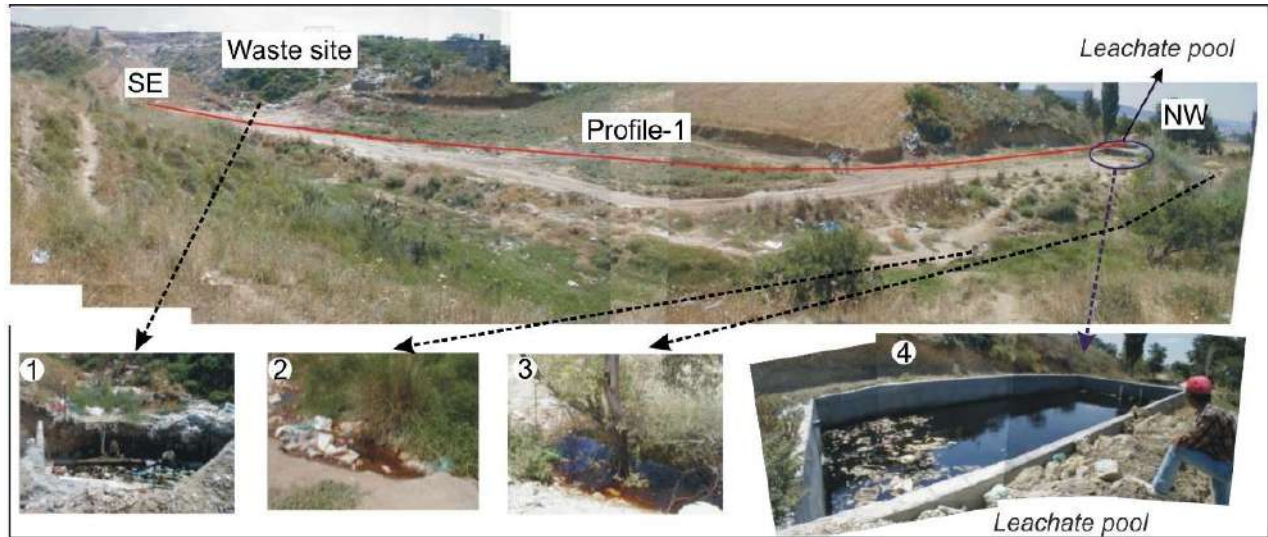


Figure3 Study area, the locations of water samples for the in-situ pH and conductivity measurements (Şengül, 2004, Aksakal, 2008).

Table1 PH and the electrical conductivity variations obtained in water samples in the years of 2004 and 2009 (during the survey periods-summer 2004 and 2009, the average temperature of the samples is 30,9 °C and 25,32 °C, respectively, Şengül, 2004, Aksakal, 2008).

Sample #	2004- pH	2009- pH	2004 Conductivity(mS/cm)	2009 Conductivity(mS/cm)
1	7,91	8,61	33,4	23,4
2	7,13	8,47	7,03	31,8
3	7,75	8,06	8,49	35,5
4	8,38	8,83	22,5	50,5

CONCLUSION

Geophysical results reveal that pollution from leachate characterized by low resistivity zones continued over years during the geophysical survey in 2004–2008–2009. Water analyses also show that conductivities increased from 22,5 mS/cm to 50,5 mS/cm in the pool (Table 1) over time due to pollutant concentration.

Overall, our findings provide important insight into the long-lasting effects of environmental pollution caused by open waste disposal sites. As shown here, geophysical research in collaboration with water analyses can be highly functional in urban solid waste management studies within the context of sustainable environmental policies.

ACKNOWLEDGEMENT

We would like to thank Sevgi AKSAKAL and Didem BEŞKARDEŞ, and our undergraduate students of the 2004-2009 academic years who contributed to geophysical measurements.

REFERENCES

- Aksakal, S. (2008). Katı atık depolama sahalarından toprak ve yeraltı suyuna olan sızıntıların elektrik özdirenç ve yapay uçuşma yöntemleri ile araştırılması. Lisans Tezi/Undergraduate Thesis, ÇOMÜ Mühendislik Fakültesi, Jeofizik Müh. Bölümü (in Turkish).
- Beşkardeş, G.D. (2009). Çanakkale katı atık depolama sahası için yeraltı suyu kirliliğinin modellenmesi. Uluslararası Deprem Sempozyumu (özet bildiri-poster, s. 89), 17-19 Ağustos, 2009, Kocaeli, (in Turkish).
- Kaya, M. A., Özürlan, G. & Şengül, E. (2007). Delineation of soil and groundwater contamination using geophysical methods at a waste disposal site in Çanakkale, Turkey. Environ Monit Assess. 135, 441–446.
- Öz, Ü., & Ertaş, E. (2016). Arılı Deresi (Rize)'nin fiziko-kimyasal açıdan su kalitesinin tespit edilmesi. Aquatic Sciences and Engineering, 31(1), 30-39, (in Turkish).
- Özkıdık H.Ö., 1995. Katı Atık Yönetimi ve Belediyeler, Devlet planlama Teşkilatı Müsteşarlığı (Uzmanlık Tezi) Ankara, (in Turkish).
- Şengül, E. (2004). Çanakkale düzensiz katı atık depolama sahası yüzey ve yeraltı sularına etkisinin uygulamalı jeofizik yöntemlerle araştırılması. Yüksek Lisans Tezi/Master Thesis, ÇOMÜ Fen Bilimleri Enstitüsü, (in Turkish).
- Şengül Uluocak, E. & Ulugergerli, E. (2023). Yer Bilimlerinde Modellemeye Genel Bir Bakış; Çevre Jeofiziği Uygulamalarından Çıkarımlar. Türkiye Jeoloji Bülteni, <https://doi.org/10.25288/tjb.1325550>

2.4 INVESTIGATION OF THE MINERALOGICAL-PETROGRAPHICAL AND GEOCHEMICAL PROPERTIES OF DARENDE (MALATYA) REGION LIMESTONE

M. Bağcı¹

¹Afyon Kocatepe University, Engineering Faculty, Department of Geology Engineering, Afyonkarahisar, Türkiye

*Corresponding author e-mail: mbagci@aku.edu.tr

ABSTRACT

In this study, the geological, mineralogical-petrographic and geochemical properties of limestone marbles belonging to the Alacakaya company in Darende/Malatya Hacılar Sıragöz Village were examined. Marble production is obtained from Cretaceous aged Kirankaya limestone. Limestones generally have thick layers, cracks and occasionally dissolution gaps. This situation negatively affects marble production. Limestones, which are generally massive in appearance, have acquired a fractured and fissured structure. The cracks detected in the stages within the marble quarry are generally located N40°W/80°NE. Polarizing microscope examinations were carried out to determine the mineralogical and petrographic properties of limestones. As a result of polarizing microscope examinations, it was observed that micritic textured calcite minerals formed the matrix of the rock, and also coarser-grained secondary (Spary) calcites settled in the microfractures and cracks in the limestone. In addition, to a lesser extent, calcite and opaque minerals with a brecciated structure have been detected in limestones. Fossil species such as Algae, Coral and Discocyclina Sp. have been identified in the limestones. When the major (main) element, minor (trace) element and rare earth element (REE) analysis results were examined, CaO was observed as the main element in all samples. CaO values vary between 52.68% and 55.72%. It was observed that the contents of other main oxide elements remained below 1% in all samples. It was determined that the Sr element was more enriched than other trace elements, and the Zn element was more enriched than other trace elements in some limestone samples.

KEYWORDS: Limestone, Mineralogy Petrography, Darende, Malatya

INTRODUCTION

The use of natural stones begins with human history. Human beings initially used rocks for the production of hunting weapons for nutrition and defense, and later for housing and protection. Natural stones have become an important industrial product because they are durable, have various color options, can be shaped and polished. Natural stones or marbles have been used throughout history in entire buildings or in decorating these structures (Kulaksız et al. 2012). The regions with significant potential in our country are Marmara, Western Anatolia, Southern Anatolia and Central and Northern Anatolia Regions. There are many travertine, marble and building stone quarries within the borders of Malatya and Elazığ provinces. The names of the marble fields where production is made throughout the province of Malatya are as follows. In the

region, Darende (Hacılar, Irmaklı, Başkaya, Üçpınar, Geniz and Göllüce Villages); There are marble deposits in Hasançelebi travertine, Kuluncak marble, Arguvan travertine, Akçadağ (Hançerli, Ören, Ortaköy, Gürkaynak and Dedeyazı Villages) locations. Within the scope of this study, the marble field operated by Alacakaya marble in the region located approximately 10 km away from Darende district of Malatya province was determined as the study area (Figure 1). Limestones appear in color tones ranging from light cream to dark cream. There are 3 stages opened in the marble quarry. In the studies carried out, sampling was done to reflect all levels. Detailed analysis and examinations were made on the marble samples taken and the mineralogical and geochemical properties of the marbles were determined.

MATERIAL METHOD

The limestone (beige) marble quarry within the borders of Hacılar Village in Darende District of Malatya Province was chosen as the study area. Using the TS EN 12670 (2004) standard, limestone marbles were examined in terms of grain size, texture, mineralogical composition and rock group with a Leica DM 2500P model polarizing microscope. The ground test samples prepared for XRD analysis were photographed on the Shimadzu brand XRD-6000 model XRD device between 2° and 70°. Total abundance ratios for major and trace elements were analyzed with a 0.1 g sample using an ICP emission spectrometer and treated with lithium metaborate and dilute nitric acid. Total fire loss was measured after 1000 °C heat treatment. Trace element and rare earth element values were analyzed by ICP-MS on a 0.1 g sample by lithium metaborate/tetraborate fission and dilute nitric acid treatment. Detection limits for major element are 0.002-0.1 wt%, and detection limits for trace element and rare earth element analyzes are 0.1-8 ppm and 0.005-0.1 ppm, respectively. Chemical analyzes were carried out in the Canadian (ACME) laboratory.

RESULTS

Geological Setting

The study area is located on the 1/25000 scale Elbistan K 38-C3 sheet around the Darende district of Malatya province (Figure 2). General geology, petroleum geology, tectonics and paleontology studies have been carried out in and around the study area, and Akkuş (1970,1971), Kurtman and Akkuş (1974), Kurtman (1978), Örcen (1986) and Şafak (1990) are some of them. The study area includes Cretaceous, Tertiary and Quaternary aged units. The units that make up the Cretaceous are; ophiolitic rocks and the massive limestone blocks (Geniz Limestone) found with them are the Ulupınar Formation and Kırankaya Limestone, which consists of weakly cemented coarse elastics. Tertiary aged units unconformably overlie the Cretaceous. These are, from bottom to top, the Yenice Formation consisting of sandy limestones with marl and marl interlayers, the Asartepe Formation represented by layered limestone and marls, the Balaban Formation consisting of gypsum conglomerates, and the Darende Formation consisting of marls with gypsum and sandstone interlayers. Plio-Quaternary is represented by the Çaybaşı Formation, which consists of conglomerates of different origin. The youngest units in the field are Quaternary alluvial units. Limestones, which constitute the main subject of the study and are considered marble, are

located within the Kirankaya limestones (Figure 3). Limestones generally consist of thin and medium-thick layered limestones. It is light yellow or off-white in color (Akkuş 1971).

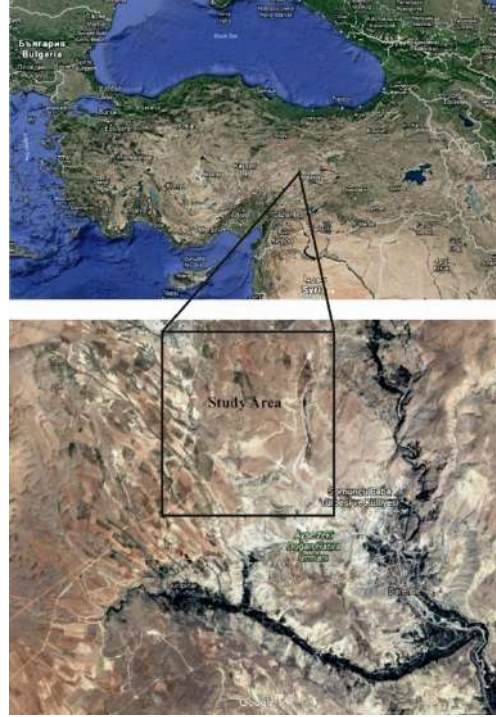


Figure1 Locator Map of the Study Area

MINERALOGICAL INVESTIGATIONS

Polarizing microscope analyzes

Most of the limestone samples consist of cream, beige and greyish-beige colored micritic limestones. In addition to beige colored micritic limestones, brecciated limestones are also encountered. Beige - white colored limestones: generally represented by micritic limestones containing oolites and algal shells (Figure 4). The limestones remaining in the quarry are generally beige, cream, grayish-beige in color. Oolite and occasionally pellet clasts, fossil shells such as algae and coral, and rock fragment sections were observed in thin sections made on limestone samples. Brecciated and nodular limestones and sparite-veined micritic limestones constitute the main rock types. Limestones are mostly micritic, occasionally sparitic and contain bioclasts. In sparitic veined micritic limestones, micritic limestone clasts and secondary sparitic calcites are seen to be connected to each other. During polarizing microscope examinations, grain size measurement results were measured as $1.9\ \mu\text{m}$ - $11.2\ \mu\text{m}$ in primary calcite grains and $300.4\ \mu\text{m} \pm 405.17\ \mu\text{m}$ in secondary calcite grains, respectively.

XRD Analysis

XRD images were taken between 2° - 70° with the Shimadzu brand XRD-6000 model XRD device at AKU TUAM Center. When XRD images taken on limestone samples were examined, it was seen that calcite mineral was dominant in all samples (Figure 5).

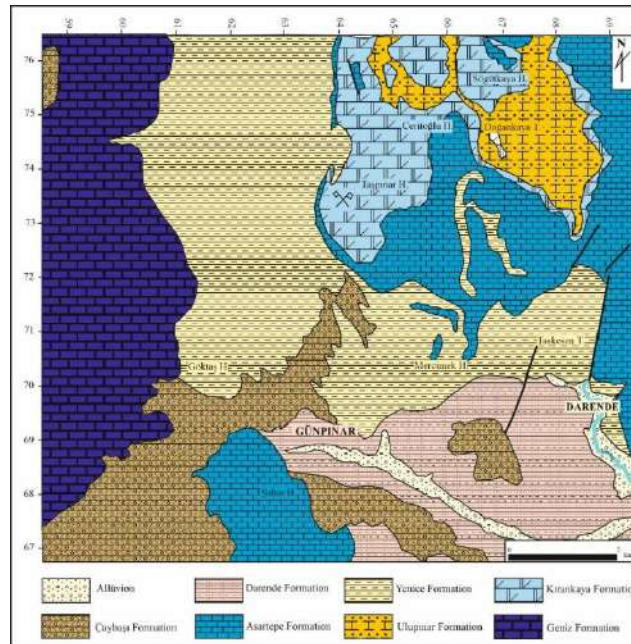


Figure2 Geological map of the study area.



Figure3 General view of the limestone quarry where block marble is produced.

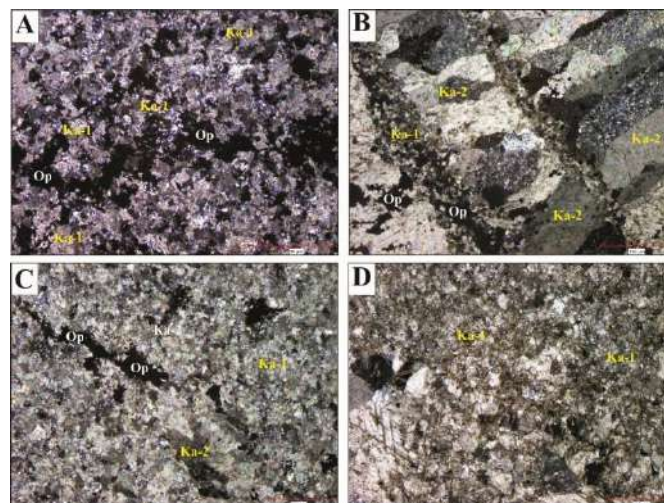


Figure4 Polarizing microscope image of limestone marbles. Primary and secondary (Secondary calcite crystals are observed. The matrix generally consists of carbonate micrites. Additionally, opaque minerals have been observed in microcracks in some places. Ka1: Primary calcite, Ka-2: Secondary (Secondary calcite), Opaque mineral: Op.

Geochemistry

Major, trace and rare earth element (REE) analyzes were performed on a total of 26 limestone samples taken for geochemical studies. Graphs showing the major, trace and rare earth element (REE) analysis results of all samples taken are given in Figure 6. Major (Ca, Mg) and trace elements (Sr, Na, Mn and Fe) provide very important information about the diagenesis processes, chemical properties and mineralogical properties of carbonate rocks (Rao and Naqvi, 1977). In the diagenesis of limestones and dolomites, their fabric properties are related to the Mg /Ca ratio and salinity in the solution (Folk and Land 1975). Strontium and original carbonate mineralogy varies with facies and salinity (Veizer and Demovie, 1974). Sodium is considered as a possible salinity index of precipitation and salinity. Minor Mg and trace (Fe, Mn, Sr) elements are incorporated into carbonate minerals during precipitation and are reintroduced during diagenesis. Stratigraphic variations are related to Sr, Na and Mn deposition environments and diagenesis (Rao, CP, 1990). To understand the precipitation and chemical environment of chemicals, representative limestone samples were collected from the limestone quarry operated by Alacakaya Mermer in Darende district. Samples were taken on the stove mirror and step surfaces. Representative samples were taken to represent the marble quarry. Limestones generally vary in beige, cream and light brown colors. The main oxide elements on the samples were SiO₂, Al₂O₃, TiO₂, Fe₂O₃, MgO, CaO, Na₂O, K₂O, P₂O₅ and trace elements such as Loss of Fire (LOI), Sr, Mn, Ba, Rb, Cr, Ni, V, Cu, Co, Sc, U, Th, Cs, Zr, Hf, Nb, Ga, Pb and Y and Rare Earth Elements (REE) were analyzed.

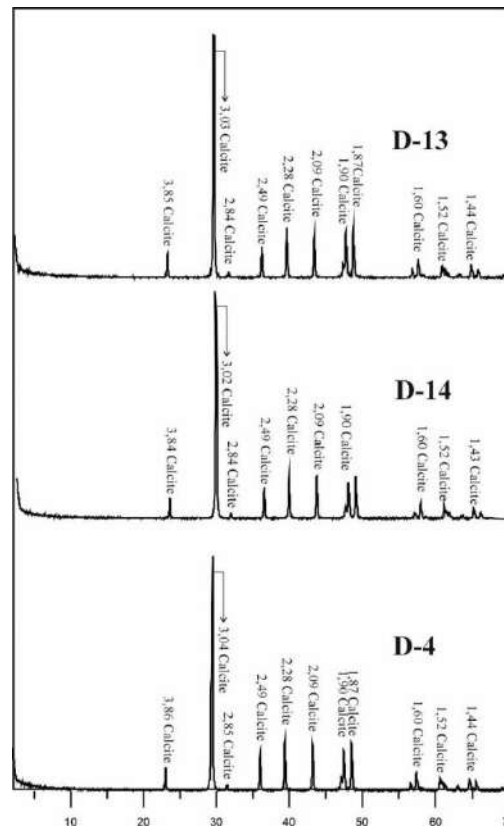


Figure5 XRD graphs of some Limestone samples.

Limestone samples have high Ca contents but very low Mg contents. CaO wt% contents vary between 52.68% and 55.77%, and MgO wt% contents vary between 0.12% and 0.66%, with an average of 0.26% .The Ca/Mg ratio ranges of the samples vary between 83% and 464%. In all limestone samples, the contents of main oxide elements such as SiO₂, Fe₂O₃, Al₂O₃ and MgO remained below 1%. Since the ionic ratio of Sr and Ca elements are similar, Sr element has the highest values among trace elements.

DISCUSSION AND CONCLUSION

Limestone marbles, which constitute the main subject of this study, are cream and light brown colored limestones seen in Hacılar Village and its surroundings within the borders of Darende (Malatya) district. The unit, known as Kirankaya Limestone in the literature, spreads over very wide areas in the region. There is a marble quarry operated by Alacakaya Marble Company, which operates economically in this region. Within the scope of the study, this marble quarry was studied in detail and systematic limestone samples were taken. Cretaceous aged Kirankaya Limestones are thick-layered, massive in appearance and contain abundant cracks and joint systems. In this respect, the block yield of marbles seems low. In polarizing microscope and XRD images, the main component in all samples is calcite mineral. There are two different calcite mineral formations in limestone: primary and secondary. Primary calcites generally form matrix (dough). The matrix consists of calcite minerals in micrite size. In addition, larger secondary calcite minerals were observed in the rock as micro veins or stylolite. In addition, the presence of algae, coral and Discocyliina Sp fossils were also detected in the rock. According to petrographic examinations of limestone samples, limestones are tightly packed biomicrite according to Folk (1959) and wackestone according to Dunham (1962). When the major (main) element, minor (trace) element and rare earth element (REE) analysis results were examined, CaO was observed as the main element in all samples. CaO values vary between 52.68% and 55.72%. It was observed that all other oxide elements remained below 1%. It was determined that Sr trace elements and Zn elements were more enriched in some samples than other trace elements. Since Zn enrichment in limestones is important, it would be useful to examine this situation in more detail in another study.

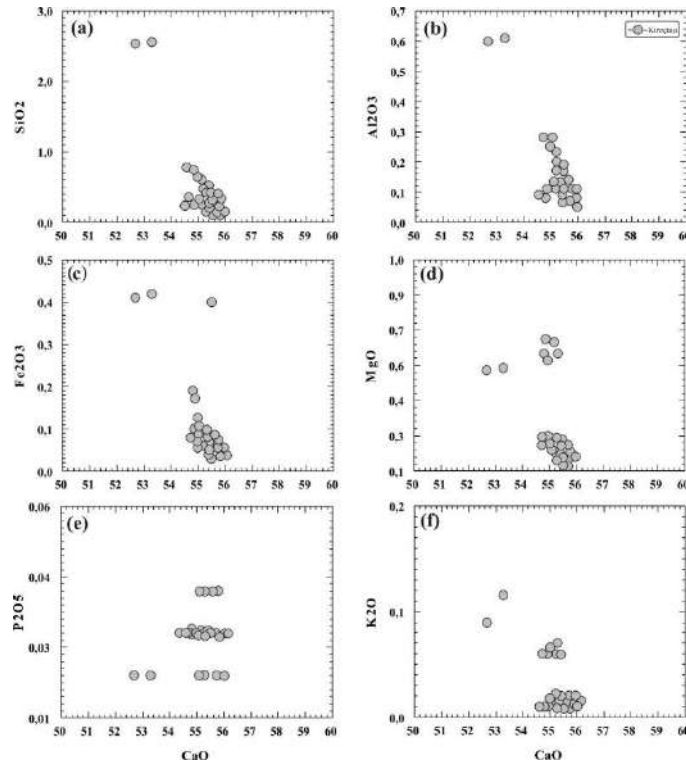


Figure6 Binary phase diagrams of Darende Limestone samples.

ACKNOWLEDGEMENT

This study was supported by Afyon Kocatepe University Scientific Research Projects Unit (AKU BAPK) with the project number 15. FENBİL.04. I would like to thank Afyon Kocatepe University for their support.

REFERENCES

- Akkuş, M. F. (1970). Darende-Balaban havzasının (Malatya, Anadolu) jeolojik ve Stratigrafik incelenmesi . Maden Tetkik ve Arama Enstitüsü Dergisi, 1–80.
- Akkuş, M. F., 1971. Darende-Balaban havzasının (Malatya, ESE Anadolu) jeolojik ve stratigrafik incelenmesi, MTA Dergisi, No: 76, Ankara, 1-60.
- Dunham, R.J. 1962, Classification of Carbonate Rocks according to Depositional Texture. American Association of Petroleum Geologists, 1, 108-121.
- Folk, R.L. and Land, L.S. 1975. Mg/Ca ratio and salinity: two controls over crystallization of dolomite. *Bull. Geol. Soc. Am.*, 59: 60–68.
- Kulaksız, S., Özçelik, Y., Bayram, F., Engin, İ. C., 2012, Doğal Taş (Mermer) Maden İşletmeciliği Ve İşleme Teknolojileri, TMMOB Maden Mühendisleri Odası, Ankara.
- Kurtman, F, Akkuş, M.F. (1974): Malatya-Gürün havzasının jeolojisi ve petrol olanakları. Türkiye İkinci Petrol Kongresi Tebliğler, Ankara
- Kurtman, F. 1978. Gürün Bölgesinin jeoloji ve tektonik özellikleri. MTA Dergisi, No: 91, Ankara, 1-12
- Örçen, S., 1986. Medik-Ebreme (KB Malatya) dolayının biyostratigrafisi ve paleontolojisi, MTA Dergisi, No: 105-106, Ankara 39-74.
- Rao, CP. and Naqvi, IH. 1977. Petrography, geochemistry and factor analysis of a Lower Ordovician subsurface sequence, Tasmania, Australia. *J. Sedim. Petrol.*, 47: 1036–55.
- Rao, CP., 1990, Petrography, trace elements and oxygen and carbon isotopes of Gordon Group carbonates (Ordovician), Florentine Valley, Tasmania, Australia: *Sedimentary Geology* (In press).
- Şafak, Ü., 1990. Malatya kuzeybatısının (Medik Ebreme yöresi) Üst Lütésiye ostrakod faunası, Ç. Ü. Müh. Mim. Fak. Derg., C: 5, No: 135-156.

3.1 NON- DESTRUCTIVE GEOPHYSICAL INVESTIGATION OF SUPPORT STRUCTURE ELEMENT BY USING 3D INVERSION OF DIRECT CURRENT RESISTIVITY DATA

C. Arıcan^{1*}, M.C. Candansayar¹ and N.Y. Gündoğdu¹

¹Geophysical Engineering Department, Ankara University, Ankara, Türkiye

*Corresponding author e-mail: carican@ankara.edu.tr

ABSTRACT

The multi-electrode and multi-channel resistivity measurement systems has long been used for Direct Current Resistivity (DCR) measurement to investigate underground resistivity structures. Although small-scale DCR studies are generally preferred in laboratory research, they are also used in the examination of structural system elements of reinforced concrete engineering structures such as buildings, bridges, etc. In this study, a new data measurement tools with multi-electrode DCR measurement systems that is suitable for small scale measurement on concrete structures was developed. In addition, different electrode array setup for concrete structure investigation taking into account the measurement time and the inversion results of synthetic data were compared. First, the 3D resistivity models generated for the concrete structure contains iron reinforcement, cracks and a moist region. For this model, we calculated sythetic data with 3D modeling for the different electrode layout that are positioned on a single surface, opposite surfaces and adjacent surfaces on a columnar structure. DCR data collected on the column structure with the developed measurement tools and determined electrode layout according to synthetic study. Measured data inverted by using 3D inversion algorithm that use unstructured finite element mesh. The synthetic and field data studies showed that it is possible to determine the concrete cover thickness of the element, the distribution of reinforcement within the element and possible fracture/crack/humidity conditions by applying the DCR method on the structural load-bearing elements

KEYWORDS : Direct Current Resistivity, Small-scale application, Construction Geophysics, 3D inversion

INTRODUCTION

The earthquakes damage the concrete structure such as buildings and bridges. In order to decide whether buildings can be used after the earthquake or not, it is very important to investigate damaged parts of load-bearing structural elements in a short time. Non-destructive geophysical methods, such as ultraseismic, structure radar and structure DC resistivity methods, are main tool for this kind of investigation (Candansayar, 2012). In this study, we used multi-electrode and multi-channel resistivity measurement systems for structure investigation. We first investigated the most suitable electrode arrays, and electrode layouts on a single side, opposite side and adjacent side by using 3D modeling and inversion algorithm. We calculated synthetic data with 3D modeling algorithm for column model. We added %2 Gaussian noise to data and invert it by

using 3D inversion algorithm. We used R3t modeling and inversion algorithm based on unstructured tetrahedron finite element mesh (Binley, 2013).

As real data, we collected DC resistivity data on column for three different electrode layout: on a single surface, on opposite surfaces and on adjacent surfaces. 3D inversion was performed by adding noise to the synthetic data obtained as a result of modeling studies.

METHOD and APPLICATION

The basic principle of the DCR method is to measure the potential difference between two pair of potential electrodes created by the direct current applied to the ground from two pair of current electrodes. The purpose of the method is to map the resistivity structure of the investigated area or region of the structures according to the electrical resistivity parameter.

DISCUSSION and RESULTS

First, a column model was designed to be used in synthetic data applications (Figure 1). In order to be more realistic, structures representing longitudinal reinforcement and stirrups were placed into the column model. In the model, the resistivity of the concrete is determined as 100 ohm.m and the resistivity of the reinforcement is determined as 1 ohm.m.

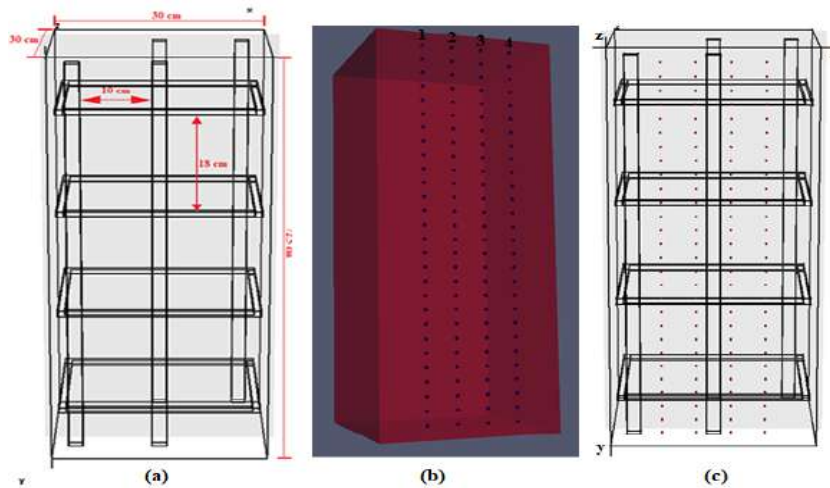


Figure1 (a) Schematic representation of the distribution of stirrups and longitudinal reinforcements within the column model (b) Demonstration of the distribution of electrodes on a single surface on the column model (1,2,3,4: Profile numbers) (c) representation on the structures within the model (electrode spacing 2.5 cm, profile spacing 5 cm)

Afterwards, sounding profiling data on a single surface electrode layout with 112 electrodes (4x28) for Wenner and Dipole-dipole electrode arrays (Arıcan, 2023) was calculated. The inversion result for each array given in Figure 2. When the inversion results are compared with the column model, it is seen that the DD array gives better results than the Wenner array.

In addition to the studies in which the electrodes were located on a single surface of the column model, modeling and inversion studies were also carried out for the situation in which the electrodes were located on the adjacent (front and left) surfaces (Figure 3).

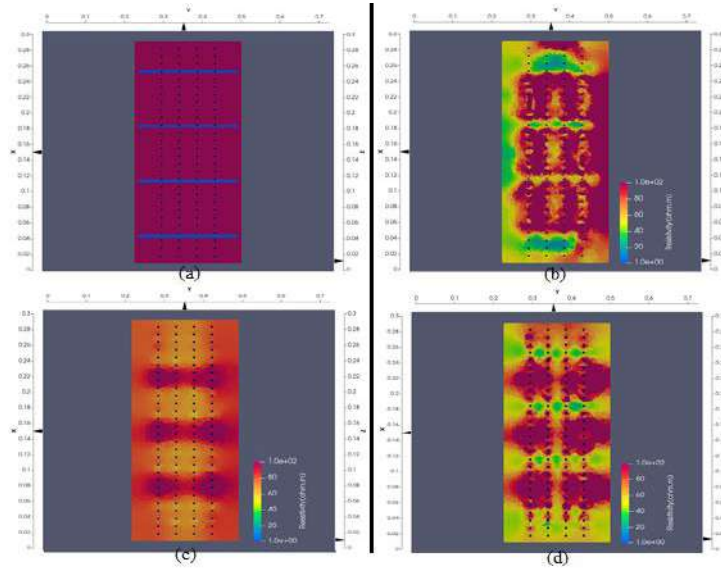


Figure2 xy-resistivity sections for $z=1$ cm depth: (a) real model (b) DD array 3D inversion result (c) W ($n=1$ level) array 3D inversion result, (d) W ($n=1$ and 3D inversion result of the sequence) for level 2.

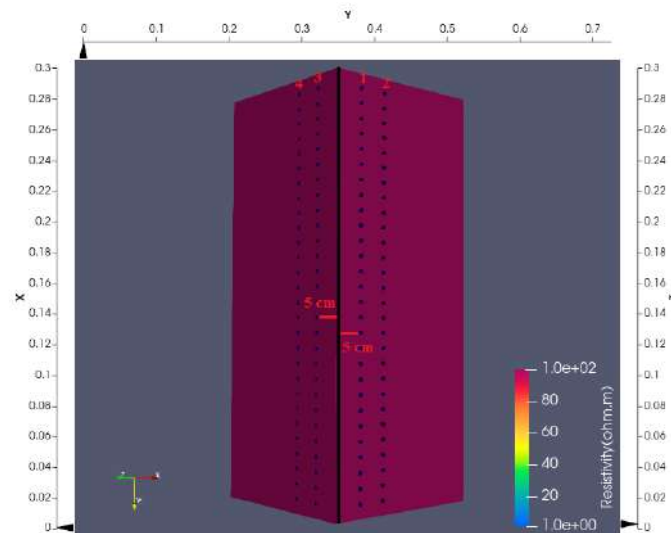


Figure3 The black line is the intersection of the front and left surfaces, and the representation of the electrodes on the front surface, located 5 cm away from the edge in the x direction, and on the side (left) surface, located 5 cm away from the edge in the z direction, on the model (1,2,3,4: profile numbers).

In the studies carried out on adjacent surfaces, inspired by the cross-gole DCR measurement, investigations were also carried out for situations where the profiles on two different surfaces were considered as one well. In the examinations, the pol-tripole (PT, ABMN) electrode array recommended by Demirel and Candansayar (2017) was used. The inversion result for DD,PT arrays and different location of electrodes on the adjacent sides of column given in Figure 4. In the 3D resistivity models of the PT array, it is seen that the artificial effects and the effects in the regions where there are no electrodes are reduced and a resistivity distribution closer to that of the real model is obtained in these regions.

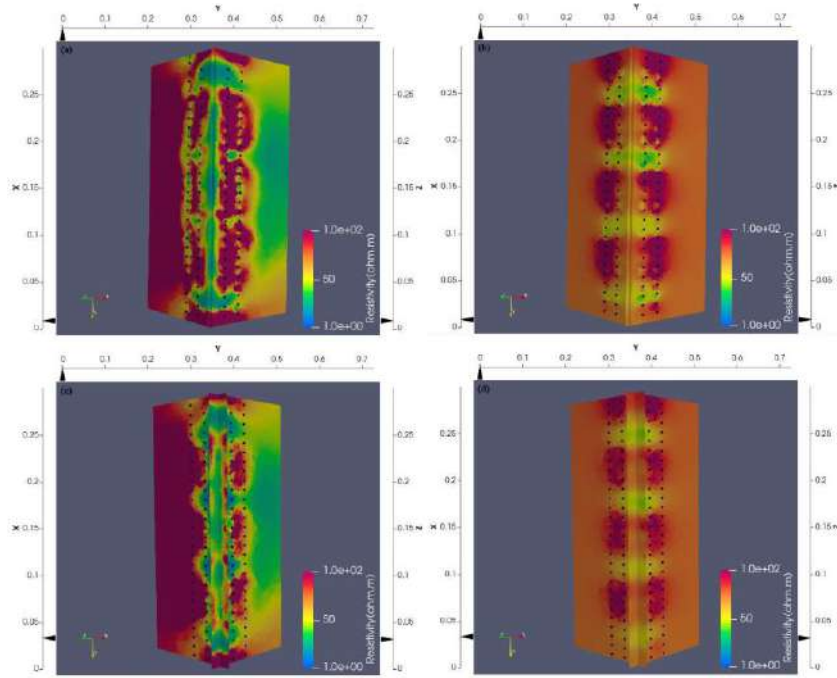


Figure4 From the 3D resistivity models obtained when the electrodes are 5 cm away from the edge, (a) Dipole-Dipole (b) $x = 1$ cm and $z = 1$ cm for PT arrays, (c) DD (d) $x = 3$ cm and Sections taken from $z = 3$ cm

CONCLUSION

When collecting data in structural geophysics, W Array with 5 cm electrode spacing is generally used. In this study, W, DD, PD sequences measured on a single surface were compared. It has been shown that PD data collected on one surface gives better results than other arrays. It is shown that the PT array data gives better results than the others when the inversion results obtained for adjacent surfaces and a single surface are compared. Inversion results of real data collected on a column also support the synthetic data results.

ACKNOWLEDGMENTS

This study was supported by TUBITAK with grant number 121Y281.

REFERENCES

- Arıcan, C., Candansayar, M.E. & Gündoğdu, N.Y. Yapı Elemanları Üzerinde Küçük Ölçekli Doğru Akım Özdirenç Yönteminin Uygulanabilirliğinin Araştırılması [Investigation of the Applicability of Small-Scale Direct Current Resistivity Method on Structure Elements]. 8. YER ELEKTRİK ÇALIŞTAYI, Trabzon, Türkiye, 16 May 2022.
- Arıcan, C. Doğru Akım Özdirenç Yöntemi İle Yapı Jeofiziği Araştırmaları: Taşıyıcı Yapı Elemanlarının 3B Görüntülenmesi [Construction Geophysics Investigation With Direct Current Resistivity Method: Three Dimensional Visualization Of Support Structure Element], Yüksek Lisans Tezi. Ankara Üniversitesi, Fen Bilimleri Enstitüsü, Ankara.
- Binley, A. 2013. R3t version 2.31 manual. Lancaster University, Lancaster. <http://www.es.lancs.ac.uk/people/amb/Freeware/R3t/R3t.htm>. Erişim tarihi:11.10.2021
- Candansayar, M. E. 2008. Two-dimensional individual and joint inversion of three-and four-electrode array dc resistivity data. *Journal of Geophysics and Engineering*, 5(3), 290-300.
- Candansayar, M.E. 2012. Yapı Jeofiziği [Construction Geophysics]. *Jeofizik Bülteni*, 69-70-71, 6.
- Demirel, C., & Candansayar, M. E. 2017. Two-dimensional joint inversions of cross-hole resistivity data and resolution analysis of combined arrays. *Geophysical Prospecting*, 65(3), 876-890.

4.1 (NOT PRESENTED) STRATIGRAPHY FROM THE PUNGALLA SECTION, ASHDAGH MOUNTAIN, NORTH EASTERN IRAQ

Imad GHAFOR (UNIV. OF SULAIMANI)

This abstract not presented during the congress.

4.2 EXHIBITION SIMILARITIES AND DISPARITIES UPPER CRETACEOUS SOURCE ROCKS FROM SOUTHEASTERN ANATOLIA FROM LITHOLOGICAL CONTENT PERSPECTIVE

M. Hazar^{1*}, T. İşçimen¹, Y.D. Erdal¹ and Ş.G. Köse²

¹Senior Petroleum System Analyst, Basin Analysis Team of TPAO Exp. Dept., Ankara, Türkiye

²Manager, Basin Analysis Team of TPAO Exp. Dept., Ankara, Türkiye

*Corresponding author e-mail: mthazar@gmail.com

ABSTRACT

As it can be examined from literature, The Arabian Plate consists of various proven and prolific hydrocarbon systems that have wide ranges of age, lithology, productivity, maturity, and areal extent. The Southeastern Anatolia Basin which constitutes the northern edge of the Arabian Plate contains at least three different active petroleum plays: Paleozoic, Jurassic and Upper Cretaceous. The Upper Cretaceous play has also its branches in at least three different carbonate source rock intervals. Although these source rocks deposited in a consecutive order at similar paleogeographic and paleoclimatic conditions, their effectiveness as a source rock can vary according to their lithological contents. In this study, we used basin analysis and petroleum system modeling principles in order to perform a substantive compare and contrast of their source rock potentials. Basically, we prepared 1D models which encapsulate all distinctive characteristics of three Upper Cretaceous source rock intervals and we applied same source rock kinetics, similar thicknesses, mechanical compactions, and other petrophysical properties. We changed carbonate amount, type and content in the rock percentage of these source rocks while most of other lithologic characteristics kept constant. This peculiar feature of different source rocks directly affected the timing or amount of generated and expelled of hydrocarbons and it can be utilized as an effectiveness parameter of source rocks especially in terms of critical timing of the aforementioned petroleum system.

KEYWORDS: Basin modeling, Upper Cretaceous Source Rocks of Southeastern Anatolian Basin, Source Rock Analysis, Carbonate Source Rocks

4.3 CHARACTERIZATION OF AN UNCONVENTIONAL ORGANIC-RICH CARBONATE MUDSTONE, LATE JURASSIC OF SAUDI ARABIA

J. Humphrey^{1*}, S. Chan¹

¹*Department of Geosciences, College of Petroleum Engineering & Geosciences, King Fahd University of Petroleum & Minerals, Dhahran, Saudi Arabia*

*Corresponding author e-mail: humphrey@kfupm.edu.sa

ABSTRACT

Five cores from a late Jurassic (Kimmeridgian) carbonate mudstone succession from Saudi Arabia were evaluated for sedimentologic, stratigraphic, organic geochemical, and geomechanical properties. A broad range of data allowed a comprehensive characterization of this potential source-rock interval that was deposited in a basinal setting during Kimmeridgian time in the Jafurah basin of eastern KSA.

Twelve lithofacies were identified through centimeter-scale core descriptions, standard petrography, and XRD and XRF characterization. Lithofacies are grouped into two distinct facies associations based on similarities in sedimentological and geochemical properties. Organic-rich facies of calcareous and mixed-calcareous mudstones with low bioturbation indices, high-redox sensitive elements, medium to high paleo-productivity indices, and good to excellent TOCs, corresponded to anoxic to dysoxic oxygen levels. In contrast, calcareous- and silica-rich mudstones with high bioturbation indices, light coloration, poor TOC values, and low redox-sensitive elements were deposited in more oxygenated water in a more proximal setting. Based on multiple data sets, a high-resolution sequence stratigraphic interpretation will be discussed.

The twelve lithofacies have also been characterized by their organic richness and hydrocarbon potential. Organic richness and hydrocarbon generation potential are good to excellent in the more anoxic facies association. Thermal maturity estimates from pyrolysis Tmax and maturity related biomarker ratios suggest a medium- to high-maturity source rock, analogous to the mature oil and wet-gas windows.

KEYWORDS: Carbonate mudstone, unconventional petroleum system, sedimentology, stratigraphy, geochemistry

4.4 UNDERSTANDING THE ORIGIN OF QUARTZ CEMENTATION IN SANDSTONES FOR BETTER PRE-DRILL RESERVOIR QUALITY PREDICTION

K.A.H. Al-Ramadan^{1*}

¹*Department of Geosciences, College of Petroleum Engineering & Geosciences, King Fahd University of Petroleum & Minerals, Dhahran, Saudi Arabia*

**Corresponding author e-mail: ramadank@kfupm.edu.sa*

ABSTRACT

Predicting and understanding the distribution patterns of diagenetic quartz cemented zones and their impacts on fluid flow within a reservoir unit is a crucial goal of reservoir characterization. Such prediction requires a comprehensive understanding of key factors. Qualitative and quantitative information on the thickness and completeness of coatings within various stratigraphic units and detailed knowledge of grain size is essential to making accurate predictions. The origin of silica cements is closely linked to the burial history, temperature, pressure, and composition of pore fluids within the sedimentary basin. Silica sources for quartz cementation could be derived from pressure dissolution of detrital quartz grains, feldspar and mica alteration, dissolution of chert, and clay mineral transformation reactions. Highly soluble biogenic silica from shale sequences is identified as an essential source of silica in some basins.

Clay coatings and micro-quartz are found to be key inhibitors to the nucleation and growth of quartz cements. Additionally, understanding the burial history of the reservoir is crucial. The type and grain size of detrital quartz grains plays a significant role in the extent of silica cementation. For example, monocrystalline quartz grains are more likely to have well-developed overgrowths, particularly in coarse sand sizes. These findings provide a better understanding of the diagenetic evolution in sandstone reservoirs and have important implications for reservoir quality prediction and hydrocarbon production.

KEYWORDS: Diagenesis, Quartz cementation, Sandstones, Reservoir Quality

5.1 LEVERAGING GENERATIVE ADVERSARIAL NETWORKS (GANS) TO ENHANCE WELL LOGGING DATA INTERPRETATION FOR SUSTAINABLE NEAR-FIELD EXPLORATION

A. Al-Fakih^{1*}, S.I. Kaka¹, A. Koeshidayatullah¹

¹ Department of Geosciences, College of Petroleum Engineering & Geosciences, King Fahd University of Petroleum & Minerals, Dhahran, Saudi Arabia

*Corresponding author e-mail: alja2014ser@gmail.com

ABSTRACT

This study focuses on the utilization of Generative Adversarial Networks (GANs) to improve the interpretation of well logging data, a critical element in near-field exploration within the oil and gas industry. Limited data accessibility and confidentiality constraints have historically posed challenges to the accuracy and efficiency of well logging data interpretation, significantly impacting exploration outcomes and environmental stewardship. Our research presents an innovative approach where GANs, a machine learning model capable of generating synthetic data indistinguishable from real data, are employed to enhance well logging data interpretation. We have trained a GAN model using a dataset of actual well logs to produce synthetic well logs. These synthetic logs are seamlessly integrated into the well logging data interpretation workflow alongside authentic well logs. The outcomes of this study reveal that the incorporation of synthetic well logs generated by GANs leads to a substantial improvement in the well logging data interpretation process for near-field exploration. The augmentation of the dataset with synthetic logs provides a more comprehensive understanding of reservoir properties and geological heterogeneities, enhancing reservoir characterization and supporting more accurate decision-making processes. This novel approach holds significant promise for sustainable near-field exploration. By leveraging GANs to generate synthetic well logs from limited data sources, operators can gain deeper insights into their near-field reservoirs, ultimately leading to more informed decisions regarding exploration strategies and environmental practices. This innovation has the potential to reduce drilling costs, enhance exploration success rates, and minimize environmental impacts.

KEYWORDS: Well logging, Generative Adversarial Networks (GANs), near-field exploration, reservoir characterization, sustainable practices, data interpretation

INTRODUCTION

Near-field exploration in the oil and gas industry plays a pivotal role in meeting the ever-growing energy demand while minimizing the environmental impact. However, this critical process often faces challenges due to limited data availability and confidentiality constraints, impeding the accuracy and efficiency of well logging data interpretation. This paper introduces an innovative approach that

leverages Generative Adversarial Networks (GANs) to enhance well logging data interpretation for sustainable near-field exploration.

Well logging data interpretation is essential for understanding reservoir properties and geological heterogeneities, which are crucial for making informed decisions in near-field exploration activities. Traditional methods rely heavily on real well logs, but these are often scarce and confidential. To address this limitation, our approach harnesses the power of GANs, a machine learning model capable of generating synthetic data that closely resembles real data. In this study, we have trained a GAN model using a dataset of real well logs, enabling it to produce synthetic well logs that are indistinguishable from actual data. These synthetic logs are then seamlessly integrated into the interpretation workflow alongside the authentic well logs.

METHOD

The methodology involves the following steps:

- **Data Collection:** Initially, a comprehensive dataset of real well logs is collected. This dataset serves as the foundation for training the GAN model.
- **GAN Training:** A Generative Adversarial Network is trained using the real well logs dataset. The GAN consists of two neural networks, a generator, and a discriminator, engaged in a competitive learning process. The generator aims to create synthetic well logs that are realistic, while the discriminator evaluates whether the generated logs are real or synthetic. This iterative process continues until the generator produces logs that are nearly indistinguishable from real data.
- **Integration:** Once the GAN is successfully trained, the synthetic well logs are incorporated into the well logging data interpretation workflow. These synthetic logs are treated as additional data points alongside the actual well logs.

Interpretation Enhancement: The results indicate that the integration of synthetic well logs significantly enhances the interpretation process. By expanding the dataset with synthetic logs, a more comprehensive understanding of reservoir properties and geological characteristics is achieved. The synthetic logs complement the real data, leading to improved reservoir characterization and more precise decision-making in near-field exploration.

Examples (Optional)

Figure 1 depicts a flowchart outlining a novel strategy for leveraging Generative Adversarial Networks (GANs) in multi-dimensional reservoir characterization, as proposed by Shahbazi et al. (2020). The strategy involves pre-processing seismic, well logs, and core data before utilizing them to train a GAN model for the generation of synthetic reservoir models. These synthetic models serve various purposes, including reservoir characterization and optimization. Figure 2: In this visualization, real and synthetic well logging data are compared using Principal Component Analysis (PCA) and t-Distributed Stochastic Neighbor Embedding (t-SNE). Preliminary results demonstrate that a GAN-based approach holds significant promise for multi-dimensional reservoir modeling. Experiments indicate that Timeseries GANs can effectively generate realistic and accurate 1D well logging data. This synthetic data has versatile applications in reservoir characterization, production optimization, and hydraulic fracturing design. While further research is needed to address limitations and refine the approach,

these findings suggest the potential of this methodology for enhancing reservoir management decisions.

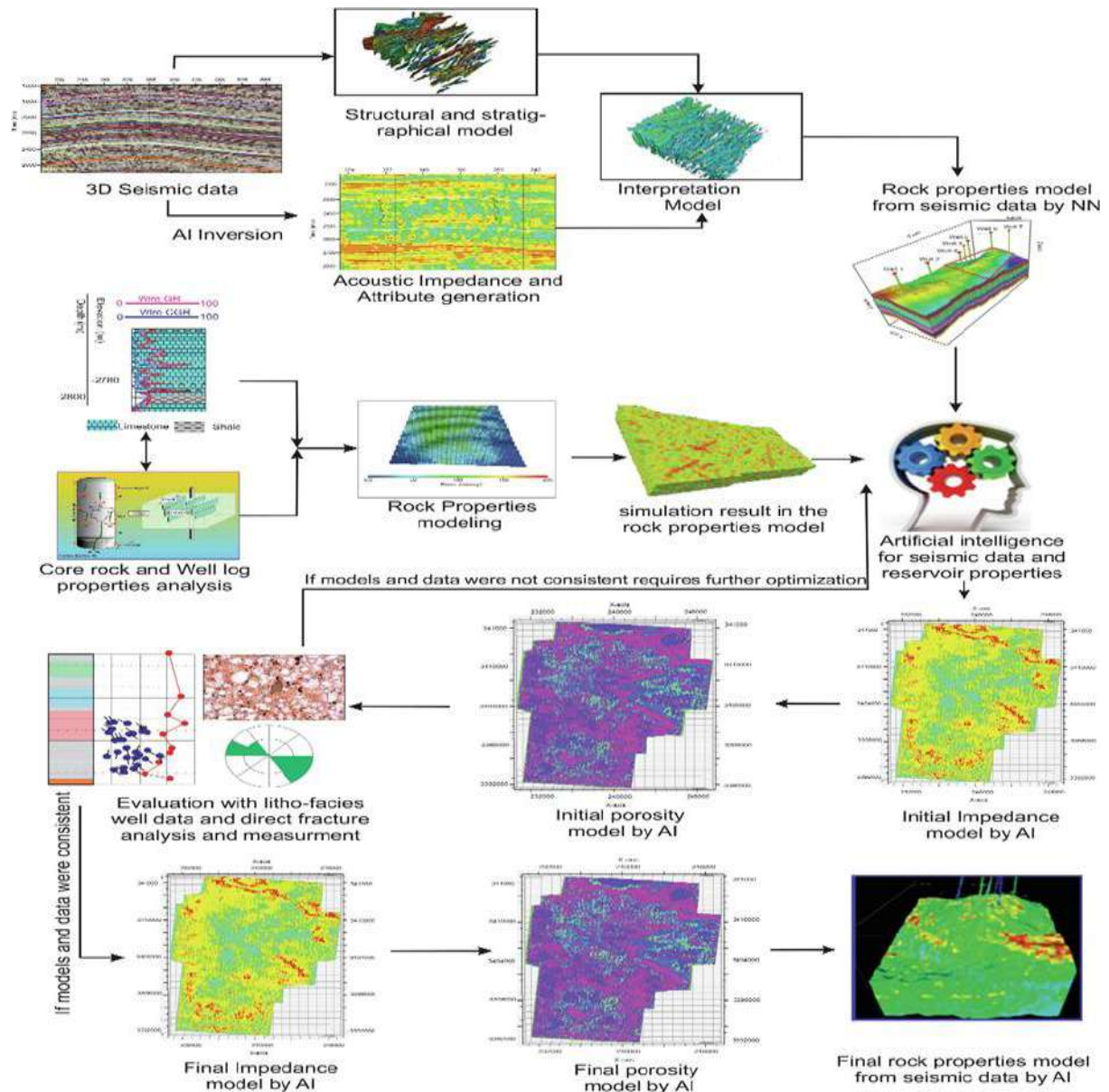


Figure 1 This is an example of the proposed strategy for using GANs for multi-dimensional reservoir characterization, as proposed by Shahbazi et al. (2020). Seismic, well logs, and core data are pre-processed before being used to train a GAN to generate synthetic models. These models can be used for reservoir characterization and optimization. GAN Training - The GAN model will be trained using the integrated dataset to generate synthetic reservoir models..

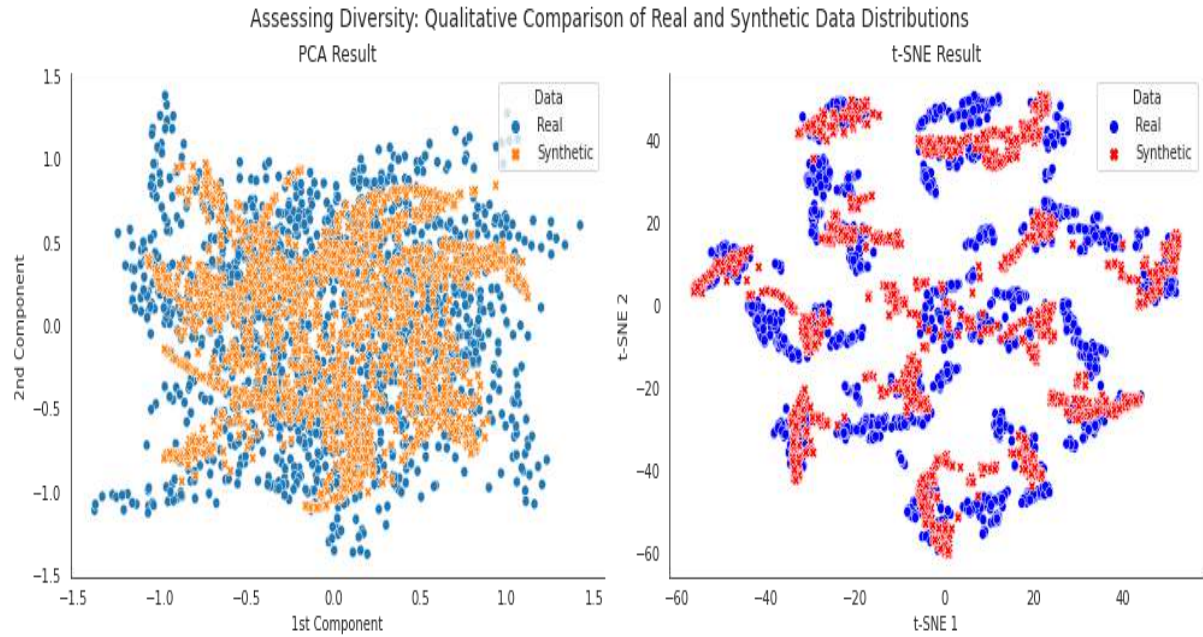


Figure 2 Visualization of real and synthetic well logging data using PCA and t-SNE

CONCLUSIONS

This paper presents a groundbreaking approach to revolutionize well logging data interpretation for sustainable near-field exploration. By harnessing GANs to generate synthetic well logs from limited data sources, operators can gain a deeper understanding of their near-field reservoirs. This, in turn, enables them to make more informed decisions regarding exploration strategies and environmental practices. The potential benefits are substantial, including reduced drilling costs, improved exploration success rates, and minimized environmental impact.

REFERENCES

Shahbazi, A., Monfared, M. S., Thiruchelvam, V., Ka Fei, T., & Babasafari, A. A. (2020). Integration of knowledge-based seismic inversion and sedimentological investigations for heterogeneous reservoir. *Journal of Asian Earth Sciences*, 202, 104541. 10.1016/j.jseae.2020.104541

5.2 POTENTIAL USE OF SONIC DATA FOR ROCK TYPING AND GEOSTEERING IN BIOTURBATED CARBONATE STRATA

A. El-Husseiny^{1*} and H. Eltom¹

¹Geosciences Department, King Fahd University of Petroleum and Minerals, Dhahran, Saudi Arabia

*Corresponding author e-mail: ammar.elhusseiny@kfupm.edu.sa

ABSTRACT

Earlier work showed that bioturbation can impact the reservoir quality of the Upper Jurassic Hanifa Formation in central Saudi Arabia which consists of burrowed and non-burrowed carbonate strata. While permeability varies drastically between the bioturbated and non-bioturbated strata, their porosity and mineralogy are very similar. This introduces a challenge in differentiating between the different rock types based on conventional well logs. This study investigated the impact of bioturbation attributes (intensity, expressed here as burrow percentage, BP and burrow-fills) on the sonic velocity of these carbonate strata. The ultimate goal is to find an sonic-derived approach to perform rock typing in such bioturbated rocks. Burrowed units were classified as highly bioturbated rocks (UB unit with BP > 15%) and rocks with low BP (LB unit with BP range of 2–15%). On the other hand, the non-burrowed strata were classified as NB unit. Seventy-seven core plugs were extracted from these three units and were characterized using different laboratory techniques including petrography, petrophysical measurements of porosity, permeability, and velocity, as well as computed tomography scanning to estimate BP. The laboratory analysis results were complemented by rock-physics modeling. Examining the permeability–porosity and velocity–porosity relationships of the combined dataset, we observed a noticeable scatter which could be explained largely by variations in BP: samples characterized by BP of > 15% (UB samples) have higher permeability and compressional velocity at any given porosity compared to LB and NB samples. These observations are explained by two factors. First, bioturbation created pathways for diagenetic fluids which resulted in the stronger cementation within the host microporous matrix (in UB samples) compared to the weakly cemented microporous matrix (LB and NB samples). Second, burrows are filled with grainy sediments characterized by dominant macro interparticle, moldic, and vuggy pores, which result in higher velocity in UB samples compared to microporosity dominated samples of LB and NB. The experimental velocity–porosity data and the pore type observations were consistent with rock-physics modeling which was also utilized for rock typing. This work shows an example where sonic data can be used to perform rock typing and assist the geo-steering by differentiating between good reservoir quality rocks (UB unit) and other non-reservoir zones (LB and NB units). This is particularly important given the similarities between all three units in terms of mineralogy and porosity.

KEYWORDS : Rock-physics, Carbonates, Rock-Typing, reservoir quality, bioturbation.

5.3 CHALLENGES IN MICROSEISMIC TECHNOLOGY FOR RESERVOIR CHARACTERIZATION AND MONITORING: A BRIEF REVIEW

S. I. Kaka^{1*}

¹Associate Professor, Geosciences Department, King Fahd University of Petroleum & Minerals, Dhahran, Saudi Arabia

*Corresponding author e-mail: skaka@kfupm.edu.sa

ABSTRACT

As the use of microseismic technology in reservoir monitoring and characterization has been steadily growing, this paper examines the challenges in detecting and locating microseismic events based on my years of experience in processing microseismic data in the Middle East as well as referred to relevant examples from literature. The microseismic events do help in understanding specific reservoir information such as the network of pre-existing planes of weakness within the reservoir that are not easily available through 3D active seismic. It also plays an essential role in hydraulic fracturing simulation where it can identify injection locations on target or that need to be adjusted. However, the key issue in the success of reservoir monitoring and characterization is the accuracy of detecting and localizing microseismic events within the reservoir. In fact, the accurate localization of microseismic events depends on many factors including array geometry, sensor orientation, picking correct arrivals, and accurate velocity models. One factor that most significantly impacts the accuracy is to detect arrivals of microseismic events due to the low signal-to-noise ratio. Specifically, microseismic energy recorded at surface array sensors has no observable arrivals due to a low single-to-noise ratio. In this paper, I review current challenges in the processing of microseismic events and, when possible, provide potential solutions.

KEYWORDS: Microseismic Technology, Reservoir Monitoring and Characterization, Processing Microseismic Events.

5.4 ELASTIC REVERSE TIME MIGRATION FOR IMAGING THROUGH GAS CLOUDS

C. Ören^{1*} and S. İleri¹

¹Senior Geophysicist, Data Processing Center, Turkish Petroleum (TPAO), Ankara, Türkiye

*Corresponding author e-mail: coren@tpao.gov.tr

ABSTRACT

The presence of complex gas clouds in the subsurface poses significant challenges in seismic imaging. One approach to tackle this longstanding problem is to exploit shear (S)-wave energy as such seismic data tend to be less sensitive to the gas clouds in comparison with pressure (P) waves. In this study, our primary goal is to accurately image beneath the gas clouds through elastic reverse time migration (E-RTM). Our E-RTM procedure includes the normalized energy-norm imaging condition that allows one to conveniently combine P and S wavefield energy leading to improved illumination of sub gas clouds. We illustrate the effectiveness of the proposed elastic imaging method using a realistic synthetic model that mimics the geology of Valhall field in the North Sea. By leveraging the capability of S waves, our secondary goal is to identify commercial- and fizz-gas reservoirs where imaging with P waves alone fails to do so. We similarly employ the aforementioned elastic imaging concept on a relatively simple synthetic model to distinguish whether a gas accumulation is commercial or non-commercial.

KEYWORDS: Elastic seismic imaging, shear wave, gas clouds

5.5 AVA ANALYSIS OF MULTI-COMPONENT SEISMIC WAVE MODES (P-SV, SV-P)

Saygın İleri¹

¹Senior Geophysicist, Data Processing Center, Turkish Petroleum (TPAO), Ankara, Türkiye

*Corresponding author e-mail: sileri@tpao.gov.tr

ABSTRACT

The amplitude variation with angle (AVA) analysis contributes significantly in quantitative seismic interpretation by delineation of rock properties consisting of lithology, porosity and pore fluids. P-P AVA analysis has become a common practice in the oil and gas industry to reduce the hydrocarbon exploration risks. In this study, rather than using conventional P wave mode, converted wave modes (P-Sv and Sv-P) are examined through the well log measurements from Midland basin and a worldwide collection on adjacent shale, brine and gas sands. With the fact that Sv-P data can be recorded with vertical displacement source and receivers, Sv-P AVA analysis plays a critical role to exploit shear wave information with less cost in comparison with P-Sv wave mode analysis. This work represents a pioneer study to distinguish brine and gas sands on converted mode AVA investigations by leveraging the potential of shear waves with a new cross-plot attribute developed from Sv-P reflectivity.

KEYWORDS: AVA, converted wave modes, P-Sv, Sv-P

5.6 GAS-WATER DETECTION TECHNOLOGY AND APPLICATION OF LOTEM COMBINED WITH WELL LOGGING AND SEISMIC DATA

X. Xie, L. Yan^{1*}, L. Zhou, X. Wang, K. Xiang, Y. Mao, H. Hu, X. Huang

¹Key Laboratory of exploration technologies for oil and resources (Yangtze university), Ministry of education of China, 430100

*Corresponding author e-mail: yjiemlab@163.com

ABSTRACT

Accurate detection of gas-water front and oil-water boundary is crucial for efficient development of oil and gas fields. The comprehensive geophysical technology of fully integrating seismic methods with high spatial resolution in fluid identification and electromagnetic methods with high sensitivity to reservoir fluids is currently a major research topic in oil and gas field development. This paper is based on the multi-component LOTEM observation data of the Feixianguan Formation reservoir in the main structural area of Puguang Gas Field. Through the static shift correction and the joint inversion of electrical and magnetic components under well seismic constraints, the resolution of resistivity and polarizability inversion is improved. A method for defining the gas-water identification factor Q based on linear coupling of multiple sensitive parameters, using resistivity and polarization as sensitive parameters, combined with seismic attribute parameters Vp/Vs, phase, and formation dip angle, was proposed. A Q-value gas-water identification template was established through the calibration with logging interpretation data and water invasion parameters of production gas wells. The gas-bearing properties of the I-VI sequences in the Feixianguan reservoir of the Puguang gas field experimental area were explained, The correctness of its interpretation results was verified by P103-2C lateral drilling. The test shows that the gas-water detection technology integrated by seismic and LOTEM has the ability to detect deep gas-bearing degree, and can be an important technical means for unconventional oil and gas development gas-water detection.

KEYWORDS: LOTEM, Gas-Water detection, resistivity, polarizability, water invasion.

INTRODUCTION

The gas-water detection is a research hotspot in the exploration and development of unconventional oil and gas, and it is also a global challenge. Currently, in the mid-to-late stage of unconventional gas reservoir development, water flooding is a serious issue in China, posing significant challenges to the sustainable development. Seismic method has strong detection capabilities and high resolution, making it the primary means of gas and water detection. However, the application effectiveness is seriously affected by the poor acoustic properties of unconventional oil and gas reservoirs. Meanwhile, the analysis of electrical testing for the unconventional reservoir rocks indicates that resistivity and polarization are remarkably sensitive to reservoir fluids. Compared to the seismic method, electromagnetic (EM) method has the physical advantages in the identification of gas and water in unconventional reservoirs. To achieve

the identification of gas and water in deep and ultra-deep conditions (with depths greater than 5000 meters) by EM method, we should focus on the accurate extraction method of the EM parameters and the modeling of the relationship between the EM parameters and gas-water content. And we also should make full use of the benefits from seismic and EM methods, and finally develop a multi-parameter joint identification technique for gas and water using seismic and EM data.

METHOD and APPLICATION

Based on the Long Offset Transient Electromagnetic Method (LOTEM) multi-component data, we achieve the resolution capability improvement for the electrical resistivity and polarization inversion, by using the magnetic component to correct the static shift of the electric component and employing well-constrained joint inversion of the electric and magnetic components. We define the gas-water identification factor Q based on the linear coupling of the main sensitive parameters, including electrical resistivity, polarization, seismic attribute parameters (V_p/V_s ratio, phase, and formation dip angle). The calculation formula is as follows:

$$Q = a_1R + a_2M + a_3V_p/V_s + a_4I_{mp} + a_5D$$

where R represents the normalized electrical resistivity, M represents the normalized polarization rate, V_p/V_s is the normalized P-wave to S-wave velocity ratio, I_{mp} is the normalized impedance, D is the normalized formation dip angle, a_1 , a_2 , a_3 , a_4 , a_5 are the weighting coefficients for the sensitive parameters. $a_1 + a_2 + a_3 + a_4 + a_5 = 100\%$. a_1 and a_2 have values between 30% and 55%, while a_3 , a_4 , and a_5 have values between 10% and 25%. Commonly, the gas-water interpretation results from multiple wells and the specific calculations of the gas-water identification factor (Q) are compared to determine the weighting coefficients that best match the well logging interpretation results. This establishes a mathematical and physical board for gas-water detection.

The Puguang Gas Field, located in the northeastern part of the Sichuan Basin, is a large-scale, fully developed, high-sulfur, ultra-high-pressure unconventional carbonate gas field in China. The main producing reservoir layers are the Feixianguan Formation, with burial depth of 5900 meters and thickness of 400 meters about. Currently, the Puguang Gas Field has entered the middle and later development stage. Water flooding is extremely common and has a serious impact on gas production. It is urgent to study the water flooding patterns in the reservoir and understand the distribution of formation water. This information is crucial for logging production control and development drilling. To address this, test on the joint detection of gas and water using integrated with LOTEM, seismic, and well logging data has been conducted in the Puguang Gas Field. Firstly, 19 survey lines were arranged in the main structural area of the Puguang Gas Field, totaling 1,138 measurement sites. The line interval is 200 meters, and the site interval is 50 meters, covering an area of 56.25 square kilometers. The data acquisition overcame the complex terrain conditions and the reliable LOTEM data had been obtained by increasing the transmitter current and extending the observation time. Secondly, based on well logging and seismic data, a spatially constrained initial model for LOTEM data inversion was established. In the inversion objective function, a cross-gradient term of the well-seismic spatial constraint model was added, which

resulted in high spatial resolution and accuracy in the inversion of resistivity and polarization models. Finally, based on the pre-existing 3D seismic data and static and dynamic production data of gas wells in the testing area, the identification of gas and water at the edge of the main structure of Puguang Gas Field and the analysis of the spatial distribution characteristics of the leading edge were carried out.

RESULTS and DISCUSSION

The specific results are as follows:

- (a) The electrical characteristics of the Feixianguan reservoir show significant variations when it contains fluids. The variation pattern of resistivity is as follows: the resistivity of the dry layer is greater than that of the layer bearing gas or gas-water mixture or water. The polarization characteristics are as follows: The polarizability of the aquifer, dry layer, and gas layer is the highest, while the polarizability of the gas layer is lower. Based on these observations, a gas-water identification model was established for this area.
- (b) With the well and seismic constrained LOTEM multi-parameter inversion and the seismic parameters inversion, time profiles and contour maps of sensitive parameters for the I to VI sequences of Feixianguan formation were obtained. Based on the gas-water distribution data from multiple production wells, the Q coefficients were calibrated, and a Q interpretation template was established. It was determined that when Q is less than 0.4, it indicates a water-invasion layer, when Q is between 0.4 and 0.6, it indicates a gas-water coexisting layer, and when Q is greater than 0.6, it indicates a gas layer or a dry layer. This model provides a basis for the quantitative interpretation of gas content detection analysis in the testing area.
- (c) In terms of physical properties, sequences I, II, and III have relatively better physical properties than sequences V and VI. From a plane perspective, the physical properties near the Puguang Fault and in the northeast are poor. Vertically, the I, II, IV, and V sequences exhibit low resistivity, with the III sequence having the lowest resistivity, and the VI sequence showing relatively higher resistivity. The I, II, IV, and V sequences have high polarizability, while the III and VI sequences have relatively lower polarizability. From a horizontal perspective the properties of the northeastern part are relatively poor. The central and southeastern parts exhibit characteristics of medium to low resistivity, while the northeastern and northwestern parts have higher resistivity. The central and southeastern parts show high anomalies in polarization rate, while the northeastern and northwestern parts have lower polarizability.
- (d) The Q planar distribution maps of the I-VI sequences indicate that water invasion occurs from the east and southeast, with the water body advancing towards the P103-4, P103-1, P105-2, and PG4 lines. The water body exhibits a trend of north-northeast to south-southwest, with a width varying between 1.5 to 2.0 km. The width of the gas-water interface varies between 200 to 500 m. The sequences with faster water invasion are I, II, III, and V, while the V and VI sequences, characterized by higher elevation and poorer properties, exhibit slower westward water invasion.

After the completion of the test, the gas field manager arranged the P103-2C lateral drilling near the P103-4 well, targeting the Feixianguan Formation reservoir. The logging results show that the area with high Q value anomalies is distributed in the IV-VI sequence area in the northwest of the survey line, which is a gas producing area. The area with medium to low anomalies in Q-value is distributed in the southeastern part of the I-III sequences, primarily representing a gas-water transition zone. The correctness of its interpretation results was verified by P103-2C lateral drilling.

CONCLUSION

We define the gas-water identification factor Q based on the linear coupling of the main sensitive parameters, including electrical resistivity, polarization, seismic attribute parameters (Vp/Vs ratio, phase, and formation dip angle), and a technology of gas-water detection combining seismic and LOTEM are proposed based on five sensitive parameters of electrical resistivity, polarization, Vp/Vs ratio, seismic phase, and formation dip angle. The correctness of its interpretation results was verified by drilling well.

5.7 SIP DETECTION AND QUANTIFICATION OF IRON SULFIDE (FeS) MATERIALS: A PATHWAY TO EARLY MONITORING

P. Kirmizakis¹, A. El-Husseiny¹, M. Mahmoud² and P. Soupios^{1*}

¹Department of Geosciences, College of Petroleum Engineering & Geosciences, King Fahd University of Petroleum & Minerals, Dhahran, Saudi Arabia

²Department of Petroleum Engineering, College of Petroleum Engineering & Geosciences, King Fahd University of Petroleum & Minerals, Dharan, Saudi Arabia

*Corresponding author e-mail: panteleimon.soupios@kfupm.edu.sa

ABSTRACT

The presence of iron sulfide (FeS) scale poses a substantial threat to oil and gas (O&G) production, with significant potential for operational disruption. Unfortunately, current monitoring approaches fail to detect the FeS scale at its early stages, rendering timely remediation impractical. Spectral Induced Polarization (SIP), an established geophysical technique widely employed in near-surface environmental contexts, emerges as a promising solution. Notably, SIP's unique attributes, which encompass sensitivity to both bulk and interfacial properties of materials, position it as a potential tool for characterization and monitoring purposes. SIP's heightened sensitivity to metallic targets, including FeS, holds profound implications for identifying, assessing, and quantifying the FeS scale. This study conducted a controlled column experiment involving varied concentrations of pyrite (FeS₂), a prevalent form of FeS scale, embedded within calcite. The primary objective was to explore SIP's discernment capabilities and to establish correlations between SIP signals and the properties of FeS₂. The research revealed that the concentration of FeS₂ within the samples exerted a direct influence on the SIP signals; greater concentrations correlated with amplified SIP parameter magnitudes.

Notably, the SIP method exhibited remarkable efficacy by detecting the presence of FeS₂ at concentrations as low as 0.25% within the sample's bulk volume. This pivotal finding underscores SIP's potential as a reliable FeS₂ detection technique, signifying a significant stride toward proactive monitoring and intervention. Furthermore, the study sets the stage for subsequent investigations to harness SIP's inherent strengths as a robust and dependable method for characterizing and monitoring FeS scale. This research highlights the dire need for early detection and mitigation of FeS scale's detrimental impacts on O&G production. The study showcases SIP's proficiency in pinpointing FeS₂ even at minute concentrations, substantiating its promise as an effective detection methodology. Moreover, the findings illuminate the path for future inquiries into employing SIP as a cornerstone for precise and steadfast characterization and monitoring of FeS scale. Ultimately, the study's outcomes contribute significantly to the drive for enhanced operational reliability and efficiency within the O&G industry.

KEYWORDS: spectral induced polarization, disulfides, pyrite

5.8 RECONSTRUCTION OF THE 3D SUBSURFACE OF THE AL-HASSA OASIS, EASTERN SAUDI ARABIA

A. Khogali¹, P. Kirmizakis¹, K. Chavanidis¹, A.L. Ashadi¹, A. Stampolidis², M.E. Candansayar³, P. Soupios^{1*}

¹Department of Geosciences, College of Petroleum Engineering & Geosciences, King Fahd University of Petroleum & Minerals, Dhahran 31261, Saudi Arabia.

²Aristotle University of Thessaloniki, Thessaloniki 54124, Greece.

³Geophysical Engineering Department, Ankara University, Ankara, Türkiye

*Corresponding author e-mail: panteleimon.soupios@kfupm.edu.sa

ABSTRACT

Al-Hassa city contains the largest oasis in Saudi Arabia and one of the world's largest naturally irrigated land. 280 natural springs provided massive groundwater discharging and watering of agricultural land. Moreover, the water in some of the springs is used to be warm. The quality was also spatially varied. The characteristics above indicate a complex subsurface that has to be characterized. Four geophysical methods were applied to reconstruct a 3D subsurface for the study area. Four non-seismic geophysical methods were applied, to reconstruct with the highest accuracy, a 3D model of the subsurface of the study area. Five hundred seventy-one gravity stations were acquired, covering the whole Al-Hassa Oasis, an area of 353 Km². 52 magnetotelluric-MT stations, 12 audio-magnetotelluric-AMT stations, and 25 transient electromagnetic-TEM stations, were acquired within the Al-Hassa National Park to reconstruct a 3D subsurface model. All EM soundings were processed and combined to achieve the highest resolution from the surface till the maximum depth of investigation. Gravity data were processed and lately integrated with the final 3D EM model. Preliminary 1D modeling of the TEM data till the maximum depth of 200m shows a lateral discontinuity of resistivity, which agrees with spatial variation of the EC of groundwater samples in the study area. 2D and quasi-3D modeling of the MT data acquired along a N-S profile and 2 E-W profiles clearly show a salt dome structure that agrees with the low resistivity (brine) shallow water analysis and previously published paper. 3D modeling of the gridded gravity data acquired covering the whole Al-Hassa Oasis, agrees with the expected NNW-SSE and ENE-WSW fracture zones that probably act as pathways or barriers to groundwater. All acquired geophysical data and collected geochemical data in the broader study area will be imported into PETREL and integrated to provide a more precise indication of the complexity of the study area. The 3D geophysical subsurface modeling of Al-Hassa Oasis reveals a complex underground structure. The integration of various geophysical data sets, including TEM, MT, and gravity data, uncovers lateral discontinuities in resistivity, a salt dome structure, and fracture zones acting as pathways or barriers to groundwater flow. This comprehensive modeling approach provides valuable insights into the subsurface dynamics of the oasis, contributing to a better understanding of its hydrogeological characteristics and potential water resources management strategies.

KEYWORDS : EM modeling, Gravity/Magnetic, Basin Analysis

5.9 DETERMINATION OF DEEP-SEATED FAULTS USING GRAVITY AND MAGNETIC METHODS: PRELIMINARY RESULTS FROM NORTH ADIYAMAN, SOUTHEASTERN TURKIYE

B. Dinçer¹, V. Isik², R. Saber³, A. Caglayan⁴ and Z.N. Bektaş⁵

¹Mrs., Exploration Department TPAO, Ankara, Türkiye

²Prof. Dr., Department of Geological Engineering, Ankara University, Ankara, Türkiye

³Dr., Department of Geological Engineering, Ankara University, Ankara, Türkiye

⁴Dr., Ministry of Environment, Urbanisation and Climate Change, General Directorate of Spatial Planning, Department of Geological Survey, Ankara, Türkiye

⁵Miss., Department of Geological Engineering, Ankara University, Ankara, Türkiye

*Corresponding author e-mail: badincer@tpao.gov.tr

ABSTRACT

Gravity and magnetic methods are among the geophysical methods used to determine specifically geological structures at depth. It is possible to clarify the zones of depression and/or uplift, shallow and deep mass distributions, sediment thickness of basins, and the location, distribution and characteristics of deep faults using gravity-magnetic methods. The study area is represented by widespread faulting along the Southeastern Anatolian Orogeny. The topography shows significant changes over short distances, and the exhumed faults are mainly characterized by reverse/thrust faults, together with a minority of relatively younger strike-slip faulting. With over 3000 gravity and magnetic measurements obtained from the area, fault traces cutting the lithological units were detected at depth. Fault traces observed at -1000, -2000 and -3000 from sea level, striking predominantly to the NE-SW and NW-SE. A small number of fault traces strike in an approximately E-W direction. Our preliminary investigations reveal that the fault traces we identified at depth using gravity and magnetic methods can be correlated with the surface faults observed in the study area.

KEYWORDS: Gravity-Magnetic method, Derivation, Downward extension, Analytical signal, Fault, Southeastern Anatolia

INTRODUCTION

The Southeastern Anatolia is part of the Alpine-Himalayan Orogeny, which is called the Southeastern Anatolian Orogeny (e.g., Yılmaz, 1993, Korucu and Isik 2023). The Southeastern Anatolian Orogeny is one of the main complex of continent-continent collision's active mountain belt development. Orogeny occurred as a result of the relative approach of the Eurasian and African/Arabian Plates to each other during the Late Cretaceous-Cenozoic, the subduction of the southern branch of the Neotethys Ocean, the overhanging of oceanic crustal rocks, and continent-continent collision (e.g., Perinçek, 1980; Şengör and Yılmaz, 1981; Robertson, 2000; Yılmaz, 2019). In the region, the closure of the Neotethys Ocean in the Late-Middle Miocene caused intense deformation of the Arabian and Eurasian Plates along the suture zone;

widespread reverse/thrust faults, folds and basin developments associated with these structures are characteristic (e.g., Şengör and Yılmaz, 1981; Kelling et al., 1987; Robertson et al. 2016; Korucu and Isik 2023).

Considering the structural character of the Southeastern Anatolian Orogenic zone, it is divided from north to south into the Nappe zone, imbricate zone and Arabian Platform (Yılmaz and Yiğitbaş (1991, Yılmaz 1993, Korucu and Isik 2023). The Nappe zone is primarily composed of tectonics formed by the ophiolitic and metamorphic rocks in the region. (Yılmaz and Yiğitbaş, 1991). The southern part of the orogeny consists of the lithologies of the Arabian Platform (e.g., Kara and Isik 2021). This study uses gravity and magnetic methods to model sub-surface geology and structural elements.

MATERIAL and METHOD

Gravity and Magnetic methods are the basic methods used in geophysics (Telford et al., 1990). The gravity method is based on the use of density, and the magnetic method is based on the use of susceptibility parameters (Blakely, 1995). The fact that the underground consists of rocks with different densities and different susceptibility causes small changes in the Earth's gravitational force. These changes are measured and evaluated with special devices. Horizontal changes in density and magnetization indicate the transition between different geological units, and this situation appears as an anomaly on the maps. Determining buried faults with this method allows for mapping geological structures. In the field, 1665 Total Magnetic Intensity measurement values were taken with the Proton magnetometer, and 2896 Gravity measurements were taken in the same region with the Scintrex CG5 Gravity meter. Since alluviums predominate throughout the region, a 2.5 g/cm³ reduction density was used. In detecting faults, a density value of 2.20 gr/cm³ was taken. An isostatic gravity map was obtained, and an isostatic gravity map was used in all other process maps.

DISCUSSION and CONCLUTIONS

The study area of approximately 1200 km² was examined by gravity and magnetic methods. It has been detected that the gravity anomaly has a high value, and the wavelength expands in areas where the basic units are close to the surface and/or outcrop. The foundation depth is predicted to vary between approximately 2.5-3 km depending on the applied process method. Faults were detected up to 2 km depth from the sea surface, and it was determined that the characteristics of these faults were reverse faults. When looking at the x and y-directional faults, it was observed that they gained offset at a certain level (Figure 1).

The study continues to determine the distribution, depth and thickness of the Mardin Group, allochthonous and other units on 12 models, four of which are NS and 8 of which are NE-SW. The maps to be made aim to find the thickness and entrance of allochthonous units and the depth of entrance to the Mardin Group.

Within the context of the study, faults in the determined region were tried to be detected by analysis of gravity measurements. By evaluating the anomalies created by measurements, fault

traces in the region from sea level to -2000 m depth were determined. It has been detected that the foundation depth varies between 2.5 and 3 km (Figure 1).

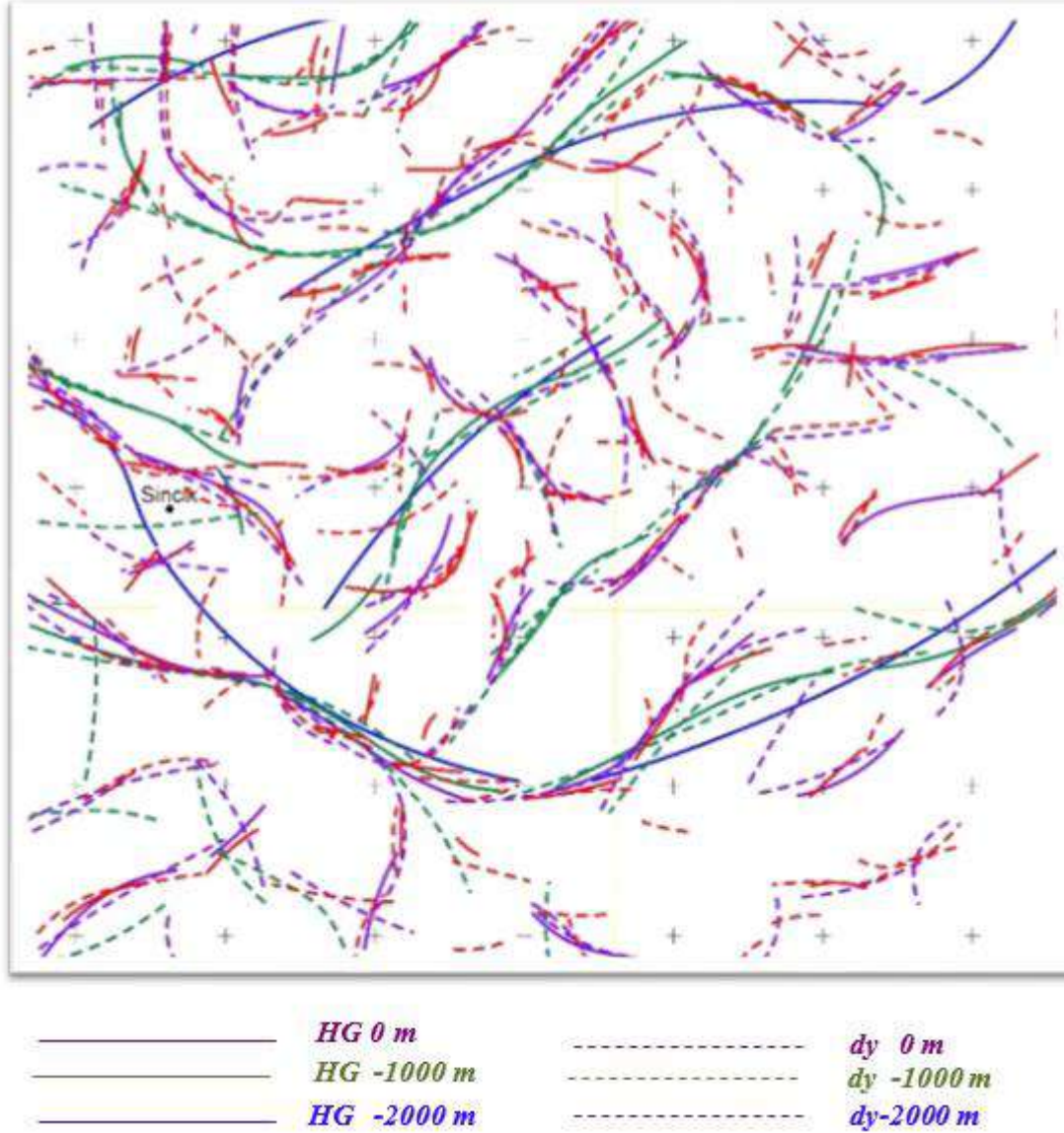


Figure1 Map showing fault traces in-depth obtained from gravity anomalies in the study area and its surroundings. HG: Horizontal gradient, dy: fault in the y direction, dx: fault in the x direction.

The following results were obtained from all data:

- 1-By using gravity anomaly data, faults at sea level (0 m), -1000 m, and -2000 m depth were determined in the study area. Fault traces are shown in different colors on the prepared maps.
- 2-When the general fault trends are examined, it has been determined that the stress comes from the northwest, and in general, the faults in the map area are determined to be reverse faults.

REFERENCES

Blakely, R. 1995. Potential Theory In Gravity and Magnetic Applications. Cambridge University Press, 441 p.

- Kara, B., and Işık, V., 2021. Reservoir characteristics and unconventional oil potential of Silurian aged Dadaş shale in southeast Turkey. *Journal of Petroleum Science and Engineering*, 200. DOI: 10.1016/j.petrol.2021.108365
- Kelling, G., Gökçen, S.L., Floyd, P.A., and Gökçen, N.D., 1987. Neogene tectonics and plate convergence in the eastern Mediterranean: new data from southern Turkey. *Geology*, 14, 425-429.
- Korucu, Ö. ve Isik, V., 2023. Güneydoğu Anadolu Orojenezinde Aksu-Samsat (Adıyaman) Profil Hattının Jeolojik Özellikleri. *Yerbilimleri*, 44 (1), 22-63, 1129329.
- Perinçek, D., 1980. Arabistan Kıtası Kuzeyindeki Tektonik Evrimin, Kıta Üzerinde Çökelen İstifteki Etkileri. *Türkiye Beşinci Petrol Kongresi, Ankara, Jeoloji- Jeofizik Bildirileri*, 77-93.
- Robertson A.H.F., 2000. Mesozoic–Tertiary tectono-sedimentary evolution of a South Tethyan oceanic basin and its margins in southern Turkey. In: Bozkurt E, Winchester JA, Piper JDA (eds) *Tectonics and Magmatism in Turkey and Surrounding Area*. Geol Soc, London, Spec Publ 173, 97–138. DOI: 10.1144/gsl.sp.2000.173.01.05
- Robertson, A., Boulton, S.J., Taslı, K., Yıldırım, N., İnan, N., Yıldız, A., and Parlak, O. 2016. Lower Cretaceous–Miocene Sedimentary Development of The Arabian Continental Margin In Se Turkey (Adıyaman Region): Implications For Regional Palaeogeography and The Closure History Of Southern Neotethys, *Journal of Asian Earth Sciences* 115, 571-616. DOI: 10.1016/j.jseas.2015.01.025
- Şengör, A.M.C., and Yılmaz, Y., 1981. Tethyan Evolution of Turkey: A Plate Tectonic Approach. *Tectonophysics*, 75, 181-241. DOI: 10.1016/0040-1951(81)90275-4
- Telford, W.M., Geldart, L. P., Sheriff, R.E., Keys, D.A. 1990. *Applied Geophysics*, 2nd Edition. Cambridge University Press, Cambridge 770 p.
- Yılmaz, Y., 1993. New Evidence And Model On The Evolution Of The Southeast Anatolia Orogen. *Geological Society of America Bulletin*, 105, 251-271. DOI:10.1130/0016- 7606
- Yılmaz, Y., 2019. Southeast Anatolian Orogenic Belt revisited (geology and evolution). *Can. J. Earth Sci.*, 56, 1163–1180. DOI: 10.1139/cjes-2018-0170
- Yılmaz, Y., and Yiğitbaş, E., 1991. The different ophiolitic-metamorphic assemblages of SE Anatolia and their significance in the geological evolution of the region: 8th Petroleum Congress of Turkey, *Geology Proceedings*, Ankara, Turkey, 128-140.
- Isik, V., Saber, R., Caglayan, A. 2021. November 08, 2019 Turkmanchay earthquake (Mw 5.9) in NW Iran: an assessment of the earthquake using DInSAR time-series and field evidence. *Natural Hazards*. <https://doi.org/10.1007/s11069-020-04439-1>

5.10 DETERMINING THE STRUCTURAL FEATURES OF THE GULF OF ANTALYA AND ITS OFFSHORE BY USING GRAVITY-MAGNETIC METHODS

A. Kirmızıtaş¹, M.A. Sünnetçioğlu²

¹TPAO, Nizami Gencevi Cad., Çankaya, Ankara, Turkey

*Corresponding author e-mail: akirmizitas@tpao.gov.tr

ABSTRACT

The geophysical modeling study of the Gulf of Antalya and its offshore was conducted by combining both seismic and gravity-magnetic methods in order to reveal regional structural features of the area. Gravity and magnetic methods are used for differentiating geological units with their density and susceptibility differences. These methods have been used to designate base topography, structure, depth, location of magmatic intrusions, and tectonism in the study area.

This study aims determining fault trends of the region and Mesozoic age autochthonous and allochthonous units of the offshore Antalya Neogene Basin. In addition to that, the purpose of this study is identifying the boundary and thicknesses of ophiolitic units by using these magnetic data sets. Three models (two of them are East – West, one of them is North – South) were created to be utilized in the study area. In this model, it has been observed that there was a difference in susceptibility in the region interpreted as ophiolite. In other regions (the magnetic anomaly shows little change) the sedimentary thicknesses display some variations.

KEYWORDS: Gulf of Antalya, Gravity-Magnetic methods, Mesozoic

6.1 AI-BASED INTEGRATION OF GEOSCINCE AND OTHER DATA FOR CARBON SEQUESTRATION AND ENHANCED OIL RECOVERY

F. Aminzadeh^{1,2*}

¹Co-founder, Energy Transition International, Houston, TX USA

²President, FACT, Santa Barbara, USA

*Corresponding author e-mail: famin@fact-corp.com

ABSTRACT

CO₂ sequestration and monitoring its injection into carbon storage sites (often times old oil fields) is becoming an important issues. This is done to address enviromental issues. In addition, when CO₂ is injected into and old oil resrvoir for the additional objective of extracting the oil “behind the pipe” and to extend its life, it has the potential to make the entire process more cost effective. We will refer to this procrss as carbon sequestration-EOR or CS-EOR. This paper highlights everal new ideas on how to use artificail intelligences (AI) to intgrate different types of geoscience data (seismic, micro-seismic, electromagnetics, petrophysics and rock physics) with other data types for an effective CS-EOR. One of the reasons to use AI is the difficulty in data integration due to what we call: SURE challenge. By SURE challenge we mean the fundemental diffeernces in Scale, Uncertainty, Reseolution and the Environment associated with diffeernt data types. Finally, a dynamic updating procedure is introduced for real time monitoring of potential induced seimicity due to the CO₂ injection process. Although in this abstrcat we focus on carbon sequestration, similar techniques could be ustilized for other energy transition applications, including geothrmal exploration and production.

KEYWORDS : GeoScience Data Integration, Artificial Intelligence, Carbon Sequestration, Enhanced Oil Recovery, Dynamic model updating, Energy Transition

INTRODUCTION

This paper focuses on the increasingly important topic of reducing the amount of CO₂ emmission by its sequestration in carbon storage sites (usually in old and abandoned oil fields). Of course when CO₂ is injected into an old oil resrvoir with the additional objective of extracting the residual oil, it offers the opportunity to extend the life of field, resulting in economic benefits and postponment of encouring the field abandonment cost. We will refer to this process as carbon sequestration with enhanced oil recovery or CS-EOR. Given the limited capital budget in most CS-EOR projects cost effectiveness of the employed methods is an important factor. The proposed AI- Based methods take this factor into consideration. Naturally, an effective CS-EOR operation requires reservoir (site) charcaterization through integration of different geoscinces and other data types. Furthermore, to monitor the effctiveness of carbon sequestration and EOR we need to monitor changes in the reservoir parametes as the CO₂ plumes moves in the reservoir.

METHOD and APPLICATION

From many issues associated with CS-EOR we will highlight two key elements in this paper. They include data intergration and dynamic reservoir updating. It should be emphasized that other energy transition problems such as geothermal exploration and production can also benefit from proposed techniques with minor modifications.

Integration of Data with different Scales, Uncertainty, Resolution and Environment

Use of committee machines (modular neural networks) to integrate data from various sources with different Scale, Uncertainty, Resolution, and Environment will improve carbon storage site characterization as well as imaging and monitoring CO₂ plumes. Committee neural networks can also quantify the incremental benefit of each data component on the results, both in the accuracy of the characterization and reduction in the level of uncertainty. Integration of data from different measurements, including conventional 3D seismic, micro-seismic, VSP, cross-well, electromagnetic, well log, and geochemistry data is an important goal. Different scale, uncertainty, data resolution and environments (e.g., lab-scale core-flooding data and CT imaging generated from the CO₂ injection experiments to 4D seismic measurements at the field scale) are consistent with the “SURE” challenge (Figure 1).

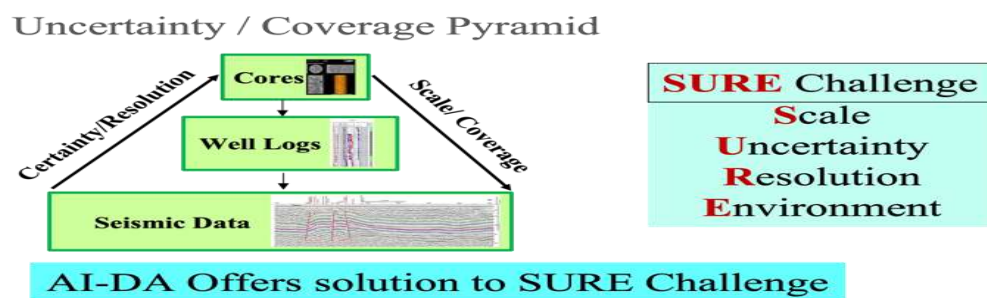


Figure5 SURE Challenge to be addressed by FACT Proprietary AI-DA Based Technology, Adopted from Aminzadeh (2021)

Dynamic updating of the reservoir parameters and potential risk factors during the CO₂ injection and monitoring is very important. The real time or near real time requirements for assessing the dynamic changes in. To reduce the cost and time for updating of the subsurface model and evolution of the fracture system, we have implemented a fast recursive updating technique borrowed from control theory.

The concept is illustrated the Figure 2 (right). The Feedback loop schematically demonstrates how the recursive updating uses the old model, the new input data and the feedback parameter to calculate the new model. The process involves (1) collecting data (D_{old}), (2) creating preliminary model of the “system” S , relating the input data D_{old} to the “output” or model parameters (M_{old}), based on D_{old} and system (3) measure new data (D_{new}), and (4) update the model by tweaking the original model M_{old} through the “innovation process: (adaptive control), using D_{new} , to create the updated model (M_{new}).

An example of application of this approach for updating the fracture system from microseismic data before and after different intervals of CO₂ injection process is shown in Figure 2 (left). In this case, the slope of the fracture grouping at the top of “stage 1” of injection is changed at the second stage of injection, indicating changes in the “b” value which may indicate increased risk associated with induced seismicity because of the new injection.

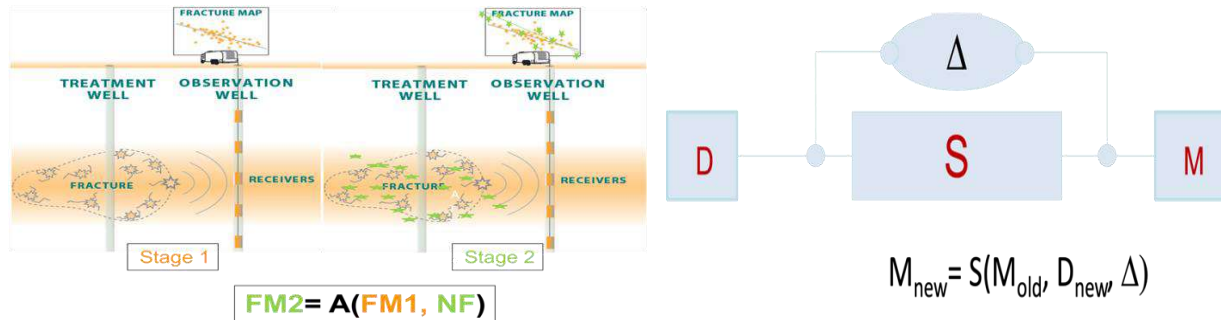


Figure2 Model updating (FM2) as a function of the old model and new fracture (MEQ) Data (left), A- FAST Recursive model updating for fracture mapping in CS-EOR (right) (Aminzadeh 2019)

DISCUSSION and RESULTS

The results shown in Figures 1 and 2 shows the benefits of using AI based method to address the SURE challenge associated with the data integration problem caused by vast differences in Scale, Uncertainty level, data resolution and the environment of different data types for reservoir characterization required for effective CS-EOR. It also show the power of dynamic recursive model updating for real time monitoring of CS-EOR that reduces cost and speeds up the process.

CONCLUSION

Data integration is an important part of any site characterization for CS-EOR. The associated challenges can be overcome by employing AI-Based methods. Furthermore for fast and cost effective model updating, recursive model updating borrowed from control theory can be useful. These tools can be more valuable as move towards interdisciplinary collaboration as we attempt to address more challenging problems.

ACKNOWLEDGEMENT

The author acknowledges contributions of many past and current collaborators.

REFERENCES

- Aminzadeh, F., 2021, Reservoir Characterization: Combining Machine Intelligence with Human Intelligence, E&P Plus, April 2021, Vol. 96 Issue 4, E&P Plus, Hart Energy,
- Aminzadeh, F. and Temizel, C and Hagizadeh, Y., 2022 Artificial Intelligence and Data Analytics for Energy Exploration and Production, John Wiley, ISBN9781119879695: <https://www.wiley.com/en-us/Artificial+Intelligence+and+Data+Analytics+for+Energy+Exploration+and+Production-p-9781119879879>
- Aminzadeh, F., 2021, Reservoir Characterization, Fundamentals and Applications, ISBN 9781119556213, Wiley & Sons
- Aminzadeh, F. 2018, Aminzadeh, F., 2019 Hydraulic Fracturing, ISBN 978111955698, John Wiley: Hydraulic Fracturing and Well Stimulation | Wiley Online Books
- Aminzadeh, F. 2018, Recursive Modeling for Fast Model Updating in Reservoir Surveillance, SPE Workshop: Improve Business Impact and Value with Advanced Data-Driven Analytics 19 - 20 Feb 2018, Houston, TX.
- Aminzadeh, F., 2019 Hydraulic Fracturing, ISBN 978111955698, John Wiley: Hydraulic Fracturing and Well Stimulation | Wiley Online Books

6.2 USING ELECTROMAGNETIC FLUID IMAGING DURING THE ENERGY TRANSITION

K.M. Strack ¹, C. Barajas-Olalde ², P. Soupios ³

¹KMS Technologies, Houston, Texas, USA

²Energy & Environmental Research Center, Univ. of ND, Grand Forks, USA

³ King Fahd University of Petroleum and Minerals, Dhahran, Saudi Arabia

*Corresponding author e-mail: kurt@kmstechnologies.com

ABSTRACT

The controlled-source electromagnetic (CSEM) method provides critical information about reservoir fluids and their spatial distribution. This feature is ideal for carbon dioxide (CO₂) storage, enhanced oil recovery (EOR), geothermal, and lithium exploration applications. CSEM can be tailored to the specific reservoir target objectives by choosing the appropriate components of a multi-component system. First, whether the primary target reservoir is resistive or conductive must be understood. In the CO₂ monitoring case, the injected fluid is resistive. However, the monitoring must also consider the conductive reservoir parts when the injected reservoir is brine-saturated (water-wet) or oil-wet (carbon capture utilization and storage - CCUS). The data acquisition pre-survey is optimized by analyzing the target parameters and the sensitivity capability of multi-component CSEM. The essential tools are on-site noise measurements coupled with 3D anisotropic modeling. From our experience, subsequent surveys go smoothly and deliver robust measurements to meet scientific targets. Another critical element is to combine data acquisition real-time quality assurance with 3D modeling to fine-tune acquisition parameters such as acquisition time and required repeats. The data can be inspected on the fly for the information content of the subsurface while the acquisition is ongoing. As a result, a high-quality data set is usually obtained for processing and (first) interpretation with minimum user interaction. The sensitivity analysis in the inversion is used to verify that acquired data are sensitive to the expected depth range of the target reservoirs. A CO₂ storage site example from North Dakota, USA, describes these steps and shows how the surface measurements achieve log scale (appropriately upscaled) sensitivity. Further, the sensitivity of the CSEM method in other case histories, including EOR, geothermal, and lithium application examples where the target reservoirs are conductive, is presented and discussed.

KEYWORDS: CO₂ storage monitoring; fluid imaging; controlled source electromagnetics (CSEM); CCUS; EOR; geothermal monitoring; lithium exploration.

6.3 HOW IMPORTANT IS MULTIPHYSICS FOR ELECTROMAGNETIC IMAGING

K.M. Strack¹

¹KMS Technologies, Houston, Texas, USA

*Corresponding author e-mail: kurt@kmstechnologies.com

ABSTRACT

Electromagnetic exploration methods, applied to depths ranging from 800 meters to 6 kilometers, can be categorized into three distinct classes for mapping various geological targets:

1. Conductive Anomalies: These anomalies include geothermal heat sources, water floods, and other conductive materials.
2. Resistive Anomalies: This category encompasses hydrocarbon accumulations, carbonates, CO₂ plumes, and other resistive geological features.
3. Anomalous Responses: This includes detecting thin resistive layers, induced polarization, and mapping fault zones.

These methods are inherently limited by their resolution capabilities. However, their effectiveness is often enhanced when combined with other geophysical techniques and geological insights. When consistent results emerge, the risk associated with the solution significantly decreases.

By employing a multi-physics approach, where different physical principles are leveraged, we have developed a strategic method over the years. This approach involves capitalizing on the strengths of each method to compensate for the weaknesses of others, resulting in maximum synergy. Case studies from various environments, such as carbonate formations, sub-salt structures, and sedimentary regions, demonstrate the effectiveness of this combination. These examples also illustrate how this approach accelerates the derivation of project value.

KEYWORDS: Multi-physics, fluid imaging, controlled source electromagnetics (CSEM)

6.4 VOLCANIC MASSIVE SULFIDE (VMS) ORE DEPOSIT IN WESTERN SAUDI ARABIA: A GEOPHYSICAL STUDY

A. Khogali¹, K. Chavanidis¹, A. Stampolidis², R. Coles³, S. Hanafy¹, P. Soupios^{1*}

¹ King Fahd University of Petroleum and Minerals, College of Petroleum and Geosciences, Department of Geosciences, Dhahran, Saudi Arabia

² Aristotle University of Thessaloniki, School of Geology, Greece

³ Golds and Minerals Company Ltd. Al Taif City, Saudi Arabia Al Taif City, KSA

*Corresponding author e-mail: panteleimon.soupios@kfupm.edu.sa

ABSTRACT

In the past ten years, significant progress has been made in developing geophysical technologies specifically designed for mining exploration directly relevant to Volcanogenic Massive Sulfide (VMS) exploration. The utilization of different geophysical methods, such as seismic, DC, EM, gravity, and magnetic, has proven to have a significant practical value in the exploration of VMS deposits. This paper briefly describes the application of gravity, magnetic, and Transient ElectroMagnetic over the Hawiah VMS deposit in Saudi Arabia. The Hawiah deposit has been well constrained through drilling and more standard geophysical methods, allowing the study to validate the various geophysical methods against a known structure and, after that, investigate the subsurface geological uncertainty in specific areas of the site away from known mineralization and to evaluate the ore characteristics and geophysical response and compare back to the constrained areas. The resulting geophysical images were confirmed by seismic and geoelectrical surveys. The geophysical images helped improve the preliminary conceptual model developed using the borehole data and other geophysical information. This research aims to enhance exploration planning, efficiency, and sustainability by reducing costs and saving time.

KEYWORDS: Mining geophysics, VMS, Saudi Arabia

6.5 (NOT PRESENTED) GEOCLUSTER-EXPERTNET: A PROPOSED MODEL INTEGRATING UNSUPERVISED LEARNING WITH EXPERT FOR OPTIMAL GEOTHERMAL DRILLING

Orkun TEKE (Manisa Celal Bayar Univ.)

This abstract not presented during the congress.

6.6 (NOT PRESENTED) INVESTIGATION OF THE RELATIONSHIP BETWEEN THE TOPOGRAPHY AND THE FLUID CIRCULATION DEPTH ON THE GEOTHERMAL SYSTEMS OF CENTRAL ANATOLIA REGION

Sultan BURHANUDDIN (Marmara Univ.), Kamil ERKAN (Marmara Univ.)

This abstract not presented during the congress.

6.7 3D VELOCITY STRUCTURE AND FLUID FLOWS INFERRED FROM THE MICROSEISMIC EVENTS IN THE GEOTHERMAL FIELD, TURKEY

B. Turhan^{1*}, T. Bilgiç², Ü.S. Selek², K. Balci³, A. Yıldırım³, B. Kaypak⁴

¹TPAO, Nizami Gencevi Cad., Çankaya, Ankara, Turkey

²Mikrosismik Mühendislik Danışmanlık Ltd.Sti., Hacettepe Teknokent, Ankara, Turkey

³MASPO Energy San. and Tic.A.Ş., Manisa, Turkey

⁴Jeofizik Mühendisliği Bölümü, Ankara Üniversitesi, Ankara, Turkey

*Corresponding author e-mail: buturhan@tpao.gov.tr

ABSTRACT

Geothermal energy, being a renewable energy source, holds significant potential, particularly in our country. Once exploration methods are employed to identify suitable locations for production wells and the optimal placement of geothermal power plants, there is often a lack of further studies focused on reservoir monitoring or reservoir management within the field. However, it is crucial to implement microseismic monitoring as a customary practice to ensure the sustainability of geothermal reservoirs. This method has been extensively applied worldwide in various geothermal projects. Nonetheless, the first comprehensive application of this method in an industrial context in our country was carried out at the Manisa Geothermal site, supported by TÜBİTAK (1501 TÜBİTAK-TEYDEP Project no: 3200756). Initially, we selected seven borehole sensors strategically positioned around production and injection wells in the geothermal field based on noise analysis results. Continuous data records were analyzed to detect and locate microseismic events, calculate their magnitudes, and determine focal mechanism solutions for assessing stress changes. These events occurred underground during the operations of re-injection, production wells, and overall geothermal activities. Finally, 3D seismic tomography studies were conducted to determine the velocity structure of the field, the mapping of the current reservoir conditions, and the movement of water within the subsurface.

KEYWORDS: Geothermal Energy, Microseismic Monitoring, Reservoir Monitoring, Induced Seismicity.

INTRODUCTION

Renewable energy sources have garnered global significance due to the depletion of fossil fuels and the escalating demand for energy. Our country holds the highest potential with regards to geothermal resources. Geothermal energy is a renewable and environmentally friendly form of energy derived from natural heat sources situated deep within the Earth's crust. The production of geothermal energy involves the extraction of subterranean water or steam, which is subjected

to high temperature and pressure, for the purpose of energy generation. During these operations, microseismic events occur, which are characterized by low energy, high frequency, small amplitude, and rapid attenuation.

The microseismic method entails the precise measurement of seismic wave characteristics, including velocity, frequency, and shape. The standardized implementation of this method is significant for the effective monitoring and management of geothermal reservoirs, ensuring safety and operational efficiency in geothermal field operations. Numerous academic and industrial studies have been conducted worldwide in this field. For instance, it has been used to estimate the spatiotemporal behavior of reservoirs, as demonstrated by studies such as Fehler et al. (1987) and Baria et al. (1999). In a seismic cluster in Basel, Switzerland, Asanuma et al. (2008) successfully determined the locations of microseismic events. The concept of diffusion in fluid-saturated rocks, as proposed by Shapiro et al. (1997), established a relationship between microseismic events and the advancement of the water front (Shapiro et al. 2002). Several studies have endeavored to elucidate pore-pressure migration by incorporating selective water flow in permeable fractures and faults, commonly referred to as the water flow model, as demonstrated by works such as Evans et al. (2005), McClure and Horne (2011), and Mukuhira et al. (2016).

Unfortunately, there is a lack of studies regarding the application of the microseismic method and reservoir monitoring through microseismic events in our country. This study represents the first comprehensive application of this method in our country, supported by TÜBİTAK. To record continuous data, seven borehole sensors were installed in the geothermal production area. The positioning of these stations was determined based on a noise analysis study, allowing for the elimination of background noise sources such as wind, ocean waves, tides, traffic, industrial activities, and artificial explosions (Tunc et al., 2023). Microseismic events were selected from a two-year dataset collected between July 2021 and July 2023. The locations of these events, along with their magnitude calculations and focal mechanism solutions, are presented to illustrate the current state of the reservoir and water flow path (Turhan et al., 2023). In addition, this study presents tomography results obtained through the analysis of the located microseismic events. These results enabled us to determine the velocity structure of the geothermal field and the current status of the reservoir.

GEOLOGICAL SETTING OF THE STUDY AREA

The study area is situated within the boundaries of the Alaşehir district in Manisa province, Turkey. The region is characterized by a combination of pre-Neogene basement rocks and Neogene and Quaternary sedimentary units. Information regarding the geology and stratigraphy of the study area has been compiled from various sources, including Karamenderesi (1994), Karahan (2007), Yolal and Karahan (2010), and Batum et al. (2012). The presence of ancient faults and graben tectonics, which originated during the closure of the Menderes Massif and the İzmir-Ankara Zone, represents significant geological structures within the region. Based on the overall geological framework, two distinct stratigraphic sequences have been identified in the study area. The lowermost units consist of basement rocks belonging to the Menderes metamorphic complex, which have undergone high-pressure and high-temperature metamorphism. Above the

basement units are Tertiary sedimentary rocks. The youngest geological formations in the study area are travertines, which form at the outlets of hot and cold water sources, as well as old and recent alluvial deposits.

The study area represents a reservoir-like region situated within a geological formation known as the Gediz Graben. The Gediz Graben is a rift basin formed by continental rifting processes (Koçyiğit, 2000). During the Miocene period, the graben initially developed as a half-graben, with only the southern margin exhibiting active faulting. Subsequently, in the Plio-Quaternary period, the graben acquired its current asymmetric configuration with the activation of the fault system along the northern margin. The sediments deposited in front of the normal faults constitute the oldest sedimentary fill within the Gediz Graben (Yılmaz et al., 2000). In the study area, the Quaternary sediments can be classified as alluvial fan sediments, fluvial sediments, lacustrine sediments with intercalated fan deltas, and delta sediments. The tectonic structure of the Gediz Graben has significantly contributed to the geothermal potential observed in the region.

RESERVOIR MONITORING and MICROSEISMIC TOMOGRAPHY

In the initial phase of this study, we conducted the localization of microseismic events and determined their depth values by utilizing velocity information obtained from seismic reflection data collected in the field area. The arrival of P- and S-waves was manually identified, and precise hypocenter locations were determined using the Geiger algorithm (Geiger, 1910) and the HYPO2000 program (Klein, 2002). Upon analyzing the spatial distribution of event locations, it becomes evident that there is a higher concentration of events toward the north in the southern portion of the field. This suggests a greater occurrence of fractures during the movement of water in the southern section. This result implies that the lithological formations in the southern part of the field are more prone to fracturing, allowing the reservoir water to circulate at greater depths with less pressure. Another significant finding is that the depth range of the events falls within approximately 1-5 km, which corresponds to the depths associated with geothermal activity. To determine the size of fractures, duration magnitude calculation was employed. Examining the magnitude distribution of microseismic events, it can be observed that induced events with smaller magnitudes tend to occur in proximity to the production and injection wells, whereas naturally occurring tectonic events located at greater depths exhibit larger magnitudes. Figure 1 illustrates the microseismic events located, their magnitudes, and depth values over a two-year period.

Furthermore, focal mechanism solutions were computed for 115 events using the moment tensor inversion algorithm. The solutions indicate predominantly strike-slip faulting. The orientation of the fractures aligns with the geological structure of the field, trending in a northwest-southeast direction. This information allowed us to determine changes in stress distribution and the path of fluid flow within the reservoir. Moreover, we were able to track the distribution of microseismic events in relation to the activities of production and injection wells, thus gaining insights into the pressure and flow variations. It was observed that induced events often coincided with changes in well activity.

Subsequently, seismic travel wave tomography was conducted using microseismic events located over a two-year period. Three-dimensional seismic tomography involves recording the elastic waves emitted by seismic sources in a region using seismographs. The travel times of these seismic wave phases (P- and S-waves) were then subjected to a series of inverse solution processes to visualize the 3D seismic velocity structure of the subsurface. For this study, 1368 events were selected from the 1635 microseismic events detected between July 2021 and the June 2023. The selection process involved applying limited value criteria such as a gap value equal to or smaller than 300° and RMS values below 0.2. Consequently, 5555 P-wave travel time data and 5519 S-wave travel time data were used in the tomography analysis. This allowed us to estimate the P-wave velocity (VP), S-wave velocity (VS), and their ratio (VP/VS) based on a seismic wave tomography method.

Tomographic imaging of the field involved modeling based on the distribution of microseismic events and stations, the number of P- and S-phase readings within the dataset, and the depth variations of the events. The inversion grids employed for forward modeling had dimensions of $500 \times 500 \times 1000$ m. The inverse solution process consisted of two steps. Initially, a 3D VP structure of the region was obtained using only P-wave travel times. The VP/VS structure was then obtained by referencing this VP structure and incorporating the S-wave travel times.

The 3D velocity structure composed of VP (P-wave velocity) and VP/VS (ratio of P-wave velocity to S-wave velocity) for the region was determined up to a depth of approximately 6 km. However, it should be noted that areas without seismic ray paths were unable to be imaged. The velocity values obtained along the existing ray paths can be considered to have lower error values and yield more realistic outcomes. Figure 2 illustrates the calculated ray paths employed in the tomography analysis. VP sections corresponding to specific depth intervals are displayed in Figure 3. Borehole station points are represented by triangles, well locations by rectangles, and events by points. In addition, the VP/VS sections for the selected depth intervals are presented in Figure 4. VP/VS values play a crucial role in interpreting reservoir conditions and fluid pathways, as they serve as important indicators of the fluid content within the reservoir. Higher VP/VS values are often associated with geothermal reservoirs dominated by hot water (Muksin et al., 2013). Conversely, the occurrence of a low VP/VS structure can be attributed to the depletion of pore liquid water and its replacement with steam, particularly in areas with low VP and high VS (Gunasekera et al., 2003). Another possible explanation for the low VP/VS structure is the presence of granite.

The prospective region extending westward from the AKU station, which is characterized by a high VP/VS velocity ratio, is of particular interest. This region coincides with areas where cracks and fractures are likely to occur due to water circulation, as evidenced by an increased number of microseismic events. Changes in the VP and VP/VS values along a selected longitude section are shown in Figure 5. Finally, to facilitate the 3D interpretation of the tomographic results, numerical data were visually represented volumetrically using an isosurface representation, as depicted in Figure 6. In the figure, anomalies that signify the presence of a reservoir and indicate the presence of fluid are believed to correspond to areas where the VP/VS ratio is elevated (light green and red volumetric areas). These anomalies are predominantly located in the southern part of the area, within depth intervals of approximately 2–6 km.

CONCLUSION

The data used in this study were collected over a 24-month period through the deployment of seven borehole sensors within the study area. A total of 1635 microseismic events were selected from continuous passive seismic records. Notably, these events were found to be predominantly concentrated in the southern part of the field rather than in the northern part. This spatial distribution suggests that the movement of reservoir fluid in the southern region contributes to the higher occurrence of fractures and cracks. The locations of these microseismic events are closely linked to injection and production activities and pressure changes within the wells. The calculated magnitudes of the microseismic events were relatively small in scale, as expected. These magnitude values provide insights into the size of the fractures.

Geothermal systems encompass reservoirs characterized by favorable tectonic and geological structures, as well as specific fluid compositions. Seismic waves propagating through such structures are significantly influenced by the geological framework and, in particular, the fluid content within rock fractures. Among the seismic velocities, the S-wave velocity is most sensitive to the presence of fluids and gases and exhibits the fastest response. Consequently, the VP/VS ratio, a tomographic parameter, becomes a vital quantity that can characterize subsurface fluid behavior. In this seismic tomography study, it was observed that the 3D VP and VP/VS structures of the field could be reliably resolved to a depth of 6 km. Distinct variations in the P-wave velocities were identified across different areas. Shallow depths with low VP values could be associated with young sedimentary structures, fractured formations, and porous rocks. Conversely, high VP values across all depth intervals could be attributed to volcanic and basaltic rock formations. Sections displaying low VP and low VP/VS values indicate fractured rocks with pore spaces saturated with gas or water vapor. Furthermore, sections exhibiting high VP and low VP/VS values were observed more frequently. This pattern suggests the presence of pore spaces saturated with gas or water vapor. Consequently, anomalies characterized by low VP values and high VP/VS ratios, particularly in the southern part of the field, indicate locations saturated with fluid and exhibiting high pore pressure.

REFERENCES

- Asanuma H, Kumano Y, Niitsuma H, Schanz Y, Häring M (2008) Interpretation of reservoir structure from super-resolution mapping of microseismic multiplets from stimulation at Basel, Switzerland in 2006. *Trans Geotherm Res Counc* 32:53–58
- Baria R, Baumgärtner J, Gérard A, Jung R, Garnish J (1999) European HDR research program at Soultz-sous-Forêts (France) 1987–1996. *Geothermics* 28:655–669
- Evans KF, Genter A, Sausse J (2005) Permeability creation and damage due to massive fluid injections into granite at 3.5 km at Soultz: 1. Borehole observations *J Geophys Res* 110:B04203.
- Fehler M. House L. Kaieda H., 1987. Determining planes along which earthquake occur: method and application to earthquakes accompanying hydraulic fracturing, *J. geophys. Res.*, 92(B9), 9407–9414.

- Geiger, L. (1910). Herdbestimmung bei Erdbeben aus den Ankunftszeiten. Nachrichten von der Königlichen Gesellschaft der Wissenschaften zu Göttingen, MathematischPhysikalische Klasse, 331-349.
- Gunasekera R.C. , Foulger G.R. , Julian B.R. (2003), Reservoir Depletion At The Geysers Geothermal Area, California, Shown By Four-Dimensional Seismic Tomography, J. Geophys. Res., 108 p. 2134,
- Karahan C, S. Bakrac, H. Dünya, 2003. Alasehir-Kavaklıdere-Gobekli Jeotermal Enerji Arastırma Sondajının Değerlendirilmesi. Sondaj Sempozyumu MTA Ege Bolge Müdürlüğü Ve TMMOB Maden Müh. Hamdi Deliormanlı A., Seçkin C, İzmir Subesi, 10–11 Nisan 2002. Bildiriler, Pp 39–43
- Karamandere İ. H., 1997. Salihli-Caferbeyli (Manisa İli) Jeotermal sahası potansiyeli ve geleceği., Dünya Enerji Konseyi Türk Milli Komitesi, Türkiye 7. Enerji Kongresi teknik oturum bildiri metinleri, pp 247-261
- Klein, Fred W., 2002, User's Guide to HYPOINVERSE–2000, a Fortran Program to Solve for Earthquake Locations and Magnitudes: U.S. Geological Survey Open-File Report 02-171, 123.
- Koçyiğit, A., H. Yusufoglu, E. Bozkurt, 1999. Evidence from the Gediz graben for episodic two-stage extension in Western Turkey. Journal of the Geological Society, London, 156, 605- 616.
- McClure M, Horne R (2011) Investigation of injection-induced seismicity using a coupled fluid flow and rate/state friction model. Geophysics 76(6):181–198
- Mukuhira Y, Dinske C, Asanuma H, Ito T, Häring MO (2016) Pore pressure behavior at the shut-in phase and causality of large induced seismicity at Basel, Switzerland. J Geophys Res Solid Earth. <https://doi.org/10.1002/2016JB013338>
- Muksin, K. Bauer, C. Haberland, (2013), Seismic Vp And Vp/Vs Structure Of The Geothermal Area Around Tarutung (North Sumatra, Indonesia) Derived From Local Earthquake Tomography, J. Volcanol. Geotherm. Res., 260, 27-42
- Tunç, S., Selek, B., Koca, B., Selek, Ü. S., Balci, K., Yıldırım, A., & Kaypak, B. (2023). Installation of microseismic monitoring networks in geothermal fields. Journal of the Faculty of Engineering and Architecture of Gazi University, 38(3), 1307-1319.
- Turhan B., Bilgiç T., Selek Ü. Balci K., Yıldırım, A., & Kaypak, B. (2023). Jeotermal Sahalarda Mikrosismik İzleme Yöntemi ile Rezervuar Takibi, IPETGAS 2023, Oral Presentation, Ankara
- Shapiro S.A. Huenges E. Borm G., 1997. Estimating the crust permeability from fluid injection-induced seismic emission at the KTB site, Geophys. J. Int., 131, F15–F18.
- Shapiro S.A. Rothert E. Rath V. Rindschwentner J., 2002. Characterization of fluid transport properties of reservoirs using induced microseismicity, Geophysics, 67(1), 212–220.
- Yılmaz, Y., S.C. Genç, O.F. Gürer, M. Bozcu, K. Yılmaz, Z. Karacık, I. Altunkaynak, and A. Elmas, 2000. When did the western Anatolian grabens begin to develop. in Bozkurt, E., Winchester, J.A., and Piper, J.D.A., eds., Tectonics and magmatism in Turkey and the surrounding area: Geological Society of London Special Publication, 173, 353–384.
- Yolal, A. and Ç. Karahan, 2010, Aydın Pamukören AP-3 Jeotermal Sondajı Kuyu Bitirme Raporu. MTA report, No. 11280.

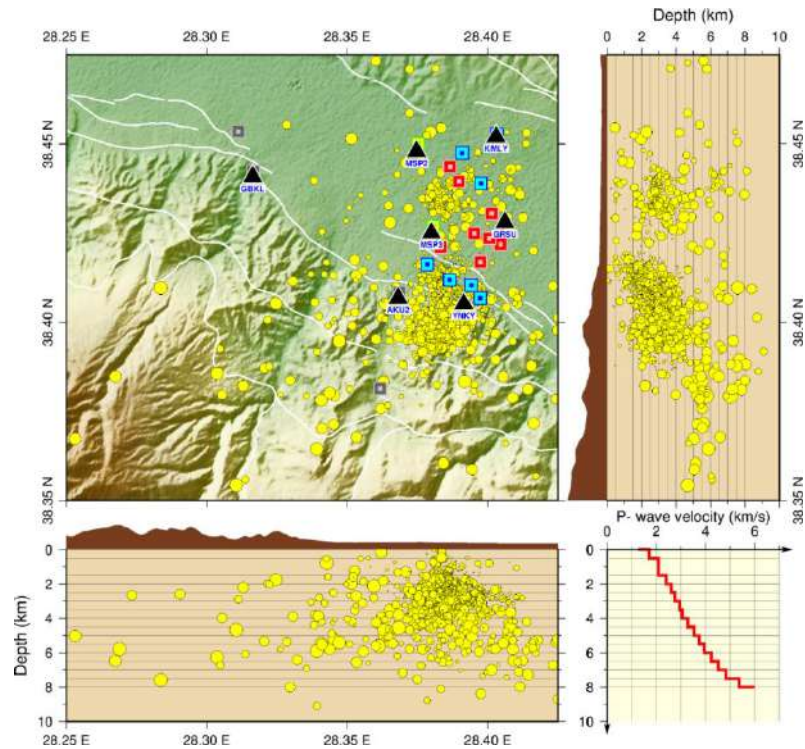


Figure6 Representation of microseismic event locations (yellow colored circles) in relation to magnitude and depth, along with the distribution of sensors (blue triangle symbols) over a two-year period. The 1-D seismic velocity model used for determining the locations is provided in the lower right corner

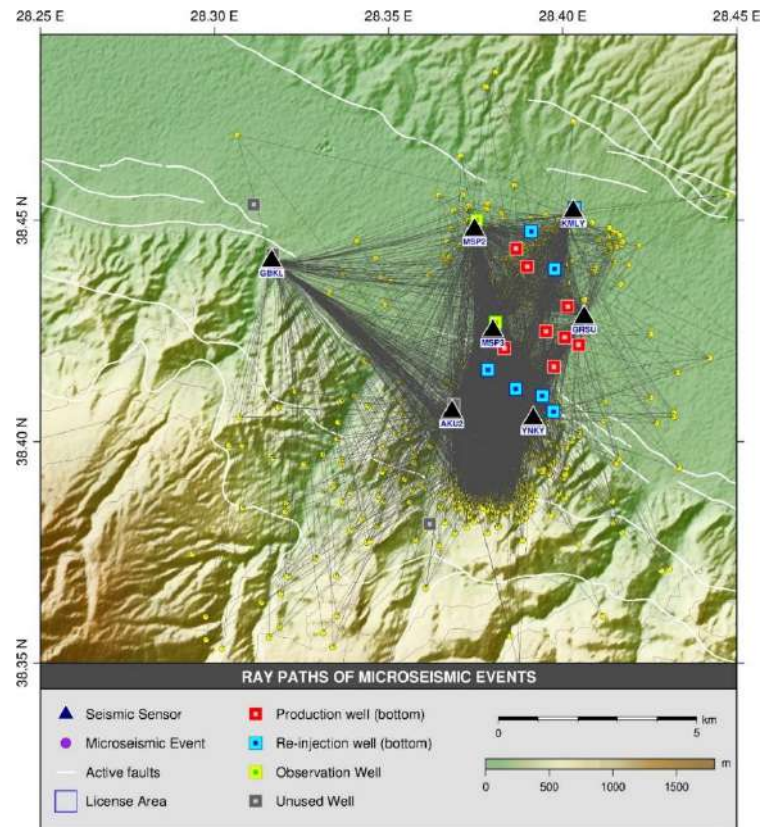


Figure7 Ray paths used in obtaining tomography results.

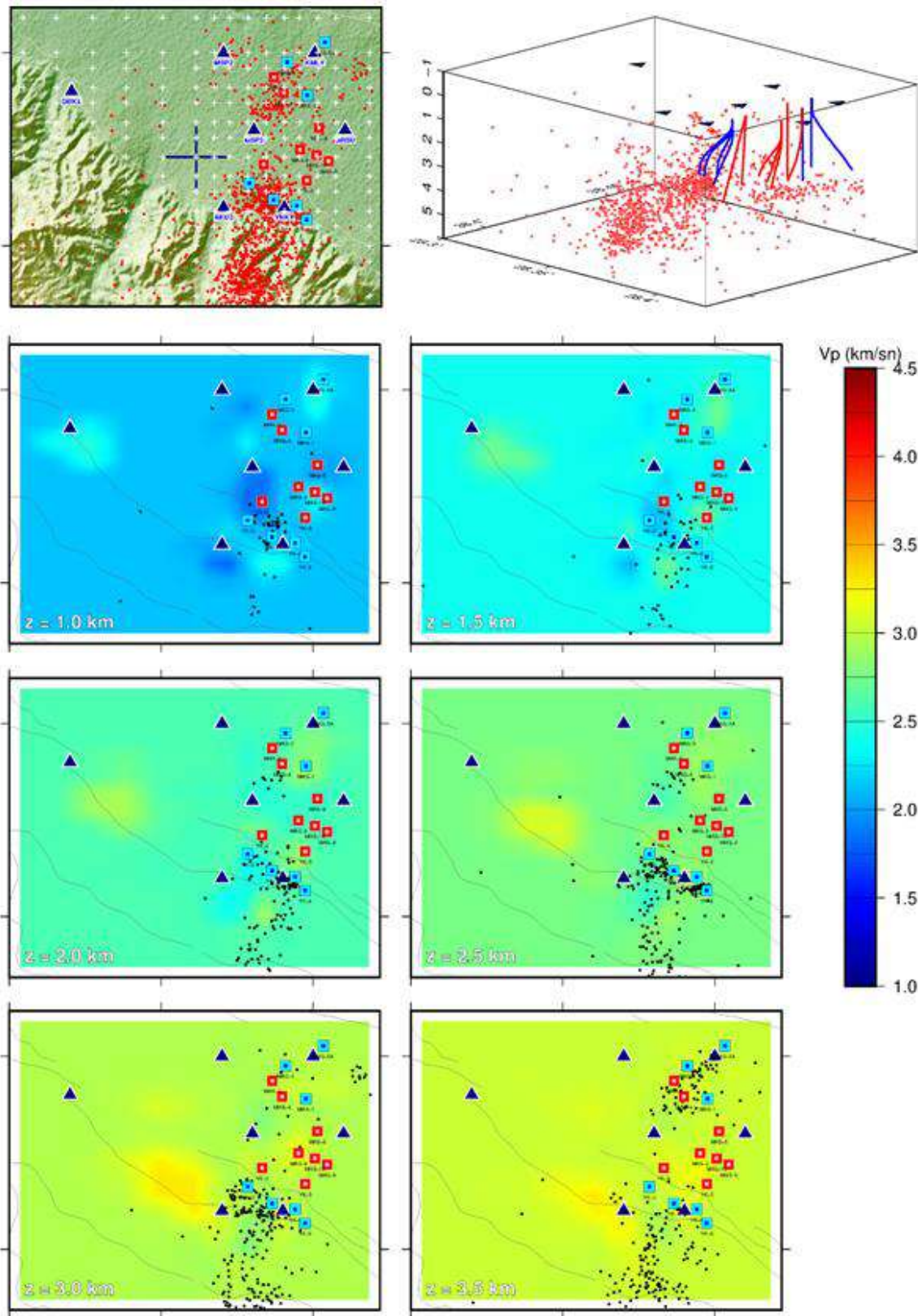


Figure8 Absolute VP layer maps obtained from the 3D inverse solution. Stations are represented by triangles in the sections, microseismic events are indicated by black/red dots, and faults are shown as white lines.

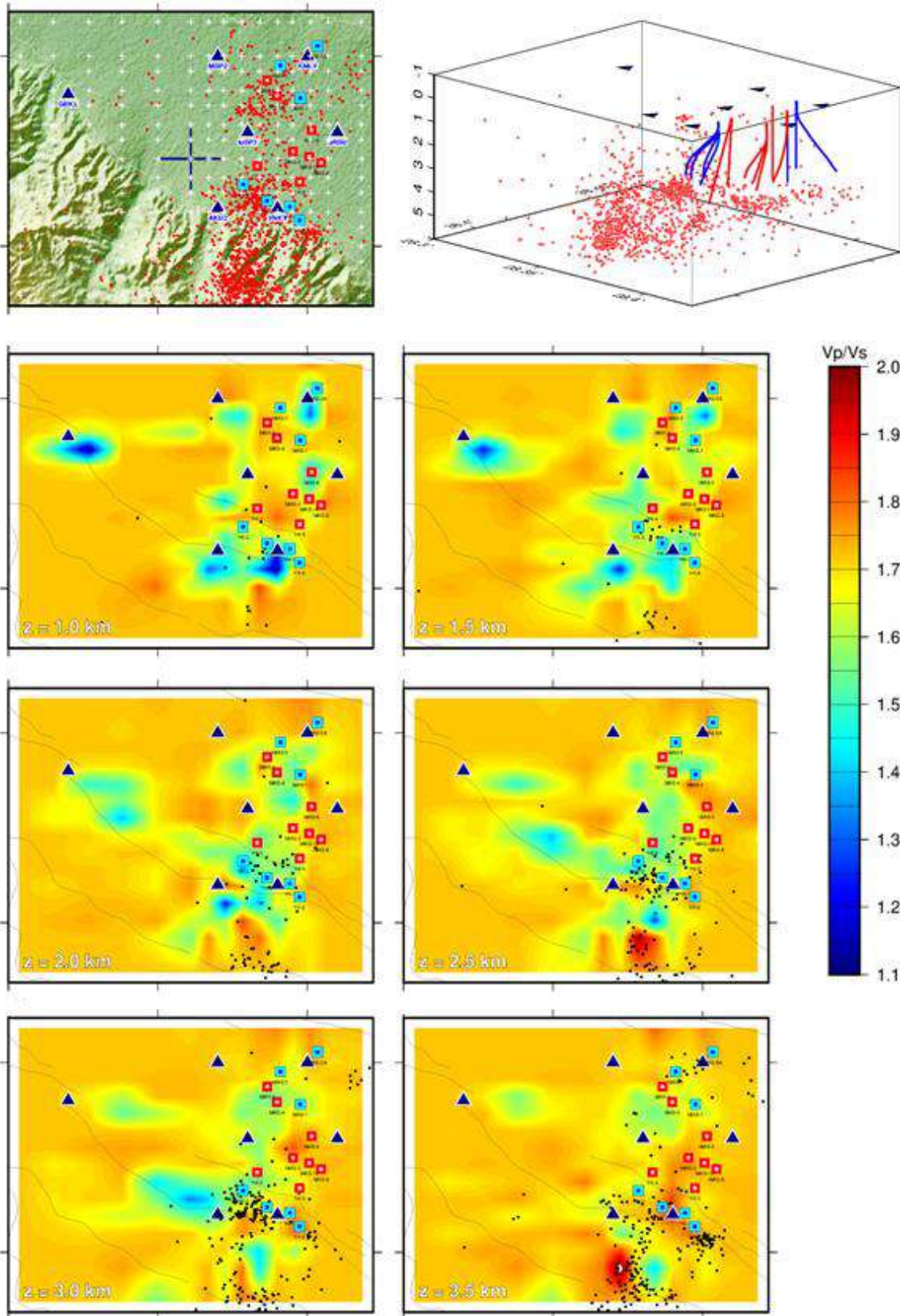


Figure9 Absolute VP/Vs layer maps obtained from the 3D inverse solution. Stations are represented by triangles in the sections, microseismic events are indicated by black/red dots, and faults are shown as white lines.

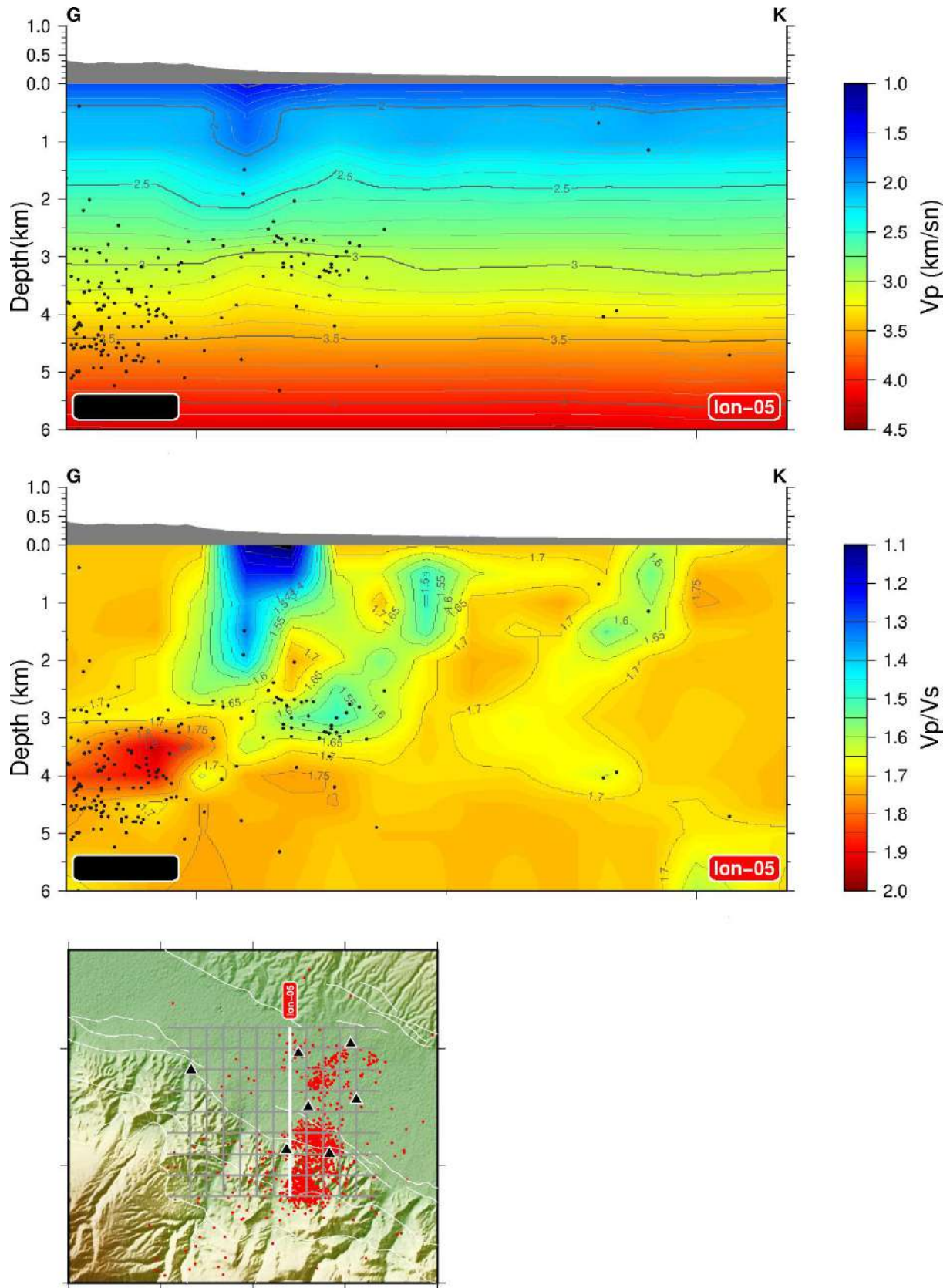


Figure10 Vertical cross-sections of absolute VP (top) and absolute VP/VS (bottom) for Profile 5. The black dots represent the locations of microseismic events projected onto the cross-section.

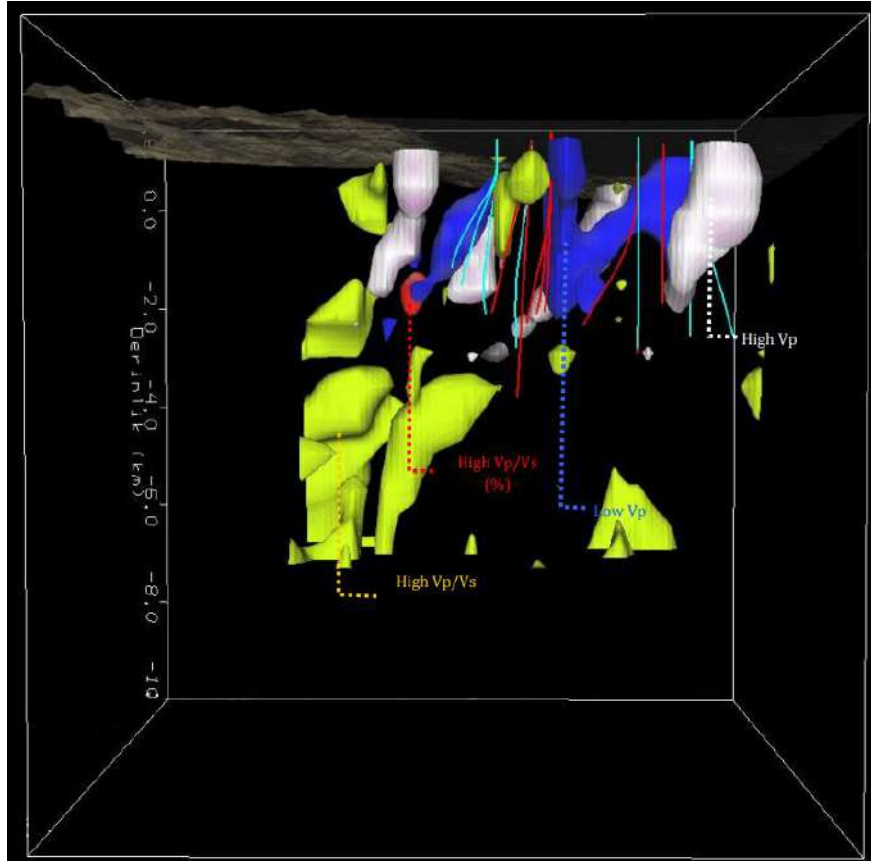


Figure11 3D Volumetric Representation of Velocity Anomalies Obtained from Tomographic Calculations (View from East to West)

6.8 MAGNETOTELLURIC SYSTEM NORD

D. Epishkin^{1,2*}, A. Yakovlev³ and N. Zorin^{1,3}

¹STC Nord-West, Moscow, Russia

²Schmidt institute of physics of the Earth, GEMRC, Moscow, Russia

³Lomonosov Moscow State University, Moscow, Russia

*Corresponding author e-mail: dmitri_epishkin@mail.ru

ABSTRACT

Key features of the new magnetotelluric system NORD are: wireless operation with options of real-time quality assessment and data processing, measuring complex impedance of each electric line, robust data processing algorithms, light weight, reliability, low self-noise and power consumption. The receiver has a built-in calibration system as well as telemetry that allows to monitor the status of the device and identify common problems. The system allows to obtain high-quality MT data in the range from 50 000 seconds up to 20 000 Hz. In this paper we show some results of recent field tests of the NORD system which show that it meets the highest standards and requirements imposed on the modern geophysical equipment.

KEYWORDS : electromagnetic instrumentation, MT acquisition system.

6.9 DIG: A RESEARCH PROJECT TO ASSESS IRELAND'S GEOTHERMAL ENERGY POTENTIAL

D. Kiyan^{1,2}, B. O'Reilly^{1,2}, J. Fulla^{1,3}, S. Lebedev^{1,4}, C.J. Bean^{1,2}, P. Meere^{2,5}, E.L. Chambers¹, T. Ye¹, M. Rezaeifar¹, A. Scully⁵, and the DIG team

¹DIAS, School of Cosmic Physics, Geophysics Section, Dublin Institute for Advanced Studies, Dublin, Ireland

²ICRAG, SFI Research Centre in Applied Geosciences, Dublin, Ireland

³UCM, Department of Physics of the Earth & Astrophysics, Universidad Complutense de Madrid, Madrid, Spain

⁴UC, Department of Earth Sciences, University of Cambridge, Cambridge, UK

⁵UCC, School of Biological, Earth and Environmental Sciences, University College Cork, Cork, Ireland

*Corresponding author e-mail: duyqu@cp.dias.ie, bor@cp.dias.ie

ABSTRACT

Potential deep (greater > 400 m) geothermal resources, within low to medium temperature settings remain poorly understood and largely untapped in Europe. DIG (De-risking Ireland's Geothermal Energy Potential) is an academic project started in 2020, which aims to develop a better understanding of Ireland's (all-island) low-enthalpy geothermal energy potential through the gathering, modelling and interpretation of geophysical, geological, and geochemical data. In the island-scale strand of the project, we develop a novel approach to determine the geothermal gradient using a new joint geophysical-petrological inversion where seismic velocities and density in the mantle are related to temperature and bulk composition within a thermodynamic framework. Large datasets of phase velocities of seismic surface-waves are now incorporated into the inversion, and provide essential constraints on the lithospheric thickness and temperature, which shape the crustal geotherms to a significant extent. We also include all available measurements of the surface heat flow, radiogenic heat production and thermal conductivity within the crust, to further constrain the temperature and geothermal gradient, in particular in the top few kilometres of the crust. Local-scale research aims to evaluate the geothermal energy potential of the Upper Devonian Munster Basin within the Variscides of southern Ireland. A more specific objective is to focus on the Mallow Warm Springs Area (MWSA) which is sited along the Killarney-Mallow Fault Zone (KMFZ). The constraints gathered by the magnetotelluric and passive seismic data within the KMFZ are integrated with rock physics and geochemical data. This substantial body of work will also include a fluid chemistry program to understand the fluid rock interactions within the KMFZ and their impact on physical properties (MT and seismic). Collectively, using this expertise, the study evaluates the geothermal and economic potential of the region and more specifically the MWSA. This local focus on the MWSA aims to directly image fault conduits and fluid aquifer sources at depth, within a convective/conductive region associated with the known occurrence of warm thermal springs. This will determine the scale of the geothermal anomaly, its correlation with our gathered data: and will so evaluate the potential for both local and industrial-scale space heating in the survey locality. The project is funded by the Sustainable Energy Authority of Ireland under the SEAI Research, Development & Demonstration Funding Programme 2019 (grant number 19/RDD/522) and by the Geological Survey Ireland.

KEYWORDS: Low-Enthalpy Geothermal, Mallow Warm Springs Area, Ireland

6.10 GEOELECTRICAL CHARACTERIZATION OF GEOTHERMAL RESERVOIRS – CASE STUDIES FROM GEDİZ GEOTHERMAL AREA (TÜRKİYE)

Ö. Hacıoğlu^{1*} and A. T. Başokur²

¹*Geophysical Engineering Department, Karadeniz Technical University, Trabzon, Turkey*

²*Lemnis Geoscience, Ankara University Technological Development Center, Ankara, Turkey*

*Corresponding author e-mail: ozlem.hacioglu@ktu.edu.tr

ABSTRACT

The extensional tectonics in western Anatolia result in the development of grabens oriented in an approximately east-west direction and low-to-high enthalpy geothermal systems along the margins of the grabens, large-scale detachment surfaces, normal faults, and high heat. The convection-dominated geothermal systems in this area are primarily controlled by the deformation zones, namely faults and fracture zones. We acquired wide-band magnetotelluric data in different parts of the Gediz basin, western Anatolia, to derive upper crustal electrical resistivity models of the geothermal prospects. The resistivity models provide significant implications for a better understanding of the deep structural image of the subsurface and, therefore, the structure of geothermal reservoirs and flow pathways for the geothermal environment. Accordingly, the circulation of geothermal fluids in reservoirs is dominantly controlled by normal faults, namely the low-angle detachment fault and main graben-bounding fault. Besides, fracture zones developed under north-south extensional stress within the metamorphic basement play an important role in locally trapping of fluids to form geothermal reservoirs. We classify the reservoir types taking into account the zones exhibiting low resistivity anomalies, namely i) reservoirs in the shallow sedimentary layers, ii) reservoirs underlying alteration zones consisting of smectite and illite minerals, and iii) reservoirs in the metamorphic basement that the fractures and faults filled with conductive fluids.

KEYWORDS: Geothermal systems, normal faults, extensional tectonics, Gediz, magnetotellurics, 3D inversion

7.1 PHOENIX NEW GENERATION MT/CSAMT TECHNOLOGIES WITH REAL TIME DATA TRANSFER CAPABILITIES

E.Erdogan^{1*}

¹Phoenix Geophysics Limited, Toronto, ON, Canada

*Corresponding author e-mail: eerdogan@phoenix-geophysics.com

ABSTRACT

Phoenix Geophysics is a pioneering geophysical instrument manufacturing company that has played a leading role in the electromagnetic (EM) community, meeting the needs of both academia and industry. Since the release of the first natural EM field data loggers (MT-16, 1980), with the data processor initially mounted on a minivan for a single Magnetotelluric (MT) station, Phoenix has maintained a focus on downsizing the equipment while simultaneously improving accuracy and reliability. Second generation MT receivers (V5, 1987) were more compact but still needed wired connection for remote reference synchronization. In 1997, Phoenix invented and developed the first Satellite Synchronized MT (SSMT) systems (US Patent 6,191,587, 1996). This was a significant milestone in the field of EM geophysics, allowing users remote reference processing with satellite synchronization. This generation of receivers was the first model of MT data loggers which had sensor processing and data processing in the same unit. Recently, Phoenix Geophysics introduced another groundbreaking feature that allows users to access their data on-site from anywhere in the world via a network connection. This feature has been employed for natural source EM field monitoring applications over the last couple of years and is expected to accelerate similar applications within the EM community.

KEYWORDS: magnetotellurics, natural EM signals, real time, monitoring

7.2 JOINT APPLICATION OF ELECTROMAGNETIC PROSPECTING METHODS FOR MINERAL EXPLORATION: CASE STUDIES

A. Solovyeva^{1*}, D. Epishkin¹, V. Kulikov¹, D. Yakovlev¹ and N. Zorin¹

¹Nord-West Limited, Moscow, Russia

*Corresponding author e-mail: soloway.msu@gmail.com

ABSTRACT

Electromagnetic geophysical methods allow determining the spatial distribution of the low-frequency resistive (electrical resistivity) and capacitive (chargeability) characteristics of rocks. Since both properties are affected by lithology, pore fluid chemistry, water, graphite and ore mineral content, some combinations of electromagnetic methods could be especially useful in mineral exploration. In this paper we consider several examples of electromagnetic method application in mineral exploration performed by Nord-West company.

KEYWORDS: resistivity, induced polarization, magnetotellurics

7.3 REAL TIME MONITORING OF THE NATURAL BROADBAND EM SIGNALS: APPLICATIONS FOR MONITORING OF ACTIVE VOLCANOES

E. Erdoğan^{1*}, Y. Avram¹, G. Hill², M. Moorkamp³

¹Phoenix Geophysics Limited, Toronto, ON, Canada

²Czech Academy of Science, Prague, Czech Republic

³University of Munich, Germany

*Corresponding author e-mail: eerdoqan@phoenix-geophysics.com

ABSTRACT

In recent years, there have been notable advancements in remote network data transfer methods that have had a transformative impact on various geophysical techniques. The monitoring of natural electromagnetic (EM) fields, in particular, has proven to be a valuable tool for gaining insights into tectonic events. However, permanent monitoring stations have historically encountered challenges related to the transfer of data due to the substantial file sizes involved. Fortunately, recent developments in network systems and the state-of-the-art technology employed in magnetotelluric (MT) data loggers have paved the way for real-time access to MT data, presenting an innovative approach to monitoring natural electromagnetic fields.

In this study, we present an examination of several case studies that showcase real-time volcano monitoring, with a particular emphasis on active volcanoes, such as those found in Hawai'i, Mount St. Helens, and Stromboli. Through these case studies, we aim to underscore the practicality and effectiveness of utilizing real-time MT data for volcano monitoring.

KEY WORDS : magnetotellurics, natural EM signals, real time, monitoring, volcanos

7.4 MAGNETOTELLURICS IN DEEP MINING OPERATIONS: CASE STUDIES FROM NORTH AMERICA

E.Erdogan^{1*}, Y. Avram¹, G. Hill², M. Moorkamp^{3,1}

¹Phoenix Geophysics Limited, Toronto, ON, Canada

²Czech Academy of Science, Prague, Czech Republic

³University of Munich, Germany

*Corresponding author e-mail: eerdoqan@phoenix-geophysics.com

ABSTRACT

Over the past decade, the utilization of Magnetotellurics (MT) has experienced significant growth. By 2023, its applications have become critical in deep mining operations at deposit and regional scales, serving both commercial and research purposes, sometimes concurrently. The global demand for critical minerals has acted as a catalyst for the widespread adoption of MT techniques. Furthermore, large-scale national projects have emerged with the objective of comprehending the profound structure of the lithosphere and its impact on near-surface deposits. In this study, we have reviewed various case studies related to mining exploration in North America.

KEYWORDS: magnetotelluric, mining, exploration, ore deposits

7.5 KMS ARRAY SYSTEM FOR CSEM/MT

K.M. Strack¹

¹KMS Technologies, Houston, Texas, USA

*Corresponding author e-mail: kurt@kmstechnologies.com

ABSTRACT

The KMS array system is founded on an innovative array concept that seamlessly integrates wireless and wired data acquisition, with full cloud connectivity. The system comprises both land-based acquisition units, the KMS-820, and borehole receivers, the KMS-888, along with transmitters, KMS-5100. Specialized marine versions are also available. Each individual unit is capable of functioning as an independent node while also having the ability to create sub-arrays when connected to a wired sub-acquisition controller, thereby expanding the channel count to virtually unlimited number of channels.

Our target market primarily consists of applications that demand long-term stability and precision, made possible through our patented technology. While it finds widespread use in magnetotellurics, our system is designed with a focus on the more exacting requirements of Controlled Source Electromagnetics, particularly in borehole environments. Our receivers can seamlessly connect to various sensor types, facilitating data acquisition across a frequency range spanning from DC to 40 KHz, with support for up to 6 channels simultaneously. Our super broadband MT sensors extend from 0.0001 to 10 kHz, offering the lowest noise levels in the industry. Low frequency fluxgate sensors can be added via the digital port. These induction coils are trusted by numerous space research institutions.

For reservoir monitoring applications, the system demonstrates exceptional long-term stability for both transmitters and receivers, as evidenced by several monitoring projects in which it successfully detected conductive and resistive anomalies. Real-time monitoring of any receiver from anywhere in the world is easily achievable. Additionally, part of the Quality Assurance process is already available through a machine learning modules within the cloud. Currently, we are further integrating 3D survey design and quality assurance with the data acquisition process, enabling seamless merging of borehole, marine, and land receivers/transmitters.

KEYWORDS: Real time monitoring; fluid imaging; controlled source electromagnetics (CSEM); magnetotellurics; array acquisition.

7.6 LITHIUM-THE IMPORTANT RESOURCE OF GREEN TECHNOLOGY: PROPERTIES, GEOLOGY AND TURKEY'S POTENTIAL

A. Yıldız^{1,2}

¹Afyon Kocatepe University Engineering Faculty Department of Geological Engineering, Afyonkarahisar, Turkey

²Afyon Kocatepe University The Application and Research Center of Geothermal and Ore Deposits

*Corresponding author e-mail: ayildiz@aku.edu.tr

ABSTRACT

Lithium has become one of the indispensable elements of modern industry due to its unique properties, such as its lightness ($\rho = 0.53 \text{ g/cm}^3$ at 20 °C), high specific heat capacity, the lowest ionic radius among alkali metals, and high electrochemical potential. The Action Plan on Critical Raw Materials of European Commission published in September 2020 predicted that the demand for lithium will increase 50 times in the next 2050. For this reason, the exploration of lithium deposits in the earth's crust has become very important. This study reveals the lithium's properties, geology and Turkey's lithium potential.

According to the United States Geological Survey (USGS), the world's total lithium reserve is 98 million tons, and the world's total lithium production in 2022 is 130,000 tons. The lithium resources occur in three different geological environments. These are (1): Pegmatites, (2): Sediment-hosted deposits and (3): Brines. The world's current lithium production is produced from three resources: brines (64%), pegmatites (29%) and clays (7%). The lepidolite minerals in magmatic rocks, clay sediments in boron deposits, current and dried lake basins (Tuz Lake, Acıgöl, Lake Van) and geothermal waters constitute the most important lithium resources in Turkey.

KEYWORDS: Lithium, Properties, Geology, Turkey's Potential

INTRODUCTION

Lithium is the alkali metal with the lowest density ($\rho = 0.53 \text{ g/cm}^3$ at 20 °C), high specific heat capacity, low ionic diameter and high electrochemical potential among the alkali metals (Garrett, 2004; Christmann et al., 2015). Due to its physical and chemical properties, lithium and its compounds are used in a wide variety of industrial applications such as ceramics, lubricants, aerospace, polymers, metal additives and especially Li-ion batteries (Dessemond et al., 2019; Zhao et al., 2023).

Lithium is widely distributed in the earth's crust and is found in rocks, soil, salt lakes, seawater, oil reservoirs, geothermal waters and many natural waters (Wietelmann and Bauer, 2000; Helvacı et al., 2006;). Lithium occurs in three types of geological environments. These are (1): Pegmatite deposits, (2): Clays and (3): Brines. The brine deposits constitute 66% of global lithium reserves.

The EU aims to be climate-neutral by 2050 – an economy with net-zero greenhouse gas emissions. It is estimated that annual electric vehicle sales will increase to 10 million in 2025 and 28 million in 2030, and electric vehicles will constitute more than half of all passenger vehicle sales in 2040 due to net-zero greenhouse gas emissions. These developments in electric vehicle sales are

expected to increase global demand for lithium (EU 2020). For this reason, the exploration of lithium deposits in the earth's crust has become very important. This study aims to reveal the properties of lithium, its geological formations and Turkey's lithium potential.

RESULTS and DISCUSSION

Properties

Lithium is the metal with the lowest density, coming after hydrogen and helium in the periodic table. Its atomic number is 3, and its atomic weight is 6.941. The name lithium comes from the Greek word "lithos" meaning "stone", represented by the symbol Li. Lithium is a soft, silver-white metal in the alkaline element group. Like all alkaline elements, Li is highly reactive and flammable. Therefore, it never occurs freely in nature and only occurs in compounds, usually ionic compounds (Vikström et al., 2013).

There are approximately 130 known lithium minerals. The silicates, phosphates or borates are mostly lithium carriers, except for 14 minerals in the carbonate or fluoride group (e.g., griseite [LiF], zabuyelite [LiCO₃], cryolithionite [Na₃Li₃Al₂F₁₂]) (Christmann et al., 2015).

Lithium Deposits

Economical lithium deposits occur in three different geological environments. These; (1): Pegmatites, (2): Clays and (3): Brines (Christmann et al., 2015; Bowel et al., 2020). There are three different types of brines as continental (lacustrine), geothermal and petroleum.

Lithium resources in brines 66% of global lithium reserves are in saltwater reservoirs. There are three different types of brine reservoirs: continental (lake), geothermal and petroleum. There are studies on lithium production from pegmatites, clays and brines in the world. The lithium production from brines is the least costly and least laborious of the known methods. The method includes precipitation, purification, ion exchange and absorption processes.

Turkey's Lithium Potential

The lepidolite minerals in magmatic rocks, clay sediments in boron deposits, current and dried lake basins (Tuz Lake, Acıgöl, Lake Van) and geothermal waters are the most important lithium resources in Turkey (Akgök and Şahiner, 2017; Gülez et al., 2019).

One of the main resources of lithium is granitic pegmatites. Petalite in these rocks is another important lithium source. Potential sources are acidic rocks containing lithium-rich mica, such as lepidolite and tin granites (Gülez et al., 2019). The presence of lithium was found in the aplites and pegmatites of the granitoids located between Kırşehir-Yozgat-Akdağ Madeni (Kadirioğlu, 2002), in the pegmatites of the Menderes Massif in Çine (Aydın) district, and in the migmatites of the Menderes Massif in the Manisa (Gördes-Demirci) region (Selim, 1967).

Clays in boron deposits contain high amounts of lithium. It is located in the octahedral layer of the clay mineral of the lithium hectorite type. High lithium values were obtained throughout the boron deposits in Turkey (Bigadiç (0.02-0.21%) and Kırka (0.16-0.30%) clays). It is closely related to minerals in which lithium sodium element is found in high amounts in boron deposits (Mordoğan et al., 1995). Lithium values of 1256 - 3,009 ppm were found in the Kırka (Eskişehir)

boron deposit, 25 - 982 ppm in Emet (Kütahya), 254 - 770 ppm in Mustafakemal Paşa (Bursa), and 152 - 2,709 ppm in Bigadiç (Balıkesir) (Gülez et al., 2019).

Lithium values in salt water are quite high. Lithium values between 20 and 365 ppm were found in Salt Lake. Lithium values up to 100 ppm have been measured in Konya-Karapınar Meke and Acı lakes. A lithium value of 29 - 48.5 ppm was found in Kayseri Sarioğlan Tuzla lake. Values of 270 ppm were obtained in Tersakan Lake and 50 ppm in Bolluk (Gülez et al., 2019).

The geothermal resources in Turkey contain high amounts of easily soluble minerals and metals due to the geological characteristics of the environment. Lithium concentration reaches a maximum of 68ppm in geothermal resources in Turkey. Lithium is produced from geothermal fluids that reach the earth through drilling to take lithium's heat in geothermal resources. The geothermal fluid, from which heat energy is extracted and the lithium it contains, is pumped back into the reservoir with a closed system. Therefore, in the lithium production facility to be established in enterprises operating on the use of geothermal fluid, the transportation of the fluid to the lithium enrichment facility and the process of pumping it back to the reservoir will not impose an extra cost burden on the enterprises (Yıldız et al., 2021).

CONCLUSIONS

This study aims to reveal the properties of lithium, its geological formations and Turkey's lithium potential. Lithium is the metal with the lowest density, coming after hydrogen and helium in the periodic table. Its atomic number is 3, and its atomic weight is 6.941. There are approximately 130 known lithium minerals. Economical lithium deposits occur in three different geological environments. These; (1): Pegmatites, (2): Clays and (3): Brines (Christmann et al., 2015; Bowel et al., 2020). There are three different types of brines: continental (lacustrine), geothermal and petroleum. The lepidolite minerals in magmatic rocks, clay sediments in boron deposits, current and dried lake basins (Tuz Lake, Acıgöl, Lake Van) and geothermal waters are Turkey's most important lithium resources. It is very important to explore in detail these geological environments containing lithium in the future and to conduct technological tests on lithium extraction from these resources.

REFERENCES

- Akgök, Y., Şahiner, M., 2017. Dünyada ve Türkiye’de Lityum. General Directorate of Mineral Research and Exploration (MTA) Department of Feasibility Studies, 25p, Ankara, (In Turkish).
- Bowell, R.J., Lagos, L., Hoyos, C.R., Declercq, J., 2020. Classification and Characteristics of Natural Lithium Resources. *Elements*, 16, 259-264.
- Christmann, P., Gloaguen, E., Labbé, J.-F., Melleton, J., Piantone, P., 2015. Global lithium resources and sustainability issues. *Lithium Process Chem.* 1–40.
- Dessemond, C., Lajoie-Leroux, F., Soucy, G., Laroche, N., Magnan, J.-F., 2019. Spodumene: the lithium market, resources and processes. *Minerals* 9 (6), 334.
- EU, 2020. Action Plan on Critical Raw Materials. 4p.
- Garrett, D.E., 2004. Part 1. Lithium. *Handbook of Lithium and Natural Calcium Chloride*.
- Gülez, B., Çiçek, M., Bakır, S., Yiğit, E., Tan, S., Topsakal, H., Akalın, N., 2019. Türkiye Endüstriyel Aramaları Lityum Aramaları Projesi (Türkiye Geneli Raporu). General Directorate of Mineral Research and Exploration (MTA) Project No: 2012-32-13-07, 2013-32-13-14, 531p, Ankara, (In Turkish).

- Helvacı, C., Mordoğan, H., Çolak, M., Gündoğan, İ., 2006. Presence and Distribution of Lithium in Borate Deposits and Some Recent Lake Waters of West-Central Turkey. *International Geology Review*, 46 (2): 177-190.
- Jaskula, B.W., 2022. Lithium. U.S. Geological Survey (USGS), Mineral Commodity Summaries, 2p.
- Kadirioğlu, F.T., 2002. Yozgat - Akdağmadeni Güneyinde Li-Be-W ve Sn aranması ve Sarıkaya Kargalık Li-Be İçeren Pegmatitlerin Maden Jeolojik İncelenmesi. Msc Thesis, Ankara University, 94p, Ankara, (In Turkish).
- Mordoğan, H., Helvacı, C., Malayoğlu, U., 1995. Bor Yatakları Killeri ve Güncel Göllerdeki Lityum Varlığı ve Değerlendirme Olanakları. *Endüstriyel Hammaddeler Sempozyumu*, 12p, İzmir, (In Turkish).
- Selim, M., 1967. Gördes Demirci ve Simav Bölgelerindeki Pegmatitlerin Genel Prospeksiyonu. General Directorate of Mineral Research and Exploration (MTA) Report No: 5098, Ankara, (In Turkish).
- Vikström, H., Davidsson, S., Höök, M., 2013. Lithium availability and future production outlooks. *Appl. Energy* 110, 252–266.
- Yıldız, A., Can, M.F., Başaran, C., 2021. Jeotermal Kaynaklardan Lityum Üretimi ve Kazanılması. *JESDERGİ*, 15, 24-28, (In Turkish).
- Zhao, H., Wang, Y., Cheng, H., 2023. Recent advances in lithium extraction from lithium-bearing clay minerals. *Hydrometallurgy* 217 106025.

7.7 THE GEOCHEMISTRY OF CLAYS ÇAVUŞÇUGÖL (ILGIN, KONYA)

H. Fidan^{1*}, G. Yanik¹, A. Yıldız², C. Özkul¹

¹Kütahya Dumlupınar University, Engineering Faculty, Department of Geology Engineering, Kütahya, Türkiye

²Afyon Kocatepe University, Engineering Faculty, Department of Geology Engineering, Afyonkarahisar, Türkiye

*Corresponding author e-mail: hakan.fidan.one@gmail.com

ABSTRACT

The Harmanyazı graben and the Çavuşçugöl graben, located in the north of Ilgın district of Konya province, host clay formations, which are the main subject of this study. The Harmanyazı graben is a fault controlled basin and widespread an approximately east-west direction. Çavuşçugöl graben, on the other hand, is a large basin bounded by the north-south diirection Ilgın fault in the west and approximately north-south direction Tekeler fault in the in the east. Over time, as these basins became lake environments, phyllites and metasandstones belonging to the Bahçecik formation and Bağrıkurt formation, which surrounded the basins, started to accumulate in the basin. Lignite coals were formed in both basins in the lakeside swampy environment and in semi-tropical climatic conditions. Due to the formation of lignite coal, with the effect of groundwater, humic acid flowed onto the clastic material previously transported to the basin floor from the surrounding units, and this humic acid enabled the muscovite and arkosic material in the phyllite and metasandstones of the Bahçecik Formation and the Bağrıkurt Formation to become clay with the contribution of hydrothermal processes. During clay formation, Al, which is immobile in the phyllites and metsandstones belonging to the Bahçecik and Bağrıkurt formations, was enriched in the illite, kaolinite and pyrophyllite minerals of the Çavuşçugöl clays, while K was enriched in the illite mineral. In the study area, the Harmanyazı graben is the place where the upper-coal clays are clearly observed, while the under coal clays are observed more clearly in the Çavuşçugöl graben. While illite is the most common mineral at both levels, the ratio of other kaolinite and quartz is higher in the upper-coal clays, while the rate of pyrophyllite is higher in the under-coal clays. This is due to the conversion of kaolinite and quartz in the under-coal clays to pyrophyllite and water by burial diagenesis and hydrothermal effects.

KEYWORDS: Clay, coal, geochemistry, Konya, Ilgın

7.8 A LARGE SCALE ERT SURVEY FOR LOCATING CLAY MINERALS

A. Stampolidis^{1*}, P. Louvaris¹, E. Amanatidou¹, K. Polydoropoulos¹ and N. Kordatos¹

¹Department of Geophysics, School of Geology, Aristotle University of Thessaloniki, Thessaloniki, Greece

*Corresponding author e-mail: astamp@geo.auth.gr

ABSTRACT

Geophysical methods are very successful in prospecting for ceramic raw materials. The resistivity method is sensitive to several parameters; in the case of clay minerals in the soil it is reduced due to their electrochemical characteristics, such as the absorption of water molecules. IP method is also sensitive to the presence of clay minerals.

The electrical resistivity tomography (ERT) and the IP method were applied to determine clay content in near-surface formations. Clays are the most crucial raw materials in the ceramic industry, so discovering new clay deposits with good ceramic properties is very important.

More than 60 line kilometers of ERT data and some IP data were collected with an electrode spacing of 5m, using a 10-channel Syscal Pro Switch 48e. The survey was performed mainly on public agricultural roads and followed by core sampling at specified locations that showed good correlation with resistivity data. Areas with high potential for clay horizons were detected and presented in this research.

KEYWORDS: Geoelectrical methods, Ceramic industry, Clay minerals, Mining Geophysics

7.9 USING MARINE CSEM FOR RESERVOIR MONITORING BASED ON PETROPHYSICAL MODELING

M. Ettayebi¹, S. Wang^{2*} and M. Landrø³

¹PhD candidate, Department of Electronic Systems, Norwegian University of Science and Technology, Trondheim, Norway

²Senior Researcher, Department of Electronic Systems, Norwegian University of Science and Technology, Trondheim, Norway

³Professor, Department of Electronic Systems, Norwegian University of Science and Technology, Trondheim, Norway

*Corresponding author e-mail: shunquo.wang@ntnu.no

ABSTRACT

The Marine Controlled-Source Electromagnetic (CSEM) method is a technique used to measure electromagnetic fields transmitted by an active source either at the seafloor or just a few tens of meters above it. This method allows us to image the electrical resistivity beneath the seafloor, making it valuable for identifying resistivity anomalies, particularly those related to high saturations of petroleum. Since its introduction in 1981 by Cox, the marine CSEM method has been gaining popularity in petroleum exploration. However, the applications of electromagnetic research have started to expand beyond petroleum exploration into an active production monitoring tool, which is the focus of our study. To achieve this, we created realistic geoelectric models by utilizing dynamic reservoir properties obtained through reservoir simulation of the Wisting field in the Norwegian part of the Barents Sea. The geologically consistent rock physics models developed in our study can also allow us to transform the simulation results into resistivity maps. Using a Finite Difference Time Domain (FDTD) forward modeling workflow, we demonstrate that the resistivity map for each time-step can be used as an input model to generate synthetic EM data. This synthetic EM data is then studied and analyzed to understand production-induced changes in the reservoir during different production phases. This helps us develop a technically feasible reservoir monitoring workflow suitable for time-lapse CSEM. Our findings indicate that the CSEM responses vary during different production phases, making the method effective for production monitoring purposes. Additionally, our study enables the testing of other time-lapse workflows with realistic complexities, allowing us to evaluate the potential of this technology for field application. We investigate resolution limitations and repeatability requirements to gain valuable insights for future implementations of the technique.

KEYWORDS: 4D, controlled-source electromagnetic method, reservoir monitoring

INTRODUCTION

The controlled-source electromagnetic (CSEM) method is a reliable technique for hydrocarbon exploration, complementing seismic studies due to its sensitivity to resistive and conductive anomalies like oil reservoirs and water. Researchers are increasingly exploring its potential for

time-lapse production monitoring, especially in realistic reservoir models at various production phases.

Our research focuses on enabling time-lapse 3D CSEM for reservoir monitoring by using geologically consistent rock-physics models. These models convert dynamic reservoir properties of the Wisting field in the Norwegian part of the Barents Sea into resistivity models for different time steps. These resistivity models are used as inputs in a Finite Difference Time Domain (FDTD) workflow (Werthmüller et al., 2021) to generate synthetic EM data for studying time-lapse production effects.

The Wisting discovery was made in 2013 at well 7324/8-1, located on the Wisting Central prospect (Figure 1). The reservoir, part of the Realgrunnen Subgroup (Fruholmen, Nordmela, and Stø Formations), was penetrated at a depth of 662 meters with a water depth of 400 meters. Wisting has notable electric properties, with a background resistivity of up to 20 Ωm (Granli et al., 2017), making it favorable for CSEM applications. The primary objective of drilling well 7324/8-1 was to explore hydrocarbons in the Jurassic Realgrunnen Subgroup, and it proved successful as a discovery well (NPD, 2022).

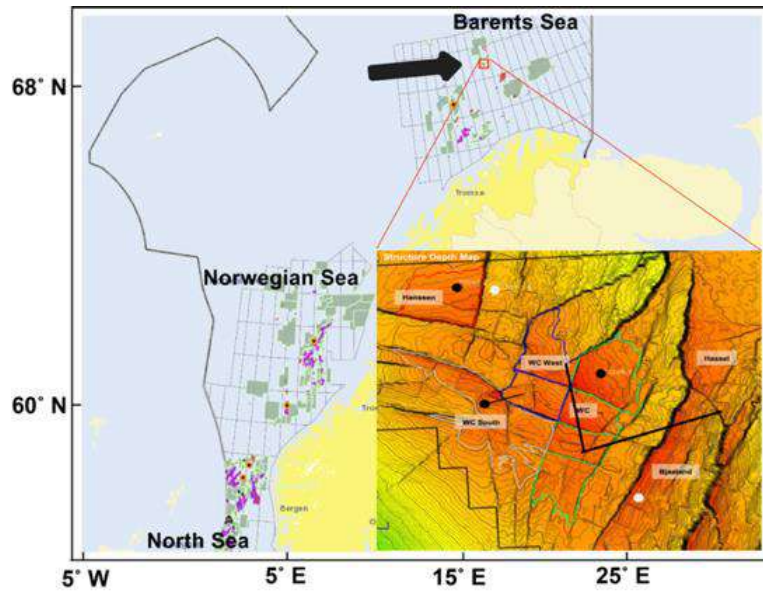


Figure1 The Wisting field is situated in the Barents Sea, marked by a red rectangle on the map.

In this research, we've compiled a comprehensive dataset, including production simulation models, well-logs, and 3D CSEM inversion results. Our main goal is to use this data within a rock physics framework to create realistic resistivity models representing various oil production phases. These models will be used to assess the potential of time-lapse CSEM for reservoir monitoring, considering survey parameters and feasibility. The study consists of two main parts. The first part involves constructing and calibrating the reservoir model to match observed data, establishing a reliable foundation. The second part explores the viability of time-lapse CSEM using the realistic resistivity models. We analyze synthetic EM data to gain insights into CSEM's potential for monitoring production changes over time. Note that repeatability requirements are not addressed here but remain a crucial aspect for future research.

METHODS AND PETROPHYSICAL MODELS

CSEM data is crucial for imaging subsurface resistivity structures, especially for time-lapse reservoir monitoring in fields like Wisting. Key factors influencing resistivity include the saturation exponent "n" and rock wettability, with complex effects in clay-containing

reservoirs. Wisting's possible oil-wet nature, as suggested by Alvarez et al. (2018), allows for adjustments to "n" to yield higher resistivities. Our study explores the non-linearity of "n" in oil-wet formations, dependent on water saturation. Oil-wet formations exhibit higher "n" due to isolated non-conductive water globules in larger pores. Wettability effects are pronounced as

brine saturation decreases. A connate water saturation threshold (10%) was established using capillary pressure curves and FWL depth maps, enhancing resistivity modeling accuracy. Gas-bearing zones require special "n" considerations; a gas saturation threshold of 70% effectively distinguishes them from oil-wet rocks. Our non-linear saturation exponent model assigns "n" based on these thresholds. We set saturation exponent values depending on a 10% connate water saturation threshold and a 70% gas saturation threshold. We used a rock physics model to convert water saturation simulations into resistivity maps for time-lapse CSEM studies in Wisting. Figure 2 illustrates this application.

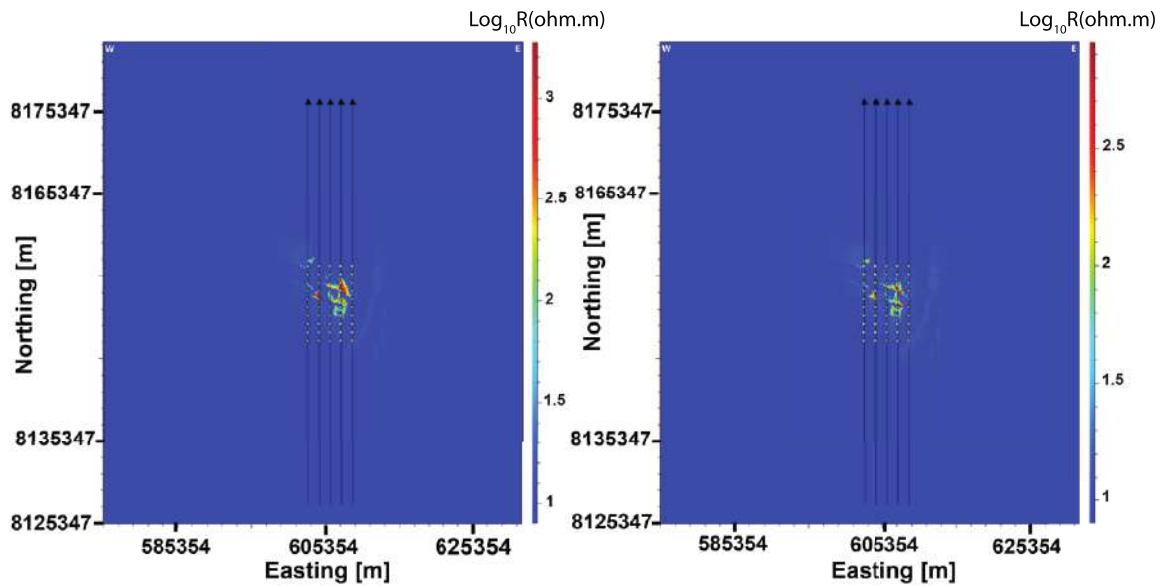


Figure2 The provided 2D resistivity maps howcase the subsurface conditions at two different time steps. The left for the year 2027, the right for the year 2057. The white rectangles are receivers and the black vertical lines going through them are owl lines.

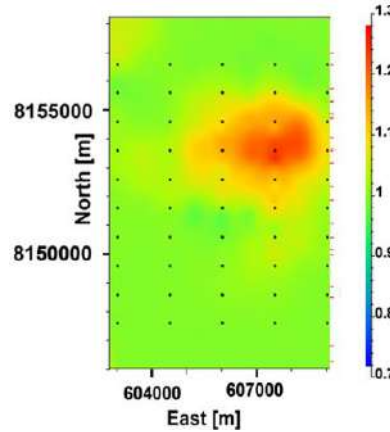


Figure3 The provided 2D maps display the Normalized Magnitude (NM) of the Ex field component for two distinct time steps. The plot represents the Ex fields of the year 2057 normalized by the Ex fields of the year 2027

4D CSEM RESPONSES

The simulation, conducted with a source-receiver offset of 2667 meters and a 5.0 Hz frequency, focuses on two critical time points: production onset in 2027 and 30 years into production in 2057. Figure 3 displays Ex-field normalized magnitude (NM) maps for these time steps. NM values of 1 (light green) signify no change in subsurface reservoir fluid content, while values greater or smaller than 1 indicate changes.

Figure 3 clearly reveals production-induced changes, seen as red positive anomalies, matching the resistivity maps in Figure 2. These anomalies align with the predicted production activity location. In hydrocarbon fields, decreasing petroleum volumes due to water injection result in lower resistivity values over time. Towards the field's end, the target resistor depletes, leaving a final resistivity response without it. Figure 3 emphasizes this with the positive anomaly, showing the 2027 response exceeds the 2057 pseudo-background response. The relatively high frequency in Figure 3 indicates higher resolution. This is also related to the combination of higher background resistivity and shallow burial depth. These results in Figure 3 offer valuable insights into subsurface reservoir changes during 30 years of production, showcasing CSEM's potential as an effective monitoring tool for tracking production-induced alterations.

CONCLUSIONS

In this study, we demonstrated the process of converting dynamic reservoir simulations at different time steps into resistivity spatial distributions using a detailed, realistic, and geologically consistent rock-physics model. These resistivity maps served as inputs in a FDTM forward modeling workflow to generate synthetic CSEM data. By studying and analyzing the CSEM data using various approaches, we aimed to develop a practical workflow for time-lapse CSEM studies. The results of the study revealed the capability of CSEM data to effectively detect and capture production-induced changes in the fluid content of a hydrocarbon reservoir during production. The presented workflow demonstrated the feasibility of using time-lapse CSEM as a monitoring tool in reservoir management. Future research will focus on investigating the repeatability requirements and limitations of time-lapse marine CSEM, and optimize and refine the workflow

for practical applications in the oil and gas industry. Understanding the repeatability of the method is essential to ensure the reliability and consistency of the data obtained in multiple monitoring surveys over time.

ACKNOWLEDGMENTS

We appreciate Equinor and the license partners for generously providing us with valuable data that have been essential for conducting this research. We are also grateful for their permission to publish the findings of this research. Additionally, we acknowledge the support of the Norwegian Research Council (294404, 309960, 324442, and 90484802), the GAMES consortium, and the Center of Geophysical Forecasting for funding this study. We are grateful to Friedrich Roth for his software support and Jan Petter Morten for his inputs. We would also like to thank Sigma2 - the National Infrastructure for High-Performance Computing and Data Storage in Norway (nn9872k) - for providing the necessary computing resources for conducting the modeling and simulations required for this research. The extended paper of this research has been published in the journal of Sensors (<https://doi.org/10.3390/s23167197>).

REFERENCES

- Alvarez P, Marcy F, Vrijlandt M, et al. (2018) Multiphysics characterization of reservoir prospects in the hoop area of the barents sea. Interpretation 6(3):SG1–SG17, DOI 10.1190/int2017-0178.1
- Granli JR, Veire HH, Gabrielsen P, et al. (2017) Maturing broadband 3D CSEM for improved reservoir property prediction in the Realgrunnen Group at Wisting, Barents Sea. SEG Expanded Abstracts 2017 pp 2205–2209
- NPD F(2022)7324/8-1general information <https://factpages.npd.no/en/wellbore/pageview/exploration/all/7> accessed: 2022-06
- Werthmüller, D.; Rochlitz, R.; Castillo-Reyes, O.; Heagy, L. Towards an Open-Source Landscape for 3-D CSEM Modelling. Geophysical Journal International 2021, 227, 644–659.

8.1 COMPARING THE EFFICIENCY OF SYNTHETIC VS NATURAL-BASED LIQUID ACTIVATED CARBON IN REMOVING ORGANIC POLLUTANTS FROM CONTAMINATED WATER

B.S. Tawabini^{1*}, T. Saleh², M. Alrayaan², R. Nasser³, P. Soupios¹, P. Kirmizakis¹

¹ Geosciences Dept., King Fahd University of Petroleum & Minerals, Saudi Arabia.

² Chemistry Dept., King Fahd University of Petroleum & Minerals, Saudi Arabia.

³ Saudi Arabian Oil Company, Saudi Arabia.

*Corresponding author e-mail: bassamst@kfupm.edu.sa

ABSTRACT

In recent years, more attention was given to the use of the in-situ injection of liquid activated carbon (LAC) to clean contaminated groundwater sources. This lab-scale study is carried out to investigate the capacity of synthetic and natural-based LAC adsorbents coated on solid materials (i.e. sand and limestone) for the removal of organic compounds such as MTBE and BTEX. The synthesized LAC material was characterized using SEM/EDXS, XRD and FTIR to study its morphological and chemical features. Batch treatment runs were conducted under various treatment conditions such as LAC dosage, pH and conductivity. Results showed that LAC may reach more than 95% removal of BTEX compounds by both types of LAC. However, the removal of MTBE was not high with a maximum removal of around 50% only. The study demonstrated that LAC can be used effectively in removing BTEX compounds, but more work is still needed to reach the same level of removal of MTBE.

KEYWORDS: liquid activated carbon (LAC); biochar; MTBE; BTEX; adsorption; groundwater

INTRODUCTION

BTEX and MTBE are common organic pollutants frequently encountered in contaminated groundwater sources near underground fuel leaking storage tanks. These compounds may impose serious health risks to humans [1] and thus are regulated for drinking purposes [2]. The high solubility of MTBE has resulted in contaminated water supplies around the world. Moreover, MTBE has low biodegradability rate, low log K_{ow} (1.24) and low Henry's constant (0.022) makes it difficult to remove with traditional treatment methods such as biodegradation, adsorption or air stripping [3]. Advanced oxidation processes (AOPs) were successfully applied to treat water contaminated with BTEX and MTBE but with high energy and chemical costs [4]. Adsorption is still an attractive method when considers the removal of both BTEX and MTBE from contaminated waters. In groundwater remediation, both ex-situ (pump & treat) and to a lesser extent in-situ adsorption treatment methods were applied using synthetic-based AC [5] or naturally-based AC [6] or polymeric materials [7]. However, due to the high cost of ex-situ adsorption and varying rates of efficiencies, more attention was given, in recent years, to using the in-situ adsorption method through injecting nano-sized AC in liquid form (i.e. LAC)

downstream of the contaminated groundwater plume forming a film on the subsurface material to act as a permeable reactive barrier. Limited studies investigated the efficiency of LAC in remediating contaminated aquifers and no reports were found that address the use of in-situ LAC adsorption for multiple contaminants, such as BTEX and MTBE in the middle east region. Therefore, this study was carried out to demonstrate the efficiency of using biochar and commercial-based LAC in treating groundwater contaminated with MTBE and BTEX compounds for their removal through lab-scale batch experiments.

METHOD and APPLICATION

The natural-based LAC was produced from local palm fibres that were cleaned, grinded ($\varnothing = 1-2$ mm), and combusted at 450°C under N₂ gas (99.9%). 5% H₂O₂ solution was added to the prepared biochar, treated with 1.0 M HNO₃ and then heated to 90°C while stirred for 3 hours. after which it was cooled down to room temperature. The biochar-based LAC was then liquefied with distilled water at wt. %, ratio of 1:10 and 0.5% poly-ethyleneimine. The commercial AC was crushed to a very fine powder (d₉₉ < 10µm) to prepare the LAC. One g of the powder commercial AC was sonicated in 100 mL of water for 1 hr. Then, 10 mL of polyethyleneimine solution at a concentration of 0.5 % was added to the sonicated AC. After that, the volume of CCAC was made up to 250 mL and mixed for 1 hr, using a high-shear mixer at 3660 rpm to obtain a homogeneous mixture. Both types of LAC were characterized using SEM/EDXS, FTIR, and XRD techniques. Moreover, different subsurface materials (i.e. Ottawa sand (OS), limestone (LS) and mix (OS/LS)) were used in the experiments. The LACs were mixed with these materials to mimic the in-situ injection of LAC. Highly pure BTEX and MTBE solutions were prepared in distilled-deionized water at concentrations of 2000 ppb and their concentrations levels before and after adsorption were measured using GC/MS instrument. In each run, certain amounts of material (OS, LS, 1 OS/LS, and GAC) were well mixed with certain amounts of LAC. The mixed materials were then added to the conical beakers and shaken at 150 rpm for 60 minutes. Samples were taken every at 0, 15, 30, 45 and 60 min for analysis of residual pollutants

DISCUSSION and RESULTS

The main characteristics of natural-based LAC were: Total C (86%), N (2%), O (12%), O/C (0.14), ash content (5%), surface area (786 m²·g⁻¹) and total pore volume (0.68 cm³/g). The commercial LAC, particle distribution analysis showed that the sample that was ground using the balls mill have the smallest particle sizes d₉₉ < 10 µm. The SEM images (Fig. 1) indicate that the LAC is slides-like shape of the prepared carbon, while the EDXS EDXS shows that the main elements are C and O, which indicates the presence of the oxygen functional groups on the carbon surface.

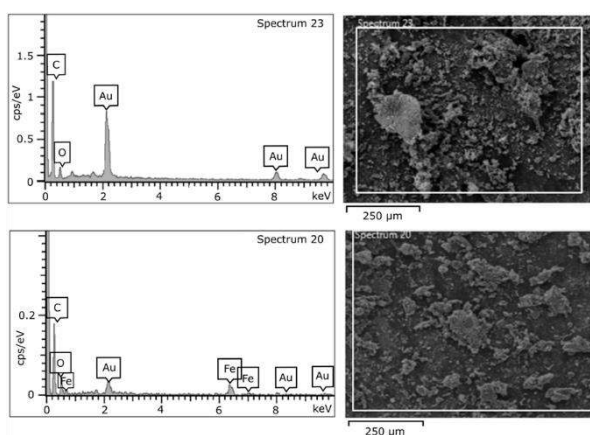


Figure1 SEM and EDX of LAC

The adsorption performance of bio and commercial LAC are presented in Figs.2 and.3 respectively. Fig.2 shows that the adsorption by the bio-LAC-coated materials were generally low, compared to GAC. On the other hand, the adsorption performance of commercial LAC presented in Fig.3 shows better removal of the 3 pollutants, compared to bio-LAC. The maximum removal efficiencies by the coated with bio-LAC were 2, 25 and 40% for MTBE, Benzene and Toluene, respectively.

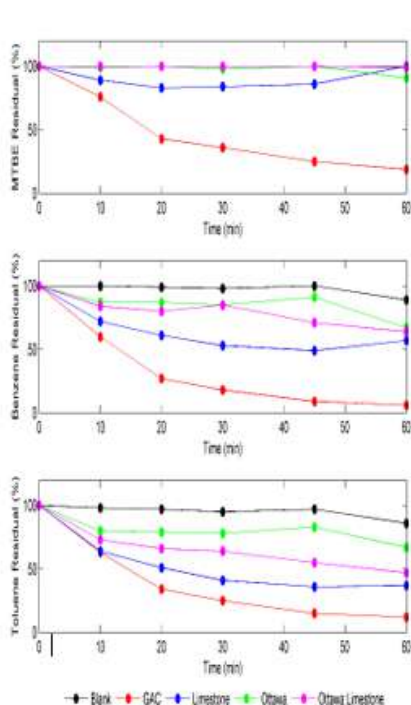


Figure 2

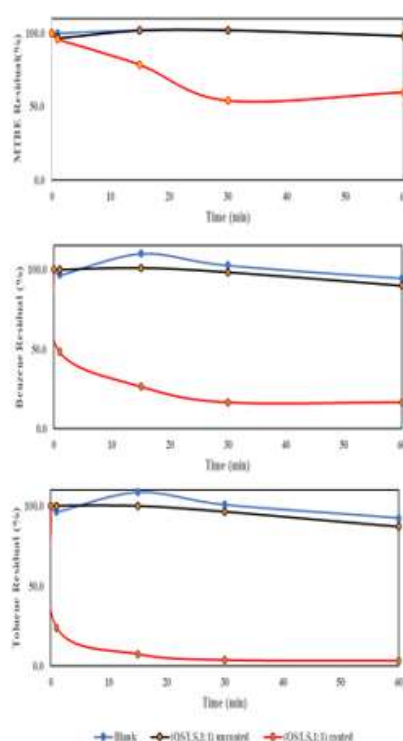


Figure3

CONCLUSION

While commercial LAC showed maximum removal efficiencies of 45, 75 and 95 % for MTBE, Benzene and Toluene, respectively. It was also noticed that both bio and commercial LAC have low adsorption behaviour for MTBE, compared to Benzene and Toluene.

ACKNOWLEDGEMENT

The authors wishes to thank King Fahd University of Pteroleum & Minerals (KFUPM) and Saudi Aramco for supporting this work under funded project CIPR 2354.

REFERENCES

- Dąbrowski, A. Adsorption — from theory to practice. *Adv. Colloid Interface Sci.* 2001, 93, 135–224, doi:10.1016/S0001-8686(00)00082-8.
- Levchuk, I.; Bhatnagar, A.; Sillanpää, M. Overview of technologies for removal of methyl tert-butyl ether (MTBE) from water. *Sci. Total Environ.* 2014, 476–477, 415–433, doi:10.1016/j.scitotenv.2014.01.037.
- Pan, L.; Nishimura, Y.; Takaesu, H.; Matsui, Y.; Matsushita, T.; Shirasaki, N. Effects of decreasing activated carbon particle diameter from 30 Mm to 140 nm on equilibrium adsorption capacity. *Water Res.* 2017, 124, 425–434, doi:10.1016/j.watres.2017.07.075.
- Crane, R.A.; Scott, T.B. Nanoscale zero-valent iron: Future prospects for an emerging water treatment technology. *J. Hazard. Mater.* 2012, 211–212, 112–125.
- Abubakar, R. Evaluation of benzene, toluene and p-xylene from produced water using locally available adsorbents and granular activated carbon. *Int. Res. J. Eng. Technol.* 2020, 2619–2639.
- Carey, G.R.; McGregor, R.; Pham, A.L.T.; Sleep, B.; Hakimabadi, S.G. Evaluating the longevity of a PFAS in situ colloidal activated carbon remedy. *Remediation* 2019, 29, 17–31, doi:10.1002/rem.21593.
- Sorengard, M.; Kleja, D.B.; Ahrens, L. Stabilization of per- and polyfluoroalkyl substances (PFASs) with colloidal activated carbon (PlumeStop®) as a function of soil clay and organic matter content. *J. Environ. Manage.* 2019, 249, 109345, doi:10.1016/j.jenvman.2019.109345.

8.2 RESISTIVITY IMAGING OF AQUIFER STRUCTURE WITH 2D/3D INVERSION OF DIRECT CURRENT RESISTIVITY AND AUDIO- MAGNETOTELLURIC DATA

N.Y. Gündoğdu^{1*}, M.E. Candansayar¹

¹Dr., Prof. Dr., Department of Geophysical Engineering, Geophysical Modeling Group (GMG), Ankara University, Ankara, Türkiye

*Corresponding author e-mail: gundogdu@eng.ankara.edu.tr

ABSTRACT

In this study, direct current resistivity (DCR) and audio-magnetotellurics (AMT) methods were applied to identify aquifer structures and/or fracture zones in limestone units that are likely to supply wells located near the study area and actively covering the water demand. DCR studies were performed along 5 lines and AMT measurements were taken in 13 stations. The orientations of the DCR lines were selected considering the determination of the aquifer recharge direction. DCR measurements were collected using a pol-dipole electrode array (left and right-sided) for better lateral separation. A total of 4650 apparent resistivity data were measured on 5 lines. The measurement time of AMT data collected as a time series at each station varies between approximately 2-5 hours. Station intervals are approximately 100 metres to cover the entire study area. Both the 2D and the 3D inversion were carried out separately for the data collected using the two methods. The resistivity distribution of a total area of 30 hectares (500 m x 600 m) was revealed. In 2D inversion, the RMS values of DCR models and AMT models were below 3% and 5%, respectively. In the 3D inversion, the RMS values are 3.2% and 9.7%, respectively. All the models obtained were interpreted separately and together and aquifer structures and fracture zones were identified on the subsurface resistivity models. Interpreted geophysical models, geologic, hydrogeologic and drilling information were evaluated and interactions of these structures and zones with the existing water well were revealed.

KEY WORDS: Direct current resistivity, audio-magnetotellurics, resistivity, inversion, aquifer

INTRODUCTION

By using geophysical methods, the structure of the earth's interior can be revealed with data measured on the ground. Each geophysical method sensitive to one physical parameters. Hydrogeophysics one main branch of applied geophysical studies. The geophysical methods are used to investigate groundwater.

In hydrogeophysical studies, mainly "Direct Current Resistivity (DCR)" method is used to investigate aquifer structures (Binley and Kemna, 2005; Rubin and Hubbard 2006; Candansayar 2008; Gündoğdu and Candansayar 2018; Demirci et al. 2017, 2020). Additionally, the deep structure of the aquifer or geothermal areas are successfully revealed by the Audio Magnetotelluric (AMT) method (Giroux et al. 1997; Falgas et al. 2011; Erdoğan and Candansayar, 2018; Gomo, 2023).

In this study, it was investigated whether the activities of a limestone quarry located within the borders of Ankara province would affect the well that provides water to the nearby settlement. For this purpose, the aquifer feeding the water well and/or limestone fracture zones were imaged by using 2D/3D DCR and AMT data inversion. Thus, the interaction of the water well and the limestone quarry was revealed.

METHOD and APPLICATION

In the study, the structure of the aquifer from the surface to a depth of 150 meters was investigated using the DCR method, and the structure up to 500 meters was investigated using the Audio-Magnetotelluric (AMT) method.

Direct current resistivity (DCR) method is one of the oldest geophysical methods that examine geological units depending on the resistivity parameter. Today, DCR data are collected by sounding-profile measurement technique along a line using multi-channel/electrode measurement systems and these data are evaluated with 2D or 3D inversion algorithms. In this study, DCR data were collected with the sounding-profile measurement technique on five separate lines using AGI SuperSting R8/IP brand multi-electrode and multi-channel measurement system. A pole-dipole electrode array was used to achieve high lateral resolution (Candansayar 2008). The number of electrodes used varies depending on the condition of the lines in the field (ranging from 34 to 112). A total of 4650 apparent resistivity data were obtained from measurement (potential differences) on five lines and subsurface resistivity models were obtained by performing 2D inversion of each line separately. Additionally, 3D inversion was performed using three lines that were almost parallel to each other out of these five lines.

Magnetotelluric (MT) is a geophysical method that determines the subsurface resistivity structure using naturally occurring electric and magnetic field variations. In the AMT method used in this study, the internal field created by atmospheric events containing frequencies greater than 1 Hz is used as a source. In the method, two components of the electric field (E_x and E_y) and three components of the magnetic field (H_x , H_y , and H_z) are measured as a function of time using pots and coils, respectively. The first measured E and H fields are transferred to frequency domain by using FFT and impedance and tipper tensors are estimated in frequency domain from the electric and magnetic field components.

MT data is generally measured along a line and the measured data is interpreted using 2D inversion algorithms. In this study, we measured AMT data on 13 stations (Fig. 1). The measurement time of AMT data collected as a time series at each station varies between approximately 2-5 hours. Before performing the 2D inversion of the MT data, the ground-electric direction, which is assumed to be constant, was determined by phase tensor (Caldwell et al., 2004) analyses. After decomposition analysis, impedance tensor is rotated by using estimated rotation angle and TE and TM mode impedances are selected after the rotation. We interpreted TE and TM mode data by using 2D inversion algorithm (Candansayar, 2008; Candansayar and Demirci, 2012).



Figure1 Blue polygon: current boundaries of the limestone quarry, white polygon: geophysical study area boundaries, yellow symbols: AMT stations, white lines within the study area: DCR lines, the white down arrow: current water well. The settlement can be seen in the east of the study area.

RESULTS and CONCLUSION

The resistivity distribution of a total area of 30 hectares (500 m x 600 m) was revealed. In 2D inversion, the RMS values of DCR models and AMT models were below 3% and 5%, respectively. In the 3D inversion, the RMS values are 3.2% and 9.7%, respectively.

While interpreting the models, they were divided into three resistivity zones (A: $\rho < 40$, B: $40 < \rho < 100$, C: $\rho > 100$) using the geological map and stratigraphy of the region and the water drilling log. While zone A shows talus and weathered metamorphics, zone B is associated with Central Anatolian Volcanics and zone C is associated with Karakaya Complex. All obtained models were interpreted separately and together. Three DCR and AMT lines are parallel to each other in direction (P4-AMT2, P5-AMT1 and P6-AMT3). Here, two parallel lines (P4-AMT2, P5-AMT1) are presented and the mentioned zones are shown on the models (Figure 2). In both interpreted models, conductive zones on the surface correspond to talus and weathered rocks. If we compare the drilling log and the resistivity models (from DCR and AMT), groundwater is around the border of zone C and zone B just above it. It is seen that the deep part of the Karakaya volcanics retains water because it is not weathered, and its aquifer feature is the clastic units within the Karakaya volcanics and the Central Anatolian Volcanics.

The slope of the limestone blocks in the Karakaya Complex, which is exposed on the surface in the study area, is seen to be towards the west from the AMT models. Therefore, there is no fault zone towards the aquifer in the east. Considering all the results, it has been demonstrated by geophysical models that the existing water well will not be affected.

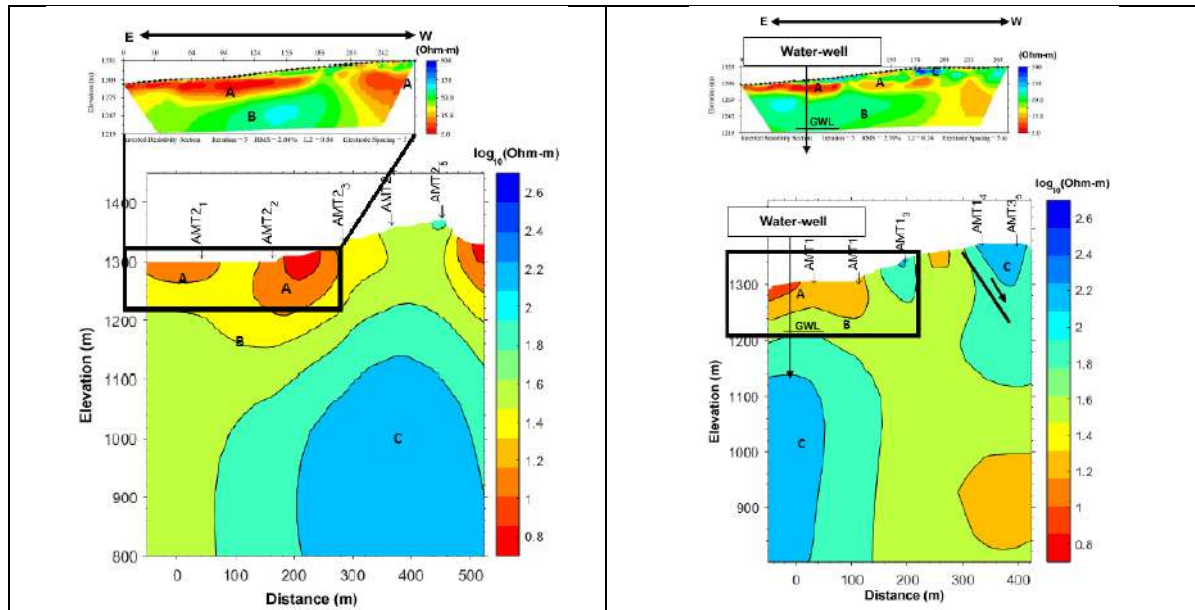


Figure2 Interpretation of P4-AMT2 and P5-AMT1 profiles.

REFERENCES

- Binley, A., & Kemna, A. (2005). DC resistivity and induced polarization methods. In *Hydrogeophysics* (pp. 129-156). Dordrecht: Springer Netherlands.
- Candansayar, M. E. (2008). Two-dimensional individual and joint inversion of three-and four-electrode array dc resistivity data. *Journal of Geophysics and Engineering*, 5(3), 290-300.
- Candansayar, M.E.,2008. Two-dimensional inversion of magnetotelluric data with consecutive use of conjugate gradient and least-squares solution with singular value decomposition algorithms, *Geophysical Prospecting*, 56, 141–157 (2008).
- Demirci, İ., Gündoğdu, N. Y., Candansayar, M. E., Soupios, P., Vafidis, A., & Arslan, H. (2020). Determination and evaluation of saltwater intrusion on bafra plain: joint interpretation of geophysical, hydrogeological and hydrochemical data. *Pure and Applied Geophysics*, 177, 5621-5640.
- Demirci, İ., Candansayar, M. E., Vafidis, A., & Soupios, P. (2017). Two dimensional joint inversion of direct current resistivity, radio-magnetotelluric and seismic refraction data: An application from Bafra Plain, Turkey. *Journal of Applied Geophysics*, 139, 316-330.
- Erdoğan, E., Candansayar, M.E., The conductivity structure of the Gediz Graben geothermal area extracted from 2D and 3D magnetotelluric inversion: Synthetic and field data applications, *Geothermics*, 65, pp. 170-179 (2017).
- Falgàs, E., Ledo, J., Benjumea, B., Queralt, P., Marcuello, A., Teixidó, T., & Martí, A. (2011). Integrating hydrogeological and geophysical methods for the characterization of a deltaic aquifer system. *Surveys in Geophysics*, 32, 857-873.
- Groom, Ross W., and Richard C. Bailey. "Decomposition of magnetotelluric impedance tensors in the presence of local three-dimensional galvanic distortion." *Journal of Geophysical Research: Solid Earth* 94.B2 (1989): 1913-1925.
- Gomo, M. (2023). Use of electric potential difference in audio magnetotelluric (AMT) geophysics for groundwater exploration. *Groundwater for Sustainable Development*, 20, 100864.
- Giroux, B., Chouteau, M., Descloîtres, M., & Ritz, M. (1997). Use of the magnetotelluric method in the study of the deep Maestrichtian aquifer in Senegal. *Journal of Applied Geophysics*, 38(2), 77-96.
- Gündoğdu, N. Y., & Candansayar, M. E. (2018). Three-dimensional regularized inversion of DC resistivity data with different stabilizing functionals. *Geophysics*, 83(6), E399-E407.
- Rubin, Y., & Hubbard, S. S. (Eds.). (2006). *Hydrogeophysics* (Vol. 50). Springer Science & Business Media.

9.1 GEOPHYSICAL AND REMOTE SENSING SURVEYS AT THE ARCHAEOLOGICAL SITE OF PHILIPPI, N. GREECE

A. Stampolidis^{1*}, A. Karamitrou² and G. Tsokas¹

¹Department of Geophysics, School of Geology, Aristotle University of Thessaloniki, Thessaloniki, Greece

²Department of Archaeology, University of Southampton, UK.

*Corresponding author e-mail: astamp@geo.auth.gr

ABSTRACT

Geophysical techniques have emerged as an integral component of archaeological field exploration. Utilizing multiple overlapping geophysical methods in tandem is important, as they provide sensitivity to varying subsurface characteristics, enabling a more comprehensive and resilient depiction of the archaeological targets.

The electrical resistivity and the magnetic gradiometry methods are commonly used in conjunction in several archaeological sites. The resistivity method is able to map features like building foundations and structural remnants, while the magnetic method shows sensitivity in objects with significant magnetic susceptibility, such as ferrous metals, ceramic artifacts, and hearths.

Furthermore, remote sensing data has become a valuable asset in archaeological research, enhancing accessibility to even remote regions. In this context, image fusion, especially the curvelet-based fusion method, facilitates the seamless integration of multiple overlapping datasets from diverse remote sensing techniques, delineating features of subsurface structures.

Geophysical data and a near infrared image from the archaeological site of Philippi in North Greece are used to demonstrate the advantages of this approach.

KEYWORDS: Archaeological prospection, Electrical methods, Magnetic methods, Fusion

ACKNOWLEDGEMENTS

This work has been accomplished on behalf of the project EKATY: Innovative imaging of the subsurface of archaeological sites and the interior of structural elements of monuments in 3 and 4 Dimensions. The project is running under the framework of the Operational Programme Competitiveness, Entrepreneurship and Innovation 2014-2020 (EPAnEK), Special Actions "Aquaculture" - "Industrial Materials" - "Open Innovation in Culture", T6YBP-00211.

9.2 IMAGING ARCHAEOLOGICAL RUINS BY GPR AND ERT SURVEYS: THE CASE OF ANCIENT SELEUKEIA SIDERA IN PISIDIA

Ç. Balkaya^{1,2*}, O. Çakmak² and H.E. Tütünsatar³

¹Geophysical Engineering Department, Süleyman Demirel University, Isparta, Türkiye

²Earthquake and Geotechnical Research Center, Süleyman Demirel University, Isparta, Türkiye

³Cultural Heritage and Tourism Program, Isparta University of Applied Sciences, Türkiye

*Corresponding author e-mail: caqlayanbalkaya@sdu.edu.tr

ABSTRACT

Ancient Seleukeia Sidera in Pisidia, located northwest of the village of Bayat in the Atabey district of Isparta, was one of the most important colonies of the Seleucid period. Since there are few visible ruins today, as most parts of the architectural structures have been lost or hidden in the ground or moved to surrounding buildings, archaeo-geophysical investigations in the city play a crucial role. The surveys are mainly conducted using ground penetrating radar (GPR) to determine the archaeological structures' location, depth, and extent. The GPR surveys, conducted as part of the city's recent three-period excavation and surface investigation campaigns between 2020 and 2022, examined an area of approximately 5.5 ha. The results of the GPR surveys to date are also consistent with those of surveys conducted in previous research periods using magnetic prospecting. In particular, they help shed light on the urban residential areas and architecture southeast of Hisar Tepe. Identifying two roads about 5 m wide in the survey area in this region, running toward SW-NE and NW-SE, clearly indicates that Seleukeia Sidera had a regular urban plan. In some cases, ERT surveys are also conducted as a supporting method to verify GPR results. Therefore, this study focuses mainly on presenting the results of GPR and ERT surveys conducted south of the city's theater ruins. In the study, the GPR scans are performed using a shielded antenna system with a center frequency of 500 MHz, while the ERT surveys are performed using a dipole-dipole array. The results of the GPR survey detect the ruins of a hidden archaeological structure with high resolution, regular geometry, and extent in the shallow subsurface. Also, the two-dimensional (2D) inversion results of the collected apparent resistivity datasets are compatible with the results of the GPR survey in this area. According to them, the anomalies of the archaeological building ruins with relatively high resistivity ($> 700 \Omega m$) and regular geometry are located within the cultural layer under the modern surface layer, which is about 30-40 cm thick. The relatively high contrasts in electrical conductivity and dielectric constant between the ground and the archaeological target allow the identification of hidden ruins to a depth of 2 m in the survey area with high resolution. According to the results of the GPR and ERT surveys, the ruins of the archaeological structures in the ancient city of Seleukeia Sidera are mainly located about 30 cm to 180 cm below the surface. Unfortunately, this indicates that agricultural activities can potentially damage the ancient city's near-surface archaeological remains when locals use tractors, rakes, and cultivators in production. As archaeo-geophysical research progresses, it will be possible to obtain more information about the residential structures, transportation routes, and architectural background of the city in this area.

KEYWORDS : Archaeogeophysics, GPR, ERT, Pisidia, Seleukeia Sidera

INTRODUCTION

An archaeo-geophysical survey efficiently determines the ruins of archaeological structures awaiting discovery beneath the surface of ancient cities at low cost, time, and effort. For this purpose, geophysical methods are often used during or prior to archaeological excavations and surveys. However, their success depends on the subsurface characteristics of an archaeological site and the degree of contrast between physical parameters such as magnetic susceptibility, dielectric constant, and electrical conductivity that these features form with the targeted archaeological structure. Since this condition is sufficiently fulfilled in the ancient city of Seleukeia Sidera in Pisidia, it is possible to identify hidden structures at a given site. The city is located on and around Hisar Tepe (1271 m), 800 m northwest of the village of Bayat (formerly Selef), which is 7 km south of the Atabey district in present-day Isparta province. It was the southern neighbor of Apollonia on the border between Phrygia and Pisidia and the northern neighbor of Sagalassos in central Pisidia. Seleukeia Sidera occupied a central position in the northern Pisidia region, as its territory borders the cities of Konane to the west and Prostanna to the east. The excavation and research work in the Seleukeia Sidera has been conducted since 2019 under the direction of Prof. Dr. Bilge Hürmüzlü Kortholt with a multidisciplinary and international team. The multidisciplinary research in Seleukeia Sidera through excavations, archaeological surface surveys, and geophysical prospecting provides essential information about the settlement plan and the settlement area's hierarchy (Hürmüzlü et al., 2023).

The sole or integrated use of magnetic prospecting, GPR, and ERT is widespread in archaeo-geophysical investigations and successful examples such as from Alacahöyük (Candansayar and Başokur, 2001), Zeugma (Drahor et al., 2008), Amorium (Ekinci et al., 2014), Pisidian Antioch (Balkaya et al., 2018), Side (Akca et al., 2019), and Doliche (Balkaya et al., 2021) can be found in the literature. In the city, the first geophysical explorations by GPR and magnetic prospecting were conducted between 2016 and 2019 by HTW (Berlin) under the direction of Thomas Schenk (2023). Since 2020, the Earthquake and Geotechnical Research Center of Süleyman Demirel University has been leading archaeo-geophysical investigations through GPR and ERT applications. The results of the GPR surveys, conducted mainly in the flat areas southeast of Hisar Tepe where agricultural activities are now taking place, are consistent with the results of the previous magnetic prospection (Balkaya et al., 2023). This study discusses the results of the GPR and ERT surveys of the archaeo-geophysical prospection near the theater ruins southwest of Hisar Tepe.

METHOD and APPLICATION

As a non-invasive method, GPR is a valuable tool in archaeological investigations. It provides high-resolution images of hidden ruins of archaeological structures without excavation using high-frequency electromagnetic waves. Seleukeia Sidera GPR surveys are conducted using a shielded antenna system (MALÅ™ ProEx) at a center frequency of 500 MHz on parallel profiles spaced 50 cm apart with 5 cm trace spacing. Depth slice maps through a three-dimensional (3D) volume of reflection data were created using the software GPR-SLICE (v7.MT, <https://www.gpr-survey.com/>) with appropriate basic data processing techniques such as dewow, time-zero correction, gain, bandpass filter, and migration. ERT is typically used in archaeological surveys to

detect buried objects such as walls, trenches, or artifacts by measuring the differences in electrical resistivity between the target objects and the

surrounding materials. The ERT survey was performed with a dipole-dipole array using the ARES GF multi-electrode resistivity measurement system with 48 electrodes on 38 parallel profiles, mainly 70 cm apart with an electrode spacing of 50 cm. ERT profile data were inverted using ResIPy (v3.4.5), an intuitive open-source software for complex geo-electrical inversion/modeling, available on GitLab (<https://gitlab.com/hkex/resipy/>), and then visualized using ParaView (v5.11.0), an open-source post-processing visualization software (<https://www.paraview.org/>).

SURVEY RESULTS

The survey area is located southwest of the ruins of the ancient theater of Seleukeia Sidera and is shown in Figure 1a within the dashed line. During the investigation, the direction of the GPR survey was approximately SE-NW, while the direction of the ERT survey was approximately NE-SW. Figure 1b shows a depth slice map of 100 cm from the GPR data analysis. Based on the map, the results of the GPR survey show the ruins of a hidden anthropogenic structure with high resolution, regular geometry, and extent in the shallow subsurface. In addition, Figure 1c shows a tomogram of Profile 21 derived from the inversion of the ERT data. The tomogram is characterized by three observations in the interpretation, including modern topsoil (1), cultural layer (2), and promising resistivity anomalies. Accordingly, the thin modern subsoil above the cultural layer is about 30-40 cm thick and has a resistivity of $< 120 \Omega\text{m}$ (Balkaya et al., 2023). On the other hand, the cultural layer contains promising anomalies that can be attributed to the remains of archaeological structures characterized by relatively high resistivity values of more than $700 \Omega\text{m}$. These 2D inversion results from Profile 21 also agree well with the results of the GPR survey and identify the walls that form the foundation of this structure.

CONCLUSION

Overall, the results of the GPR and ERT surveys indicate that the remains of the buried archaeological structures are located at a depth of approximately 30 cm to 180 cm. Considering that agricultural activities are taking place in the ancient city's flat areas, it can be concluded that these activities pose the risk of damaging the near-surface archaeological remains when the local population uses power harrows and cultivators in production. The GPR and ERT investigations will be continued in future campaigns at Seleukeia Sidera in light of the results of the previous archaeo-geophysical surveys.

ACKNOWLEDGEMENT

We owe special thanks to Prof. Dr. Bilge Hürmüzlü Kortholt, the head of the excavations in the ancient city, and the Rectorate of Süleyman Demirel University. The excavations and research of Seleukeia Sidera are carried out with the permission and financial support of the Ministry of Culture and Tourism of the Republic of Turkey, General Directorate of Cultural Heritage and

Museums. We thank M. Metin Ünyay (M.Sc) for contributing to the data acquisition during the survey.

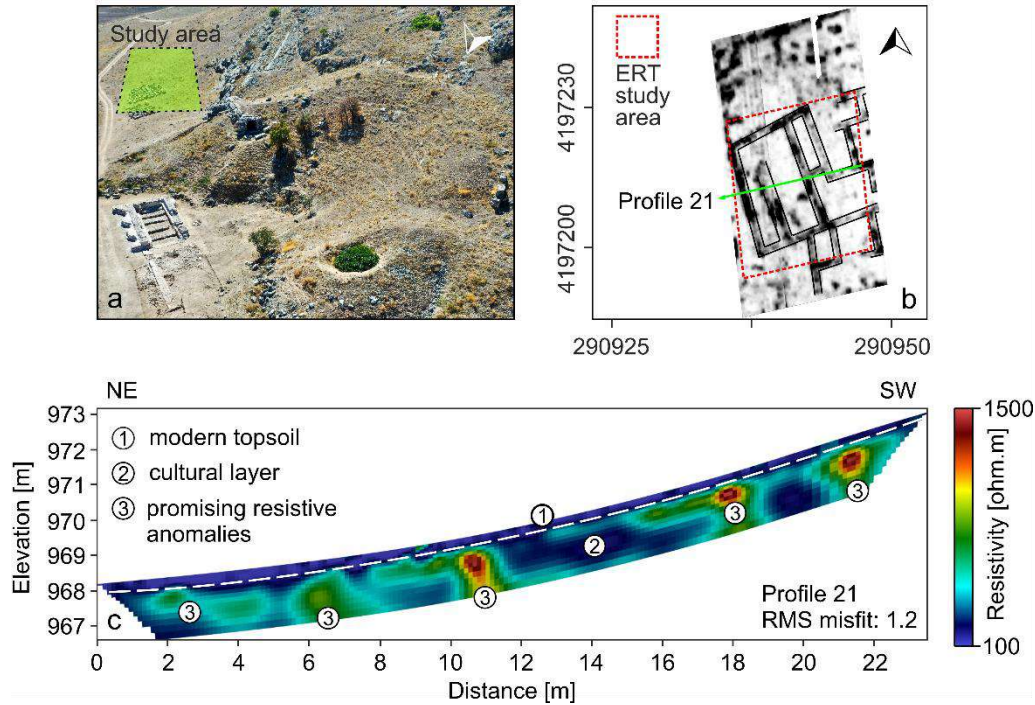


Figure1 (a) The study area southwest of the ruins of the ancient theater of Seleukeia Sidera, on an aerial photograph from the city project archive (b) A GPR depth slice map of 100 cm obtained from data analysis (c) Resistivity tomogram of Profile 21 obtained by 2D inversion (Balkaya et al., 2023)

REFERENCES

- Akca, İ., Balkaya, Ç., Pülz, A., Alanyalı, H.S., Kaya, M.A., 2019. Integrated geophysical investigations to reconstruct the archaeological features in the episcopal district of Side (Antalya, Southern Turkey). *Journal of Applied Geophysics*, 163, 22-30.
- Balkaya, Ç., Ekinci, Y.L., Çakmak, O., Blömer, M., Arnkens, J., Kaya, M.A., 2021. A challenging archaeo-geophysical exploration through GPR and ERT surveys on the Keber Tepe, City Hill of Doliche, Commagene (Gaziantep, SE Turkey). *Journal of Applied Geophysics*, 186, 104272.
- Balkaya, Ç., Çakmak, O., Tütünsatar, H.E., 2023. Archaeogeophysical investigations at Seleukeia Sidera. Eds. B. Hürmüzlü, P. Talloen, B. Sönmez, S. Togan, *Overview of the Archaeological Excavations and Research at Seleukeia Sidera (2019-2022)*, 71-87, Myrina Publications, Ankara.
- Candansayar, M.E., Başokur, A.T., 2001. Detecting small-scale targets by the 2D inversion of two-sided three-electrode data: application to an archaeological survey. *Geophysical Prospecting*, 49, 13-25.
- Drahor M.G., Berge M.A., Kurtulmuş T.Ö., Hartmann M., Speidel M.A., 2008. Magnetic and electrical resistivity tomography investigations in a Roman legionary camp site (Legio IV Scythica) in Zeugma, Southeastern Anatolia, Turkey. *Archaeological Prospection*, 15, 159-186.
- Ekinci, Y.L., Balkaya, Ç., Şeren, A., Kaya, M.A., Lightfoot, C.S., 2014. Geomagnetic and geoelectrical prospecting for buried archaeological remains on the Upper City of Amorium, a Byzantine city in midwestern Turkey." *Journal of Geophysics and Engineering*, 11, 015012.
- Hürmüzlü, B., De Jong, L., Dijkstra, T.M., 2023. The Necropoleis and burial customs of Seleukeia Sidera. Eds. B. Hürmüzlü, P. Talloen, B. Sönmez, S. Togan, *Overview of the Archaeological Excavations and Research at Seleukeia Sidera (2019-2022)*, 197-204, Myrina Publications, Ankara.
- Schenk, T., 2023. Results of geomagnetic surveys and evidence for forging activities in Seleukeia Sidera, Eds. B. Hürmüzlü, P. Talloen, P. B. Sönmez, S. Togan, *Seleukeia Sidera I, Overview of the Archaeological Excavations and Research at Seleukeia Sidera (2019-2022)*, Myrina Publications, 51-69, Ankara.

9.3 WATER-BORNE ARCHAEOGEOPHYSICAL INVESTIGATIONS AT LAKE İZNIK

I. Akca^{1*}, M. Şahin²

¹Assoc. Prof., Geophysical Eng. Department, Ankara University, Ankara, Türkiye

²Prof. Dr., Archaeology Department, Uludağ University, Bursa, Türkiye

*Corresponding author e-mail: iakca@eng.ankara.edu.tr

ABSTRACT

Waterborne geophysical investigations are playing an increasingly prominent role in various applications, including mineral exploration, solving engineering challenges, and the detection of buried objects. With the continuous development of methods and procedures, the accuracy of results, particularly in shallow research, has significantly improved. This particular study focuses on the investigation of a basilica structure located 20 meters from the shoreline of İznik Lake in the Bursa province, employing geophysical methods as its primary approach. The study utilizes two main geophysical techniques: direct current resistivity and ground-penetrating radar. For the DC resistivity method, we employed both multi-channel setups with 11 mobile electrodes and 32 fixed electrodes. Additionally, we utilized antennas operating at 200 and 500MHz frequencies for the ground-penetrating radar. Data collection was carried out along profiles, with real-time GPS data used to pinpoint each data location. Both datasets were subsequently processed using appropriate data analysis techniques, and the results are presented in the form of depth slices. It's worth noting that İznik Lake has been affected by a recent decline in water levels due to drought and excessive water consumption. Consequently, some of the structures under investigation now lie above the water's surface. While this situation has improved signal penetration for the ground-penetrating radar method, it has presented challenges for surface measurements, particularly in conducting electrical resistivity measurements using mobile setups. In the results we present, sections of the existing basilica structure's walls are clearly visible. Below the water floor, we've observed linear features that do not align with the visible structure boundaries. It is recommended that these anomalies be further explored through underwater excavations.

KEYWORDS : water-borne resistivity, GPR, underwater archaeology

INTRODUCTION

Archaeological research is predominantly conducted on land; however, underwater archaeology plays a crucial role in uncovering submerged structures and artifacts for various purposes. Conducting underwater excavations requires distinct methods and specialized equipment, contributing to increased research costs and slower progress. Geophysical studies conducted on the water's surface or seabed offer unique insights compared to land-based research. In some cases, adaptation of land-based archaeological geophysics measurement systems can be applied to underwater environments (Lawrance et al., 2004; Boyce et al., 2006; Müller et al., 2009;

Passaro, 2010; Papatheodorou et al., 2011; Kritikakis et al., 2015; Smyrdanis et al., 2016; Qin et al., 2018). However, investigating man-made structures

submerged beneath sediments on the water floor poses challenges related to water chemistry and depth, limiting measurement resolution and sensitivity. This project focuses on the basilica structure discovered when Lake Iznik's water level receded in 2014. Subsequent scientific research revealed multiple phases of the basilica's construction, making it a significant element in the Christianization of Nikaia. It is believed to have been the site of the First Council of Nicaea in AD 325 (Şahin, 2020). Moreover, being one of the few known churches from the Early Christian period in Anatolia adds to its historical importance. Consequently, a project was initiated to explore other structures associated with the Iznik Lake Underwater Basilica Church using geophysical methods, as indicated in Figure 1.



Figure1 Aerial view of the basilica structure, known as the Sunken Church, determined in 2014 in Lake Iznik

During the project's preparation phase, measurements were initially planned to be conducted by floating equipment on the water surface, allowing for rapid scanning of large areas. However, due to portions of the building protruding up to 50 cm above the water surface in some areas, creating continuous measurement profiles proved challenging. As a result, a fixed measuring system was employed for electrical resistivity measurements, enabling more precise data collection. The project utilized direct current resistivity and ground radar measurements to survey the basilica's perimeter, facilitating research up to a depth of 2 meters beneath the shallow water floor, leading to various significant discoveries.

METHOD and APPLICATION

In the geophysical investigations conducted at Lake Iznik, a combination of ground-penetrating radar and direct current resistivity methods were employed for shallow subsurface exploration. Additionally, Side Scan Sonar (SSS) was utilized to determine water depth and obtain a comprehensive overview of the lakebed. For the Direct Current Resistivity method, a measurement device equipped with two current electrodes and nine potential electrodes was deployed, with the equipment mounted at the rear of a boat. During the fieldwork, electrode spacing was consistently set at 2.5 meters. The measurements were conducted using a dipole-

dipole array configuration, and a total of eight dipole levels ($n=8$) were recorded with the nine potential electrodes integrated into the system. Figure 2 provides a visual representation of the measurement setup along with a photograph captured during the data acquisition process.

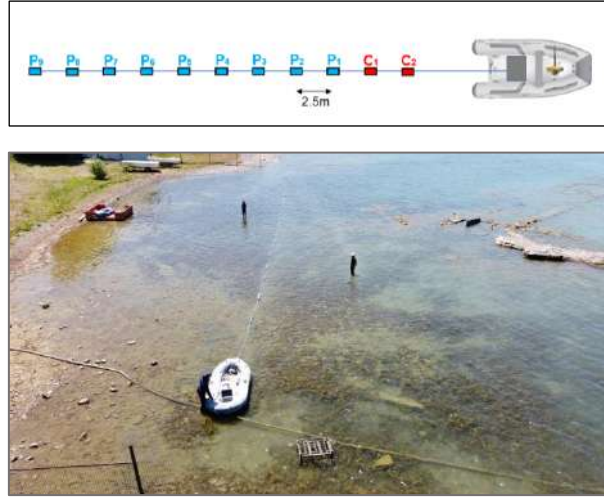


Figure2 Aerial view of DC resistivity measurements at Lake İznik

The current water depth in the study area ranges from 0 to 2 meters. Given these conditions, ground-penetrating radar was deemed suitable for the study. The radar system's antennas were floated above the water surface using an inflatable boat, allowing signals to penetrate beneath the lakebed (see Figure 3). The depicted antenna operates at 200MHz, and measurements were also conducted using a 500MHz antenna.



Figure3 GPR measurement setup with 200MHz antenna

DISCUSSION and RESULTS

The resistivity data measured at Lake İznik was inverted with a 3D smoothness-constrained least squares algorithm. The final data misfit was 3.2% which was satisfactory. A depth slice from the 3D resistivity model is given in Figure 4a. GPR data were also processed and depth slices are generated. A sample GPR depth slice for the same depth is given in Figure 4b.

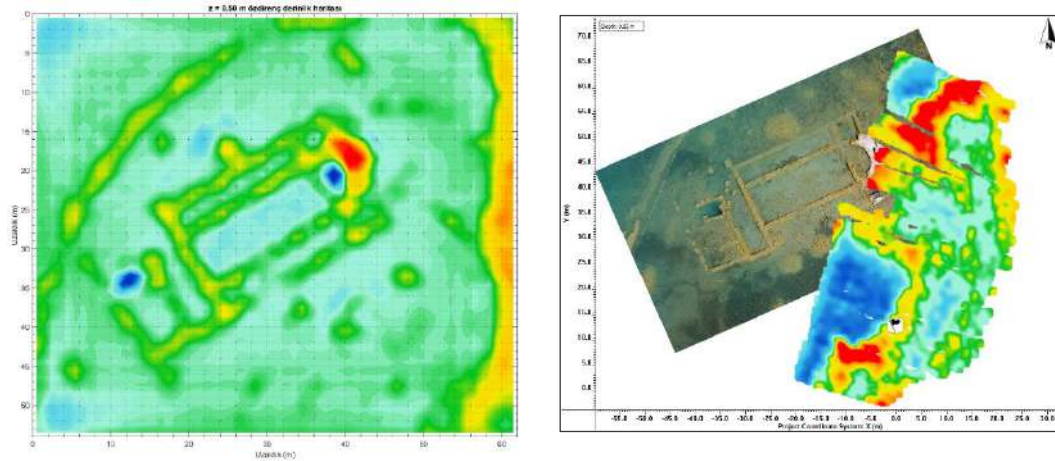


Figure4 (a) Resistivity and (b) GPR depth slices from 0.8m below water surface

CONCLUSION

GPR and DCR are highly suitable methods for near-surface research. In this study, we explore their application in an aquatic environment. Our research focuses on utilizing these methods to image submerged archaeological remains within Lake Iznik. Notably, various indicators and findings were uncovered during our investigations, which were subsequently reported to the excavation team.

REFERENCES

- Boyce, J. I., Krezoski, G., Reinhardt, E. G., Goodman, B., & Artzy, M. 2006. "Marine Geophysical Mapping of Bronze-Age Harbor Structures, Liman Tepe", Turkey. Philadelphia, PA: Geological Society of America.
- Lawrence, M., Oxley, I., & Bates, C. R. 2004. "Geophysical techniques for maritime archaeological surveys", In 17th EGS Symposium on the Application of Geophysics to Engineering and Environmental Problems (pp. cp-186). European Association of Geoscientists & Engineers.
- Müller, C., Woelz, S., Ersoy, Y., Boyce, J., Jokisch, T., Wendt, G., & Rabbel, W. 2009. "Ultra-high-resolution marine 2D–3D seismic investigation of the Liman Tepe/Karantina Island archaeological site (Urla/Turkey)", *Journal of Applied Geophysics*, 68(1), 124-134
- Papatheodorou, G., Geraga, M., Chalari, A., Christodoulou, D., Iatrou, M., Fakiris, E., Kordella, St., Prevenios M. & Ferentinos, G. 2011. "Remote sensing for underwater archaeology: case studies from Greece and Eastern Mediterranean", *Bulletin of the Geological Society of Greece*, 44, 100-115.
- Qin, T., Zhao, Y., Lin, G., Hu, S., An, C., Geng, D., & Rao, C. 2018. Underwater archaeological investigation using ground penetrating radar: A case analysis of Shanglinhu Yue Kiln sites (China). *Journal of Applied Geophysics*, 154, 11-19.
- Şahin, M. 2020. "İznik Gölü'ndeki Bazilika Kalıntısı İlk Olarak Ne Zaman Keşfedildi?", *Bursa Günlüğü Dergisi*, 9, 66-71.

ACKNOWLEDGEMENT

This study was supported by TUBITAK with grant number 122Y040. We would like to thank the project scholars İrem Baysal, Özgür Ulaş and geophysical engineers Seçkin Sertaç Lallı, Murat Gölebatmaz, Bengisu Taşkın and the vice chairman of excavation Suha Cura.

10.1 ESTIMATING THE ELECTRICAL ANISOTROPY COEFFICIENT, STRIKE DIRECTION, AND DIP ANGLE USING SQUARE ELECTRODE ARRAY DATA WITH GENERALIZED REGRESSION NEURAL NETWORKS

E. Pekşen^{1*}, D. Durdağ² and E. Gasimov²

¹Assoc. Prof., Department of Geophysical Engineering, Kocaeli University, Kocaeli, Türkiye

²Ph. D.(c), Department of Geophysical Engineering, Kocaeli University, Kocaeli, Türkiye

*Corresponding author e-mail: ertanpeksen@kocaeli.edu.tr

ABSTRACT

The Direct Current Resistivity (DCR) method is established as one of the oldest and most extensively used techniques in applied geophysics. DCR measurements are influenced by electrical anisotropy (EA). Electrical anisotropy characterizes the directional dependence of electrical resistivity measurements. This study focuses on the integration of a square electrode array with electrical anisotropy, offering an effective tool for estimating the strike, dip, and electrical resistivities of subsurface layers along both the x and y directions of the medium using a generalized regression neural network.

KEYWORDS: square array, electrical anisotropy, generalized regression neural network

INTRODUCTION

The Direct Current Resistivity (DCR) method is one of the oldest and most extensively employed techniques in applied geophysics (Telford et al., 1990). DCR measurements are influenced by several factors, including formation porosity, cementation factor, water saturation, fracturing, resistivity of formation water, temperature, and electrical anisotropy (EA). Electrical anisotropy, denoting the directional dependence of electrical resistivity measurements, has been a subject of investigation since Maillet's pioneering work in 1947. Numerous studies on electrical anisotropy have been conducted to date. In this study, we focus on the application of a square electrode array with electrical anisotropy. Square arrays have proven valuable for investigating the strike and dip of subsurface layers (Habberjam, 1972; 1975), a particularly relevant technique given the prevalence of karstic geological features in Türkiye, as demonstrated by Şener et al. (2021) in their work on the Menekşe karst plateau.

Herein, we present an innovative approach that uses this effective square electrode array in conjunction with the Generalized Regression Neural Network (GRNN) to estimate the strike and dip of subsurface layers, as well as the electrical resistivities along both the x and y directions of the medium.

METHOD and APPLICATION

Figure 1 illustrates a geological model incorporating a square electrode array. Within this model, ρ_x represents the resistivity measured along the x direction, while ρ_y corresponds to the resistivity measured perpendicular to the x-direction. The apparent resistivity value (ρ_a) can be calculated using Equation (1):

$$\rho_a = \frac{\rho_n}{2 - \sqrt{2}} \left\{ \left(\frac{2}{(1 + (N^2 - 1) \cos^2(\theta))^{\frac{1}{2}}} \right) - \left(\frac{1}{(2 + (N^2 - 1)(1 + \sin(2\theta)))^{\frac{1}{2}}} \right) \right. \\ \left. - \left(\frac{1}{(2 + (N^2 - 1)(1 - \sin(2\theta)))^{\frac{1}{2}}} \right) \right\}$$

where $N = ((1 + (f^2 - 1) \sin(\alpha)^2))^{\frac{1}{2}}$ is the effective anisotropy coefficient. $f = \sqrt{\frac{\rho_{hy}}{\rho_{hx}}}$ is the electrical anisotropy coefficient of electrical. $\rho_n = \sqrt{\rho_{hy}\rho_{hx}}$ is the mean resistivity. θ is the strike and α the dip angle (Habberjam, 1972). Figure 1 also provides examples of the horizontal electrical anisotropy model, depicting variations in electrical anisotropy, strike directions, and dip angles.

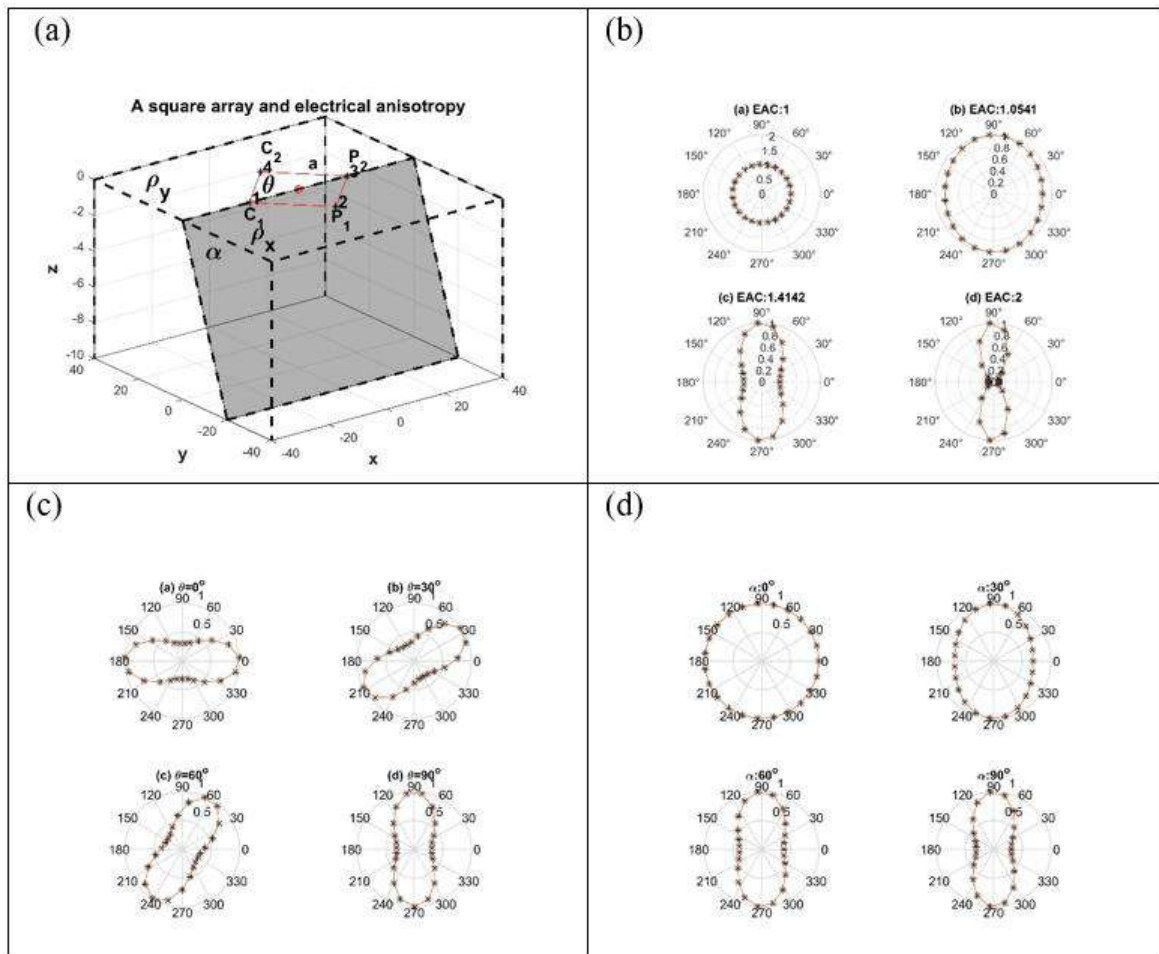


Figure1 (a) A square array and electrical anisotropic model. C_1 ve C_2 are current electrodes. P_1 ve P_2 are potential electrodes. The distance among electrodes is a . (b) Various electrical anisotropies of the earth model response. (c) Various strike directions of the earth model response. (d) Various dip angles of the earth model response.

Artificial neural networks (ANNs) are a class of nonlinear models designed to mimic biological nervous systems. ANNs have been widely applied to solve many difficult problems, including in different fields such as pattern recognition, signal processing, language learning, function approximation, prediction, and modeling. Typically, a biological nervous system (consisting of several layers, each composed of multiple neural units (neurons)) can process information in a parallel manner. Models with these features are known as ANN models (Haykin, 1999).

GRNN was proposed by Specht in 1991. Its general structure consists of four layers divided into input pattern collection, and output sections. GRNN has many advantages over other nonlinear neural network techniques. A benefit of GRNN is that it does not require an iterative training phase. In other words, the network learns directly (single pass learning) from the input data. Another advantage is that predicted model individuals can encounter minimums and maximums of the input data. Moreover, although local regime methods converge to undesirable solutions corresponding to local minima, the GRNN method does not. The calculation time of GRNN includes fast calculation time, database-based prediction ability, and low error rate.

RESULTS

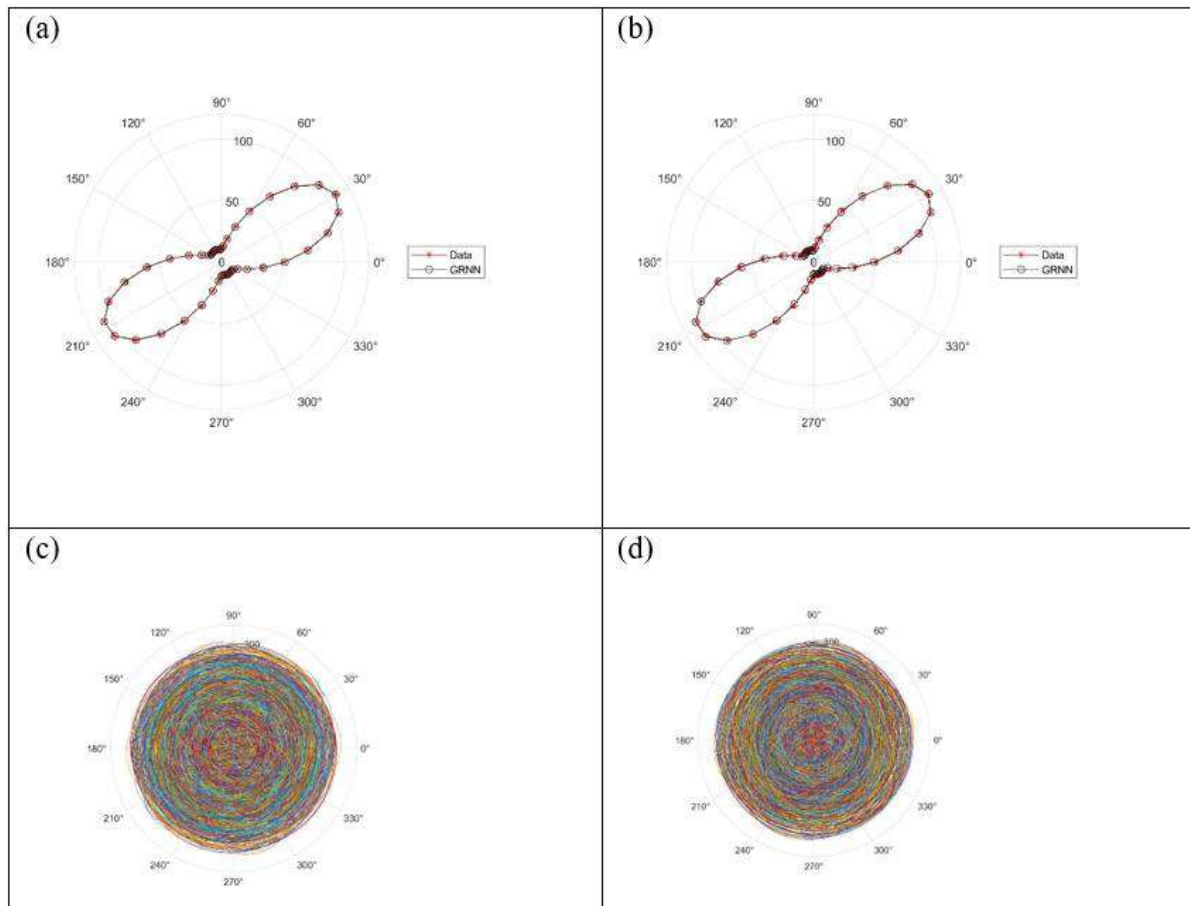


Figure2 (a) Polar plot of a model with two parameters estimated by GRNN using synthetic data. (b) Polar plot of a model with four parameters estimated by GRNN using synthetic data. (c) Training set of parameters space for model (a) with two unknowns. (d) Training set of parameters space for model (b) with four unknowns.

Figure 2 shows the estimated model parameters using the GRNN method with synthetic data. The estimated model parameters are given in Table 1.

Table1 Estimated model parameters using the GRNN.

Parameters	ρ_x (ohm.m)	ρ_y (ohm.m)	θ (degrees)	α (degrees)
Model	100	15	120	45
Noise-Free 2 Parameters			119.21	44.94
Noise-Free 4 Parameters	100.94	14.58	120.17	45.70
Training Set Range	(0-200]	(0-200]	[0-180]	[0-90]

CONCLUSION

This study demonstrates the successful application of the GRNN method to estimate the strike direction, dip angle, and anisotropy coefficient of an anisotropic earth model. We rigorously tested this approach using synthetic data, both with and without noise, highlighting its adaptability to karst environments and various geophysical problems. Effective parameter estimation relies on defining the solution space for the model parameters, with the training set range playing a crucial role in computational efficiency. Selecting an appropriate parameter range is essential, because an excessively large range can lead to increased computational demands.

ACKNOWLEDGEMENT

This work is supported by the Scientific and Technical Research Council of Turkey (TÜBİTAK) under grant 123Y277.

REFERENCES

- Habberjam, G.M. 1972. "The effects of anisotropy on square array resistivity measurements", *Geophysical Prospecting*, 20 (2), 249–266.
- Habberjam, G.M. 1975. "Apparent resistivity, anisotropy and strike measurements", *Geophysical Prospecting*, 23 (2), 211–247.
- Haykin, S. 1999. *Neural Networks: A Comprehensive Foundation* (second ed). Prentice Hall.
- Maillet, R. 1947. "The fundamental equations of electrical prospecting", *Geophysics*, 12 (4), 529–556.
- Specht, D.F. 1991. "A general regression neural network", *IEEE Trans Neural Netw*, 2(6):568 576.
- Şener, A., Pekşen, E., Yolcubal, İ. 2021. "Application of square array configuration and electrical resistivity tomography for characterization of the recharge area of a karst aquifer: A case study from Menekse karst plateau (Kocaeli, Turkey)", *Journal of Applied Geophysics*, 195/ 104474.
- Telford, W. M., Geldart, L. P., Sheriff, R.E. 1990. *Applied geophysics*. Cambridge: Cambridge University Press.

10.2 CONSTRAINED INVERSION OF GEOPHYSICAL DATA WITHOUT REGULARIZATION PARAMETER USING PARETO-OPTIMAL SWARM INTELLIGENCE: APPLICATION TO MAGNETOTELLURIC PROBLEM

E. Büyük^{1,2}

¹Dr., Department of Geophysical Engineering, Faculty of Engineering and Natural Sciences, Gümüşhane University, 29100, Gümüşhane, Turkey

²Dr., TÜBİTAK, Marmara Research Center, Earth Sciences Research Group, 41470, Kocaeli, Turkey

*Corresponding author e-mail: ebuyuk@gumushane.edu.tr

ABSTRACT

A drawback of traditional inversion methods in geophysics is that the solution is trapped in a local minima in the objective space due to initial model dependence. In recent years, global optimization methods such as particle swarm optimization, genetic algorithm, neighborhood algorithm, and simulated annealing have been preferred to overcome this disadvantage. The main advantage of these methods is that the parameter space is searched widely and thus almost the entire objective space is explored with the physically meaningful input arguments. However, due to the ill-posed nature of the problem with a high-dimensional model space, solution sampling is limited by the curse of dimensionality. In general, if the solution cannot be manipulated, not all dimensions of the model space will be represented by the observed data. In this case, a constraint in the objective space with a regularization parameter is required, as in traditional inversion methods. However, an initial model affects not only the solution result, but also the estimation of the regularization parameter when constrained inversion is used. This is because the regularization parameter, which is iteratively adjusted during the iteration, also indirectly depends on the initial model that initiates the inversion process. In particular, if the data are noisy, the appropriate regularization parameter cannot be determined, leading to a tradeoff between data fitting and model variance. In addition, subjective and unpredictable weights of the objective function terms can also lead to misleading results. This study provides a method that can be applied without regularization parameters in the constrained inversion of geophysical data by integrating particle swarm optimization, one of the global optimization methods, with the Pareto optimality approach. To verify the applicability of this approach, magnetotelluric data were selected and the solution accuracy was investigated using a type of synthetic analysis. The results showed that synthetic models can be successfully reproduced even with a high number of model parameters and a large search space. In order to have more confidence in the results of these analyzes, magnetotelluric field data obtained from measurements at a single station in the Çanakkale-Tuzla geothermal field were also modeled. The resistivity- depth section obtained by modeling the field data with advanced tests was compatible with the well logs in the study area. These results confirm that the presented approach can also be successfully used for constrained inversions by minimizing the objective function terms without estimating the regularization parameters.

KEYWORDS: Geophysical modeling, Magnetotelluric, Pareto optimality, Swarm Optimization, Regularization

10.3 A NEW SOFTWARE FOR 3-DIMENSIONAL INVERSION OF MAGNETOTELLURIC AND GRAVITY DATA: PART 1: SOFTWARE INTERFACE AND GRAVITY INVERSION

Ö. Özyıldırım^{1*}

¹Afyon Kocatepe University The Application and Research Center of Geothermal and Ore Deposits

*Corresponding author e-mail: ozyildirim@aku.edu.tr

ABSTRACT

There are many studies about the joint inversion of Magnetotelluric and Gravity data. This study tries to explain the completed gravity inversion part of the joint inversion algorithm, which is currently under development. Firstly, the part of creating a model mesh using tetrahedron elements is presented along with the difficulties encountered and suggestions. Then, in the forward modeling phase, the methods by which the vertical component of gravitational acceleration can be calculated from the gravity potential calculated with the finite elements method and test models for the modeling algorithm are presented. Finally, the gravity inversion algorithm is compared with the previously developed inversion algorithm that used rectangular prisms, and the developed software's user interface is introduced.

KEYWORDS: Gravity, Tetrahedron, Three, Dimensional, Modeling, Inversion

10.4 A NEW MAGNETOTELLURIC 3D MODELING ALGORITHM: COMPARISON BASED ON DIFFERENT DIRECT AND ITERATIVE SOLVER PERFORMANCES

İ. Demirci^{1*}

¹Faculty of Engineering, Department of Geophysical Engineering, Ankara University, Ankara, Turkey

*Corresponding author e-mail: idemirci@eng.ankara.edu.tr

ABSTRACT

The calculation time of the 3D magnetotelluric forward modeling algorithm is so large that traditional serial and parallel algorithms cost an extremely large computation time. Reducing the computation time in parallel computing is usually done by allocating threads to different cores for each discrete frequency. However, when sharing the threads, researchers completely focus on different frequencies and on computers that do not have a sufficient number of cores, the total time is given in proportion to the threads that takes the longest processing workload. In those algorithms, the number of cores used is generally chosen depending on the number of frequencies in distributed computing algorithms. But, solving the Helmholtz equation by iterative methods for high frequencies can reach solution faster than solving it iteratively for low frequencies. When a very low relative residual value is selected, it is observed that the algorithms did not reach a solution in low frequencies and ended with the maximum number of iterations. It is not possible for iterative algorithms to reach a solution for very low frequencies because the amplitude difference between the imaginary and real components grows proportionately too much. For this reason, the solution is generally less sensitive to phase values compared to amplitude values. To overcome this, direct methods can be used instead of iterative methods. However, the excessive RAM usage of direct methods limits the use of the methods for large model meshes. Thanks to the recently developed multifrontal methods, RAM usage has been reduced and a solution has become possible even for large model networks. During this study, dynamic selection of direct and iterative methods are studied to reduce the solution time in 3D magnetotelluric modeling studies. Thus, it has been suggested to use iterative methods in solving high frequencies and to use direct solvers after the determined threshold frequency value. Additionally, due to the high solution speeds at high frequencies, additional recommendations are made when distributing it to the cores. At the end of the study, we also compared the CPU and GPU performances of the algorithm and their contribution to performance has been discussed.

KEYWORDS : Magnetotelluric, Modeling, Direct and Iterative Solvers, 3 Dimensional, Dynamic Selection, CPU and GPU computation

INTRODUCTION

3-D forward solution in the magnetotelluric method is one of the most important research topics in recent years. In this method, solving the Helmholtz equation takes a long time and require enormous RAM consumption. For this reason, it is extremely important to develop new and rapid approaches to solving the method faster than previously developed algorithms. To do so, we need to calculate performance of the direct and iterative solvers on the solution of the Helmholtz equation.

In recent years, there have been many studies on 3-D forward solutions in frequency domain EM methods. As a forward solution method, Finite Differences (Newman and Alumbaugh, 1995, 2002; Streich, 2009), Finite Elements (Badea et al., 2001; Mitsuhata and Uchida, 2004; da Silva et al., 2012), Finite volume approach (Mackie et al., 1994; Haber and Ascher, 2001; Constable and Weiss, 2006) and integral equation (Wannamaker, 1991; Avdeev et al., 2002) methods are used. The finite element method is the most flexible method in terms of defining the model geometry (Avdeev, 2005, Erdoğan et al. 2008, Demirci et al., 2012). Although integral equation methods are very useful for simple models, there are difficulties in calculating them for complex models (Mackie et al. 1993). For this reason, the Finite Difference method and the closely related finite volume approach are preferred due to ease of calculation, application and solution stability.

To improve the efficiency of 3D flat solution algorithms, the general idea focuses mainly on the development of faster and more accurate numerical algorithms, parallelization of codes on the CPU and/or GPU-based algorithms with direct and iterative solvers. During this study, first iterative and direct solver performances were compared. Then, the combined and/or sequential use of the best solvers were tested on the CPU and their performance on the GPU was also discussed.

METHOD and APPLICATION

In MT method, the frequency domain equations of the forward solution is the Helmholtz equations obtained from Maxwell's equations. This equation cannot be solved analytically for complex models. For this reason, one of the numerical solution approaches must be used to solve the equation. The Finite Difference method (Newman and Alumbaugh, 1995; Alumbaugh et al., 1996; Champagne II et al., 2001; Weiss and Newman, 2002, Streich, 2009) is one of the most frequently preferred methods due to its ease of application and solution speed. In this study, the Finite Difference method was preferred to solve the Helmholtz equation. In the solution of method, the Finite Difference expression is obtained using the staggered grid approach of Yee (1966), scaled symmetrically and Dirichlet boundary conditions are used (Dirichlet boundary conditions were generally used in previous studies to ensure that the resulting equation is to be symmetric, see Newman and Alumbaugh, 1995; Streich, 2009). As a result, system of linear equations in the form given below is obtained.

$$KE=S \quad (1)$$

Here, K matrix defines a hermitian and sparse matrix with at most 13 non-zero elements in each row, and S defines the source term. E field values are obtained by solving the equation system,

and H fields can be derived from electric fields using auxiliary equations. In solving the system of equations, the K matrix must be inverted (direct methods) or the system of equations must be solved with Krylov environment solvers (iterative methods).

The number of rows or columns of the K matrix in the system of equations to be solved can be expressed in hundreds of thousands or even millions, depending on the number of elements in the designed 3-D model mesh. For this reason, the stationary and fast solvers used in the solution of the system of equations directly affect the speed of the method. Krylov environment solvers are frequently preferred because RAM usage is much lower than direct solvers. The main Krylov space solvers used in the forward solution in the 3-D MT method are CG (Zhdanov et al., 2000; Haber, 2004; Zhdanov et al., 2011), BICG (Sasaki et al., 2010; Farquharson and Miensopust, 2011; Sasaki, 2012), BICGSTAB (Xiao et al., 2018; Singh et al., 2017; Plessix and Mulder, 2008), QMR (Kelbert et al., 2014; Tang et al., 2015; Wang and Tan, 2017) and GMRES (Cox et al., 2010; Grayver, 2015). ; Grayver and Kolev, 2015). During this study, the performances of those iterative solvers were tested.

Recently, direct solvers have begun to be used for relatively small model networks. Since the matrix is inverted in direct solvers, there is no need to solve the equation again for each polarization and the solution speed increases. Due to developments in computer technology, the use of direct solution methods has increased in the last decades and the use of Multifrontal methods in the CPU environment has become widespread (Streich, 2009; da Silva et al., 2012; Kordy et al., 2015; Puzyrev et al., 2016; Mütschard et al., 2017). ; Liu et al., 2018). Although RAM usage of direct solvers is reduced with multifrontal methods, their use is not preferred for large model networks.

During the study, the solution sensitivities and calculation times of all iterative and direct solvers were tested and the obtained results were discussed.

DISCUSSION and RESULTS

In 2008 and 2011, during two workshops at the Dublin Institute for Advanced Studies over 40 people from academia and industry from around the world met to discuss 3-D MT modeling and inversion studies. In these workshops, to test the numerical forward solutions, a 3-D models were designed to compare the responses obtained by different codes and/or users. This model was called as Dublin Test Model-1 (DTM-1). The DTM1 test model which is used by the 3D algorithm developers in the MT method was used during the study. The results of the developed algorithm were discussed using Dublin Test Model-1 (DTM-1). In the comparison, whole algorithm reached same results and whole discussions made based on this test model.

During the study, the performances of the solvers were tested on the CPU and the BICGSTAB solver was found to be the fastest and most stable solver (Figure-1). However, it is seen that direct solvers reach the solution in the most effective solution time if more than one polarization is used. In Figure-1, the results are given according to the use of a single polarization. While it is necessary to make a new calculation for each polarization in iterative solvers, this is not necessary in direct solvers and there is no noticeable increase in calculation time. Therefore, as a result of the study,

it was concluded that it would be efficient to use direct solvers, especially at low frequencies (0.01 Hz and lower), for small model meshes. Using iterative methods for frequencies of 0.01 Hz and larger allows the algorithm to reach faster results than direct solvers. For this reason, it has been observed that making this selection in the algorithms to be developed increases the solution speed. When we look at the CPU and GPU performances of the BICGSTAB algorithm (which is the selected iterative solver), it is observed that the acceleration in the solver is 2.5 times higher, especially at low frequencies, for the algorithm developed on the GPU platform (Figure-2). However, due to GPU RAM usage restrictions, it has been observed that its use is not suitable for large model meshes.

CONCLUSIONS

The simultaneous use of direct and iterative solvers during 3D magnetotelluric modeling is important in terms of solution speed. Therefore, the use of BICGSTAB iterative solver for frequencies higher than 0.01 Hz and direct solvers for frequencies lower than 0.01 Hz makes a positive contribution to the solution speed. In addition, coding the entire algorithm in the GPU environment has shown that this selection may not be necessary in the future if there is no GPU RAM bottleneck. It has been observed that the best method for today's conditions is to use both direct and iterative methods together on the CPU.

ACKNOWLEDGEMENT

This study was supported by TÜBİTAK BİDEB under Grant number 1059B191800610.

REFERENCES

- Avdeev, D. B., Kuvshinov, A. V., Pankratov, O. V., & Newman, G. A. (2002). Three-dimensional induction logging problems, Part I: An integral equation solution and model comparisons. *Geophysics*, 67(2), 413-426.
- Badea, E. A., Everett, M. E., Newman, G. A., & Biro, O. (2001). Finite-element analysis of controlled-source electromagnetic induction using Coulomb-gauged potentials. *Geophysics*, 66(3), 786-799.
- Constable, S., & Weiss, C. J. (2006). Mapping thin resistors and hydrocarbons with marine EM methods, Part II— Modeling and analysis in 3D. *Geophysics*, 71(6), G321-G332.
- da Silva, N. V., Morgan, J. V., MacGregor, L., & Warner, M. (2012). A finite element multifrontal method for 3D CSEM modeling in the frequency domain. *Geophysics*, 77(2), E101-E115.
- Demirci, I., Erdoğan, E., & Candansayar, M. E. (2012). Two-dimensional inversion of direct current resistivity data incorporating topography by using finite difference techniques with triangle cells: Investigation of Kera fault zone in western Crete. *Geophysics*, 77(1), E67-E75.
- Erdoğan, E., Demirci, I., & Candansayar, M. E. (2008). Incorporating topography into 2D resistivity modeling using finite-element and finite-difference approaches. *Geophysics*, 73(3), F135-F142.
- Haber, E., & Ascher, U. M. (2001). Fast finite volume simulation of 3D electromagnetic problems with highly discontinuous coefficients. *SIAM Journal on Scientific Computing*, 22(6), 1943-1961.
- Mackie, R. L., Smith, J. T., & Madden, T. R. (1994). Three-dimensional electromagnetic modeling using finite difference equations: The magnetotelluric example. *Radio Science*, 29(4), 923-935.
- Mitsuhata, Y., & Uchida, T. (2004). 3D magnetotelluric modeling using the T-Ω finite-element method. *Geophysics*, 69(1), 108-119.
- Newman, G. A., & Alumbaugh, D. L. (1995). Frequency-domain modelling of airborne electromagnetic responses using staggered finite differences. *Geophysical Prospecting*, 43(8), 1021-1042.

- Newman, G. A., & Alumbaugh, D. L. (2002). Three-dimensional induction logging problems, Part 2: A finite-difference solution. *Geophysics*, 67(2), 484-491.
- Streich, R. (2009). 3D finite-difference frequency-domain modeling of controlled-source electromagnetic data: Direct solution and optimization for high accuracy. *Geophysics*, 74(5), F95-F105.
- Wannamaker, P. E. (1991). Advances in three-dimensional magnetotelluric modeling using integral equations. *Geophysics*, 56(11), 1716-1728.

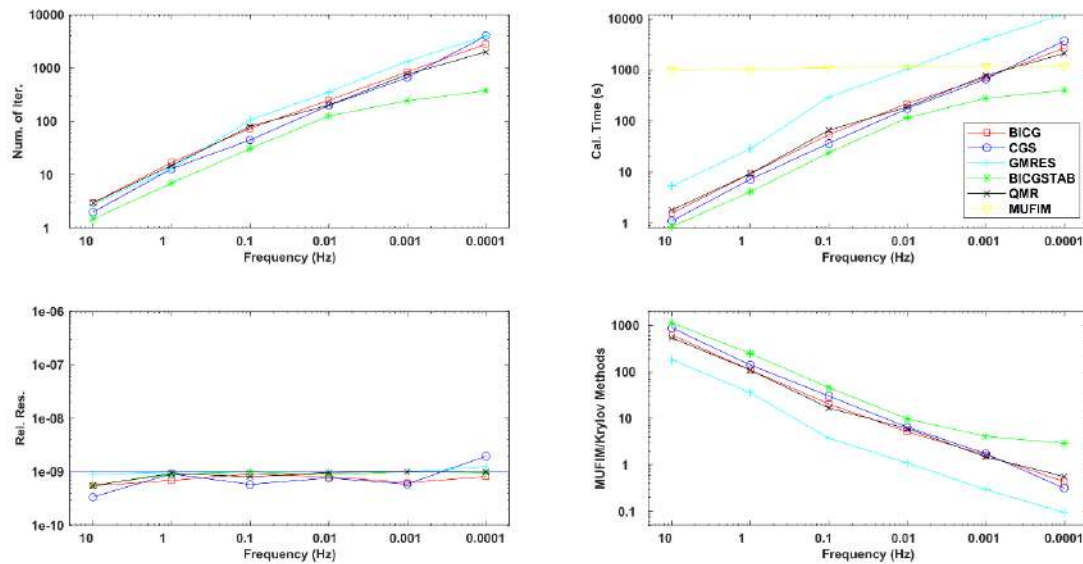


Figure1 Comparison of iterative and direct methods in terms of number of iterations, calculation time, relative error and speedup based on DTM-1

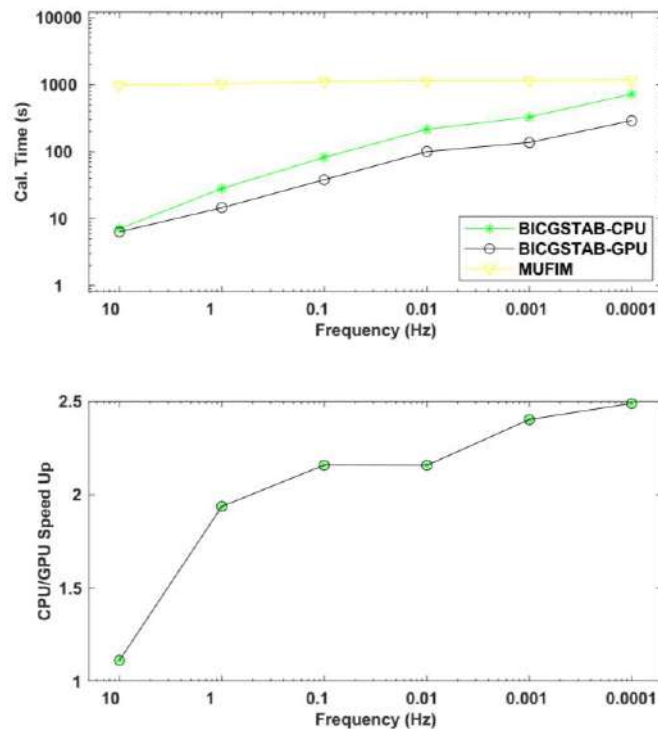


Figure2 CPU and GPU performances and relative acceleration graphs of the selected solver (BICGSTAB)

10.5 SEISMIC VELOCITY INVERSION BY IMPROVED INVERSIONNET DEEP MODEL: NOISY AND NOISELESS TRAINING DATA SETS

M. Najafikhatounabad^{1*}, H.Y. Keleş², S. Kadioğlu¹

¹Geophysical Engineering Department, Ankara University, Ankara, Türkiye

²Computer Engineering Department, Hacettepe University, Ankara, Türkiye

*Corresponding author email: najafim@ankara.edu.tr

ABSTRACT

To investigate the seismic velocity inversion process by deep neural network, we study the InversionNet deep model structure and create two learning data sets: noisy and noiseless. Two different versions of InversionNet have been published so far. We made changes in its architecture especially in the decoder part and achieved a new version of it. The new version of InversionNet can map seismic shot gathers to velocity model better with lower loss function than the others. Labeled data set is one of the essential needs in supervised deep learning methods. In our study InversionNet maps the seismic shot gathers to a related velocity model therefore seismic shot gathers are used as input and velocity models as target or ground truth. We develop a stochastic method to construct 18000 two dimensional(2D) realistic velocity models consisting of dense layers, faulty, and salt dome models. It is used as targets. To prepare the input data sets, 20 synthetic seismic shot gathers are calculated in each velocity model by using 2D acoustic wave propagation equation. In total we calculate 20×1800 shot gathers. It is used as noiseless inputs. Adding coherent and random noises to prepared seismic data made it difficult to recognize the signal patterns. Thus, on the one hand the shot gathers are more like real data and on the other hand the training ability of InversionNet can be investigated. We created a synthetic coherent noise seismogram like ground roll waves pattern and added random noise to it, then summed the outcome with related noiseless shot gather and repeated this for all of them. It is used as noisy inputs. In other words, in this study we prepared noisy and noiseless ‘seismic shot gathers-velocity model’ labeled data sets. The three versions of InversionNet are trained with two noisy and noiseless learning data sets. The results of the test phase for two different data sets are compared and analyzed.

KEYWORDS: Seismic velocity inversion, Deep learning, Convolutional neural network

REFERENCES

- Alford, R. M., Kelly, K. R., and Boore D. M., 1974. “Accuracy of finite-difference modeling of the acoustic wave equation”, *Geophysics*, 39(6), 834-842.
- Araya-Polo, M., Jennings, J., Adler, A. and Dahlke, T. 2018. “Deep-Learning tomography”, *Leading Edge*, 37(1), 58-66.
- McCulloch, W. S. and Pitts, W. 1943. “A logical calculus of the ideas immanent in nervous activity”, *Bull. Math. Biophys.*, 5, 115-133.
- Li, Sh., Liu, B., Ren, Y., Chen, Y., Yang, S., Wang, Y. and Jiang, P. 2020. “Deep-learning inversion of seismic data”, *IEEE Transactions on Geoscience and Remote Sensing*, 58(3), 2135-2149.
- Lines, Larry R., Slawinski, Raphael, Bording, R. Phillip, 1999. “A recipe for stability of finite-difference wave-equation computations” *Geophysics* 64(3), 967-969.
- Liu, B., Yang, S., Ren, Y., Xu, X., Jiang, P. and Chen, Y. 2021. “Deep-learning seismic full-waveform inversion for realistic structural models”, *Geophysics*, 86(1), R31-R44.
- Wang, Z., Bovik, A. C., Sheikh, H. R. and Simoncelli, E. P. 2004. “Image quality assessment: From error visibility to structural similarity”, *IEEE Transactions on Image Processing*, 13(4), 600-613.

P.1 ELECTRIC FIELD MEASUREMENT IN POOR GROUNDING CONDITIONS

N. Zorin¹, D. Epishkin^{1*}, A. Yakovlev¹, D. Yakovlev¹

¹*Nord-West Limited, Moscow, Russia*

**Corresponding author e-mail: dmitri_epishkin@mail.ru*

ABSTRACT

Electrical exploration on frozen or stony soil is associated with high difficulties in achieving good quality of electrode grounding. In such conditions, the results of high-frequency electric field measurements are often biased due to the electrode contact resistance (ECR) effects, i.e., the capacitive leakage between wires and ground and voltage division at the receiver's input. In this paper we discuss a method of full analytical correction of the ECR distortion implemented in the new magnetotelluric system NORD.

KEYWORDS: ECR effect, high electrode contact, electric line calibration

P.2 AIRBORNE MAGNETIC INVESTIGATION FOR DETECTION OF EXPLODED AND UNEXPLODED ORDNANCE USING UAV SYSTEMS IN A FORMER MILITARY AREA

C. Ertuğrul^{1*} And A. Keskinsezer^{1,2}

¹Sakarya Üniversitesi, Fen Bilimleri Enstitüsü, Jeofizik Müh. Anabilim Dalı

²Sakarya Üniversitesi, Müh.Fak. Jeofizik Müh. Bölümü

*Corresponding author e-mail: coskun.ertugrul@ogr.sakarya.edu.tr

ABSTRACT

Along with advanced UAV (Unmanned Aerial Vehicle) and quantum technology, geophysical devices are also developing. Investigation of structures that give magnetic anomalies has given birth to aerial magnetic researches with UAV, with the development of high technology in the last 10 years. Aerial magnetic method with UAV is one of the most effective methods used for the last 5 years in scanning faster and wider areas. It is the most effective method especially in areas where topography changes a lot and terrain conditions are difficult. It is a method that is actively used primarily in metallic mineral exploration in our country, and recently it is one of the leading methods used for archeology, forensic cases, detection of old oil wells, and exploded-unexploded ordnance (UXO) surveys.

In this thesis, it is aimed to quickly and accurately locate the explosive and unexploded munitions, which are dangerous, with high resolution magnetic data from the mortar, before the construction works to be carried out in an old military shooting range.

KEYWORDS: Aerial, Magnetic Survey, UXO, UAV

INTRODUCTION

Aerial magnetic method measurements aim to determine the Earth's magnetic field and anomalies with an airplane or unmanned aerial vehicle. Since different rocks show different magnetic properties, magnetic measurements provide information about the underground structure. Low-altitude flights are used to explore near-surface and locally confined magnetic objects such as ore deposits or artificial structures such as waste piles.

Recently, as a result of advances in quantum technology, magnetometers using Potassium, Cesium and Rubidium, called optically pumped magnetometers, have been developed in a more minimal structure.

As a result of the development of quantum and drone technologies, magnetic sensors, which are also used in military fields today, are actively used in the detection of exploded and unexploded ammunition, buried structures, tunnels and hollow structures.

In this thesis, a drone-mounted airborne magnetic scanning was carried out using the latest technologies for the detection of munitions observed in the area, which was a former military firing range in the 1960s and later used as an agricultural area until today.

1- METHOD and APPLICATION

The research site is located in Kazan district of Ankara, and access to the site is provided by the Ankara-Istanbul highway passing through the northwest of the site and the D100 highway passing through the north-east of the site (Figure 1.).



Figure 1. Location map of the survey area.

According to the satellite map in Figure 2, the research area is approximately 2.25 km longitudinally and approximately 500 meters transversely and has a total area of approximately 114.32 hectares.

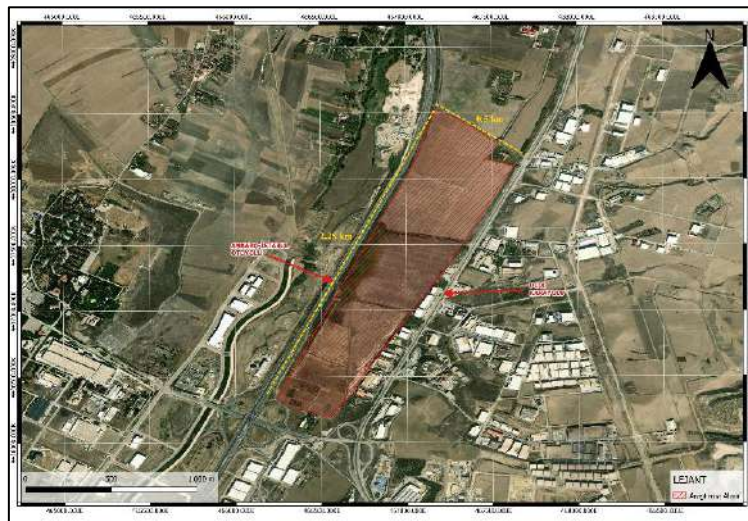


Figure 2. Google Earth satellite image of the research site.

Today, a private company has purchased the site to build commercial buildings. However, as a result of the observations and examinations made in the field, it was predicted that it would

be very dangerous to start an uncontrolled construction work here since there were many exploded and unexploded ammunition and their remains when agriculture was practiced in the field. For this reason, with the opinion of the experts in the field, it was tried to detect exploded and unexploded munitions with aerial magnetic surveys, which have been very popular in the world recently and have given good results, for the first time in Turkey (Figure 3.).



Figure 3. A view of the study in the survey area

Equipment Used and Features

The UAV Magnetometer system, as shown in Figure 4, consists of a drone, drone batteries, SkyHub real terrain tracking kit manufactured by SHP Engineering, Emlid Reach 2 GPS module, MagArrow model cesium optical pump magnetometer manufactured by the American company Geometrics, data acquisition module and power module.



Figure 4. Components of the UAV magnetic system.

Software Used and Features

In aerial magnetic surveys, various programs are used for planning, data acquisition and post-acquisition processing. In this project, the open source QGIS (Quantum Geographic Information System) program was used for the preparation and planning of flight lines in the field, a line output of which is shown in Figure 5.



Figure 5. Drawing flight blocks with QGIS program.

These flight plans need to be uploaded to the drone system as a mission. For this purpose, UgCS (UAV Mission Planning And Flight Control Software) software developed by SHP Engineering, whose interface is shown in Figure 6, was used.



Figure 6. Creating the flight plan with the UgCS program

The MagArrow sensor developed by Geometrics and the Geometrics Survey Manager package program provided by the company were used to pre-check and convert the data to other formats. Then, with the macro software made by ourselves, the lines in the form of blocks were combined into a single line throughout the survey area.

These magnetic data, which are collected with great care, are finally passed to the processing stage. At the processing stage, the Oasis Montaj Assembly 9.8 software of the Seequent software company of the American Bentley group company, which is a popular and up-to-date software in the world in the processing of magnetic data, was used, and all these magnetic data were processed line by line, bad data were extracted, necessary corrections were applied, filtered and mapped.

DISCUSSION and RESULTS

In this survey, exploded and unexploded munitions in a former military firing range in Kazan district of Ankara were tried to be detected by aerial magnetic method using drone technology, which has recently become popular in the world. Within the scope of the research, DJI M600 Pro drone, SkyHub laser altimeter kit from SHP Engineering, precision GPS system and MagArrow magnetic sensor using cesium vapor produced by the American Geometrics company for aerial magnetic studies were used.

The open source QGIS program was used for the preparation of one meter high and one meter spaced flight lines and planning of the blocks, the UgCS program of SHP Engineering was used for drone flights, the Geometrics Survey Manager program of Geometrics company was used for downloading the data and converting them into different formats, and the Oasis Montaj 9.8 program and Google Earth programs of the American Bentley group company, which produces geoscience software called Seequent, were used for data processing and mapping.

The drone flew a total of approximately 1250 km at one meter intervals. In this thesis, only the maps and some results of the magnetic data obtained in plots B1 and B4 are shown (Figure 7, Figure 8, Figure 9 and Figure 10).

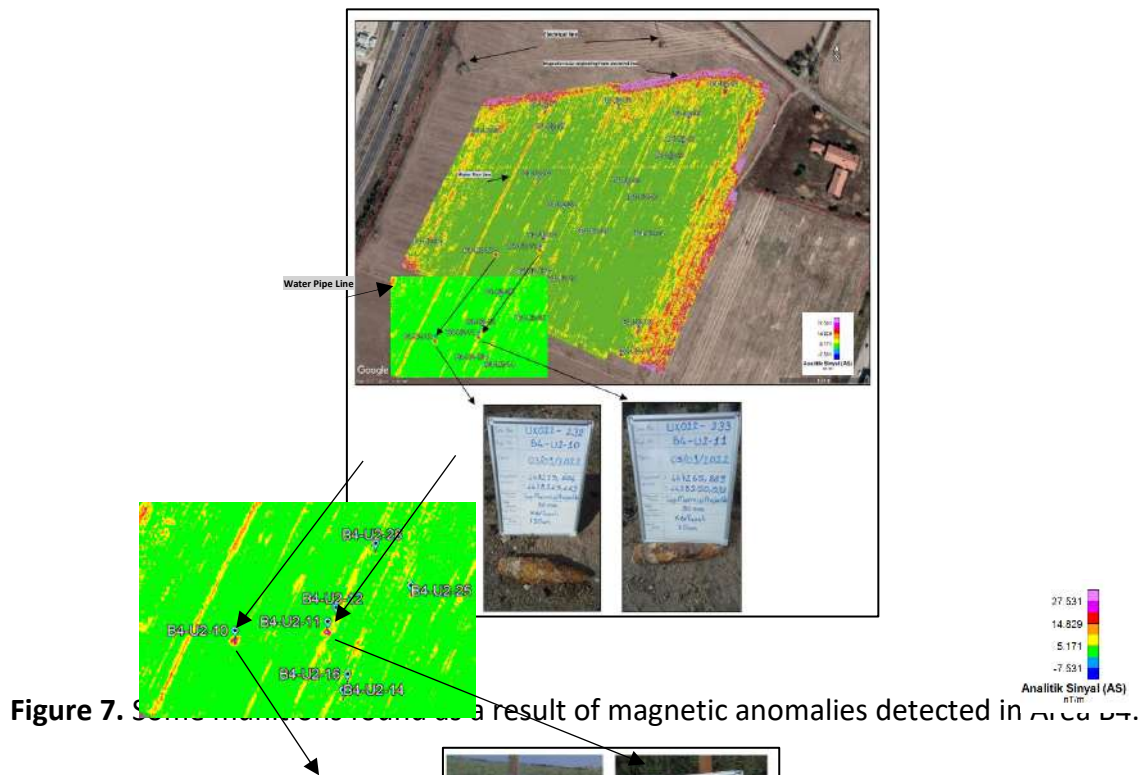


Figure 7. Some munitions found as a result of magnetic anomalies detected in area B4.



Figure 8. List-1 photographs of 90 mm long ammunition detected in area B4.

In the map shown in Figure 9, magnetic anomalies larger than 10 nT were detected at points B4-U2-10 and B4-U2-11 as a result of the magnetic data taken in Area B4, and ammunition numbered UX022-232 and UX022-233 were found at depths of 130 and 70 cm at these points.

These munitions are 90 mm long artillery shells with blunt fuze. When we carefully examine the magnetic anomaly, it is seen that the ammunition numbered UX022-232 from the B4-U2-10 point gives a stronger and more widespread magnetic anomaly because it is more oxidized. In the other anomalous points, 70-75, 90 and 155 mm lengths of ammunition without fuses, with blind fuses and with genuine fuses were detected. The list of some of the 90 mm and 155 mm ammunition recovered is given in Table 3. photographs of the recovered ammunition are shown in Figure 8.

Table 3. List of some of the 90 mm ammunition detected in area B4.

Ammunition Number	Registration Number	Excavation Date	Ammunition Diameter	Flange Type	Inferred Depth
UXO22-205	B4-355	31.08.2022	90	Blind Flange	80 cm
UXO22-206	B4-811	31.08.2022	90	Blind Flange	40 cm
UXO22-207	B4-546	31.08.2022	90	Blind Flange	40 cm
UXO22-210	B4-753	1.09.2022	90	Blind Flange	10 cm
UXO22-212	B4-972	1.09.2022	90	Original Flange	130 cm

Table 5. Magnetic anomaly distributions according to the depths of 155 mm long ammunition detected in area B1.

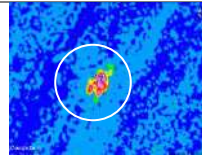
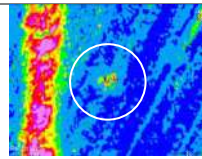
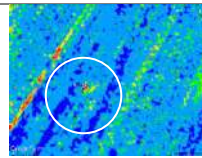
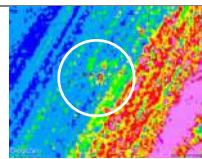
Ammunition Number	Registration Number	Inferred Depth	AS Magnetic Anomaly Map
UXO22-03	B1-358	50 cm	
UXO22-24	B1-1653	120 cm	
UXO22-29	B1-1890	110 cm	
UXO22-37	B1-2402	80 cm	

Table 5 compares the magnetic anomaly quality of some 155 mm long munitions according to their depth. According to this comparison, munitions close to the surface yielded more diffuse and higher magnetic anomalies, while the strength of the magnetic anomalies obtained from deeper munitions decreased.

CONCLUSION

In this study, drone-mounted airborne magnetic data were used to detect detonated and unexploded munitions in a former military firing range in Kazan district of Ankara province. As can be seen in the examples, although the data quality decreased at points where there was magnetic noise, very good results were obtained in the field in general.

In conclusion, the use of airborne magnetic data from drones for the identification of exploded and unexploded ordnance is advantageous in terms of both economy and speed, and the advantages of this method are the improvement of data quality by developing magnetic sensors and the rapid adaptation of new technologies to the method.

However, since high data quality brings high data, it is very difficult to store and control in field conditions. In addition, drone control is difficult in windy weather, disturbing magnetic fields affecting the surface such as power lines and natural gas lines affect the data quality in detail studies, and besides this, we can say that the disadvantages of aerial magnetic studies with drones today are that it is a new technology, the studies in the world are not at a sufficient level and the experienced trained team is not much in the sector.

Finally, although the magnetic sensor used in this study is dual, it gives a single magnetic result. As it is known, the gradient magnetic method is the most widely used method in archaeology to detect magnetic anomalies of structures close to the surface. Now, with the newly developed quantum magnetic sensor technologies, this method can be done more easily with drones. For this reason, it is useful to utilize multi-sensor measurements in the search for metallic objects and ammunition close to the surface. Gradient magnetic measurements using at least two sensors will be more useful in terms of data quality and interpretation.

P.3 THE MAGNETOTELLURIC METHOD IN GEOTHERMAL EXPLORATION: CASE STUDIES

N. Palshin¹, D. Epishkin¹, A. Yakovlev¹, D. Yakovlev¹, N. Zorin^{1*}

¹*Nord-West Limited, Moscow, Russia*

*Corresponding author e-mail: nikita.zorin.geophys@gmail.com

ABSTRACT

Among the geophysical tools employed for investigation of geothermal systems, the magnetotelluric (MT) method could be very effective since it is sensitive to the electrical conductivity, which is an important parameter characterizing a geothermal setting in a target area. Many of high temperature zones and recharge areas are characterized by reduced resistivity. Often hydrothermal processes result in forming conductive clay caps. The reliably identified low resistivity zones produced by brines and clays that cap a geothermal system represent attractive targets for EM exploration. In this paper we consider some examples of MT application in geothermal studies, performed by or in close cooperation with the Nord-West company.

KEYWORDS: Electromagnetic exploration, geothermal energy, volcanic regions

Sponsors & Exhibitors & Supporters

Diamond Sponsor



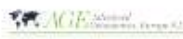
Golden Sponsor



Silver Sponsor



Exhibitors



Academic Partners



Society



Main



Media

